University of Alberta

Power System Voltage Stability Assessment Using Channel Components Transform

by

Iraj Rahimi Pordanjani

A thesis submitted to the Faculty of Graduate Studies and Research
in partial fulfillment of the requirements for the degree of

Doctor of Philosophy
in
Power Engineering and Power Electronics

Department of Electrical and Computer Engineering

Fall 2013
Edmonton, Alberta

Abstract

This Thesis proposes a novel transform called “Channel Components Transform” and presents its application to power system voltage stability assessment. The transform is based on the following observation: a power network can be represented as a multi-node, multi-branch Thevenin circuit connecting the loads to the generators. If one applies eigen-decomposition on the Thevenin impedance matrix, the network can be decoupled into a set of single-branch equivalent circuits. These circuits are much easier to analyze and they carry valuable information of a power system. Similarly, if the variations of the transformed variables can be evaluated, one may be able to predict the complex behaviours of the actual network. The eigen-decomposition of the Thevenin impedance matrix and associated operations are named “Channel Components Transform” (CCT).

The thesis shows that CCT can establish a framework to assess the voltage stability conditions of a power system. Techniques are developed to identify the critical modes (called channels) involved in voltage collapse, the associated critical buses, generators, and branches. These methods are tested using various test systems including an actual large power system. The results confirm that the developed methods are useful tools for assessing the voltage stability of a complex power system.

A wide-area scheme for the online voltage stability monitoring based on the proposed CCT-based framework is proposed. A methodology for optimal placement of Phsor Measurement Units (PMUs) is also proposed in order to minimize the number of required PMUs and as a

result, make the implementation procedure practical. A CCT-based algorithm to facilitate the planning of reactive power support is developed. Using the proposed algorithm, the optimal location and amount of reactive supports are determined in order to increase the voltage stability margin. The application of Singular Value Decomposition (SVD) in the proposed CCT is also investigated in this thesis.

Acknowledgements

I would like to express my sincere gratitude to my supervisor, Prof. Wilsun Xu, for his expert guidance, encouragement and support during my PhD program at the University of Alberta. In the thousands of hours he devoted to my education and research, he showed me how to think like a researcher as well as formulate, test, express, and defend my ideas in a clear and concise manner.

I would also like to thank my colleagues in the Power Disturbance and Signaling Research Laboratory. I would like to thank all of them specially Dr. Yunfei Wang, Dr. Hooman Erfanian, Hesam Yazdanpanahi, and Dr. Ali Arefifar for their cooperation and valuable discussions.

My family has always been supportive and encouraging. I give a hearty thanks to all my family members. I am forever indebted to them for all their endless encouragement and love for my entire life.

This thesis was supported by the Alberta Innovates Technology Future with the Graduate Student Scholarship, the University of Alberta with the Provost Doctoral Entrance Award, my supervisor and the ECE department with several terms of R.A. and T.A. This collection of financial sources made my student life a lot more pleasant, and is highly appreciated.

Table of Contents

List of Tables

List of Figures

Chapter 1: Introduction

The problem of maintaining power system stability is still one of the main concerns in the operation of power systems. Power system stability is defined as "the ability of an electric power system, for a given initial operating condition, to regain a state of operating equilibrium after being subjected to a physical disturbance, with most system variables bounded so that practically the entire system remains intact" [1]. Power system stability can be divided into different categories including angular stability, frequency stability, and voltage stability.

With the increasing demand for electrical power and due to economic and environmental constraints, power systems are currently being operated closer to their limits. This has led to an ever-increasing risk of voltage instability. As a result, a great deal of research works has been conducted during the past decade to develop methods for voltage stability analysis and mitigation. On the other hand, with the advent of Phasor Measurement Unit (PMU) technology which is the most accurate and advanced time-synchronized technology available to power engineers [5], many attempts have been carried out to adapt voltage stability analysis methods for online monitoring purposes. However, the progress is very slow in this respect. The aim of this Chapter is to discuss this problem and make it clearer. For this purpose, the basic concepts of voltage stability are reviewed first. All the existing methods for voltage stability analysis and their associated problems are then overviewed. Moreover, the problems of reactive power planning which is one of the most effective ways to improve voltage stability are discussed. The thesis contributions and outline are presented at the end of this chapter.

1.1 Voltage Stability Definition and Classification

The IEEE/CIGRE Joint Task Force [1] defines the voltage stability as "Voltage stability refers to the ability of a power system to maintain steady voltages at all buses in the system being subjected to a disturbance from a given initial operation condition". The definition suggested in [15] which is more related to the phenomena and mechanism of voltage instability is as follows: "Voltage instability stems from the attempt of load dynamics to restore power consumption beyond the capability of the combined transmission and generation systems". As this definition

describes, loads are the driving force of voltage instability. The transfer capability of transmission network and the generation capacity affect voltage stability. As a result, voltage stability is a condition of equilibrium depending on network topology, system operating conditions and the disturbance [79].

In order to briefly describe the voltage instability phenomena, a two-bus system as shown in Fig. 1.1(a) is considered. Under normal condition, system operation is described by the following equations.

$$P = -\frac{EV}{X}\sin\theta \tag{1.1}$$

$$Q = -\frac{V^2}{X} + \frac{EV}{X}\cos\theta \tag{1.2}$$

Solving (1.1) and (1.2) with respect to V yields

$$V = \sqrt{\frac{E^2}{2} - QX \pm \sqrt{\frac{E^2}{4} - X^2P^2 - XE^2Q}} \tag{1.3}$$

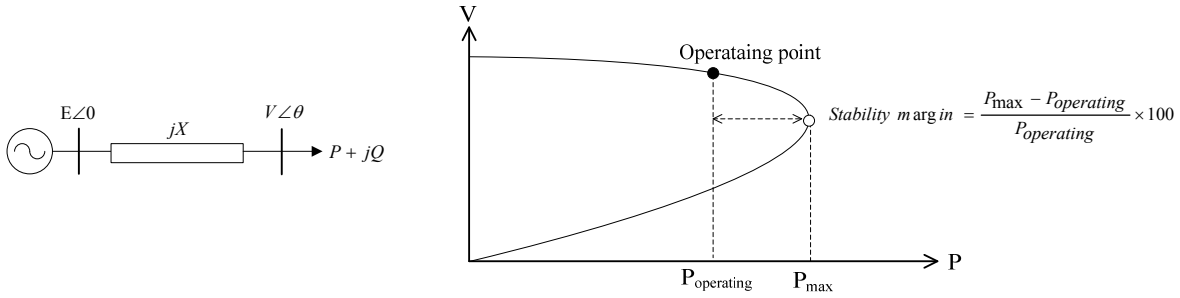

(a) The two-bus system (b) PV curve of the system

Fig. 1.1: A two-bus system and its PV curve

For many reasons and in industry practice, it is common to consider the curves which relate voltage to active or reactive power. Such curves are called PV or QV curves, respectively. The PV curve for our system can be obtained using (1.3) as shown in Fig. 1.1(b). As shown in this figure, power systems normally operate at the upper part of the PV curve. This figure also confirms the existence of a maximum load power (P_{max}). Simply stated, voltage instability results from the attempt to operate beyond maximum load power. This may result from a severe load

increase or from a large disturbance that increases X and/or decreases E to the extent that the pre-disturbance load demand can no longer be satisfied.

PV curves are usually used to determine the voltage stability level. For this purpose, the stability margin as shown in Fig. 1.1(b) is used. The stability margin shows the distance of the current operating point to the maximum loadability point. If the margin is lower than a specific value (typically 5%), the system is considered in danger and actions should be taken into account to improve the stability [9].

As seen above, voltage stability can be easily analyzed for a simple two-bus system. Similarly, if the measurements taken at the buses are available, the stability level of the system can be monitored online. In fact, the analytical expression of the PV (QV) curve shown in (1.3) makes this possible. However, as well known, power systems are much more complex than this two-bus example. They have several loads connected to several generators through a complicated interconnected transmission network. These characteristics make it difficult to obtain PV curves and asses the system stability. This becomes even more challenging when it comes to online applications where measurements are to be used for this purpose. These difficulties have led to tremendous research works in the past decade and several methods for voltage stability analysis have been proposed (these proposed methods and their limitations are discussed in the next sub-section).

It is also useful to classify voltage stability into different sub-classes. This classification will help to better understand the voltage stability phenomenon and to choose the right analyzing strategy according to the nature of the phenomenon. Voltage stability can be divided into the following two classes according to [81].

- Small disturbance voltage stability (steady-state voltage stability): This type of voltage stability is a result of a small (and usually gradual) perturbation in the system. One common type of these perturbations is a gradual increase in the system loads. Static (steady-state) analysis is usually performed to study the small disturbance voltage stability. When analyzing this type of voltage stability, usually midterm (10 seconds to few minutes) or long term (few minutes to tens of minutes) studies are considered [80].
- Large disturbance voltage stability (transient voltage stability): This type of voltage stability happens as a result of a large change in the system. This large change could

be a fault on a major transmission line, sudden outage of a transmission line or a generator. A dynamic analysis is usually preferred to capture the nonlinear dynamic behaviors of this kind of voltage stability. The time frame for the analysis is the short-term (0 to 10 seconds).

1.2 Voltage Stability Analysis Methods

As mentioned in the previous section, each class of voltage stability has its own nature and characteristics. Therefore, it is reasonable to use different analysis methods for different types of voltage stability. In this respect, the voltage stability analysis methods can be categorized into two groups.

- Static analysis
- Dynamic analysis

Static analysis is used to study the small disturbance (steady-state) voltage stability. In the event of small disturbances, the system dynamics which are related to voltage stability are usually slow. Therefore, the problem can be effectively analyzed using static approaches. In these approaches, snapshots are taken from different system operating conditions at certain time instants. At each time instant, non-linear system equations are linearized to study the voltage stability characteristics at that time instant.

Dynamic analysis uses time-domain simulations and captures the actual dynamic characteristics of the system without any approximation or linearization. Nonlinear dynamic analysis is very useful for large disturbance voltage stability where short-term and transient phenomena need to be studied. Dynamic analysis provides accurate results, but on the other hand, encounters several difficulties. Dynamic simulations require detailed modeling of all system components. Accurate models of many components in an actual power system are usually not available. In this situation, approximations in modeling might decrease the accuracy of the results significantly. Dynamic simulations are obviously much more complicated than static studies since it includes nonlinear differential equations as well as regular algebraic equations. Solving these equations require significant computational time and capacity. This limits the application of this kind of analysis in online applications where the computational time is a main concern.

In this thesis, the focus is on small-disturbance voltage stability. Therefore, the static analysis will be studied. In the voltage stability analysis, the following important tasks should be accomplished.

- Determine the stability of the current operating point
- Identify the areas (loads) which are more prone to voltage stability
- Identify the transmission lines which are weak with regard to voltage stability
- Identify the generators which have the highest impacts on voltage stability.

Most of the existing methods are based on the steady-state power flow formulation. These methods are widely used by utilities for offline studies. On the other hand, some methods have been proposed based on direct measurements. These methods aim to employ the measurements taken by PMUs to analyze some aspects of voltage stability problem in online applications.

1.2.1 Methods based on power flow formulation

Many methods which are based on power flow analysis or derived from power flow formulation have been proposed in the literature. The most popular methods are reviewed below.

A. Continuation power flow

Power flow analysis is often a useful tool in voltage stability analysis. The maximum loadability of a system can be determined by starting from the current operating point, making an increase in the loads with considering a certain load pattern such as constant power factor, and re-computing power flow until the maximum loading point is reached. In this approach, the operating point at which the power flow diverges and the system Jacobian matrix becomes singular in considered as the maximum loading point. PV (QV) curves can also be obtained to visualize the maximum loadability. A modification of this method known as continuation power flow (CPF) was proposed in [10]. In this method, the power flow equations are reformulated so that they remain well-conditioned for all scaling factors. This makes it possible to find the solutions of the power flow even for the unstable equilibrium points i.e. the lower portions of the PV curves. Therefore, plotting the complete PV and QV curves becomes possible.

CPF and PV (QV) curves are widely used by utilities in offline studies. With the support of modern computer hardware and software technology, many attempts have been made to use CPF for online applications [11]. However, the computation time is still a main concern in online applications. Moreover, it is difficult to determine the weak loads, branches, and generators by using this method.

B. Modal analysis

Modal analysis which involves eigenvalue analysis of the system Jacobian matrix (J) was proposed in [12]. The basic concepts of this method are as follows: Assuming $\Delta P = 0$, the linearised power flow equations are firstly reduced as shown below.

$$\begin{bmatrix}\Delta P \\ \Delta Q\end{bmatrix} = \begin{bmatrix}J_{P\theta} & J_{PV} \\ J_{Q\theta} & J_{QV}\end{bmatrix}\begin{bmatrix}\Delta\theta \\ \Delta V\end{bmatrix} = J\begin{bmatrix}\Delta\theta \\ \Delta V\end{bmatrix}, \quad \Delta P = 0 \Rightarrow \Delta V = J_R^{-1}\Delta Q \tag{1.4}$$

where $J_R = J_{QV} - J_{Q\theta}J_{P\theta}^{-1}J_{PV}$ is called the reduced Jacobian matrix. This matrix becomes singular at the PV curve nose point [12]. According to the eigenvalue theory, (1.4) can be written as

$$\begin{bmatrix}\Delta v_1 \\ \Delta v_2 \\ \cdots \\ \Delta v_n\end{bmatrix} = \begin{bmatrix}\lambda_1^{-1} & 0 & . & 0 \\ 0 & \lambda_2^{-1} & . & 0 \\ . & . & . & . \\ 0 & 0 & . & \lambda_n^{-1}\end{bmatrix}\begin{bmatrix}\Delta q_1 \\ \Delta q_2 \\ \cdots \\ \Delta q_n\end{bmatrix} \tag{1.5}$$

where $\Delta v = T\Delta V$ and $\Delta q = T\Delta Q$ are the modal voltage and reactive power variations, respectively, and T is the eigenvector matrix. According to (1.5), if $\lambda_i = 0$, the ith modal voltage experiences collapse when the ith modal reactive power experiences a small variation. Therefore, the voltage collapse is essentially the collapse of the voltage in a mode (critical mode). The minimum eigenvalue corresponds to the critical mode because when the system moves toward an unstable condition, it will move toward zero.

For the critical mode, the participation factors of all load buses can then be calculated to identify the locations which are most prone to voltage collapse. Identification of the weak locations (critical buses) is indeed the most important feature of the modal analysis method and is widely used in voltage stability analysis studies [13]-[16]. However, the critical generators which have the highest impacts on the voltage stability cannot be determined by modal analysis.

In fact, this method provides no information for generators since (1.4) contains no entries for the generators. In [17], another reduced Jacobian matrix which contains active power information (instead of reactive power) has been proposed. Using this Jacobian matrix, it is possible to determine the active (power) participation factors (APF) of the generators. As a result, generators can be ranked in terms of the impacts of their active powers on voltage stability. However, there is still no method to determine the impact of generators' reactive powers. On the other hand, determining the impact of generators' reactive powers on voltage stability can be very useful since the voltage collapse is typically associated with the reactive power [11].

C. Singular value decomposition

The singular value decomposition method was first introduced in [18] and [19]. This method is similar in nature to the modal analysis method. It works on the same reduced Jacobian matrix (J_R). The only difference is that instead of eigenvalue decomposition, singular value decomposition (SVD) is applied on this matrix. The singularity of the Jacobian matrix is then determined by the minimum singular value of the matrix. A fast algorithm for calculation of the minimum singular value has also been proposed in [20] to improve the computational speed of this method. As expected, [21] has shown that the minimum singular value and minimum eigenvalue provide similar information for voltage stability analysis.

D. Sensitivity based method

Sensitivity factors computed from the Jacobian matrix of the system power flow [22] have been used for a long time. Within the context of voltage stability analysis, different sensitivity factors have been proposed as indices to detect voltage instability [11], [23].To do this purpose, the sensitivities of load voltages to reactive powers [24]-[25], and the sensitivities of the total reactive power generation to the reactive loads [15], [26], [27] turn out to be a convenient system-wide index.

A general formula based on the eigenvectors and eigenvalues of the Jacobian matrix was also derived in [28] in order to obtain the sensitivity of the loadability margin to parameters. It was later applied to various parameters in [29]. This formula is within the context of loadability limit computation. An extension for the purpose of post-contingency scenario analysis was proposed in [27]. This approach has been used in [30] to determine the minimal load shedding

and in [31] to improve the secure operating margin. More recently, sensitivity based techniques were revisited and extended in [32].

Because of the computation efficiency of sensitivity-based indices, they can be implemented in protection relays to initiate remedial actions such as load shedding and capacitor switching. However, they do not provide any measure of the distance to the voltage collapse point. More importantly, they cannot be used to determine the weak loads that are more prone to the voltage instability [33].

E. Other related methods

A variety of other methods can be found in the literature which are very similar to the methods explained above, but with using different perspective. As an example, a method was proposed in [34] which is based on the fact that a stable system must have two solutions for the power flow equations, and the number of existing solution will change from 2 to 1 when the system reaches the maximum loadability. The concept of this method is similar to the PV curve approach used in CPF. The method proposed in [35] is based on the same concept and uses the pair of load flow solutions to calculate the voltage instability proximity index (VIPI). Another example is the method proposed in [36] in which a voltage stability index called the L indicator was proposed. This index is derived based on the feasibility of the power flow of an individual load bus. This index indicates the voltage collapse point when the Jacobian matrix becomes singular [37].

1.2.2 Methods based on measurements

Methods which are based on the online measurements provided by PMUs can be divided in two categories; methods based on local measurements, and methods based on wide-area measurements.

A. Methods based on local measurements

Most of these methods rely on the impedance matching concept. The method proposed in [38] uses the measurements taken at one load bus to estimate the Thevenin equivalent circuit seen from that bus. In this method, at least two sets of measurements are required and the

Thevenin circuit is estimated using a least-square method. Extensions of this concept are used in [39]-[42]. Once the Thevenin circuit is estimated, the impedance matching condition can be also expressed as the voltage matching condition. The voltage matching condition has been used in [43]-[44] to develop a voltage stability index. [45] presents another extension of the impedance matching condition.

Application of the Thevenin equivalent and the impedance matching condition encounter several limitations. First of all, from the theoretical point of view, the adequacy of observing a single load when the maximum power is reached in a set of loads is doubtful [46]. In this respect, [47] shows that the impedance matching condition is necessarily met after meeting the maximum loadability condition. Secondly, the estimation of the Thevenin equivalent based on at least two sets of measured data faces some difficulties. The measurements need to be gathered over a time window that should be wide enough for the operating conditions to change, but narrow enough to satisfy the constant Thevenin impedance assumption [6]. Also, the technique might not be robust enough to be applied over the time interval following a severe disturbance [46].

B. Methods based on wide-area measurements

Unfortunately, only a few good methods based on wide-area measurements have been reported in the literature. The method proposed in [48] uses a wide-area network of PMUs and relies on the impedance matching condition to detect the critical operating conditions and identify the critical load buses. However, since this method is based on the impedance matching concept, the difficulties discussed in the previous subsection also exist in this method.

In order to overcome the difficulties coming from the need for multiple measurements in the impedance matching, a method which needs only one snapshot was proposed in [49]. In this method, the voltage drop of the Thevenin impedance is approximated by the sum of the magnitudes of the voltage drops over the branches located on the shortest path from a particular load bus to a generator under voltage control. The impedance matching condition is then replaced by a voltage drop matching condition. However, not enough evidences have been reported to verify the practical validity of this method. In fact, since this method involves several approximations, it might lead to unacceptable errors.

More recently, a method has been proposed in [8], [46], and [50] for the detection of voltage instability from the system states provided by PMUs. In this method, an efficient sensitivity

computation is performed in order to identify when a combination of load powers has passed through the maximum. However, similar to any other sensitivity-based method, this method is not able to provide useful voltage stability-related information such as the locations that are more prone to the voltage instability.

In summary, all the existing methods for voltage stability analysis have some limitations. On one hand, the methods based on power flow formulation still encounter some unanswered questions even in offline studies. For example, none of them can determine the impacts of generators' reactive powers on voltage stability. Moreover, the required computational time makes it difficult for these methods to be used for online monitoring. Also, they are not able to fully employ the wide-area measurements provided by PMUs. On the other hand, in spite of several attempts, no complete method has been proposed for monitoring and analysis of voltage stability based on PMUs data. We believe this is partially due to the lack of a technically sound framework for PMU data interpretation and application. Therefore, the main aim of this research is to propose such a framework, and then use the framework to propose methods and indices for monitoring and analysis of voltage stability.

1.3 Reactive Power Planning

The information obtained by the voltage stability analysis can be used to manage proper countermeasures to improve the stability of the system. For this purpose, a variety of countermeasures can be taken into account [51]. Among them, reactive power planning (RPP) is one of the most effective ones since voltage collapse is typically associated with the reactive power demands of loads not being met because of limitations on the production and transmission of reactive power [11]. RPP can be performed both on the generation side and on the network side. On the generation side, RPP involves optimal reactive power scheduling to improve the stability margin. On the network side, RPP involves optimal allocation of Var sources such as capacitor banks, static Var compensators (SVC), and static compensators (STATCOM).

Over the past few years, RPP has been a concern for several researchers and several methods have been proposed for this purpose. The proposed methods can be categorized in two groups including optimization-based methods, and direct methods.

A. Optimization-based methods

Reference [52] reviews several methods that have been proposed in the literature for RPP. This reference shows that the most commonly used methodology is to introduce voltage stability requirements into the optimal power flow. These kind of methods formulate a multi-objective optimization problem based on the distance to the voltage collapse point, minimum singular value, minimum eigenvalue, or other similar indices. Examples of these methods for RPP both on the generation side and on the network side can be found in [53]-[60]. However, these methods encounter several difficulties. First of all, when considering the voltage stability-related objectives, the formulated multi-objective problem becomes very complicated and very difficult to be solved. That is why several attempts have made to use evolutionary algorithms for solving this optimization problem [52]. Therefore, these methods may not be practical for real power systems which are very large and interconnected. On the other hand, in the vicinity of the voltage collapse point, the voltage stability indices which are used as objectives present nonlinear characteristics, which make the convergence of these methods more difficult [61].

B. Direct methods

In RPP on the network side, direct methods simply estimate the best locations for placing new Var sources. For this purpose, different methods such as modal analysis or sensitivity analysis have been used in the literature. Examples of direct methods can be found in [13], [62]-[63]. However, this kind of methods has a main drawback. They are all based on the following assumption: the loadability sensitivities remain constant no matter how much Var support is added at the selected locations. The situation is similar to that of the load shedding. We have recently shown in [64] that the sensitivities vary a lot when loads are shed at different locations. Similar conclusion can be obtained when adding new Var sources. Therefore, this kind of methods may not lead to optimal solutions when more than one Var source is to be added.

In RPP on the generation side, a direct method has been proposed in [65]. In this method, the active economical dispatch is kept fixed, and the participation factors derived from the critical eigenvectors of the Jacobian matrix are used for reactive power scheduling. References [61] and [66] also use the same concept. The main problem of these methods is that they use the active (power) participation factors (APF). However, APF cannot accurately determine the

impacts of generators reactive powers on the voltage stability. Therefore, the results obtained by using this approach might not be optimal.

This research aims to overcome the problems of directs methods and propose effective methodologies for RPP. The main focus will be on the RPP on the network side, however, the ideas can be extended for the generation side.

1.4 Thesis Scope and Outline

Due to the rapid advancement of measurement and telecommunication technologies, a large amount of data are available nowadays for power system monitoring and control. One example is the synchronized phasor data. Various research works have been conducted to develop applications for the phasor data [3], [4], [73]. For example, reference [74] has documented the latest attempts to create situation awareness for power system planners and operators using the wide-area phasor data collected by PMUs. However, the progress is slow and the PMUs have not offered unique advantages in almost all of the proposed methods.

The challenges of extracting new and unique information from the phasor data may be partially due to the lack of a support theory for phasor data processing and interpretation. This situation may be understood by examining the use of three-phase voltage phasor data, V_a, V_b and V_c. One can process the data in various ways. However, operations such as $(V_a+V_b+V_c)/3$ ($=V_{zero\text{-}sequence}$) or $(V_a+a^2V_b+aV_c)/3$ ($=V_{negative\text{-}sequence}$) (where $a=1\angle 120^o$) have been recognized as the best means to analyze the data. The symmetrical components transform is the support theory for these operations. Because of the theory, converting abc phasors to 012 sequences has become a standard approach to process three-phase phasor data and a number of monitoring and protection schemes have been developed. The wide-area monitoring systems nowadays have made multi-location (positive sequence) voltage phasor data, V_1, V_2, V_3 … V_n available. Inspired by the success of the symmetrical components theory, one would wonder if operations such as $T_1V_1+T_2V_2+...+T_nV_n$ can be rigorously derived for the multi-location (i.e. multi-bus) phasor data, and if such operations can reveal unique characteristics of a power system.

This thesis shows that such a transform can be derived. The proposed transform, called "Channel Components Transform", is able to extract important information about a power system from the phasor data. The theory is likely to bring new insights into the interactions of various quantities measured by PMUs and thus leads to the establishment of a new framework

for PMU applications. The first basic idea of the proposed theory is to treat a multi-generator, multi-load and multi-branch network as a network that has one generator supplying one load through one transmission line that has multiple phases. In other words, each of the real generators can be considered as one phase of a N-phase generator and each of the loads as one phase of a N-phase load. The mutual couplings of the multi-phase transmission line represent the mutual interaction of various branches inside the actual network. The second idea of the proposed technique is to conduct a modal transform to decouple the N-"phase" network into a N de-coupled networks called "modal networks". This is very similar to the symmetrical components transform. The difference is that the former applies to a N-phase network (which represents a N-load actual power system) and the latter applies to a 3-phase line. The mathematical operation of decoupling the N-phase network results in a set of decoupled modal circuits.

The significance of this transform is the following: a complex network is converted into a set of decoupled simple one-source, one-load networks. By analyzing the characteristics of individual decoupled networks, it is possible to extract important information about the actual network. Similarly, if the variations of the modal variables can be monitored, we might be able to predict the complex behaviour of the actual network. Since the PMUs are the ideal and also the only devices available for monitoring the modal variables, we believe the Channel Components Transform has the potential to become a platform where powerfull applications can be developed for the PMUs.

The objective of this thesis is to introduce and investigate the concept of "Channel Components Transform" and to establish associated framework and methods to analyze multi-source, multi-branch and multi-loads electric networks, with a special focus on the power system voltage stability. The thesis is organized as follows:

- Chapter 2 presents the basic theory of the "Channel Components Transform" and compares it with the traditional symmetrical components transform theory. The computation procedure and the basic characteristics of the transform are also discussed in this chapter.

- Chapter 3 aims to assess the voltage stability problem in the channel domain. For this purpose, first of all, the concepts of channel PV/Pδ curves are introduced and discussed using some conceptual case studies. The concept of the critical channel is also introduced. The associated challenges are addressed and overcome by modifying the

channel circuit. The proposed modification is also presented as a simple procedure to make it simple and practical. Methods are proposed for identification of the critical channel. Finally, a procedure is presented to show how the voltage stability can be analyzed form the channel domain. This procedure can be considered as a new framework for the voltage stability analysis.

- In chapter 4, methods are proposed to analyze the voltage stability of a power system using the CCT. The proposed methods are for the identification of the critical load, critical generator, and critical branch. All the proposed methods are verified using several case studies in this chapter.

- In chapter 5, the application of the proposed methods to an actual large system is investigated. For this purpose, the CCT and its associated methods are used and the voltage stability of the Alberta Integrated Electric System (AIES) which is a 2038-bus system is analyzed. The results show the effectiveness and validity of the proposed methods.

- Chapter 6 presents one of the applications of the CCT in reactive power planning. The CCT is used and a strategy for shunt compensation is proposed in order to enhance the voltage stability of power systems. The detail algorithms of the proposed strategy are presented in this chapter. The strategy is also applied to some case studies and the results are discussed.

- Chapter 7 proposes a wide-area scheme for the online voltage stability monitoring based on the proposed CCT-based framework. For this purpose, a practical implementation procedure will be proposed. The proposed procedure will be based on the current technologies available in power systems. These technologies mainly consist of PMUs, and Supervisory Control and Data Acquisition (SCADA). A methodology for optimal placement of PMUs will also be proposed in order to minimize the number of required PMUs and as a result make the implementation procedure practical.
- In Chapter 8, the difficulties which might be faced by CCT are discussed. The main difficulties include the non-existence difficulty and the robustness difficulty. It will be shown that using the singular value decomposition instead of the eigen-decomposition could help overcoming the difficulties. Therefore, a new transformation based on singular value decomposition is proposed. The proposed transformation is also applied to several test systems to analyze the voltage stability characteristics. The obtained results are

compared to those of the CCT to verify the performance of the SVD-based transformation.

- Conclusions of the project are presented in Chapter 9.

Chapter 2: The Theory of Channel Components Transform

This chapter presents the basic ideas of the "Channel Components Transform" theory and establishes several terminologies. The new concepts are compared with those established through the traditional symmetrical components transform theory.

2.1 Basic idea of Channel components transform

A general power system is shown in Fig. 2.1. This system consists of n loads and m generators. There are many transmission lines and other components such as transformers inside the network. This network can be represented using a generalized multi-source Thevenin equivalent circuit model. The equivalent circuit has the following form:

$$\begin{bmatrix} V_1 \\ V_2 \\ \cdots \\ V_n \end{bmatrix} = \begin{bmatrix} k_{11} & k_{12} & . & k_{1m} \\ k_{21} & . & . & . \\ . & . & . & . \\ k_{n1} & k_{n2} & . & k_{nm} \end{bmatrix} \begin{bmatrix} E_1 \\ E_2 \\ \cdots \\ E_m \end{bmatrix} - \begin{bmatrix} Z_{11} & Z_{12} & . & Z_{1n} \\ Z_{21} & . & . & . \\ . & . & . & . \\ Z_{n1} & Z_{n2} & . & Z_{nn} \end{bmatrix} \begin{bmatrix} I_1 \\ I_2 \\ \cdots \\ I_n \end{bmatrix} \tag{2.1}$$

Or $$[V] = [K][E] - [Z][I] = [E'] - [Z][I]$$

In this model, $[E]$ is the terminal voltages or the internal voltages (if a generator's Q_{max} is reached) of the generators and $[V]$ is the nodal voltages at the load buses. A general circuit model for the representation of (2.1) is shown in Fig. 2.2(a).

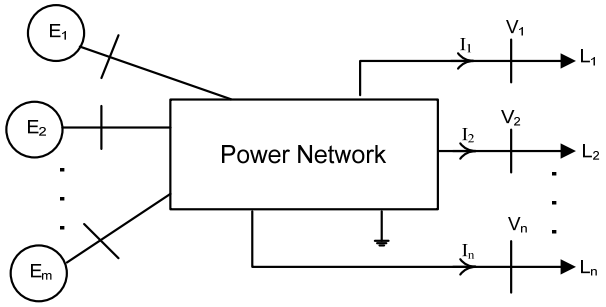

Fig. 2.1: A general electric power network

The first main idea of the transform is to treat the multi-generator, multi-load and multi-branch network shown in Fig. 2.2(a) as a network that has one generator supplying one load through one transmission line that has multiple "phases" (Fig. 2.2(b)). In other words, each of the real generators can be considered as one phase of a n-phase generator and each of the loads as one phase of a n-phase load. The mutual couplings of the multi-phase transmission line represent the mutual interaction of various branches inside the actual network. Since the actual generators and loads are not equal in their power output or consumption, each "phase" of the equivalent generator or load is loaded differently, which is equivalent to saying that the system is "unbalanced" among different "phases". The mathematical model for the n-phase system is exactly the same as (2.1). So this research first introduces a new perspective of interpreting a complex electric network as a simple one-source, one-load and one-branch network that runs on multiple "phases". The number of "phases" is equal to the number of load buses in the system.

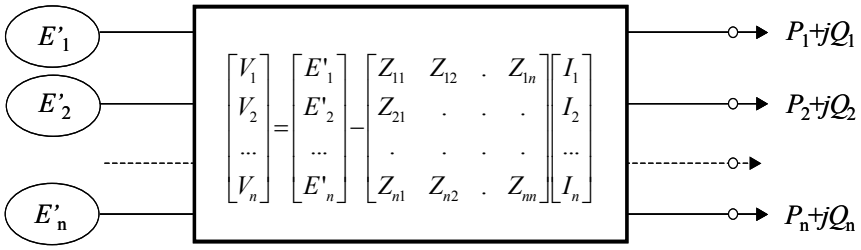

(a) Multiple branch view of a power network

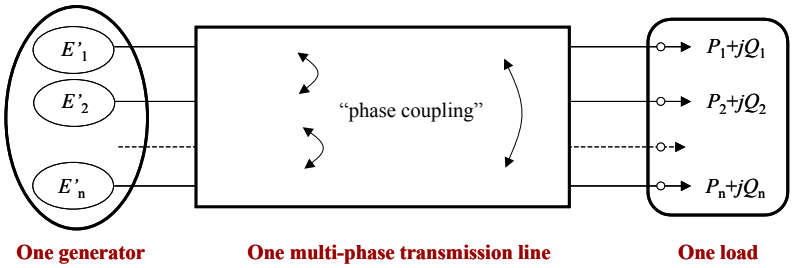

(b) Multiple "phase" view of a power network

Fig. 2.2: Two perspectives on a power network.

Once the actual complex network is viewed as a simple multiphase network, the second idea is to conduct a modal transform to decouple the n-phase network into n de-coupled networks called "modal" networks. This is somewhat similar to the symmetrical components transform which is used to decouple an actual (not equivalent) three-phase branch into positive-, negative-

and zero-sequence branches. The mathematical operation of this decoupling is shown below. First let the eigen-decomposition of the [*Z*] matrix as follows:

$$[Z]=[T]^{-1}[\Lambda][T] \tag{2.2}$$

Then: $[V]=[K][E]-[Z][I]=[K][E]-[T]^{-1}[\Lambda][T][I]$

$$[T][V]=[T][K][E]-[\Lambda][T][I] \tag{2.3}$$

Denote $[\boldsymbol{U}]=[\boldsymbol{T}][\boldsymbol{V}]$ as the modal voltage, $[\boldsymbol{J}]=[\boldsymbol{T}][\boldsymbol{I}]$ as the modal current, and $[\boldsymbol{F}]=[\boldsymbol{T}][\boldsymbol{K}][\boldsymbol{E}]$ as the modal voltage source. This leads to the following decoupled modal networks whose circuit representations are shown in Fig. 2.3.

$$\begin{bmatrix} U_1 \\ U_2 \\ \dots \\ U_n \end{bmatrix} = \begin{bmatrix} F_1 \\ F_2 \\ \dots \\ F_n \end{bmatrix} - \begin{bmatrix} \lambda_1 & 0 & 0 & 0 \\ 0 & \lambda_2 & 0 & 0 \\ 0 & 0 & . & 0 \\ 0 & 0 & 0 & \lambda_n \end{bmatrix} \begin{bmatrix} J_1 \\ J_2 \\ \dots \\ J_n \end{bmatrix} \tag{2.4}$$

The significance of the above transform is the following: a complex network has been transformed into a set of decoupled simple one-source, one-load networks. By analyzing the characteristics of individual decoupled networks, one may extract important information about the actual network.

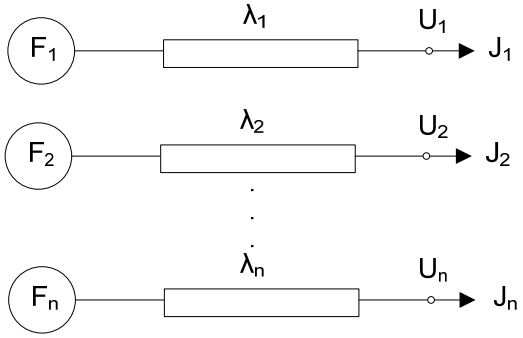

Fig. 2.3: Modal domain representation of a complex network.

2.2 Comparison with symmetrical components transform

Power systems are three-phase networks. How to analyze and interpret the behaviour of three-phase variables and networks was a challenge until the symmetrical components transform was invented. By converting a three-phase network into three decoupled sequence (i.e. modal) networks, the transform opened up a new way to study and monitor three-phase power systems. A number of power system protection schemes and associated relays were invented based on the transform.

The proposed transform shares many common characteristics with the symmetrical components transform (SCT). It is therefore useful to compare the two transforms so that more insights can be gained for the new transform.

The voltage and current relationship of a n-conductor (or n-phase) power line shown in Fig. 2.4 is the simple voltage drop relationship in a matrix form:

$$[V_R] = [V_S] - [Z][I] \tag{2.5}$$

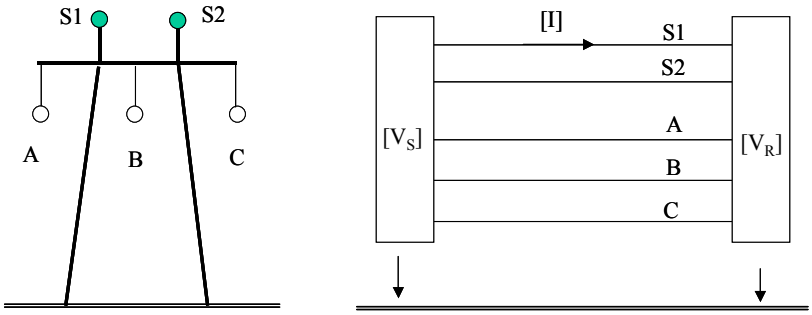

Fig. 2.4: A multi-conductor (or multi-phase) power line.

where $[Z]$ is the n-phase impedance matrix of the line. The simplest case of the above equation is the 3-phase line where $[V_R] = \begin{bmatrix} V_{Ra} & V_{Rb} & V_{Rc} \end{bmatrix}^T$ and $[I] = \begin{bmatrix} I_a & I_b & I_c \end{bmatrix}^T$. If a three-phase line has two shield wires, there are five conductors involved (Fig. 2.4), i.e. $[V_R] = \begin{bmatrix} V_{Ra} & V_{Rb} & V_{Rc} & V_{RS1} & V_{RS2} \end{bmatrix}^T$. In the EMTP analysis, such a line is called five-phase line [75]. This concept can be generalized to n-phase lines if there are n-conductors in a tower structure.

When conducting EMTP simulations or finding the modes of wave propagation in a line, the [*Z*] matrix must be diagonalized, i.e., eigen-decomposition shall be performed on [*Z*]. [75] has presented various forms of [*Z*] decomposition or transform. The symmetrical components transform is the simplest one among them. The SCT yields three single branches in the modal domain. These are the positive-, negative- and zero-sequence branches. The corresponding domain is the well-known sequence domain.

Let's now compare equation (2.5) with (2.1). These two equations have exactly the same form if we set $[E']=[V_S]$ and $[I]=[I_R]$. This clarifies why we have treated the multi-generator, multi-load and multi-branch network shown in Fig. 2.2(a) as a network that has one generator supplying one load through one transmission line that has multiple "phases", shown in Fig. 2.2(b). Once an actual complex network is viewed as a simple "multi-phase" network, the proposed transformation which is similar to eigen-decomposition techniques (such as SCT) well studied in the EMTP theory can be applied to decouple it into n simple "modal" networks.

Therefore, the symmetrical components transform is very similar in the theory with the proposed transform since both are indeed decoupling methods which are based on the eigen-decomposition of a [*Z*] matrix. However, there are some fundamental differences between these two. Each row of the [T] matrix in the proposed transformation is not "symmetric" – the vectors representing T_{ij} (j=1,…N) exhibits random positions in the complex plane. They don't have a system-independent distribution pattern. On the other hand, the symmetrical components have three elements for each row (since it is developed for 3-phase system only). The elements have the same magnitude and are spaced out by exactly 120˚. This characteristic is system independent as long as the system impedances are balanced. Fig. 2.5 shows the differences of the two transformation matrices.

(a) Symmetrical components transform (3-phase) (b) Channel components transform (5 bus example)

Fig. 2.5: Characteristics of the transform matrix [T] for a particular mode

The modal variables ([*U*], [*J*] and [*F*]) in the proposed transform are very similar to the sequence components in the symmetrical components transform. For example, modal 1 voltage may represent the root cause of a voltage collapse scenario. Similarly, the zero sequence current in a three-phase network may represent the most significant source of telephone interference. By analyzing the modal or sequence components, it is easier to identify the causes of certain power system problems.

In summary, if we consider SCT as a method for processing three-phase phasors (measured or calculated), and the transforms documented in [75] as tools for processing multi-phase phasors, the proposed CCT can be viewed as an operation for processing multi-bus phasors. It is interesting to note that the PMU was created originally for determining the sequence components needed by a power system protection scheme [76].

Since "modal components" is a very general term, the modal quantities resulted from the proposed transform will be given the specific name of "Channel Components". The associated domain is called the "Channel Domain". A channel component represents one pattern of currents flowing in a network. The terms "channel components (or channel domain)" and "sequence components (or sequence domain)" can be used interchangeably if one remembers the former applies to an equivalent multiphase system. The channel concept is also somewhat similar to that used for the telecommunication circuits. A telecommunication medium such as a cable carries one physical signal but it represents multiple information-carrying signals running on multiple non-interfering channels.

2.3 Computation Procedure for Channel Components Transform

In order to apply the proposed transform to a power system, according to (2.2) and (2.3), [*Z*] and [*K*] need to be calculated for the system. The calculation process is as follows:

The standard node equations in matrix notation are expressed as:

$$[I] = [Y][V] \tag{2.6}$$

where, [*V*] is the bus voltages, [*I*] is the net injected current, and [*Y*] is the admittance matrix.

All buses can be classified into three types:

- Generator bus (G)
- Load bus (L)
- Network bus (N) which has no generator or load

As a result equation (2.6) can be partitioned as

$$\begin{bmatrix} I_G \\ -I_L \\ I_N \end{bmatrix} = \begin{bmatrix} Y_{GG} & Y_{GL} & Y_{GN} \\ Y_{LG} & Y_{LL} & Y_{LN} \\ Y_{NG} & Y_{NL} & Y_{NN} \end{bmatrix} \begin{bmatrix} V_G \\ V_L \\ V_N \end{bmatrix} \tag{2.7}$$

Since the net injected currents of the network buses are equal to zero i.e. $I_N = 0$, we can write

$$I_N = Y_{NG}V_G + Y_{NL}V_L + Y_{NN}V_N = 0$$

$$i.e.\ V_N = -Y_{NN}^{-1}(Y_{NG}V_G + Y_{NL}V_L) \tag{2.8}$$

Substituting the obtained V_N in (2.7) will result in

$$-I_L = Y_{LG}V_G + Y_{LL}V_L - Y_{LN}Y_{NN}^{-1}(Y_{NG}V_G + Y_{NL}V_L)$$

$$i.e.\ \ -I_L = (Y_{LG} - Y_{LN}Y_{NN}^{-1}Y_{NG})V_G + (Y_{LL} - Y_{LN}Y_{NN}^{-1}Y_{NL})V_L \tag{2.9}$$

Rearranging (2.9) yields

$$V_L = -(Y_{LL} - Y_{LN}Y_{NN}^{-1}Y_{NL})^{-1}(Y_{LG} - Y_{LN}Y_{NN}^{-1}Y_{NG})V_G - (Y_{LL} - Y_{LN}Y_{NN}^{-1}Y_{NL})^{-1}I_L \tag{2.10}$$

It can be seen that equation (2.10) is the same as equation (2.1) and as a result we will have

$$[K] = -(Y_{LL} - Y_{LN}Y_{NN}^{-1}Y_{NL})^{-1}(Y_{LG} - Y_{LN}Y_{NN}^{-1}Y_{NG}) \tag{2.11}$$

$$[Z] = (Y_{LL} - Y_{LN}Y_{NN}^{-1}Y_{NL})^{-1} \tag{2.12}$$

Equations (2.11) and (2.12) give the expression of matrices [*K*] and [*Z*]. Having these two matrices for any power system, we can apply the transform to the system.

2.4 Characteristics of Channel Components

As the channel components are a new concept and represent transformed quantities, it is useful to understand their physical meanings and key characteristics first before more complex treatment is pursued.

A very simple power system is used to illustrate the meanings of channel components. The case is shown in Fig. 2.6(a). The corresponding network equation is

$$\begin{bmatrix} V_a \\ V_b \\ V_c \end{bmatrix} = \begin{bmatrix} E \\ E \\ E \end{bmatrix} - \begin{bmatrix} Z + Z_a & Z & Z \\ Z & Z + Z_b & Z \\ Z & Z & Z + Z_c \end{bmatrix} \begin{bmatrix} I_a \\ I_b \\ I_c \end{bmatrix} \tag{2.13}$$

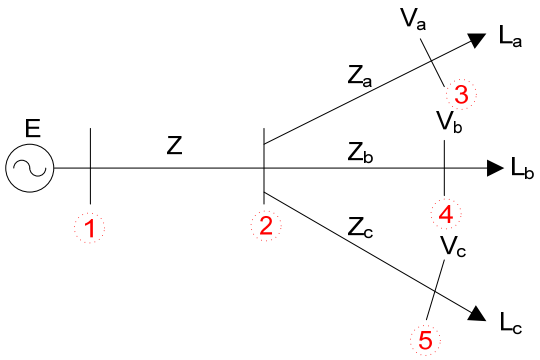

(a) physical network

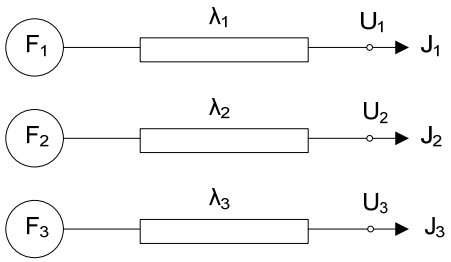

(b) channel network

Fig. 2.6: The one-source three-load system.

If Z_a=Z_b=Z_c, the [Z] matrix and its corresponding "three-phase" network is "balanced". Therefore, the symmetrical components transform can be used as a special case of the Channel components transform, which leads to the following channel or "sequence" parameters. Note that in this case, Channel components 1, 2, and 3 correspond to the zero, positive, and negative sequence components, respectively.

$$[\Lambda] = \begin{bmatrix} 3Z + Z_a & 0 & 0 \\ 0 & Z_a & 0 \\ 0 & 0 & Z_a \end{bmatrix}, and \quad [F] = \begin{bmatrix} \sqrt{3}E \\ 0 \\ 0 \end{bmatrix}$$

As seen above, only channel 1 has a voltage source. It implies that channel 1 is the only channel responsible for power transfer in this case. In fact, the channel impedance λ_1=3(Z+Z_a/3) represents the series connection of Z branch with that of a parallel combination of Z_a, Z_b and Z_c branches. This is exactly what one will do when analyzing the circuit of Fig. 2.6(a) "on the back of an envelope". There is no need to analyze the other channels. So a four-branch power network has been simplified into an one-branch network.

More interestingly, the above analysis can be performed even if loads L_a, L_b and L_c are not equal. This is because the decoupling is only dependent on the [Z] matrix and is independent of the loads connected at different buses. The load conditions will change values of channel components, not the channel circuit and its impedance parameters.

If Z_a, Z_b, and Z_c are not equal, analytical solution is difficult so numerical case is used. Assuming Z_a=0.35, Z_b=0.2, Z_c=0.1, Z=j0.3, E =1.0, S_a=0.3, S_b=0.25, and S_c=0.4, the CCT yields the following parameters.

$$[\Lambda] = \begin{bmatrix} 1.129\text{j} & 0 & 0 \\ 0 & 0.28\text{j} & 0 \\ 0 & 0 & 0.14\text{j} \end{bmatrix}, \ and \ [F] = \begin{bmatrix} 1.7164 \\ -0.1718 \\ 0.1566 \end{bmatrix}$$

It can be seen that all channels have non-zero source voltages. The channel impedances are also different. Since the power transfer capability of a line is proportional to V^2 and inversely to X, channel 1 is the mode responsible for transferring power to loads. Table 2.1, which shows the channel currents in each branch of the system, reveals more information on how the power is

transferred to the loads. Fig. 2.7 shows the patterns of channel currents in the system. In this figure, the thickness of an arrow on a branch is in proportion to the value of the channel current flowing through that branch. Note that the scale used for each channel is different from other channels.

Table 2.1: Channel currents in each branch of the test system.

Branch		Current		
From	To	Channel 1	Channel 2	Channel 3
1	2	1.0001 ∠ 22.3°	0.0089 ∠ -2.6°	0.0169 ∠ -18.4°
2	3	0.3853 ∠ -22.3°	0.0385 ∠ 177.4°	0.0241 ∠ 161.6°
2	4	0.3231 ∠ -22.3°	0.0327 ∠ -2.6°	0.0846 ∠ 161.6°
2	5	0.2917 ∠ -22.3°	0.0147 ∠ -2.6°	0.1256 ∠ -18.4°

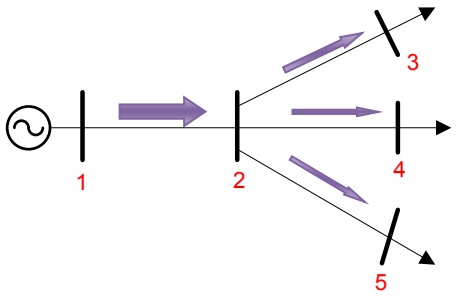

(a) Channel 1

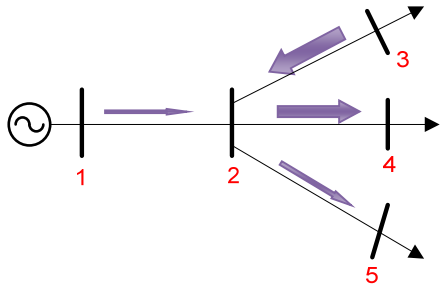

(b) Channel 2

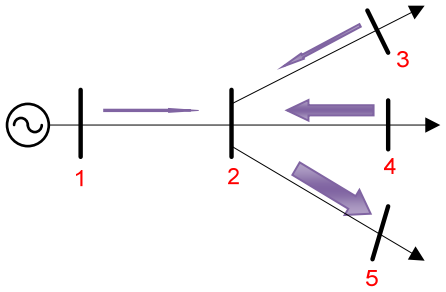

(c) Channel 3

Fig. 2.7: Channel currents in each branch of the test system.

As seen in Table 2.1and Fig. 2.7, the Channel 1 currents are all in-phase, flowing from the source to the loads. So this is the channel responsible for power transfer. The channel 2 current mostly flows from bus 3 to buses 4&5 and the channel 3 current mostly flows from buses 3&4 to bus 5. These are "loop flows" that don't help the power transfer. This shows that the channel currents can help to identify the main paths (or patterns) of power transfer in a power system.

Each channel transfers different amount of power. We can calculate the channel power at any given network operating points established by the load flow results. Fig. 2.8 shows the channel power levels of an actual 2038-bus power system. It can be seen that only a small number of channels are responsible to transfer the majority of power in a network. The implication is that one may only need to analyze or monitor a small number of channels to understand the characteristics of a power system.

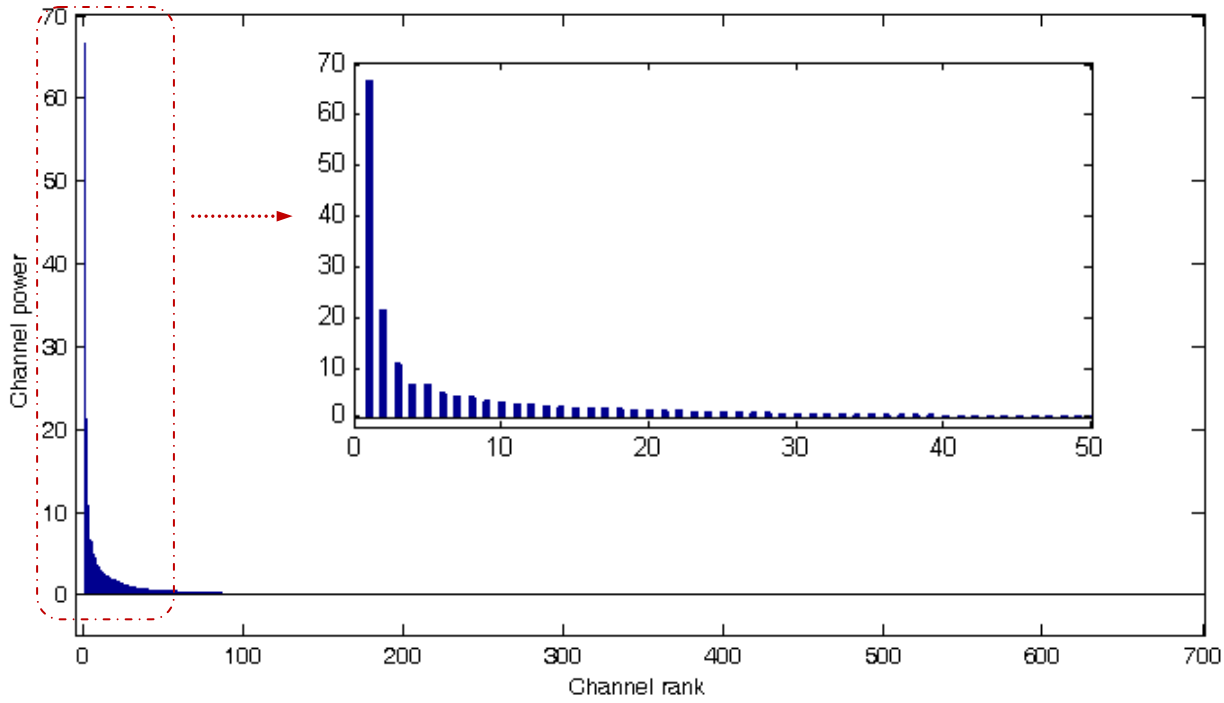

Fig. 2.8: Distribution of channel powers in a large system.

2.5 Conclusions

This chapter has shown that a multi-generator, multi-load, and multi-branch network is mathematically equivalent to a system that has one generator supplying one load through one

transmission line that has multiple "phases". Based on this observation, a transformation, called the Channel Components Transform, has been proposed to analyze complex power systems. The Transform converts a complex power system into a set of decoupled one-source to one-load networks. By analyzing the characteristics of each decoupled network, one may be able to extract important information of a complex network.

The channel components transform shares many similarities with the symmetrical components theory. The similarities have been discussed in this chapter. In view of the evolvement of symmetrical-components-based applications, the proposed channel components transform has a promising future.

Some characteristics of the channel components were clarified using some simple case studies. The results have shown that, in a multi channel system, there is usually one channel which is more responsible for the power transfer. The implication is that instead of analyzing all channels, it suffices to analyze one channel. The distribution of the channel powers in a large system was also discussed, indicating that one may only need to analyze or monitor a small number of channels to understand the characteristics of a power system.

Chapter 3: Voltage Stability Interpretation from the Channel Domain

Maintaining voltage stability is a major objective in power system planning and operation [15]. Although our understanding on the subject has increased significantly in recent years, new findings are still emerging, especially with the emergence of measured phasor data. Many research activities have been conducted on how to utilize the phase information for voltage stability monitoring [8], [48]. This research attempts to propose a new framework for the voltage stability analysis and monitoring based on the channel components transform. The proposed framework can be used both for the offline-analysis and the online monitoring using phasor data. Before presenting the complete algorithms, the characteristics of voltage stability are analyzed from the channel domain first. It is shown how the voltage stability of the actual system can be investigated frrom the channel domain.

3.1 Channel *PV* curves

Transmitting power from generators to loads is the primary objective of a power transmission system. The system has an inherent limit to the amount of power that can be transmitted. Operating a power system too close to the limit is extremely risky since a small disturbance could result in a voltage collapse. The stability level of the system (margin) can be investigated using *PV* curves as shown in Fig. 3.1. The distance of the operating point from the nose point of the *PV* curve determines how close the system is to a voltage collapse. If the margin is lower than a specific value (typically 5%), the system is considered in danger and actions should be taken into account to improve the stability.

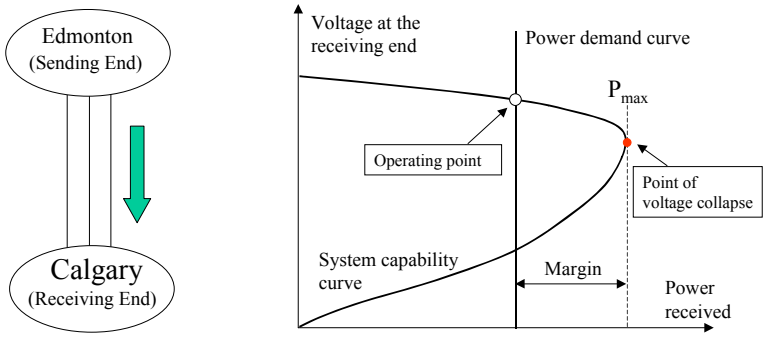

Fig. 3.1: Illustration of power transfer characteristics (PV Curve) of a transmission network

However, obtaining the PV curves is not an easy task in actual power systems. There are several loads connected to several generators through a complicated interconnected transmission network. These characteristics make it difficult to obtain *PV* curves and asses the system stability. This becomes even more challenging when it comes to online applications where measurements are to be used for this purpose.

On the other hand, using the proposed transform, we can transform a complex power system in to simple decoupled networks (channel networks). *PV* curves of these channel networks can be obtained easily. It is, therefore, interesting to examine the *PV* curves from the channel domain.

Since the channel circuit is a very simple one-branch circuit, one can actually derive the entire *PV* curve in channel domain analytically, as follows:

For a channel shown in Fig. 3.2, the relationship between the channel voltage (U_i), and the channel load power (P_i, and Q_i) is given as

$$U_i^4 + U_i^2[2(P_i R_i + Q_i X_i) - F_i^2] + |\lambda_i|^2 (P_i^2 + Q_i^2) = 0 \tag{3.1}$$

Using (3.1), the channel voltage can be plotted for different active powers assuming a constant power factor for the channel load. The resulting curve will be the channel *PV* curve.

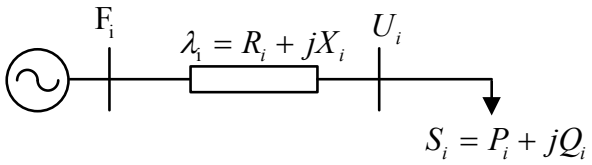

Fig. 3.2: The i[th] channel circuit

The process to map *PV* curves to the channel domain is as follows: A *PV* curve calculation procedure such as the continuation power flow is applied to the study system. At each *PV* curve point obtained by this process, the CCT is applied to calculate the channel variables corresponding to that point. The process will produce a set of data points in the channel domain. For each data point, (3.1) is used and the corresponding channel PV curves are obtained.

Two conceptual case studies are considered first to illustrate the concepts of the channel PV curves. The first case is the simple one-source three-load system shown in Fig. 2.6. As shown in the previous chapter, when Z_a=Z_b=Z_c, only channel 1 (the "zero sequence") has a voltage source. It implies that channel 1 is the only channel responsible for power transfer in this case. It suffices to analyze this pattern of power transfer (i.e. channel 1) only. Let's consider the system parameters as Z=j0.3; Z_a=Z_b=Z_c=j0.2; E =1.0. Also, the loads are considered purely active as S_a=0.3, S_b=0.25, and S_c=0.4. The corresponding physical and channel *PV* curves are shown in Fig. 3.3. One can see that there are three physical *PV* curves and only one channel PV curve. Therefore, one (channel) PV curve has captured all the characteristics of the system. It is also observed that the channel PV curve reaches its nose point when the physical PV curves reach their noise points.

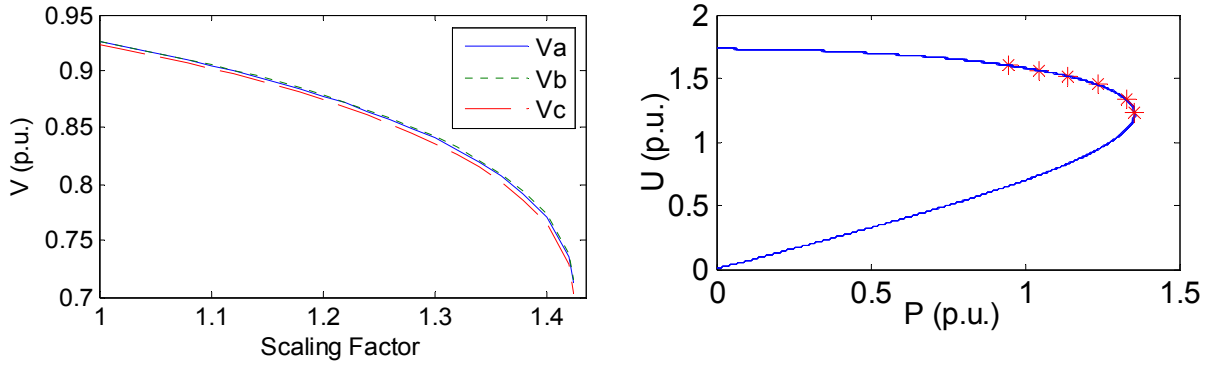

(a) PV curves of the actual system (b) Channel PV curve (Channel 1)

Fig. 3.3: PV curves for case study 1

The second case study involves the same network configuration but Z_a, Z_b, and Z_c are not equal (Z_a=0.35, Z_b=0.2, and Z_c=0.1). As shown in the previous chapter, all channels have non-zero voltage sources in this case. Therefore, all channels need to be analyzed. The channel PV curves for this case are shown in Fig. 3.4. As seen in this figure, there are three groups of channel curves. Each group corresponds to one channel as this is a three-channel system. The stars are the *PV* curve points of the actual system mapped to the channel domain. The reason that each channel has a group of curves is due to the following phenomenon. Two variables, the source voltage and the branch impedance, define the shape of a *PV* curve for a single-branch network according to (3.1). In the channel domain, the channel impedance λ is constant but the source voltage F changes with the physical voltages of the system. Each channel *PV* curve therefore corresponds to different source voltage F.

The results shown in Fig. 3.4 confirmed the observation earlier that each channel carries different amount of power. One can also notice that voltage collapse occurs when one of the channels (channel 1) reaches its maximum power transfer limit, which can be called the critical channel.

In summary, there is a critical channel among different channels of a system. The operating point of this channel goes close to its PV curve nose point when the system reaches the voltage collapse point. By analysis of the critical channel characteristics and its impact on the actual system, it is hoped that useful information about the voltage stability of the system can be extracted. This will be the main focus of the next chapter.

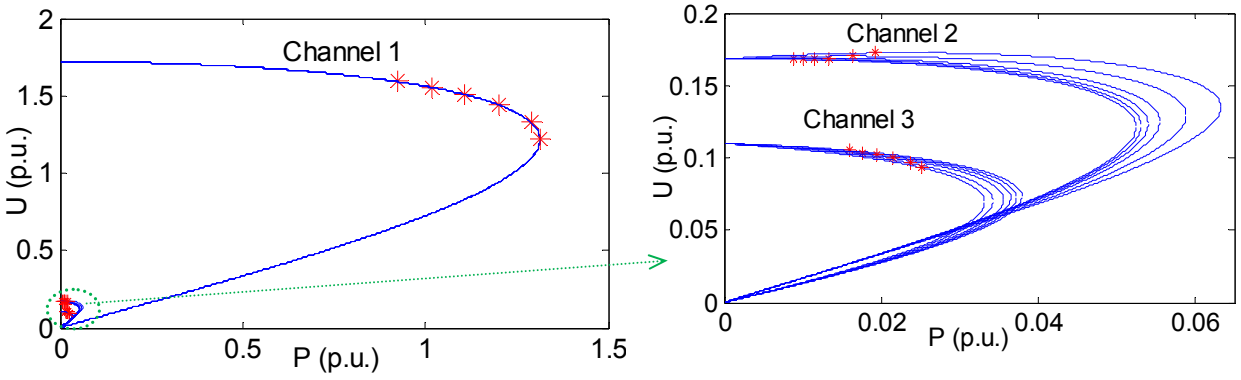

Fig. 3.4: Channel PV curves for case study 2

3.2 Channel *Pδ* Curves

Voltage stability analysis is usually performed using the *PV* curves. But it can also be examined from the *Pδ* curves, at least for the single-load system. Since industry is increasingly interested in the angle information provided by the PMUs, it is useful to examine voltage instability from the *Pδ* curve. However, there are *n×(n-1)* angle differences for a n-bus power network. It is a big challenge to examine the angle information on a *PV* curve trajectory. The CCT offers a natural solution to the problem since one can easily study the angle information in the channel domain.

Consider the i[th] channel circuit as shown in Fig. 3.2. For the sake of simplifying equation derivation, let's assume that the channel impedance is purely reactive i.e. $\lambda_i = jX_i$. The following power angle equation can therefore be developed for this channel circuit.

$$P_i = \frac{F_{eqi} U_i}{X_i} \sin \delta_i \tag{3.2}$$

Since U_i varies with P_i which is in turn varies with δ_i, (3.2) cannot be used as the Pδ relationship. However, this equation can be rewritten as follows.

$$U_i = \frac{P_i X_i}{F_i \sin \delta_i} \tag{3.3}$$

Since

$$Q_i = \frac{F_i U_i}{X_i} \cos \delta_i - \frac{U_i^2}{X_i} \tag{3.4}$$

Substituting (3.3) into (3.4) yields:

$$X_i P_i^2 - F_i^2 \sin \delta_i \cos \delta_i P_i + F_i^2 \sin^2 \delta_i Q_i = 0 \tag{3.5}$$

Dividing (3.5) by P_i yields:

$$X_i P_i - F_i^2 \sin \delta_i \cos \delta_i + F_i^2 \sin^2 \delta_i \tan \theta_i = 0 \tag{3.6}$$

where, θ_i is the power factor angle of the ith channel load and is kept constant according to the PV curve approach. P_i as a function of δ_i can be solved from the above equation as:

$$P_i = \frac{F_i^2}{X_i} \sin\delta_i \left[\cos\delta_i - \sin\delta_i \tan\theta_i\right] \tag{3.7}$$

Equation (3.7) is the analytical expression of the Pδ curve for the ith channel. Since the channel circuits are decoupled, establishing Pδ curve for each channel is straightforward. In the following, the conceptual case studies are used to illustrate the behaviours of the channel Pδ curves.

The first case is the "balanced" system shown in Fig. 2.6. As discussed before, this system has only one non-zero channel. The Pδ curve of this channel is shown in Fig. 3.5. As seen in this figure, when the actual system reaches the voltage collapse point, the channel Pδ curve reaches its maximum point. The maximum angle is about 50^o. It can be shown that for the system of Fig. 3.2 where the receiving end voltage is uncontrolled, the δ_{max} can be determined as

$$\sin\delta_{\max-i} = \sqrt{\frac{1-\sin\theta_i}{2}} \tag{3.8}$$

which is always less than 90^o due to the lack of reactive power support at the receiving end.

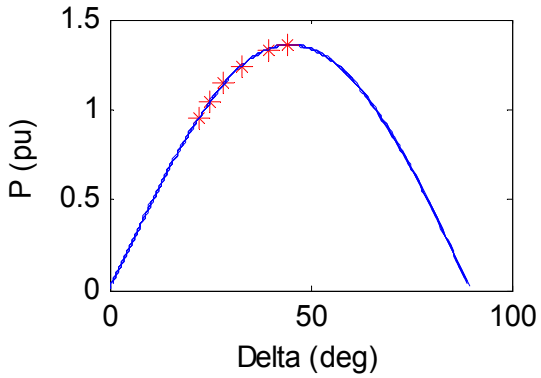

Fig. 3.5: Channel Pδ curve of for case study 1

The second case study involves the same network configuration but Z_a, Z_b, and Z_c are not equal (Z_a=0.35, Z_b=0.2, and Z_c=0.1). Fig. 3.6 shows the channel *Pδ* curves of this case study. As

seen in this figure, when the actual system reaches the voltage collapse point, the *Pδ* curve of channel 1 (critical channel) reaches its maximum point.

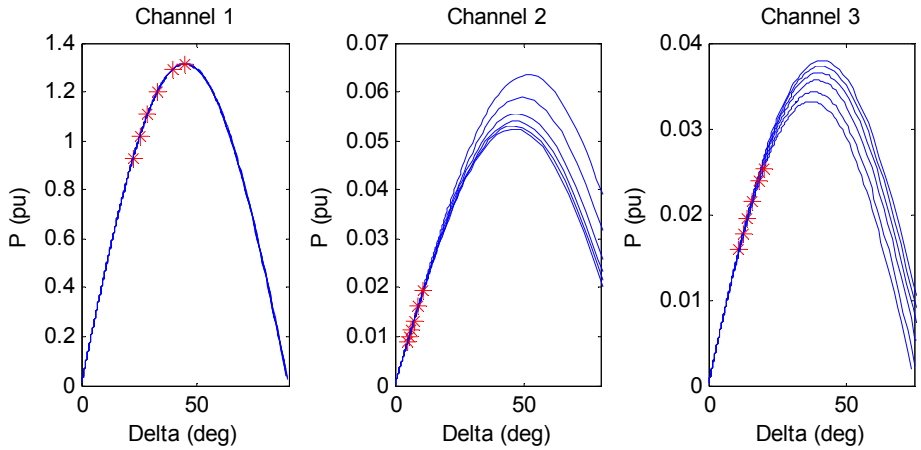

Fig. 3.6: Channel Pδ curve of for case study2

In summary, the channel *Pδ* curves can be used to interpret the voltage stability of a power system. Without the proposed transform, it is impossible to obtain any meaningful *Pδ* curves since there are many physical bus angles in an actual power system. Which bus angle differences to examine are difficult to determine.

3.3 Formal approach to PV/Pδ curve decomposition

The PV curves of many test systems have been analyzed in the channel domain. The results show that when a system is at stable conditions, the corresponding operating point in the channel domain might lie beyond the nose point of the channel *PV* curve. This situation makes it difficult to correctly identify the critical channel. Therefore, it is very important to understand the reason behind this phenomenon first and then propose a method to overcome this difficulty. Our extensive research has revealed that the phenomenon is caused by the coupling of loads in channel domain. This coupling is investigated in this sub-section.

3.3.1 Coupling Characteristics of Channel Loads

The advantage of CCT is that it can decouple the supply system into independent channel circuits. When it is applied to the loads (which are physically decoupled), however, the channel loads might become coupled. This is because the CCT is a linear transform. A load (*Z* or *S*) is a

nonlinear variable. This phenomenon can be further understood as follows: The physical loads may be modeled as constant power loads or variable impedance loads that produce the effects of constant power consumptions. Since it is easier to explain the concepts, the impedance load model is used. The physical load at various buses can be expressed as

$$Physical\ loads: \begin{bmatrix} V_1 \\ V_2 \\ \cdots \\ V_n \end{bmatrix} = \begin{bmatrix} Z_{L1} & 0 & .. & 0 \\ 0 & Z_{L2} & .. & 0 \\ .. & .. & .. & \cdots \\ 0 & 0 & .. & Z_{Ln} \end{bmatrix} \begin{bmatrix} I_1 \\ I_2 \\ \cdots \\ I_n \end{bmatrix} \tag{3.9}$$

where, Z_{Li} satisfies load's power demand constraints. In the channel domain, the loads become:

$$[V] = [Z_L][I] \Rightarrow [U] = [T][Z_L][T]^{-1}[J] \Rightarrow [U] = [Z_C][J]$$

$$\Rightarrow Channel\ loads: \begin{bmatrix} U_1 \\ U_2 \\ \cdots \\ U_n \end{bmatrix} = \begin{bmatrix} Z_{C11} & Z_{C12} & .. & Z_{C1n} \\ Z_{C21} & Z_{C22} & .. & Z_{C2n} \\ .. & .. & .. & \cdots \\ Z_{Cn1} & Z_{Cn2} & .. & Z_{Cnn} \end{bmatrix} \begin{bmatrix} J_1 \\ J_2 \\ \cdots \\ J_n \end{bmatrix} \tag{3.10}$$

It can be seen that the loads are coupled in the channel domain. This illustrates another fundamental difference between the situations encountered by the symmetrical components transform and by the proposed transform. All applications involving symmetrical components such as the short-circuit analysis deal with linear operations. For power system load flow and stability analysis, one has to deal with power that is the multiplication of voltage and current. Methods need to be developed to apply a linear transform to nonlinear problems.

For the PV curve decomposition and voltage stability analysis, the model in (3.10) can be treated as a MIMO (multiple input multiple output) system shown in Fig. 3.7 in which the channel voltages are the inputs and the channel currents are the outputs. In this approach the outputs are obtained by multiplying the input matrix in a gain matrix $[Y_C]=[Z_C]^{-1}$. In order to analyze the channel circuits separately, the channel loads should be decoupled too. In other words, the above MIMO system should be decoupled into n SISO (single input single output) systems.

The control theory states that a Relative Gain Array (RGA) can be formed for every MIMO system [67]. RGA will determine how coupled the MIMO system is. It also determines the optimal input-output variable pairings. RGA can be formed using the gain matrix $[Y_C]$ as follows.

$$RGA = [Y_C].*([Y_C]^{-1})^T \tag{3.11}$$

where (.*) indicates the element-wise multiplication.

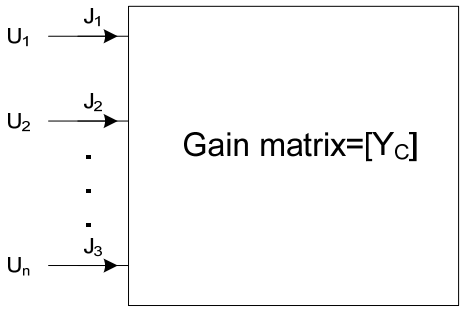

Fig. 3.7: Channel loads as a MIMO system.

As an example, the RGA for the WECC 9-bus system when it is at the normal operating condition is as follows:

$$|RGA| = \begin{bmatrix} 1.0324 & 0.0226 & 0.016 \\ 0.0226 & 1.0245 & 0.0095 \\ 0.016 & 0.0095 & 1.0228 \end{bmatrix}$$

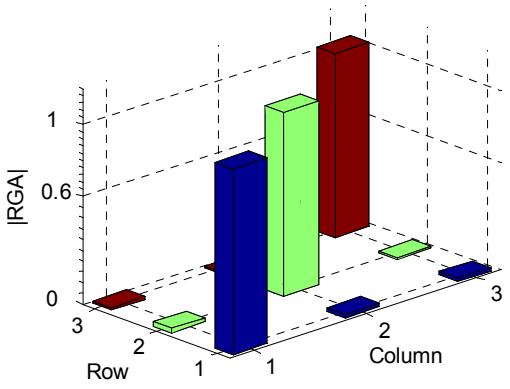

Fig. 3.8: RGA for WECC 9-bus system.

Since the diagonal elements of the RGA are much larger than the off-diagonal elements, one may conclude that the MIMO system associated with the channels loads is almost decoupled. In other words, the channel loads for this system may be expressed as the following form.

$$\begin{bmatrix} J_1 \\ J_2 \\ \dots \\ J_n \end{bmatrix} \approx \begin{bmatrix} Y_{C11} & 0 & .. & 0 \\ 0 & Y_{C22} & .. & 0 \\ .. & .. & .. & \dots \\ 0 & 0 & .. & Y_{Cnn} \end{bmatrix} \begin{bmatrix} U_1 \\ U_2 \\ \dots \\ U_n \end{bmatrix} \tag{3.12}$$

The implication is that the PV curve decomposition using the CCT works without any difficulties in this system.

The RGA has also been computed and examined for several power systems. For example, Fig. 3.9 illustrates the RGA computed for several test systems when they are at the normal operating conditions.

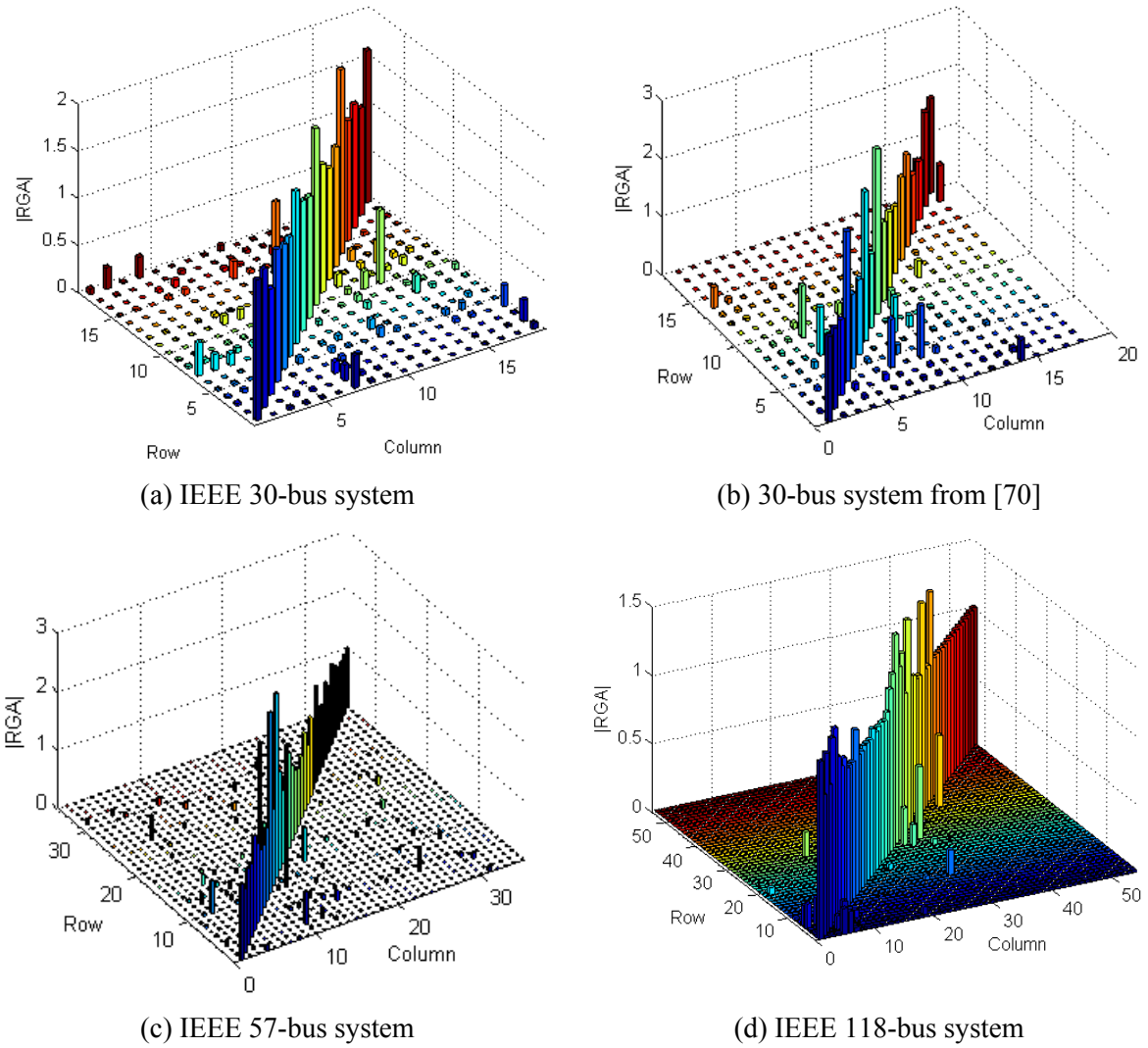

(a) IEEE 30-bus system

(b) 30-bus system from [70]

(c) IEEE 57-bus system

(d) IEEE 118-bus system

Fig. 3.9: RGA for different test systems.

As seen in Fig. 3.9, most of the channel loads are decoupled, and there are only some loose couplings among a few of them. These coupling may make the model shown in (3.12) inaccurate in some systems. Therefore, it is important to properly model these coupling so that their effects can be excluded from the channel loads. For this purpose, a method will be proposed in the next sub-section.

3.3.2 Modified Channel Circuits

Based on the investigation results of the load coupling in channel domain, a channel load representation is proposed in this subsection in order to exclude the coupling effects from the channel loads. Using this channel load representation, a simple procedure is also proposed for modifying the channel circuits based on system information at each operating condition.

As explained, the coupling of the channel loads may make the model shown in (3.12) inaccurate in some systems. In other words, there might be an approximation error (J_{Ei}) for each channel as shown below

$$\begin{bmatrix} J_{E1} \\ J_{E2} \\ \dots \\ J_{En} \end{bmatrix} = \begin{bmatrix} J_1 \\ J_2 \\ \dots \\ J_n \end{bmatrix} - \begin{bmatrix} Y_{C11} & 0 & .. & 0 \\ 0 & Y_{C22} & .. & 0 \\ .. & .. & .. & \dots \\ 0 & 0 & .. & Y_{Cnn} \end{bmatrix} \begin{bmatrix} U_1 \\ U_2 \\ \dots \\ U_n \end{bmatrix} \tag{3.13}$$

where J_{Ei} is a term in J_i which cannot be expressed as a function of U_i. In other words, J_{Ei} can be considered independent of U_i and is affected by other channel voltages, i.e. the coupling effect.

On the other hand, the channel circuits are connected as shown in Fig. 3.10. As seen in this figure, the load seen by the channel 1 circuit will contain the F and λ components associated with other channels. This indicates that the channel load can be represented by a Norton (or Thevenin) equivalent circuit shown in Fig. 3.11. More discussions on this channel load representation are provided in the Appendix A.

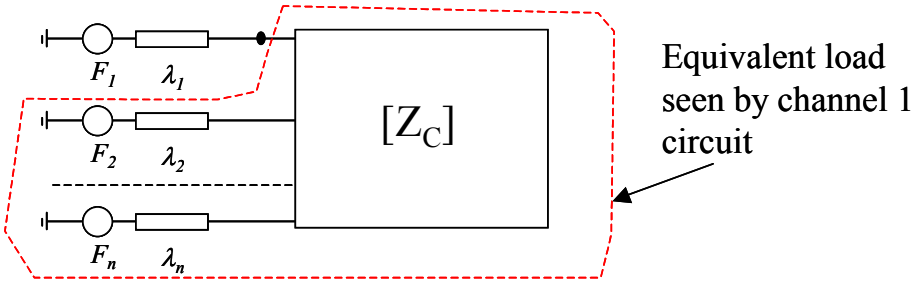

Fig. 3.10: The channel circuits.

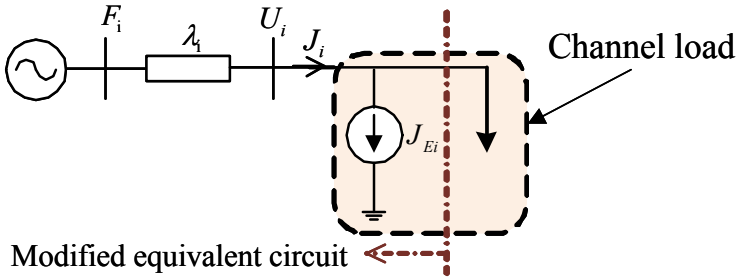

Fig. 3.11: The i[th] channel circuit with the modified load.

The current source in Fig. 3.11 is in fact the term J_{Ei} shown in (3.13). In other words, the current source for each channel can be determined from

$$J_{Ei} = J_i - Y_{Cii}U_i \tag{3.14}$$

where Y_{Cii} is the i[th] diagonal element of $[Y_C] = [Z_C]^{-1}$. In fact, the coupling has been modeled as a current source J_{Ei}. This current source representation is accurate for the operating point from which it is derived. This known current source is then merged into the supply channel circuit to form an equivalent circuit as shown in Fig. 3.12. This results in the change of the channel voltage source from F_i to $F_{eqi} = F_i - \lambda_i J_{Ei}$.

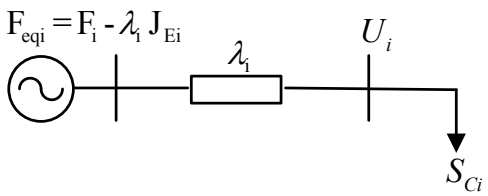

Fig. 3.12: The equivalent circuit for the ith channel.

In summary, the coupling effects have been represented as a modification to the channel voltage source F_i. This is an accurate model for the point from which the parameters are derived. It is an approximation for other points. Extensive case studies presented later have shown that this approximation works very well. In summary, the proposed method to construct the final channel circuit is as follows:

- Step 1: Calculate the load impedance for each physical bus, which is $Z_{Li}=V_i/I_i$.
- Step 2: Obtain $[Y_C]$ using (3.15). Note that the computation is minimal because no matrix inversion in needed ($[T]^{-1}$ is already available and $[Z_L]$ is a diagonal matrix).

$$[Y_C]=[Z_C]^{-1}=([T][Z_L][T]^{-1})^{-1}=[T][Z_L]^{-1}[T]^{-1} \tag{3.15}$$

- Step 3: Calculate the current source J_{Ei} for each channel according to (3.14).
- Step 4: Calculate the modified channel voltage source $F_{eqi}=F_i-\lambda_i J_{Ei}$ for each channel. The result is the equivalent channel circuit shown in Fig. 3.12.

With the above treatment, all channels are decoupled from each other. Therefore, it becomes easy to examine the *PV* curves from the channel domain. For this purpose, equation (3.16) which is the relationship between the channel voltage U_i, and channel load's power P_i+jQ_i can be applied to each of the equivalent channel circuits.

$$U_i^4+U_i^2[2(P_iR_i+Q_iX_i)-F_{eqi}^2]+|\lambda_i|^2(P_i^2+Q_i^2)=0 \tag{3.16}$$

Extensive case studies which will be presented later have shown that the proposed channel representation works very well. One of the outcomes is that whenever a physical system reaches its nose point, one of the channels will go close to its nose point as well, while no channel will pass the nose point. This channel becomes the critical channel.

3.4 Critical Channel Identification

As discussed before, among different channels of a system, there is a critical channel which can be considered responsible for the voltage collapse. The critical channel can then be used to analyze the voltage stability problem. However, before any analysis can be done, the critical channel needs to be identified. Two indices are proposed for this purpose in this subsection.

A) <u>Identification based on Channels' margins</u>

Critical channel can be identified based on the channel's margin, i.e. the critical channel is the one that has the smallest channel margin. Since each channel resembles a two-bus system as shown in Fig. 3.12, the maximum channel power can be determined analytically as follows:

$$S_{\max} = \frac{\left|F_{eqi}\right|^2 \left[\left|\lambda_i\right| - \left(X_i \sin\theta_i + R_i \cos\theta_i\right)\right]}{2\left[X_i \cos\theta_i - R_i \sin\theta_i\right]^2} \tag{3.17}$$

where θ_i is the power factor angle of the ith channel load. The channel margin can then be calculated as follows:

$$Channel\ M\arg in = \frac{S_{\max} - S_{operating}}{S_{operating}} \times 100 \tag{3.18}$$

where $S_{operating}$ is the channel load power at the current operating condition.

As an example, Fig. 3.13 illustrates the channel margins obtained at different load scaling factors in the second conceptual case study. As this figure shows, channel 1 has the lowest margin. When the system reaches its maximum loading point, the margin of channel 1 goes very close to zero. Therefore, this channel is identified as the critical channel in this system.

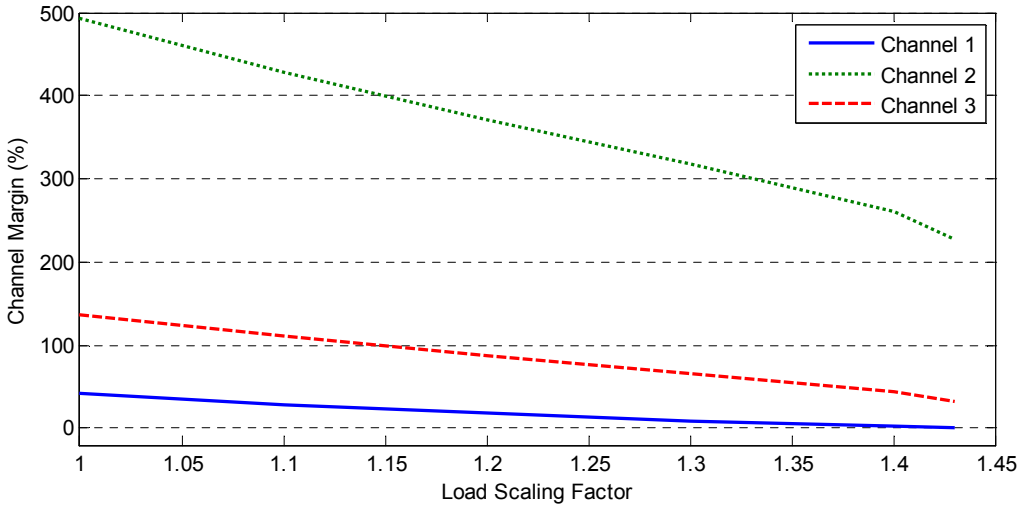

Fig. 3.13: Channel margins for case study 2

B) <u>Identification based on Normalized Voltage Drop:</u>

Consider the equivalent circuit of the i[th] channel shown in Fig. 3.12. This circuit resembles a two-bus power system. Therefore, the critical operating point of the channel can be derived from the singularity condition of the corresponding Jacobian matrix. On the other hand, if the voltage source F_{eqi} is considered as the slack bus in the two-bus system, the singularity of the Jacobian matrix can be derived from the determinant of the Jacobian matrix [68].

$$Det\, J = \frac{\partial P_i}{\partial \delta_i}\frac{\partial Q_i}{\partial U_i} - \frac{\partial P_i}{\partial U_i}\frac{\partial Q_i}{\partial \delta_i} = 0 \tag{3.19}$$

where δ_i is the phase angle difference between F_{eqi} and U_i

The above singularity condition can be expressed as the following equation which is similar to what was derived in [43] for a two-bus system.

$$U_i \cos\delta_i = \frac{F_{eqi}}{2} \quad \Rightarrow \quad \Delta U_d = \frac{F_{eqi}}{2} \tag{3.20}$$

where ΔU_d is the direct-axis component of the voltage drop $\Delta\overline{U}_i$ projected on the voltage source $\overline{F}_{eqi}$. This can be seen in Fig. 3.14 which illustrates the voltage phasor diagram of the channel.

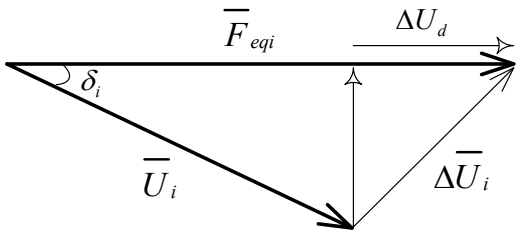

Fig. 3.14: Voltage phasor diagram of the i[th] channel

According to (3.20), the direct-axis component of the voltage drop can be used as an index to determine the stability condition of the channel. In this approach, the higher the ΔU_d is, the closer the channel operating point to the nose point is. When the channel operating point reaches the nose point of the channel PV curve, ΔU_d becomes equal to $F_{eqi}/2$.

Since the magnitudes of the channel voltage sources are quite different, a normalization process is needed so that stability levels of various channels can be compared. After extensive investigations, the following normalized voltage drop (*NVD*) index has been found adequate for critical channel identification:

$$NVD_i = \frac{|F_{eqi}| - |U_i| \cos \delta_i}{|F_{eqi}|} \times 100 \tag{3.21}$$

The normalized voltage drops are calculated for all channels. The channel which has the largest NVD is the critical channel. As an example, Fig. 3.15 shows the *NVD* results for the second conceptual case study. As seen in this figure, channel 1 has the largest *NVD* and is therefore the critical channel.

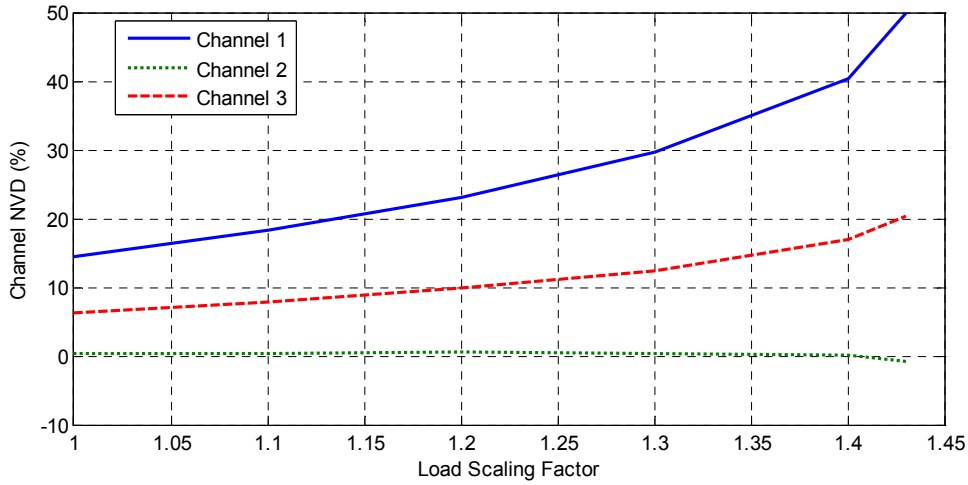

Fig. 3.15: Channel *NVD* for case study 2

3.5 Procedure of the CCT-based Voltage Stability Analysis

The CCT-based (off-line) voltage stability analysis technique is summarized in the flowchart of Fig. 3.16. As this figure shows, the transformation matrix [*T*] and the channel impedances [Λ] are first calculated based on the network admittance matrix. These parameters will remain constant unless the network impedance or topology is changed (which includes generators reaching Q limits). The *PV* curve calculation procedure (which can be the conventional *PV* curve method or the continuation power flow method) is then applied to the system. At each *PV* curve

point, the CCT is applied to calculate the channel variables and circuits corresponding to that point. The channel margins will be determined as well. The critical channel is then identified. The generation of channel *PV/Pδ* curves are optional because channel margins are sufficient for the critical channel identifications. Based on the critical channel, different aspects of voltage stability problem can be analyzed. For example, the critical load, critical generator, and critical branch can be identified. Methods will be proposed for these tasks in the next chapter.

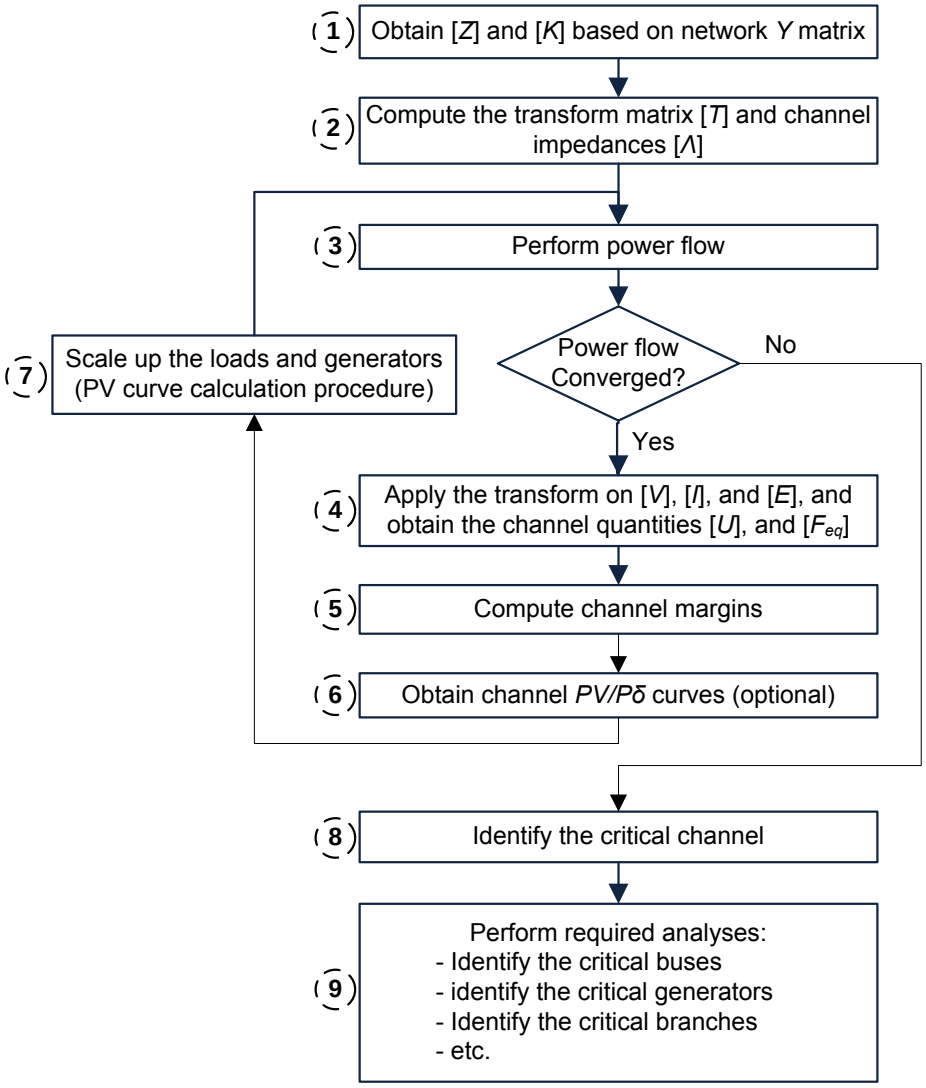

Fig. 3.16: Procedure of the CCT-based voltage stability analysis

It can be seen that the proposed algorithms can be considered as a diagnostic tool for the *PV* curves. It uses *PV* curve results to extract more useful information about the system. This procedure is similar to that used by the Jacobian matrix modal analysis technique of [12].

If one of the generators' reactive power limits is reached at a *PV* curve point, that generator shall be represented as a constant excitation voltage behind its synchronous impedance. The terminal of the excitation voltage becomes a new (*PV*) bus. Thus the network topology is changed. The network *Z* matrix and CCT transform need to be recalculated accordingly.

3.6 Case Study Results

Several standard test systems are considered in this section as case studies. The presented procedure is applied to these cases, and the voltage stability characteristics of channels are investigated.

- **WECC 9-bus system**

The first case study is the WECC 9-bus system. This system has 3 load buses, and as a result, there are three channels in this system. Fig. 3.17(a) shows the channel *NVD*s for different load scaling factors. As this figure shows, channel 1 has the highest *NVD*, and therefore, this channel is the critical channel. The same result is obtained from the channel margins shown in Fig. 3.17(b). Channel 1 has the lowest margin, so this is the critical channel. The channel Pδ, and PV curves are shown in Fig. 3.18(a), and Fig. 3.18(b), respectively. These figures verify that channel 1 is indeed the critical channel. In both the Pδ and PV curves of this channel, the operating point goes close to the curve nose point when the actual system goes close to the maximum loading point.

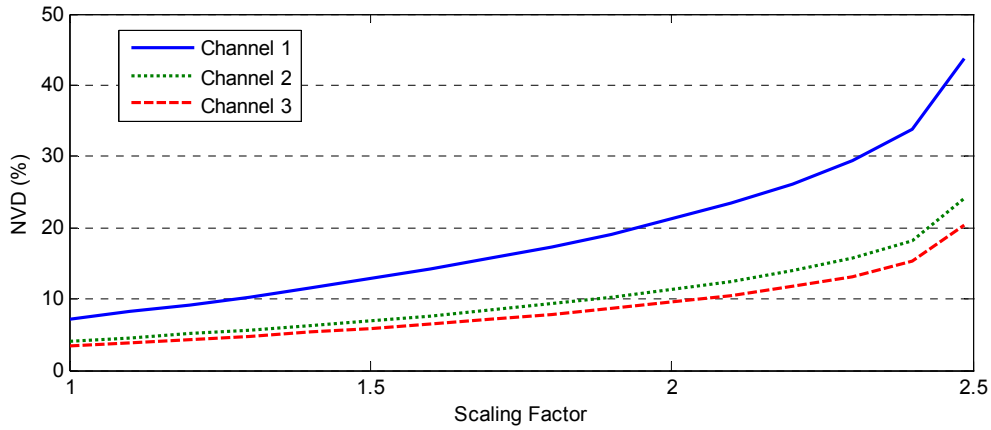

(a) channel *NVD*s

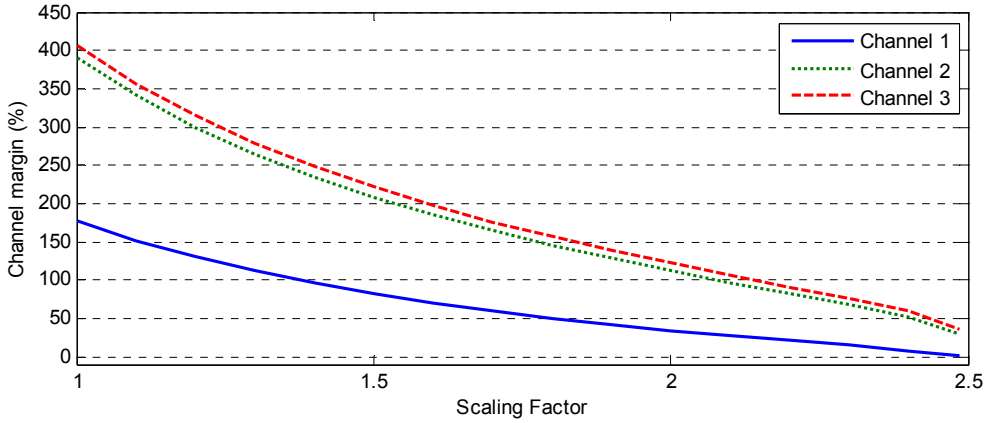

(b) channel margins

Fig. 3.17: Channels' margins and *NVD*s in WECC 9-bus system

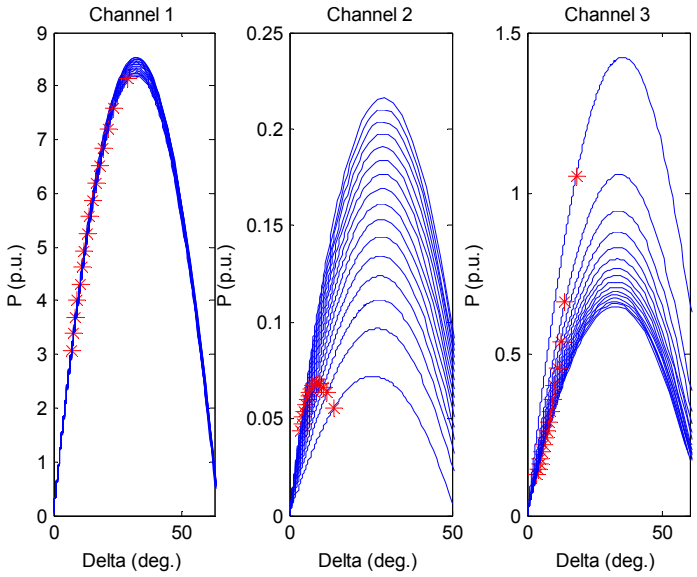

(a) channel Pδ curves

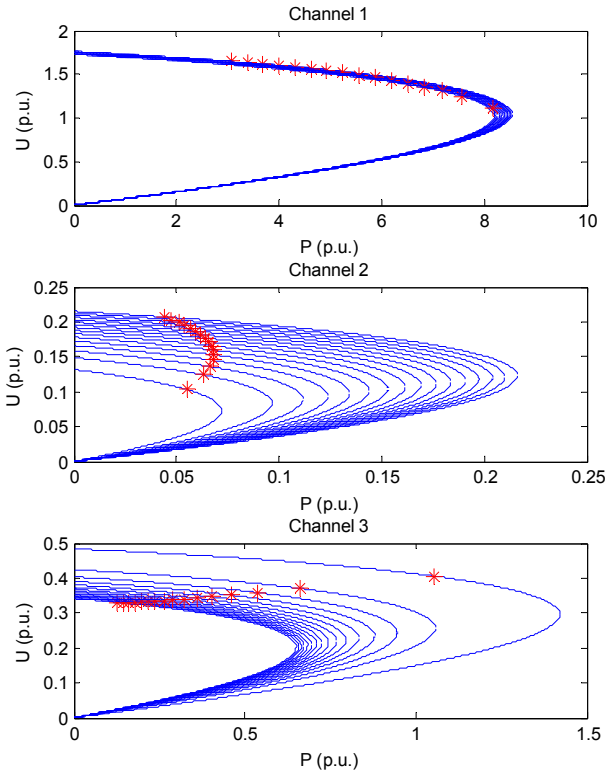

(b) channel PV curves

Fig. 3.18: Channel Pδ and PV curves for WECC 9-bus system

- **30-bus system**

The second case study is the 30-bus system from [70]. Fig. 3.19 illustrates the channel NVDs and margins of this system. As both of these figures reveal, channel 4 is the critical channel in this system. Moreover, Fig. 3.20 shows the channel Pδ and PV curves. Note that to save space, only the first 6 top rank channels are shown in this figure.

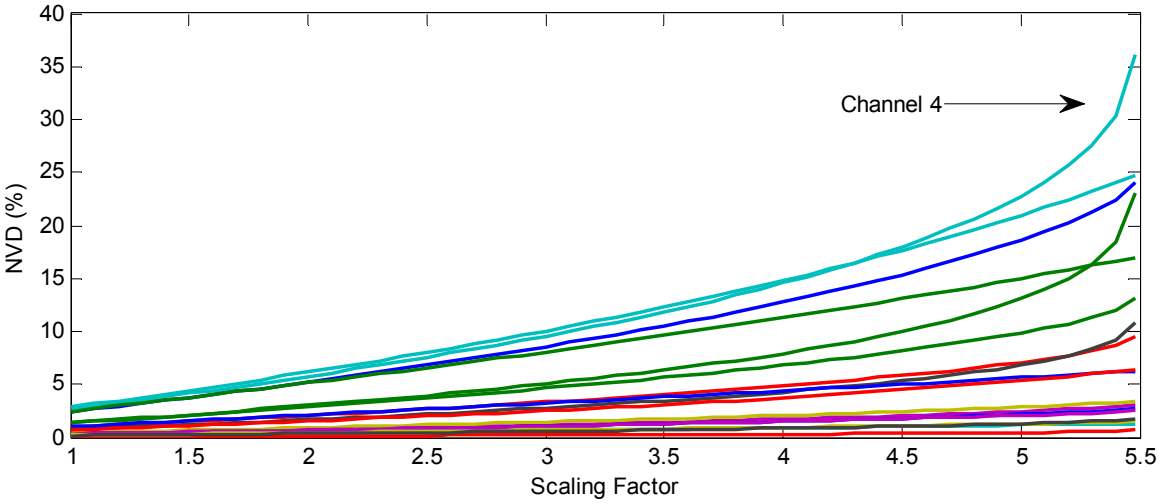

(a) channel *NVD*s

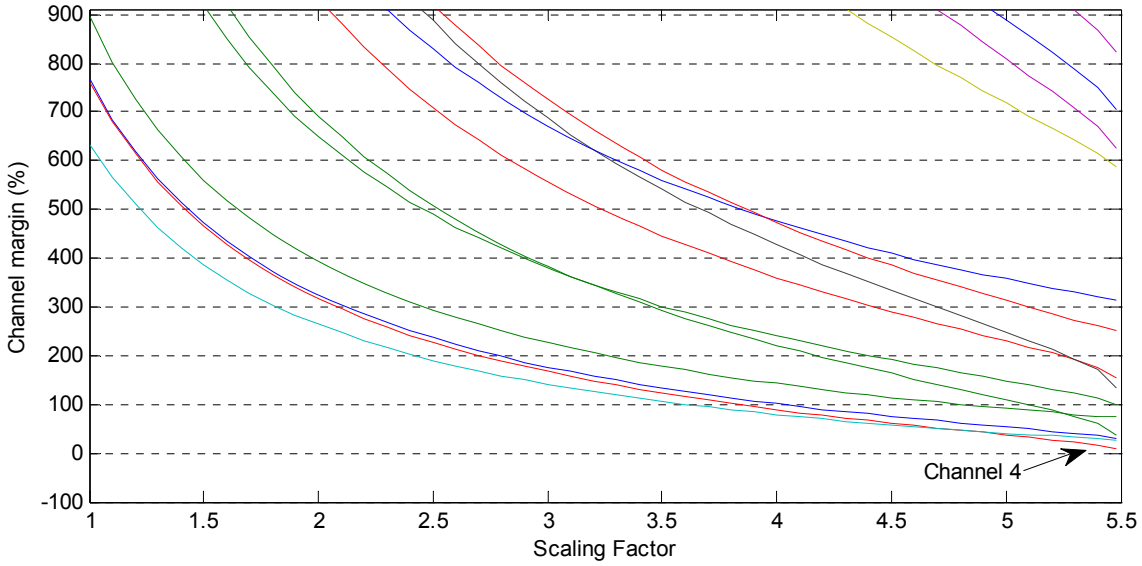

(b) channel margins

Fig. 3.19: Channels' margins and *NVD*s in the 30-bus system

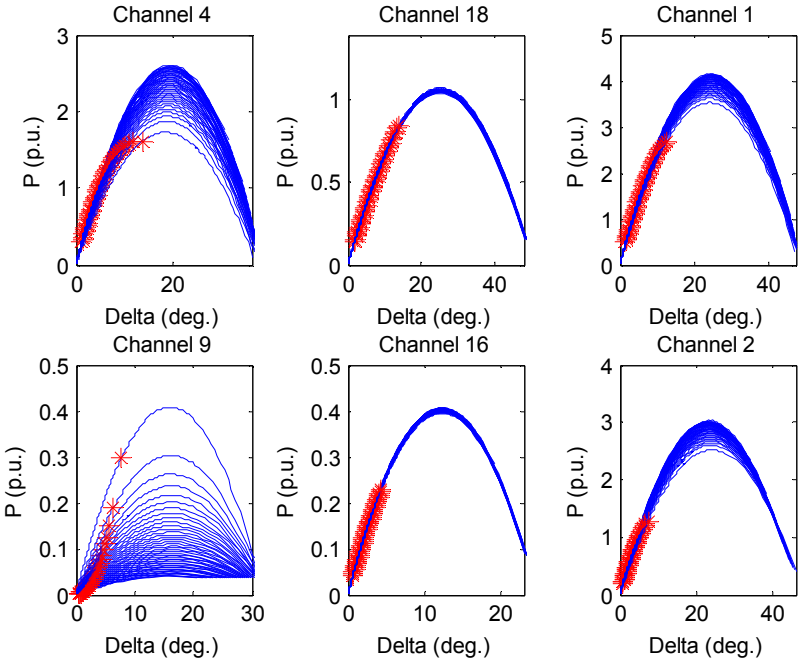

(a) channel Pδ curves of six top rank channels

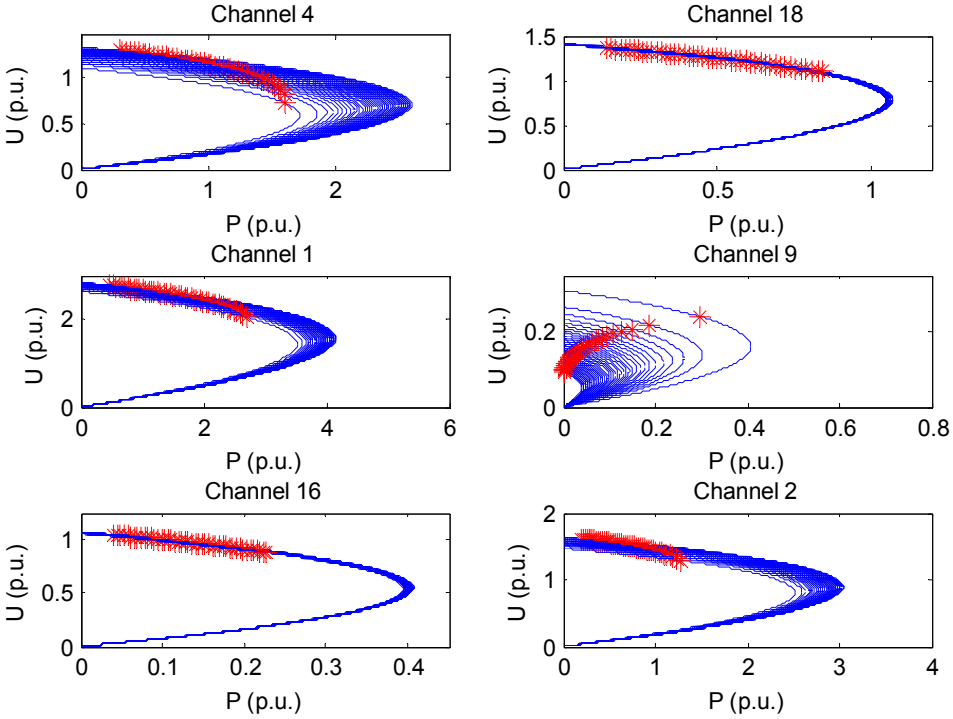

(b) channel PV curves of six top rank channels

Fig. 3.20: Top channel Pδ and PV curves for the 30-bus system

- **IEEE 30-bus system**

Fig. 3.21(a), and Fig. 3.21(b) show the channel NVDs and channel margins, respectively. As these figures indicate, channel 1 is the critical channel in this system. This can be confirmed according to Fig. 3.22 which illustrate the channel Pδ and PV curves of the top rank channels. As seen in these figures, when the actual system reaches its nose point, the operating point in channel 1 goes close to its Pδ/PV curve nose point.

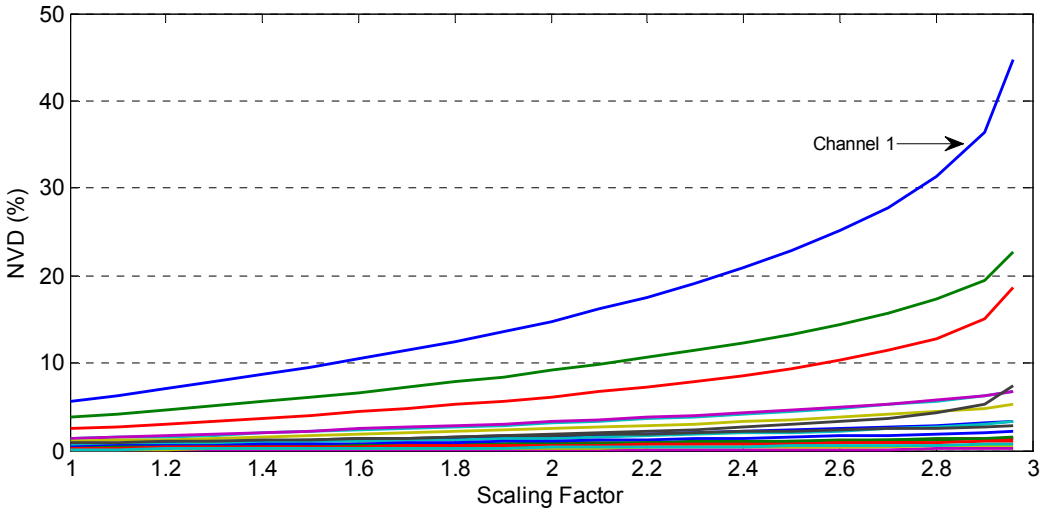

(a) channel *NVD*s

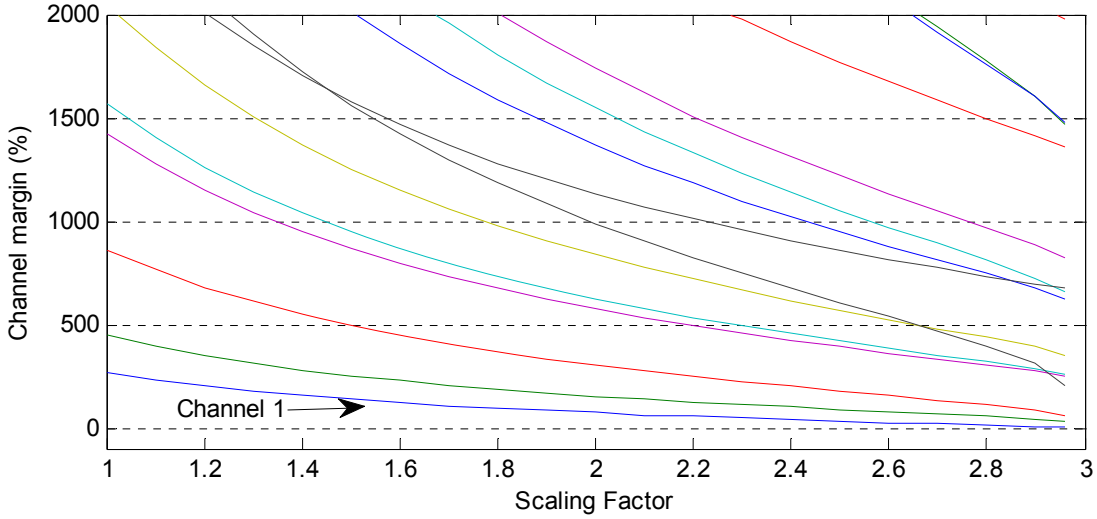

(b) channel margins

Fig. 3.21: Channels' margins and *NVD*s in IEEE 30-bus system

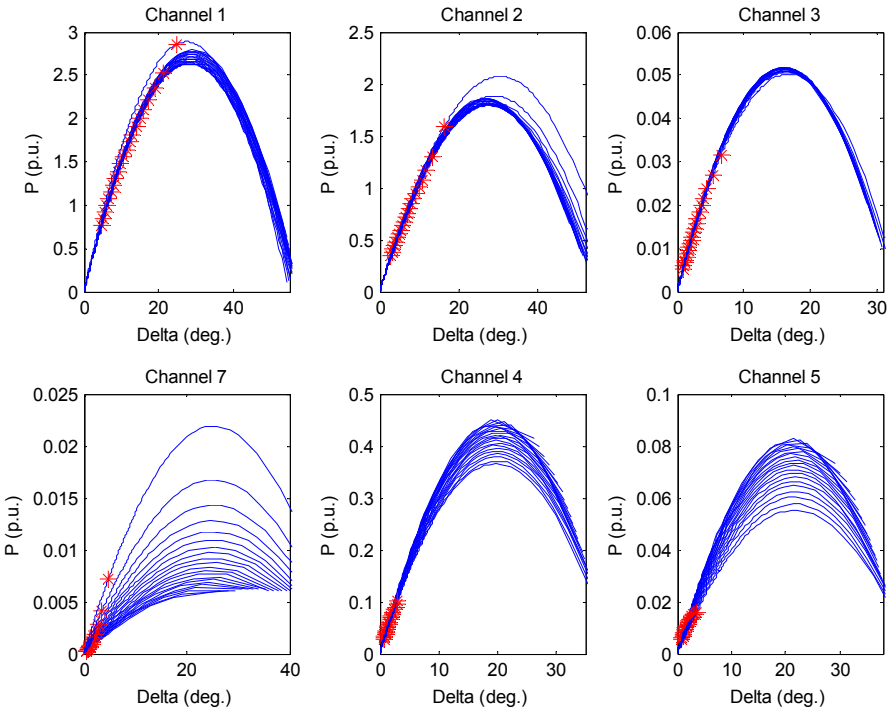

(a) channel Pδ curves of six top rank channels

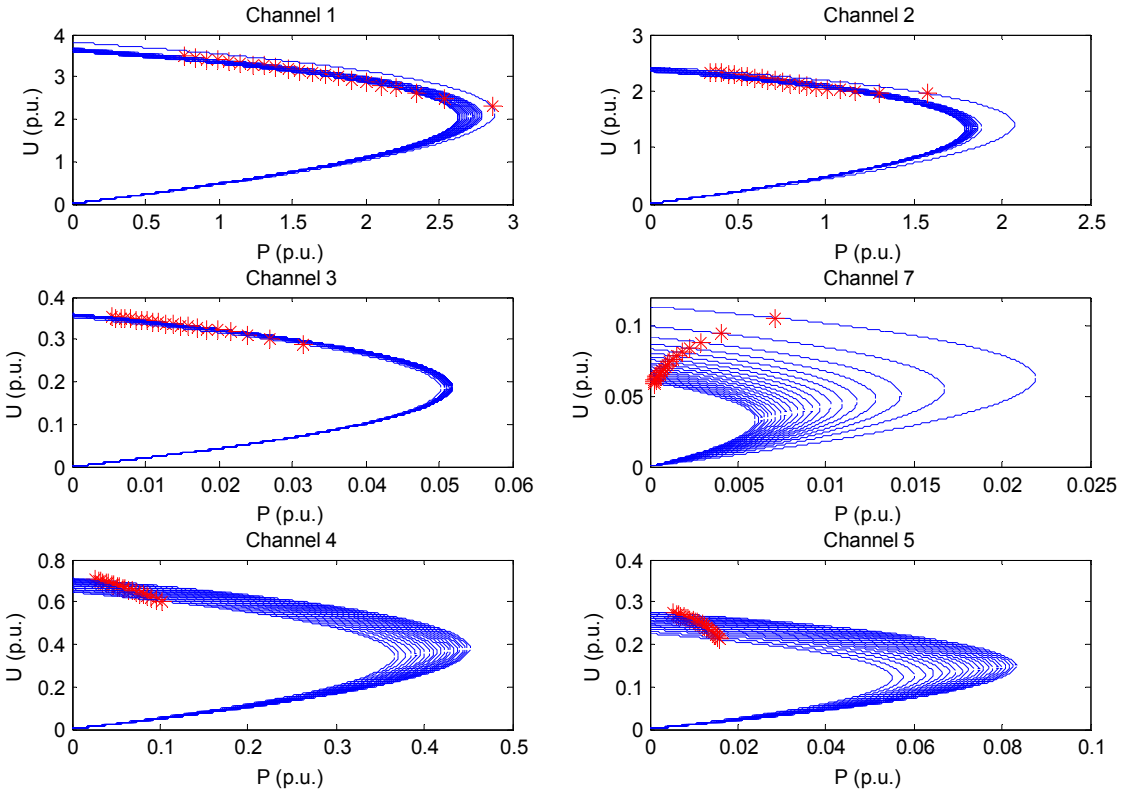

(b) channel PV curves of six top rank channels

Fig. 3.22: Channel Pδ and PV curves for IEEE 30-bus system

- **IEEE 57-bus system**

The simulation results for the IEEE 57-bus system are shown in the following figures. According to Fig. 3.23, channel 1 is the critical channel in this system. The top ranked channel Pδ and PV curves are also shown in Fig. 3.24. This figure verifies that channel 1 is the most critical channel in this system.

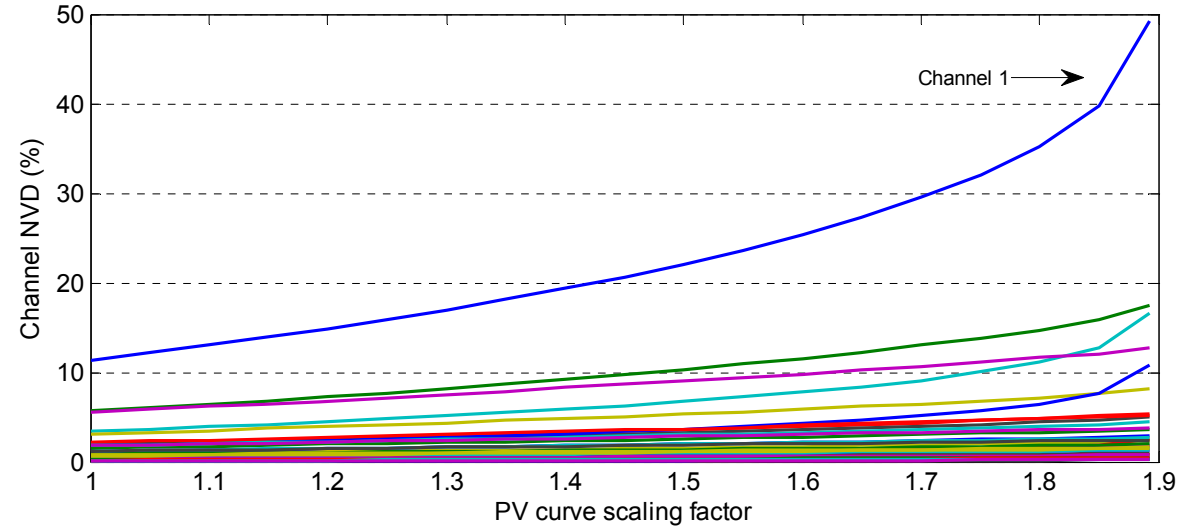

(a) channel *NVD*s

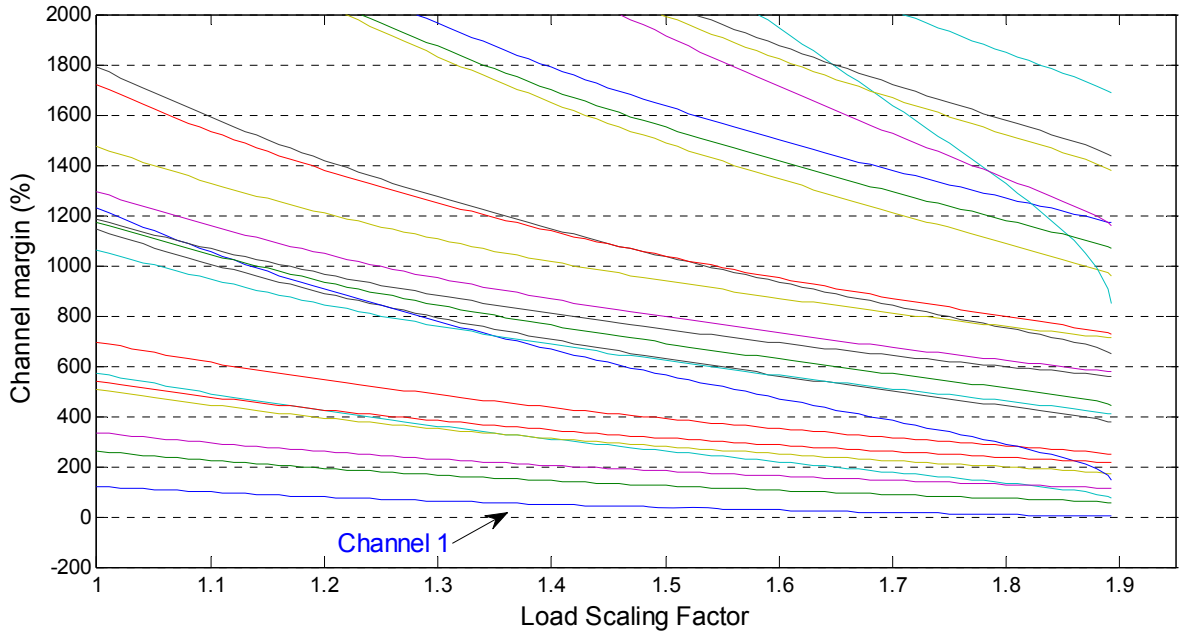

(b) channel margins

Fig. 3.23: Channels' margins and *NVD*s in IEEE 57-bus system

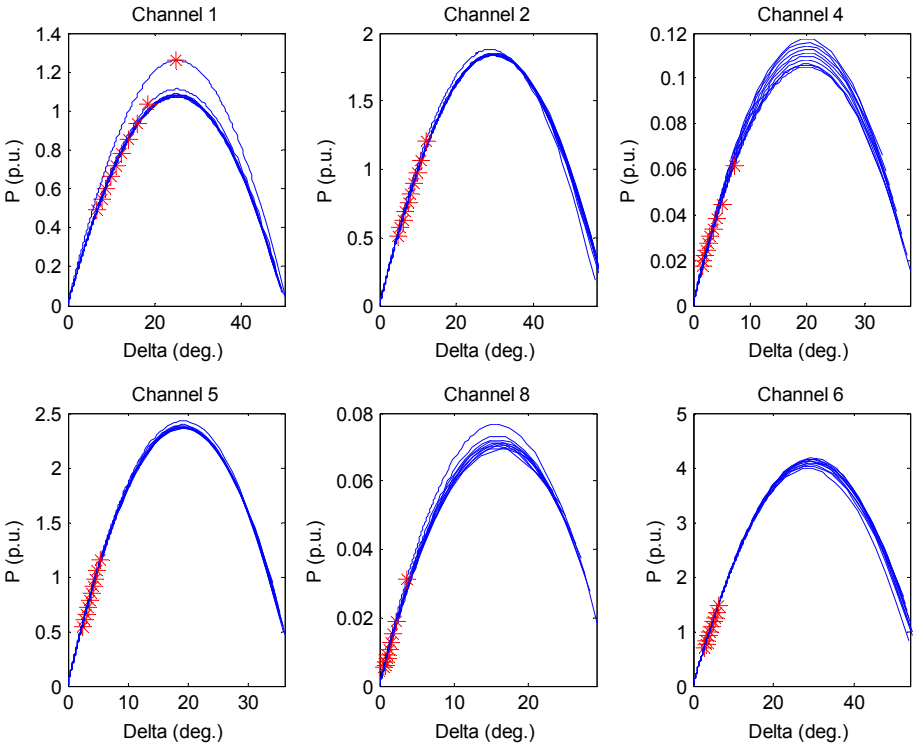

(a) channel Pδ curves of six top rank channels

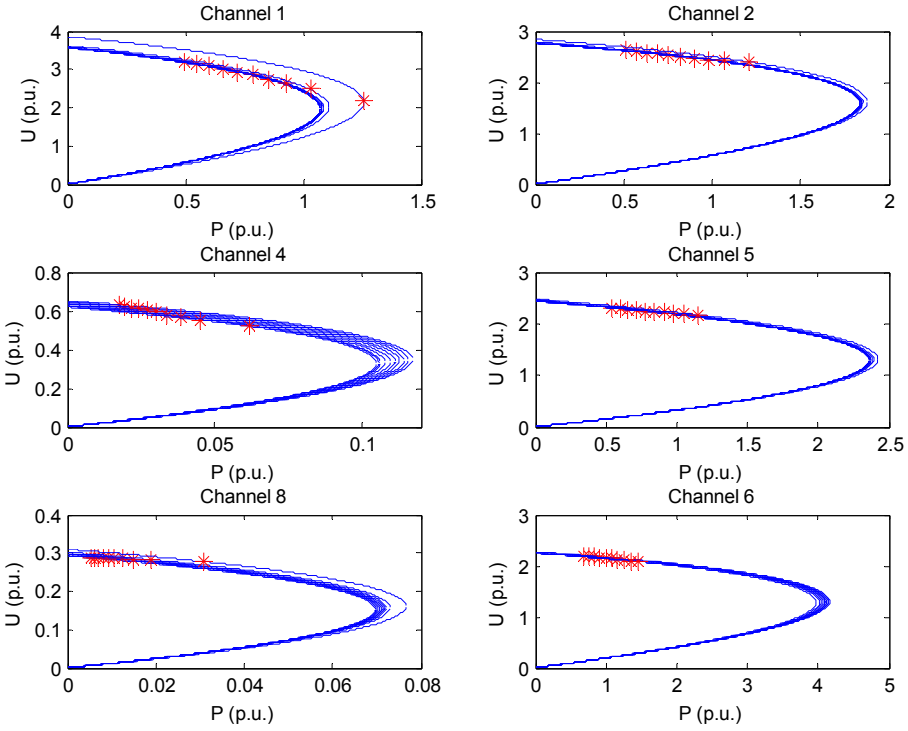

(b) channel PV curves of six top rank channels

Fig. 3.24: Top channel Pδ and PV curves for IEEE 57-bus system

3.7 Conclusions

The aim of this chapter was to establish a framework to interpret and analyze the voltage stability of complex power systems from the channel domain. For this purpose, first of all, the concepts of channel Pδ and PV curves were introduced in this chapter. It was shown that the actual Pδ/PV curves of a complex power network could be decomposed into channel Pδ/PV curves. This is a promising feature since the channel Pδ/PV curves can be easily derived from the channel circuits even in online applications.

This chapter has also shown that channel PV curves could be used instead of actual PV curves for voltage stability analysis and monitoring. This was done by evaluating the criticality of each channel in that domain and finding the critical channel which is most responsible for the voltage collapse. The implication is that for monitoring and analyzing the voltage stability, one may only need to monitor and analyze the critical channel. Moreover, it was shown that the channel $P\delta$ curves can be used to interpret the voltage stability of a power system. Without the proposed transform, it is impossible to obtain any meaningful $P\delta$ curves since there are many physical bus angles in an actual power system.

The characteristics of channel loads have been fully investigated in this chapter. It has been found out that the loads are coupled in the channel domain. The degree of coupling has been investigated using the Relative Gain Array theory which is a well accepted theory in the control society. The results have shown that although most of the channel loads are decoupled, there are some loose couplings among a few of them. These loose couplings, however, make some difficulties in the PV/ $P\delta$ curve decomposition using the channel components transform. These studies have, therefore, indicated that the couplings should be properly modeled in order to improve the performance of the CCT. Motivated by these studies, a channel load representation has been proposed. In the proposed representation, the coupling effects are excluded from the channel loads and represented as current sources. According to this channel load representation, a simple procedure has then been proposed for modifying the channel circuits based on system information at each operating condition.

Two methods were presented in this chapter to identify the critical channel. These methods are based on the channels' stability margins, and channels' normalized voltage drops. A procedure has been proposed for the voltage stability analysis using the CCT. Finally, extensive case studies have been presented to clarify and verify the concepts proposed in this chapter.

Chapter 4: Methods for Voltage Stability Analysis Using CCT

In the previous chapter, a framework was proposed for the interpretation of voltage stability in the channel domain. Using the proposed framework, a complex power system is transformed into channel components. The voltage stability is assessed from the channel domain using channel PV/Pδ curves. The critical channel which is responsible for the voltage collapse is then identified. The aim of this chapter is to show how the proposed framework can be used to analyze the voltage stability characteristics of an actual system. The basic idea is to consider the critical channel and extract important information about the actual system by analyzing this channel. The information to be extracted mainly includes:

- Identification of the critical locations (buses) which are more prone to voltage instability
- Identification of the critical generators which have the highest impacts on voltage stability.
- Identification of the weak branches which more limit the stability of the system

Details of the proposed methods are presented in this chapter. Several standard test systems are also analyzed in order to verify the performances of the proposed methods.

4.1 Identification of the Critical Bus

One of the most important issues related to the voltage stability problem is to identify which location (bus) in the system is the most prone to voltage collapse. This bus is called the critical bus. Identification of the critical bus can be very useful since it is usually the best location to apply corrective actions such as the load shedding. The aim of this section is to use the CCT and develop a method that can identify the critical bus and can be easily used in online applications. The proposed method is verified with extensive case studies. It is also compared to the Jacobian matrix (JM) modal analysis which is a well accepted method in the field.

4.1.1 The proposed method

Once the critical channel is known, one can use the information to identify the critical bus. The method proposed for this task is as follows. Since the low stability margin of the critical channel corresponds to its large channel voltage drop, one can therefore infer that the critical load bus is the one that is the most responsible for the voltage drop of the critical channel. Since the channel voltage drop is caused by the channel current, the contribution of bus currents I to the critical channel current J_i can be used to rank the contribution of different buses to the channel voltage drop. The critical channel current J_i is as follows:

$$J_i = T_{i1} I_1 + T_{i2} I_2 + \ldots + T_{iN} I_N \tag{4.1}$$

According to (4.1), the following contribution index is proposed:

$$Cont_{ik} = \frac{\left| T_{ik} I_k \right| \cos(\alpha_{ik})}{\left| J_i \right|} \tag{4.2}$$

where $Cont_{ik}$ is the contribution of load bus k to the channel current J_i and α_{ik} is the angle difference between the channel current J_i and the term $T_{ik}I_k$.

To determine the critical bus, the contributions of all load bus currents to the critical channel current are calculated using (4.2) and are compared. The bus whose current has the highest contribution to the critical channel current is the critical bus.

4.1.2 Verification methods

In order to evaluate the validity of the proposed critical bus identification method, two verification methods are used.

- *Modal analysis method:* This method, which is based on eigenvalue analysis of the system Jacobian matrix, is the most popular and accepted method for bus ranking. The details of this method can be found in [12].

- *Sensitivity-based method:* The method is based on the sensitivity of the loadability margin with respect to load shedding at different load buses. In this method, a very

small portion of each load (say 1%) is shed and the resulting increase in the loadability margin is calculated using Continuation Power Flow (CPF). Load buses are then ranked according to their associated increases in the margin. This method is similar to the one used in [71].

4.1.3 Case study results

Several standard test systems are considered as the case studies. The proposed bus ranking method is applied to these systems, and the results are compared with those of the verification methods.

- **<u>WECC 9-bus system:</u>**

Fig. 4.1(a)-(c) show the load bus ranking results obtained for this system. According to these figures, the critical bus identified by the proposed method is exactly the same as both of the verifications methods.

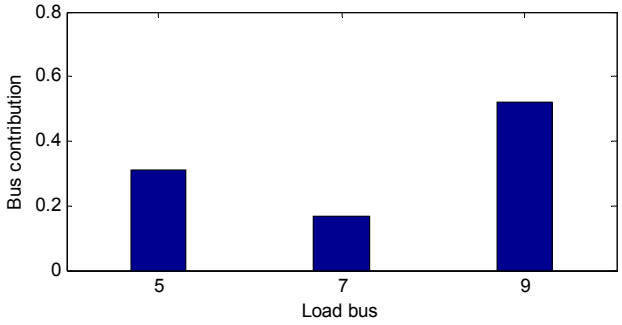

(a) using the CCT-based index

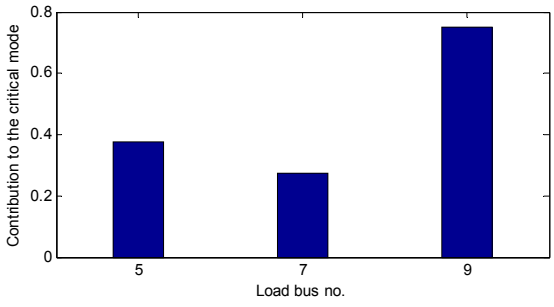

(b) using modal analysis method

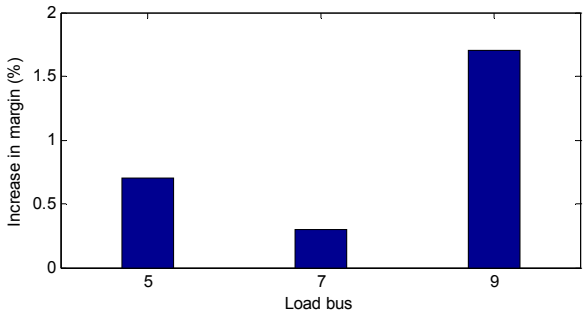

(c) using the sensitivity of loadability margin

Fig. 4.1: Bus ranking for WECC 9-bus system.

- **The 30-bus system:**

Fig. 4.2 shows the results obtained for the 30-bus system. As these figures reveal, the critical load bus is the same in all the methods.

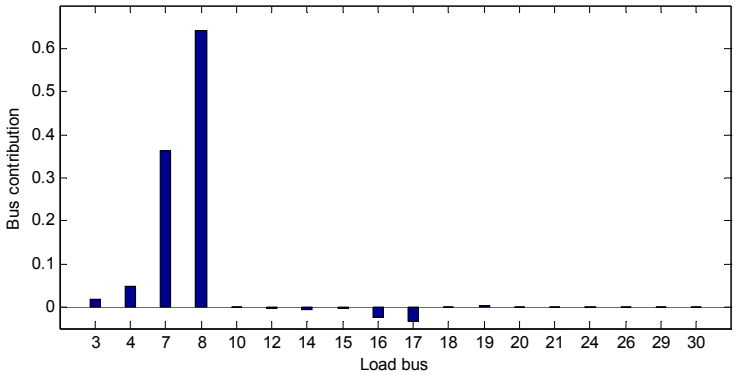

(b) using the CCT-based index

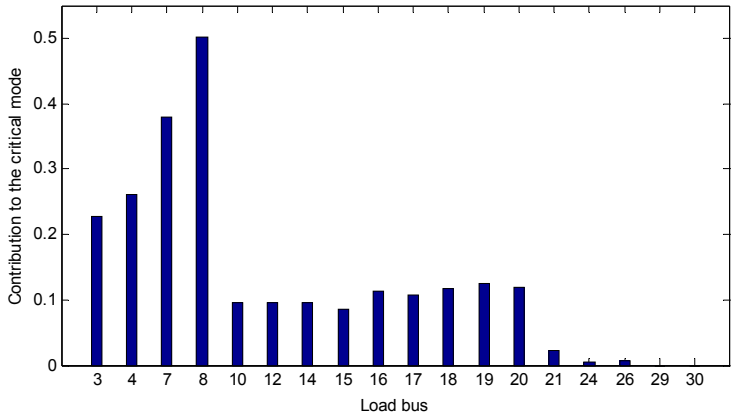

(b) using modal analysis method

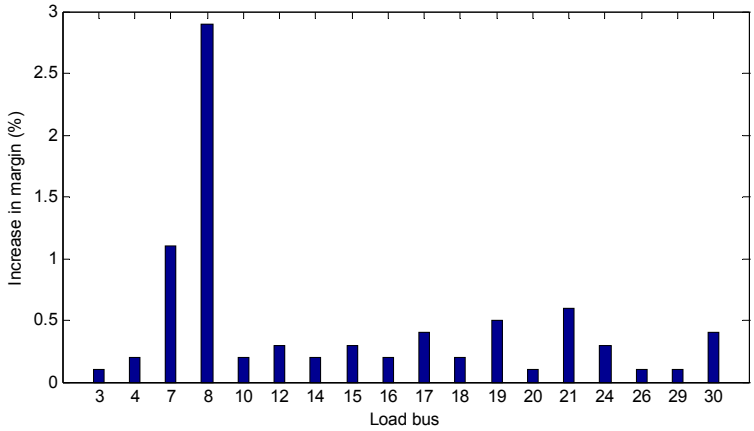

(c) using the sensitivity of loadability margin

Fig. 4.2: Bus ranking for the 30-bus system.

- **IEEE 30-bus system:**

The results obtained for this system are illustrated in Fig. 4.3. It can be seen in this figure that both of the verification methods verify the critical bus identified by the proposed method.

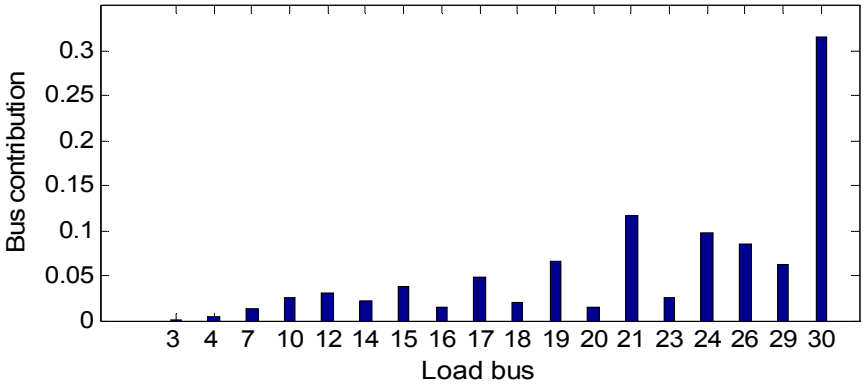

(c) using the CCT-based index

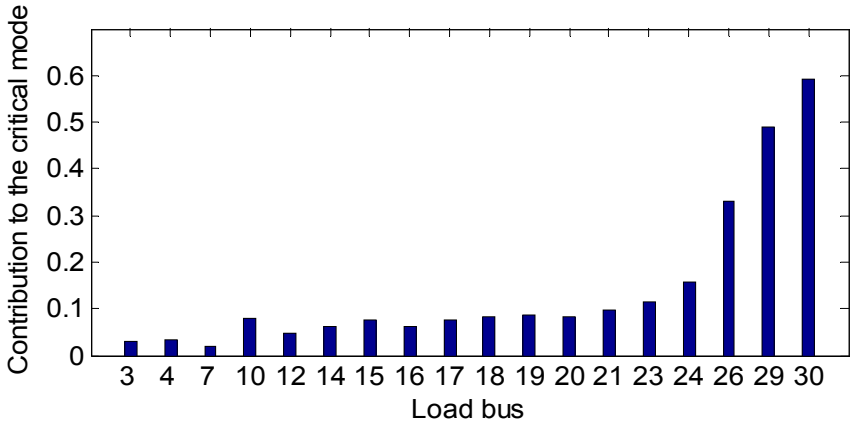

(b) using modal analysis method

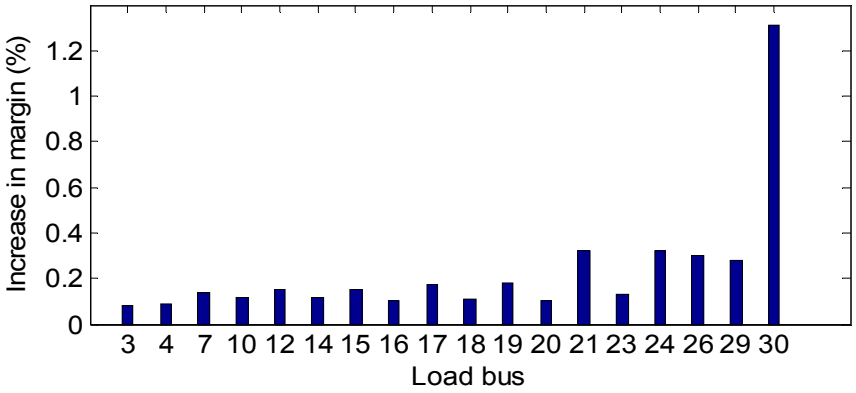

(c) using the sensitivity of loadability margin

Fig. 4.3: Bus ranking for IEEE 30-bus system.

- **IEEE 57-bus system:**

The results obtained for this system are illustrated in Fig. 4.4. According to this figure, both of the verification methods verify the critical bus identified by the proposed method.

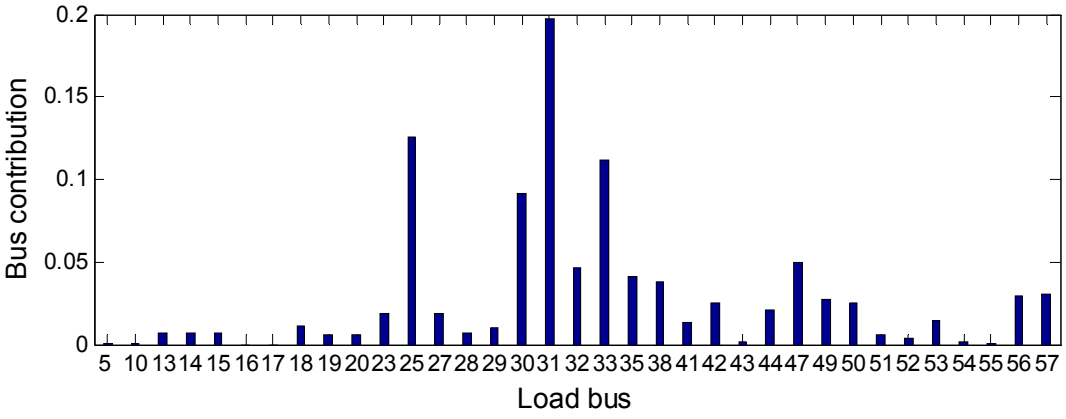

(a) using the CCT-based index

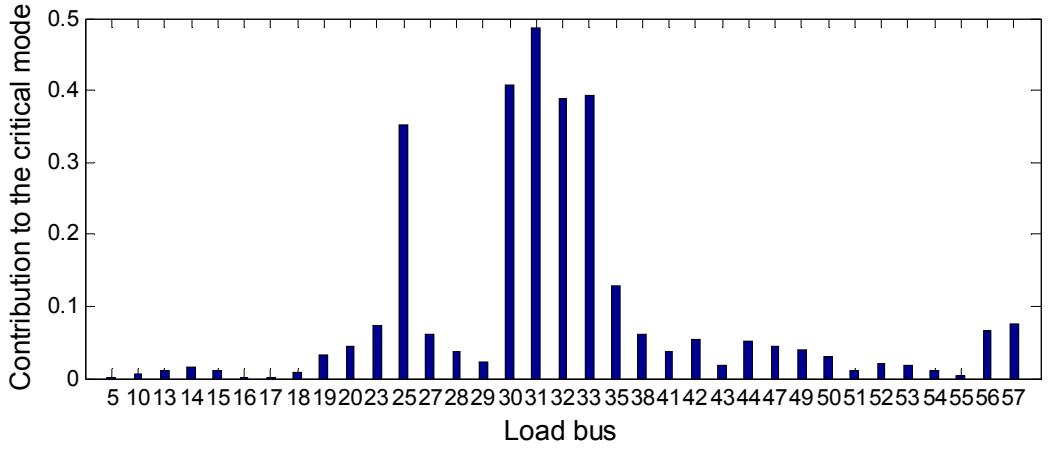

(b) using modal analysis method

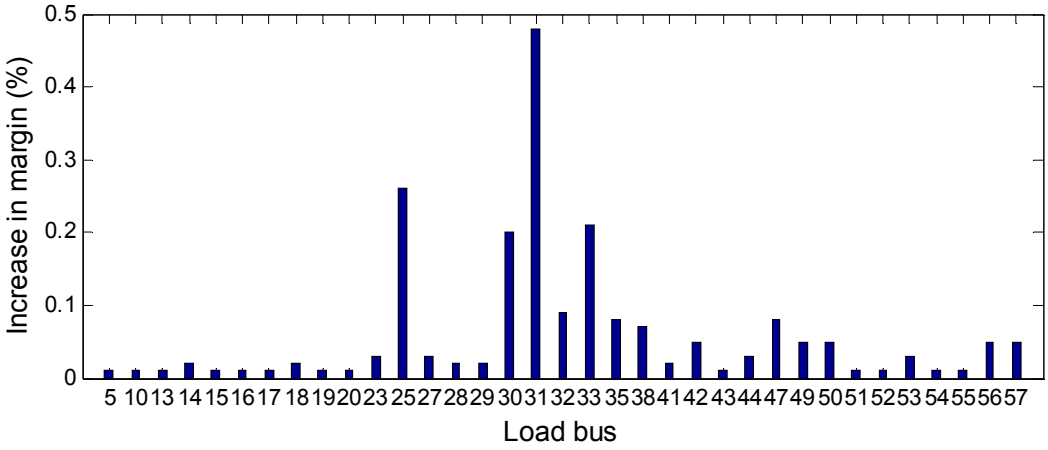

(c) using the sensitivity of loadability margin

Fig. 4.4: Bus ranking for IEEE 57-bus system.

The above case studies are summarized in Table 4.1. This table clearly indicates that the proposed method is accurate and reliable for the critical load identification.

Table 4.1: Summary of the results for critical bus identification

System	Top ranked critical load buses		
	Proposed method	JM modal analysis method	Sensitivity-based method
WECC 9-bus	9, 5, 7	9, 5, 7	9, 5, 7
30-bus from [70]	8, 7, 4, 3	8, 7, 4, 3	8, 7, 21, 19
IEEE 30-bus	30, 21, 24, 26	30, 29, 26, 24	30, 21, 24, 26
IEEE 57-bus	31, 25, 33, 30	31, 30, 33, 32	31, 25, 33, 30

4.1.4 Comparison with Jacobian Modal Analysis Method

For the critical bus identification, the application procedure of CCT technique is quite similar to that of the Jacobian matrix modal analysis (JM) technique [12]. It is therefore useful to compare the two techniques.

1) *Physical meaning:* the channel components and circuits have clear physical meanings and models. It is therefore easy to interpret the results in channel domain and extract useful information. The JM method, on the other hand, is just a numerical technique. There is no circuit model for the modal results. A domain to map and simplify the *PV* curves does not exist. The $P\delta$ curves are out of reach for the JM method.

2) *Computing effort:* If the network impedance matrix remains the same, the CCT eigen-decomposition only needs to be performed once. The whole *PV* curves can be mapped into the channel domain with little computing effort. Online implementation is straightforward. The movement of modes can thus be traced easily. The JM method needs to execute eigen-decomposition at every *PV* curve point if one wants to track the mode changes. Furthermore, a complex, yet-to-be developed mode-trace (i.e. root-locus plotting) technique is needed to relate one eigenvalue obtained at a *PV* curve point to another eigenvalue obtained at the next *PV* curve point.

3) Robustness: A significant problem that has not been solved for the JM method is which matrix, the reduced Jacobian matrix or the full Jacobian matrix, shall be used for the eigen-analysis. In theory, the full Jacobian matrix shall be used. But case studies have shown that the full Jacobian matrix yields different ΔQ bus rankings compared to those derived from the reduced Jacobian matrix. Furthermore, the full Jacobian matrix yields two bus ranking lists, one corresponding to ΔP and one for ΔQ. These two lists are different, which creates additional ambiguity in bus ranking. The CCT method does not have this problem. It includes the impact of both active and reactive power in the form of channel margin. Another practical issue is the difficulty to identify the critical mode correctly using the JM method since the index to rank modes is the magnitudes of eigenvalues. Because the *PV* curve technique cannot reach the exact nose point where λ=0, the mode ranking can only be done at a *PV* curve point close to the nose point (the continuation power flow will help to zero in the nose point but numerical differences can still exist). As a result, numerical errors and the existence of multiple small eigenvalues can mask the critical mode.

4.2 Identification of the Critical Generator

Generators, through their reactive power support to power system voltages, have a significant impact on the voltage stability of a power system. Utility planners and operators have a strong desire to know the most important generators, called the critical generators, for a given voltage instability scenario or when voltage stability margins become too small. This need was first recognized in [12] where the Jacobian matrix based modal analysis technique was used to identify the critical load points. Since the reduced Jacobian matrix used by [12] provides no reactive power information for generators, empirical indices are proposed for generator ranking [87]. In order to establish a theoretical basis for generator ranking, some references such as [17] propose to use the active power information contained in the reduced Jacobian matrix to determine the active (power) participation factors (APF) of the generators. As a result, the generators are ranked in terms of their active power impacts on voltage stability. However, APF may fail to act as a proper index since voltage stability is usually associated with the reactive power limitations. In other words, ranking the generators based on the impacts of their reactive powers on voltage stability would be very beneficial. This section will show that the CCT can be used to develop a new and effective method to do so.

4.2.1 The proposed method

Similar to the critical load identification, critical channel can be used to identify the critical generator. For this purpose, generators' contributions to the critical channel are determined first. Then, the generator which has the highest contribution to the critical channel will be the critical generator which has the highest impact on the voltage collapse.

The channel voltage sources can be written in terms of the generators' voltages as follows.

$$[F]=[T][K][E]=[C][E] \tag{4.3}$$

Matrix [C] represents the contribution of each source E to the voltage F. For example, the magnitude and angle of C_{ik} works like a weighting factor to indicate the weight of E_k on the channel voltage F_i:

$$F_i = C_{i1}E_1 + C_{i2}E_2 + \ldots + C_{ik}E_k + \ldots \tag{4.4}$$

Using the above equation, the contribution of each generator's voltage to the critical channel (say channel i) can be calculated by

$$G\_Cont_{ik} = \frac{|C_{ik}E_k|\cos(\theta_{ik})}{|F_i|} \tag{4.5}$$

where G_Cont_{ik} is the contribution of generator k to the channel voltage F_i, and θ_{ik} is the angle difference between the channel voltage F_i and the term $C_{ik}E_k$.

Assume that generator j (E_j) has the highest contribution to the critical channel. In this case, if the angles of generators' voltages are assumed to remain constant, an increase in the voltage magnitude of the generator j will lead to the highest increase in the magnitude of the channel voltage F_i. This will result in the highest increase in the stability margin of the critical channel. On the other hand, the increase in the magnitude of the generator voltage corresponds to the increase in its reactive power. As a result, the proposed contribution index can be used to determine the contribution of generators' reactive powers on the stability of the critical channel and as a result on the stability of the actual system.

4.2.2 Verification methods

The main challenge is how to verify the results because as mentioned before, there is no standard method for determining the contribution of generators' reactive powers on the voltage stability. However, to see whether the results are reasonable or not, two methods are used and their results are compared with the proposed method. These two methods are as follows:

- *Method A*: the sensitivity of loadability margin with respect to the generators' voltages is used to rank the generators. For this purpose, for each generator, a very small increase (say 1%) in its voltage magnitude is made and the increased margin of the system is calculated using the continuation power flow (CPF). This is done for all the generators and they are ranked according to their associated increases in the margin.

- *Method B*: In this method, the system is firstly stressed until it has a small margin (say 5%). The reactive power of the test generator is then frozen and the system is stressed further until a new nose point is reached and the reduced stability margin is obtained. This is done for all generators, and they are ranked according to their associated decreases in the margin.

4.2.3 Case Study Results

The standard test systems used in the previous sections are considered again as the case studies. The proposed generator ranking method is applied to these systems, and the results are compared with those of the verification methods.

- **<u>WECC 9-bus system:</u>**

The following figures show the generator ranking results obtained for this system. According to these figures, the generator connected to bus 1 is identified as the critical generator using the proposed method. Method A verifies this result since this method identifies bus 1 and bus 2 as the critical generators (both buses has the same sensitivity). Although method B identifies bus 1 as the second critical generator, the value of margin increases for the first and second critical generators are very close to each other (Fig. 4.5c).

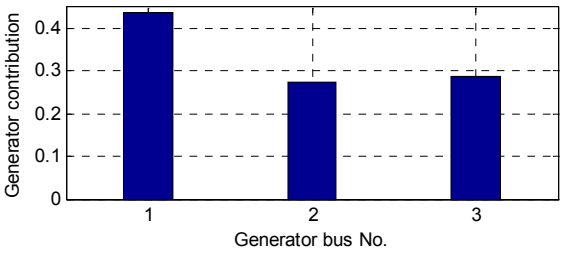

(a) using the proposed method

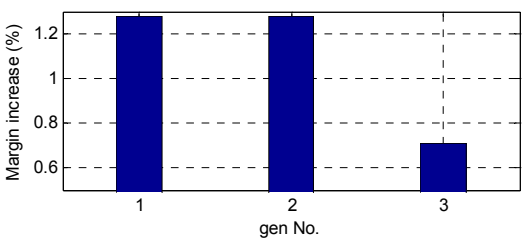

(b) using method A

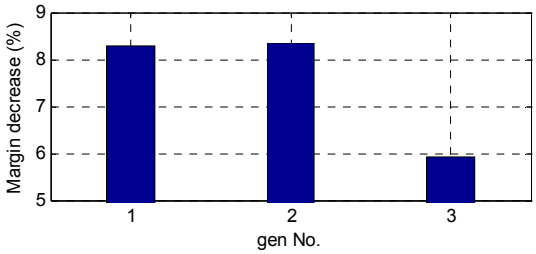

(c) using method B

Fig. 4.5: Generator ranking for WECC-bus system

- **The 30-bus system:**

Fig. 4.6 shows the generator ranking results obtained for the 30-bus system. As seen in this figure, both of the verification methods verify the critical generator identified by the proposed method.

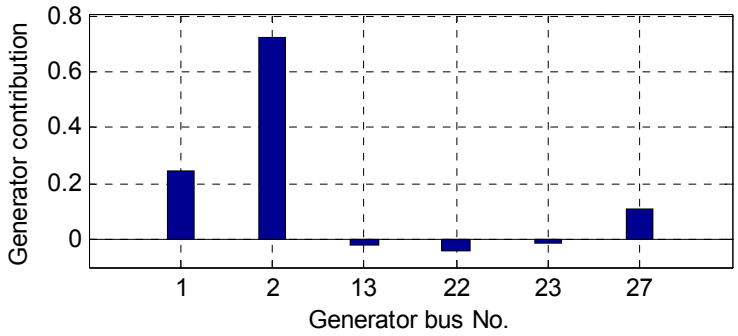

(a) using the proposed method

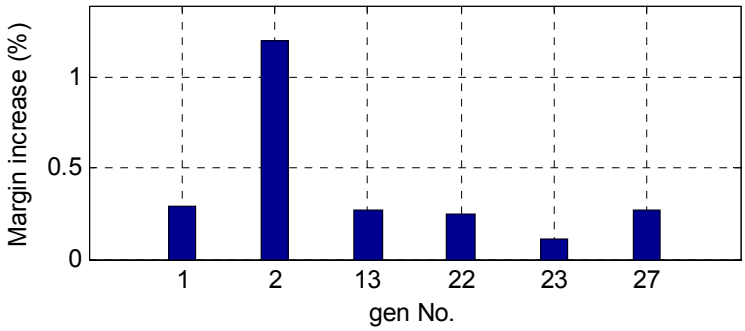

(b) using method A

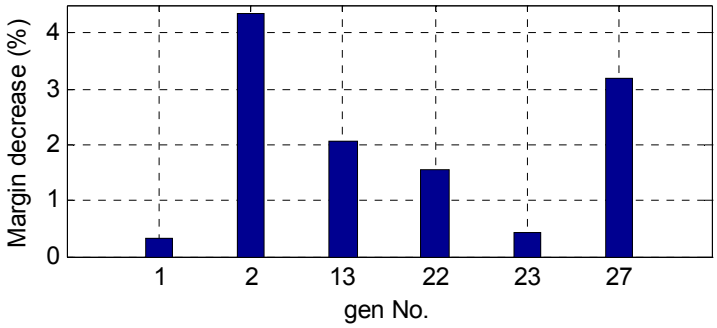

(c) using method B

Fig. 4.6: Generator ranking for the 30-bus system

- **IEEE 30-bus system:**

Fig. 4.7 illustrates the results obtained for the IEEE 30-bus system. As seen in this figure, both of the verification methods verify the critical generator identified by the proposed method.

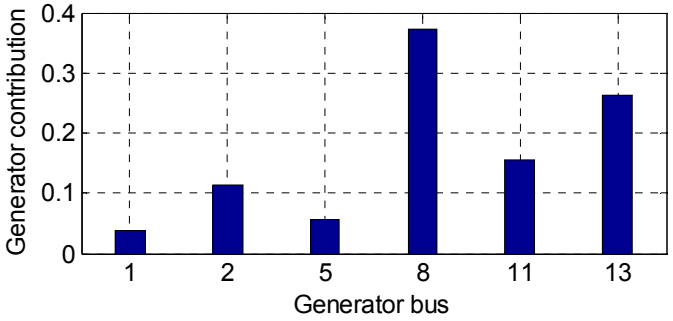

(a) using the proposed method

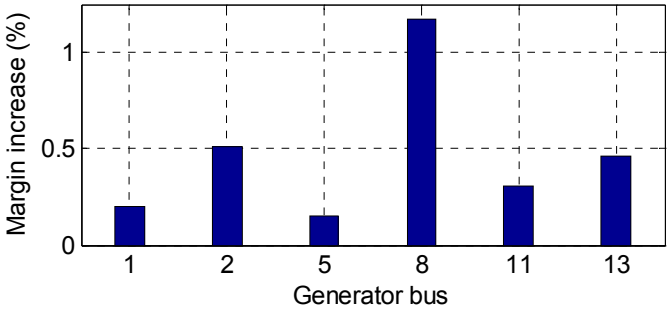

(b) using method A

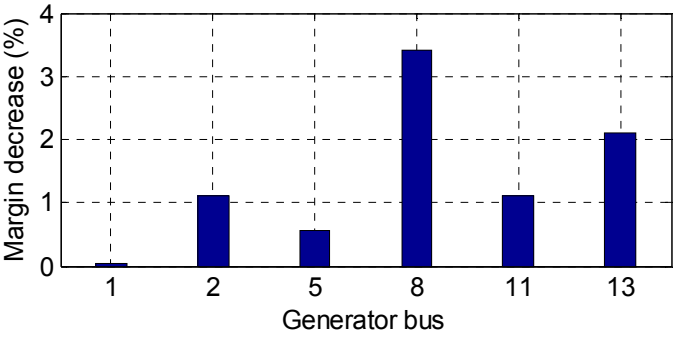

(c) using method B

Fig. 4.7: Generator ranking for IEEE 30-bus system

- **IEEE 57-bus system:**

The results obtained for the IEEE 57-bus system are shown in the following figure. As seen in this figure, the proposed method identifies bus 9 as the critical generator. This generator is identified as the critical generator using method A, and as the second critical generator using method B.

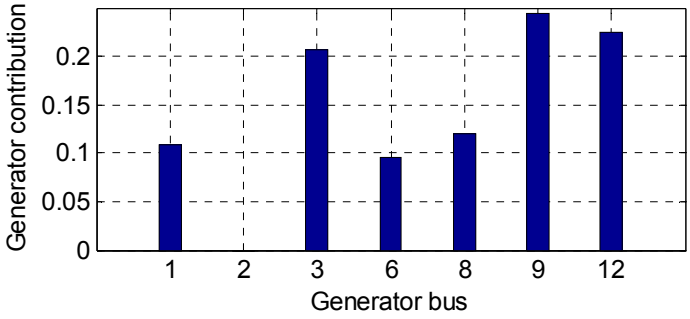

(a) using the proposed method

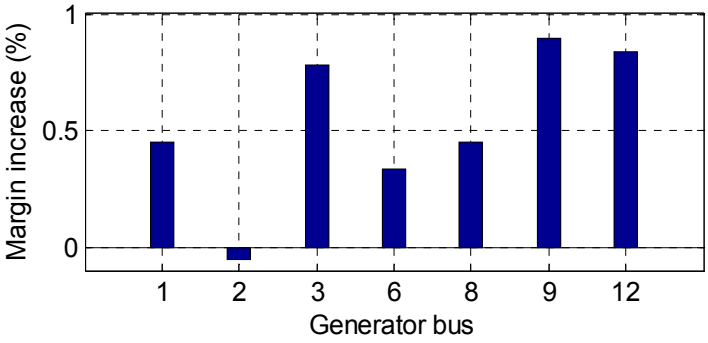

(b) using method A

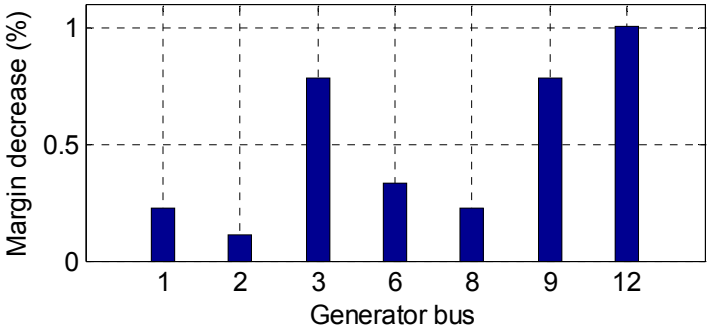

(c) using method B

Fig. 4.8: Generator ranking for IEEE 57-bus system

The above case study results are summarized in Table 4.2. According to this table, both methods A and B verify the results obtained by the proposed method in the 30-bus and IEEE 30-bus systems. In the WSCC 9-bus and IEEE 57-bus systems, the critical generator identified by

the proposed method is the same as the critical one obtained by one of the methods A and B and is the same as the second critical generator obtained by the other method. These results indicate that the generator rankings obtained by the proposed method are totally reasonable and acceptable.

Table 4.2: Summary of the results for critical generator identification

System	Critical generator bus		
	Proposed method	Method A	Method B
WECC 9-bus	1	1	2 1
30-bus from [70]	2	2	2
IEEE 30-bus	8	8	8
IEEE 57-bus	9	9	12 9

The above results indicate that the generator rankings obtained by the proposed method are totally reasonable and acceptable. It is worthwhile to emphasize again that no proven method has been proposed in the literature in order to determine the impacts of generators' reactive powers on the voltage collapse. Due to the lack of such a method, the ranking method (APF) proposed in [17] which is based on the impacts of generators' active powers, have been used in the literature ([61], [65], [66]) for optimal reactive power planning. However, as expected, by applying this ranking method on several test systems, we have found out that it cannot be used to determine the impacts of generators' reactive powers. As an example, Fig. 4.9 shows the results of this method in IEEE 30-bus system. Comparison of this figure with Fig. 4.7(b) and Fig. 4.7(c) clearly reveals that APF is not a good method to determine the impacts of generators' reactive powers. That is why we believe by using the proposed ranking method, the existing methods of reactive power planning on the generation side can be improved significantly.

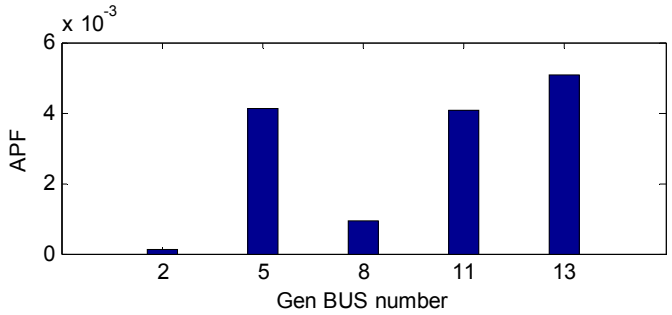

Fig. 4.9: Generator ranking in IEEE 30-bus system obtained by APF

4.3 Identification of the Critical Branch

Due to the ever increasing demand for electrical power, power systems are currently operating close to their stability limits. This situation is very risky since a disturbance can lead to a voltage collapse. Therefore, it is very important to reinforce the system stability. In addition to the countermeasures that can be taken on the load side (such as installing shunt compensation devices) and on the generator side (such as performing optimal reactive power scheduling), some preventive actions can be taken on the transmission network i.e. system branches. These actions mainly include constructing new transmission lines, adding new transformers, and installing series compensation devices such as Thyristor controlled series capacitors (TCSC).

On the other hand, due to financial and environmental limitations, it is not possible to perform these reinforcement actions on every part of the network. Therefore, it is very critical to determine what part of the system is more under pressure so that only weak locations (branches) can be reinforced. The implication is that the identification of the branches which are weak with respect to voltage stability is an important task in power system planning and operation. The aim of this section is to use the CCT in order to identify the critical branch. The main idea is to identify the critical transmission path (CTP) first, and then identify the critical segment of this path.

Therefore, the first step is to determine the critical transmission path. In [43], an index called the transmission path stability index (TPSI) has been proposed which can be used to identify the critical transmission path. For this purpose, the TPSI of all possible transmission paths should be computed first. The critical path will then be the path which has the smallest TPSI. However, since there can be too many transmission paths in a power system, this method might encounter

some difficulties and problems. The aim is to use the channel components transform and propose an improved method in order to overcome the difficulties. Using the proposed approach, the critical transmission path can be identified much easier, faster, and more accurately. Once the critical transmission path is identified, its segments (branches) can be compared to identify the critical segment.

4.3.1 Transmission Path Stability Index

Before introducing the transmission path stability index (TPSI), let's recall the critical stability condition of a two-bus (one-source one-load) system shown in Fig. 4.10(a). Assuming bus 1 as the generator bus and bus 2 as the load bus, the phasor diagram of the two-bus system is as shown in Fig. 4.10(b). On the other hand, the critical operating point of this system can be derived from the singularity condition of the corresponding Jacobian matrix, resulting in the following condition [43].

$$0.5V_1 = V_2 \cos\delta_{12} \quad \Rightarrow \quad 0.5V_1 = \Delta V_d \tag{4.6}$$

where ΔV_d is the direct-axis component of the voltage drop ΔV projected on the voltage source V_1 (see Fig. 4.10).

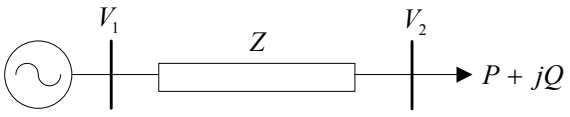

(a) The two-bus system

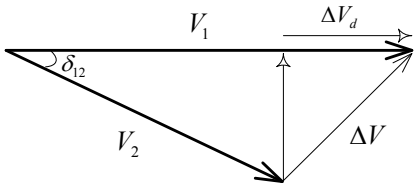

(b) The voltage phasor diagram

Fig. 4.10: A two-bus system and its voltage phasor diagram

According to (4.6), the TPSI for the two-bus system is defined as:

$$TPSI = 0.5V_1 - \Delta V_d \tag{4.7}$$

This index can be used as a measure for the stability of the system. When the system is going toward to the collapse point, TPSI is decreasing toward zero. In other words, when TPSI reaches zero, the system will experience the voltage collapse.

The above index can be extended to a n-bus radial network shown in Fig. 4.11 which results in the following equation [43]:

$$TPSI = 0.5V_1 - \Delta V'_d \tag{4.8}$$

where $\Delta V'_d$ is called the total corrected voltage drop.

The total corrected voltage drop ($\Delta V'_d$) is equal to the sum of corrected voltage drops of all segments. The corrected voltage drop of a segment is obtained by projecting the direct-axis component of its voltage drop into the voltage phasor of the supply bus. This concept is illustrated in Fig. 4.12 which shows the phasor diagram of a radial system. As an example, consider the segment n-1 connecting bus n to bus n-1. As shown in the figure, the corrected voltage drop of this segment ($\Delta V'_{dn-1}$) is indeed the projection of the direct-axis voltage drop (ΔV_{dn-1}) into the supply voltage (V_1). The corrected voltage drops of all segments should be calculated and added together to obtain the total corrected voltage drop $\Delta V'_d$ (see Fig. 4.12).

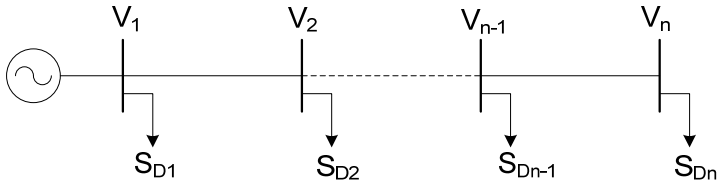

Fig. 4.11: One-line diagram of a radial network

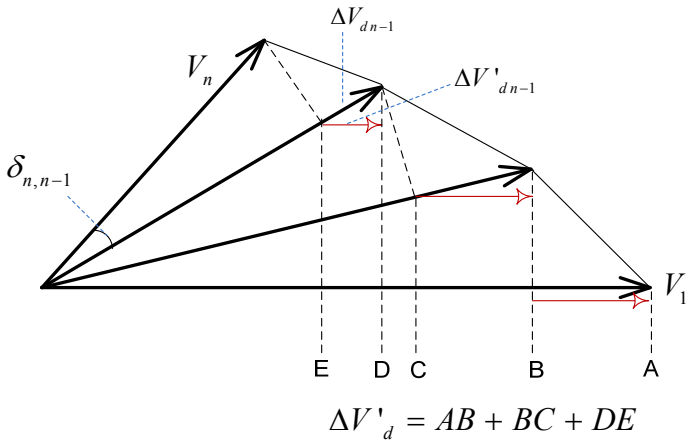

Fig. 4.12: Voltage phasor diagram of the radial system

Therefore, the TPSI of a n-bus radial system can be calculated using the voltage phasors as follows.

$$\begin{aligned} TPSI &= 0.5V_1 - \Delta V'_d = 0.5V_1 - \sum_{i=1}^{n-1} \Delta V'_{di} \\ &= 0.5V_1 - \sum_{i=1}^{n-1} \{(V_i - V_{i+1}\cos\delta_{i,i+1})\cos\delta_{1,i}\} \end{aligned} \tag{4.9}$$

Since power systems are meshed networks, a different situation exists. However, [43] has shown that TPSI can be applied to transmission paths of a meshed network as an approximate stability index. A transmission path is usually defined as a series of buses with declining voltage magnitude [68]. A transmission path always ends in a load bus, and there might be different paths supplying one load bus. In the method proposed in [43], all the transmission paths supplying all the system loads are determined and their TPSI are calculated using system voltage phsors and according to (4.9). The transmission path which has the smallest TPSI will then be the critical transmission path. It is worthwhile to mention that as shown in [43], when the system is close to the collapse point, the critical transmission path is more likely to have a negative TPSI.

4.3.2 The Proposed Method

The main problem of the above method is that there would be too many transmission paths especially in actual power systems. So the calculation efforts would be too much especially if it is intended for online applications. Furthermore, as explained in the previous section, this method is essentially accurate for radial systems. However, it may involve some approximations in power systems which are meshed networks. Therefore, when comparing too many paths, these approximations may result in identifying a wrong critical path.

The channel components transform (CCT) can help to simplify this method and overcome its problems.

- The CCT can identify the critical load bus and it is well known that the end bus in the critical transmission path is the critical load bus [43] and [68].

- The CCT can also identify the critical generator which has the highest impact on voltage collapse. So, it is totally reasonable to say that the critical transmission path must be from the critical generator.

Therefore, instead of considering every possible transmission path in the network, it suffices to only consider the transmission paths from the critical generator to the critical load. If there is only one such a path, that path will be the critical path. If there are more than one path (which will not be too many), the TPSI of these paths are determined and compared. The critical path will then be the path with the smallest TPSI.

Once the critical path is identified, its segments can be compared to determine which segment is the most responsible for the low TPSI (or the high total corrected voltage drop) of the path. For this purpose, the corrected voltage drops of the segments can be compared. The segment which has the highest corrected voltage drop is then identified as the weakest segment of the critical path. The identified segment would be the critical segment (branch) in the system.

Therefore, the proposed method can be summarized as the following steps. It is assumed that the CCT has already been applied to the system and the critical load and the critical generator has been identified.

- Determine the transmission paths which supply the critical load bus.
- From the determined paths, only consider those which start from the critical generator.
- In each path, find the corrected voltage drop of its segments and calculate the total corrected voltage drop of the path.
- Compute the transmission path stability index (TPSI) of each path.
- Compare the TPSI of all paths and identify the critical path which has the smallest TPSI (if there is only one path, that path would be the critical path).
- Consider the critical transmission path, compare the corrected voltage drops of its segments, and identify the critical segment. The critical segment is the one with the highest corrected voltage drop.

4.3.3 The Verification Method

In order to verify the results, a verification method is required. For this purpose, the sensitivity of the loadability margin with respect to the branch impedance is used. In this method, the reactance of the branch is reduced by a small percent and the increased loadability margin is obtained using the continuation power flow. This is done for all the branches (including lines and transformers) and they are ranked. The critical branch would be the one which results in the highest increase in the margin. This method is based on the findings of [88], which show that the sensitivity of the loadability margin to system line reactances can be used to find the most critical transmission lines.

4.3.4 Case Study Results

In this section, the proposed method is applied to four test systems including the WECC 9-bus, 30-bus, IEEE 30-bus and IEEE 57-bus systems and the results are compared with those of the verification method.

A) <u>WECC 9 bus system</u>

By applying the CCT on this system, bus 9 is identified as the critical load bus and bus 1 is identified as the critical generator. There is only one transmission path from the critical generator to the critical load which is bus1-bus4-bus9.

- Path 1: 1-4-9

This path is highlighted on the one-line diagram of the system shown in Fig. 4.13.

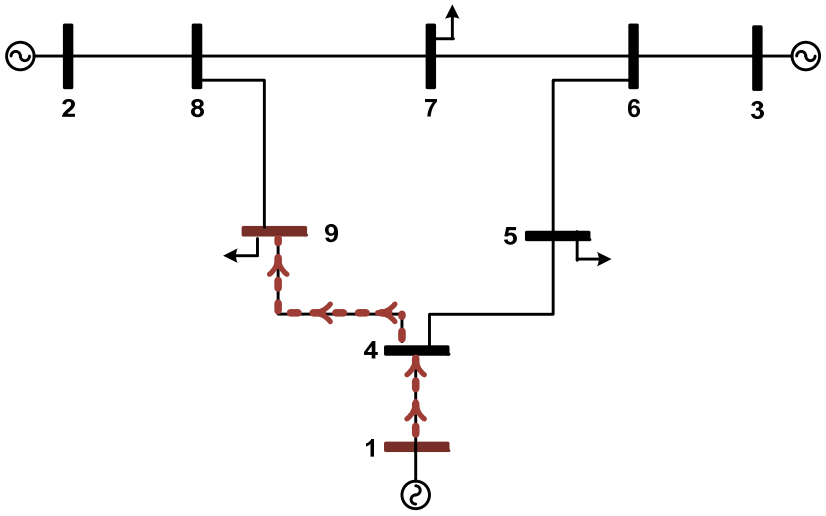

Fig. 4.13: Single line diagram of the system

Since there is only one path from the critical generator to the critical load, this path would be the critical path. This path has two segments:

- Segment 1: 1-4
- Segment 2: 4-9

Using the voltage phasors of the system when it is close to the collapse point, the corrected voltage drops of these segments are calculated and shown in Fig. 4.14.

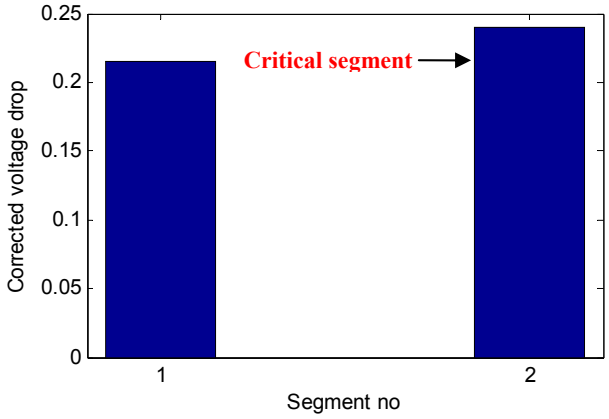

Fig. 4.14: Corrected voltage drops for the segments of the critical path

According to Fig. 4.14, the critical segment would be segment 2 (4-9) since it has the highest corrected voltage drop.

On the other hand, by applying the verification method to this system, Fig. 4.15 is obtained. As seen in this figure, the first critical segment is 8-9, and the second critical segment is 4-9. In other words, the critical segment identified by the proposed method is the same as the second critical segment identified by the verification method.

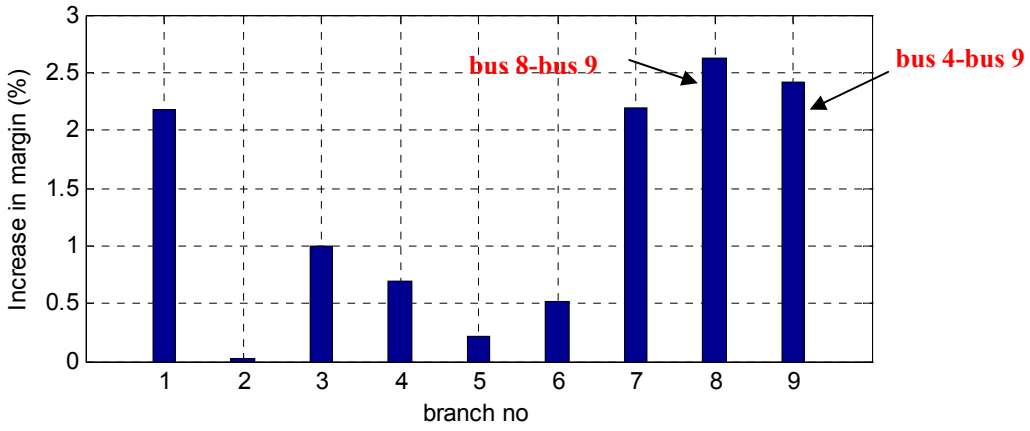

Fig. 4.15: Results of the verification method.

B) <u>The 30 bus system</u>

By applying the CCT on this system, the critical load and generator are identified as follows.

- Critical load: bus 8
- Critical Generator: bus 2

Using the voltage phasors of the system when it is close to the collapse point, transmission paths from the critical generator to the critical load are determined as follows:

- Path1: 2-6-8
- Path2: 2-4-6-8

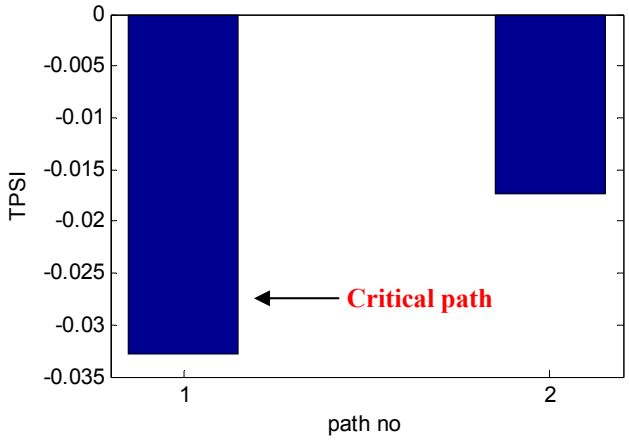

Fig. 4.16: TPSI of the transmission paths

Since there are more than one path from the critical generator to the critical load, TPSI of these paths are calculated as shown in Fig. 4.16. According to this figure, Path1 (2-6-8) has the smallest TPSI and therefore it is the critical path. This path is highlighted on the single line diagram of the system which is shown in Fig. 4.17.

Segments of the critical path are:

- Segment 1: 2-6
- Segment 2: 6-8

The corrected voltage drops of these segments are illustrated in Fig. 4.18. Based on this figure, the critical segment is the segment 2-6. This is exactly verified by the verification method which results in the Fig. 4.19.

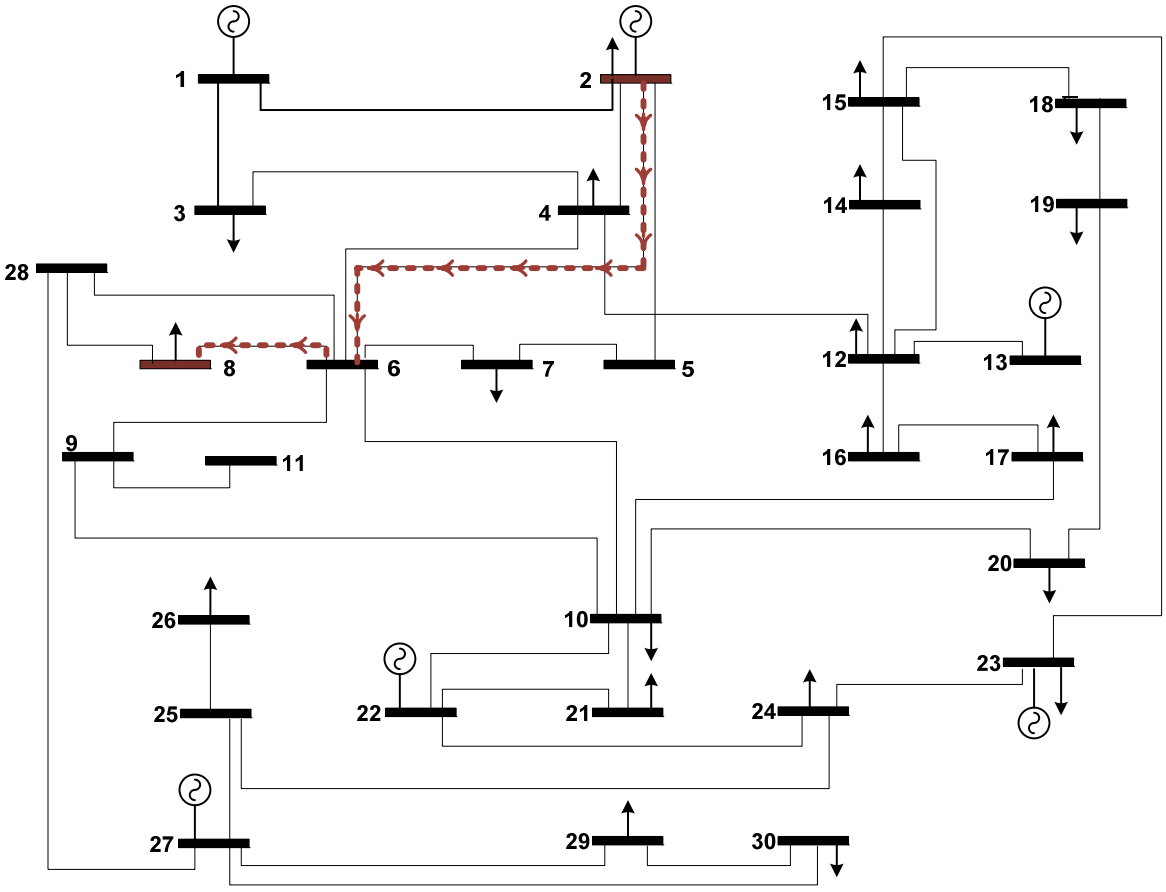

Fig. 4.17: Single line diagram of the system

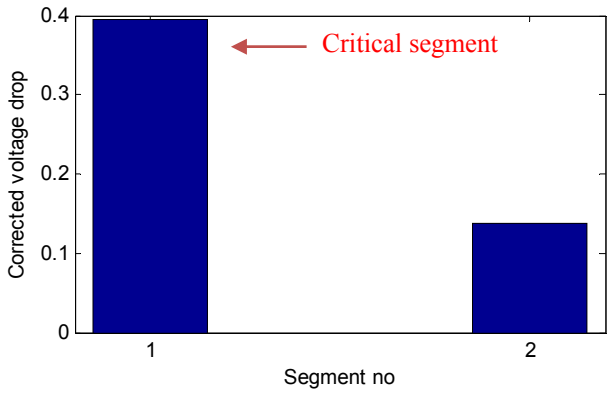

Fig. 4.18: Corrected voltage drops for the segments of the critical path

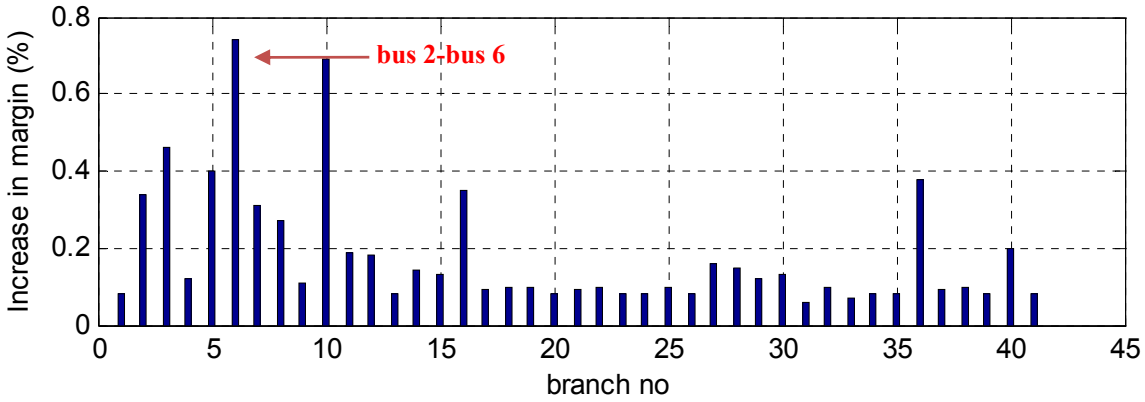

Fig. 4.19: Results of the verification method

C) IEEE 30 bus system

As seen in the previous sections, by applying the CCT on this system, the critical load and generator are identified as follows.

- Critical load: 30
- Critical Generator: 8

There are four transmission paths from the critical generator to the critical bus:

- Path1: 8-28-27-30
- Path2: 8-6-28-27-30
- Path3: 8-28-27-29-30
- Path4: 8-6-28-27-29-30

The TPSI of the transmission paths are illustrated in Fig. 4.20. According to this figure, path2 (8-6-28-27-30) is identified as the critical path. This path is shown on the system's diagram in Fig. 4.21.

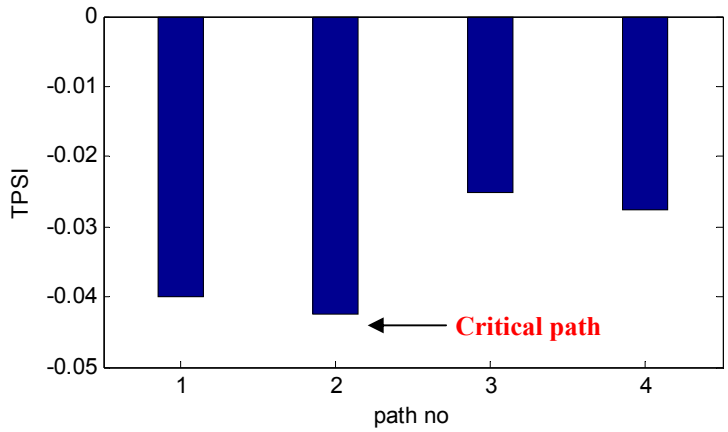

Fig. 4.20: TPSI of the transmission paths

This path has four segments:

- Segment 1: 8-6
- Segment 2: 6-28
- Segment 3: 28-27
- Segment 4: 27-30

Corrected voltage drops for all the segments are shown in Fig. 4.22. As this figure reveals, segment 3 (27-28) is identified as the critical segment.

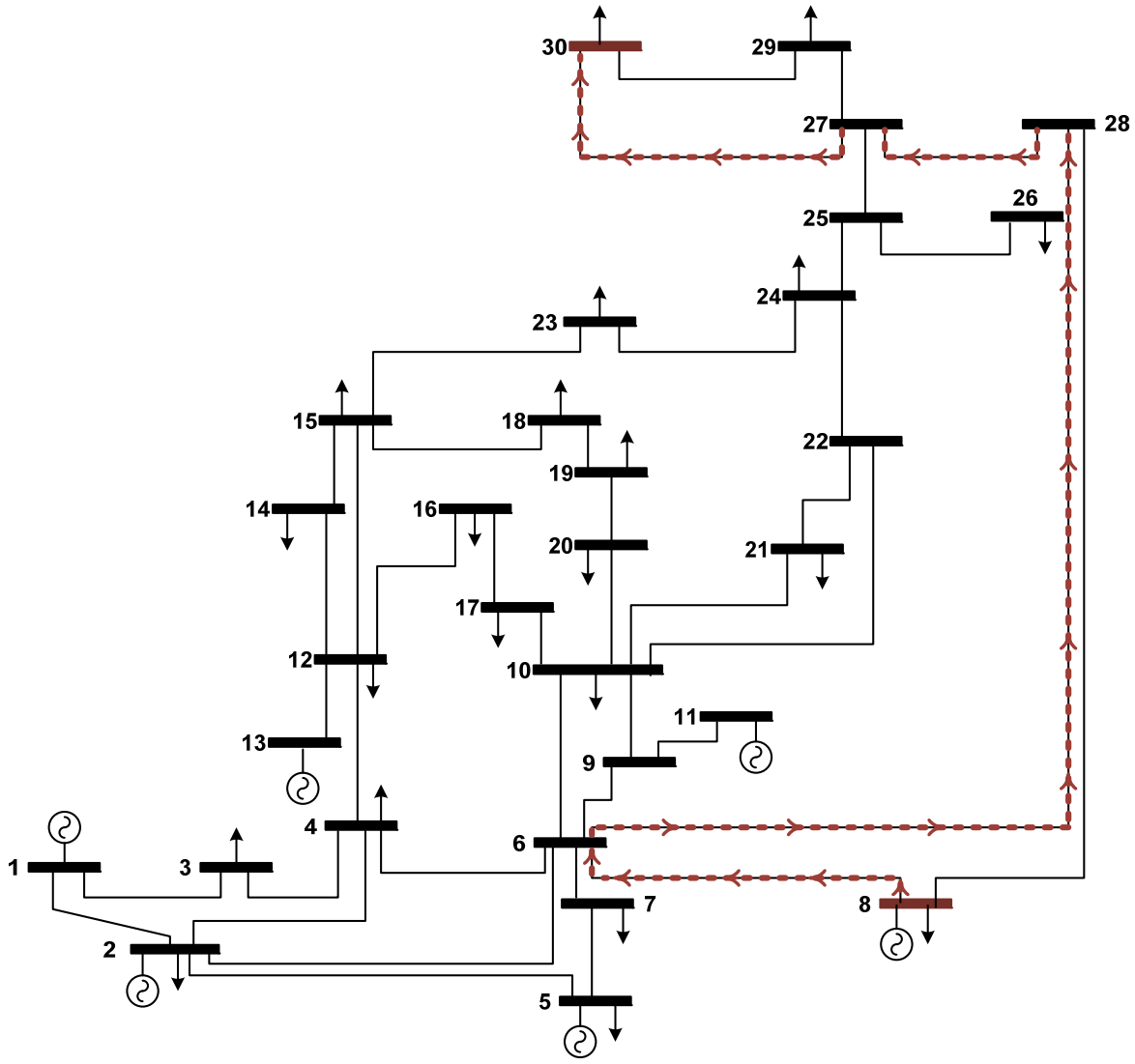

Fig. 4.21: Single line diagram of the system

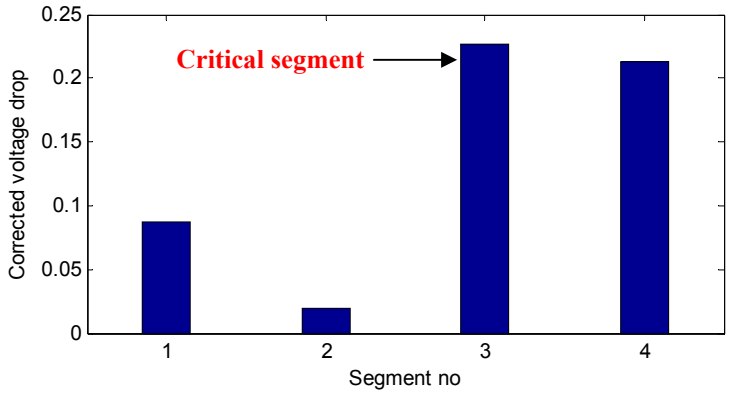

Fig. 4.22: Corrected voltage drops for the segments of the critical path

The following figure illustrates the results of the verification method. As seen in this figure, the verification method identifies the segment 27-28 as the critical branch which is exactly the same as the result of the proposed method.

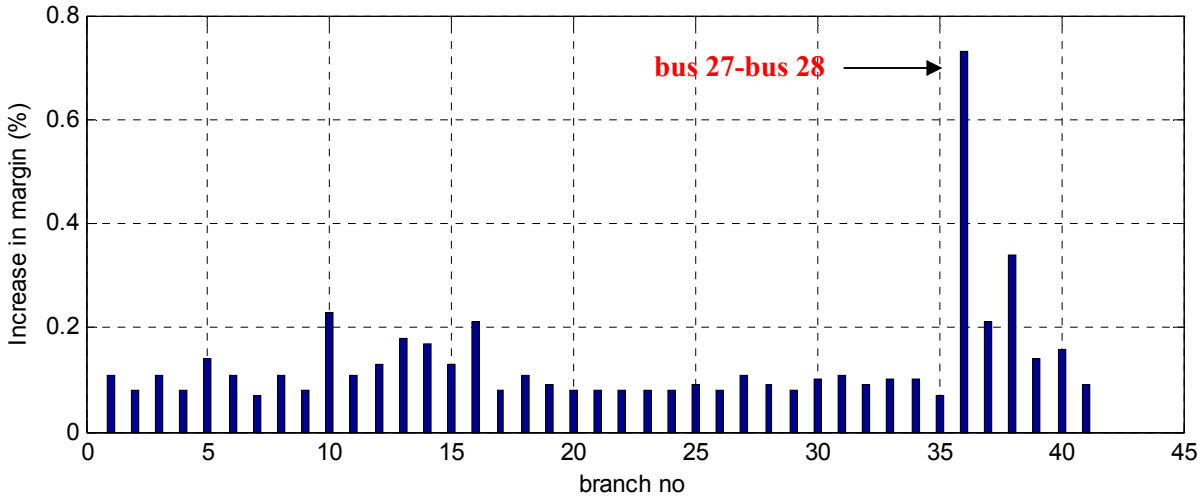

Fig. 4.23: Results of the verification method

D) IEEE 57 bus system:

By applying the CCT on this system, the critical load and generator are identified as follows.

- Critical load: bus 31
- Critical Generator: bus 9

There are four transmission paths from the critical generator to the critical bus:

- Path1: 9-13-49-38-22-23-24-25-30-31
- Path2: 9-13-49-48-38-22-23-24-25-30-31
- Path3: 9-13-49-38-37-36-35-34-32-31
- Path4: 9-13-49-48-38-37-36-35-34-32-31

The TPSI of these transmission paths are calculated and shown in Fig. 4.24. As this figure shows, path 4 has the smallest TPSI and as a result, this path (9-13-49-48-38-37-36-35-34-32-31) is the critical path. In Fig. 4.25, this path is illustrated on the single line diagram of the system.

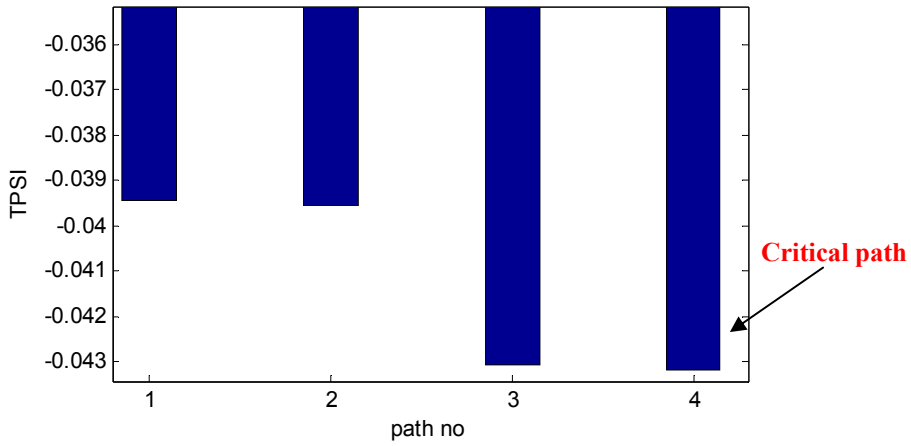

Fig. 4.24: TPSI of the transmission paths

The critical path has 10 segments as follows:

- Segment 1: 9-13
- Segment 2: 13-49
- Segment 3: 49-48
- Segment 4: 48-38
- Segment 5: 38-37
- Segment 6: 37-36
- Segment 7: 36-35
- Segment 8: 35-34
- Segment 9: 34-32
- Segment 10: 32-31

The corrected voltage drops of these segments are shown in Fig. 4.26. This figure indicates that segment 9 has the highest corrected voltage drop and as a result, this segment is the critical segment in this system.

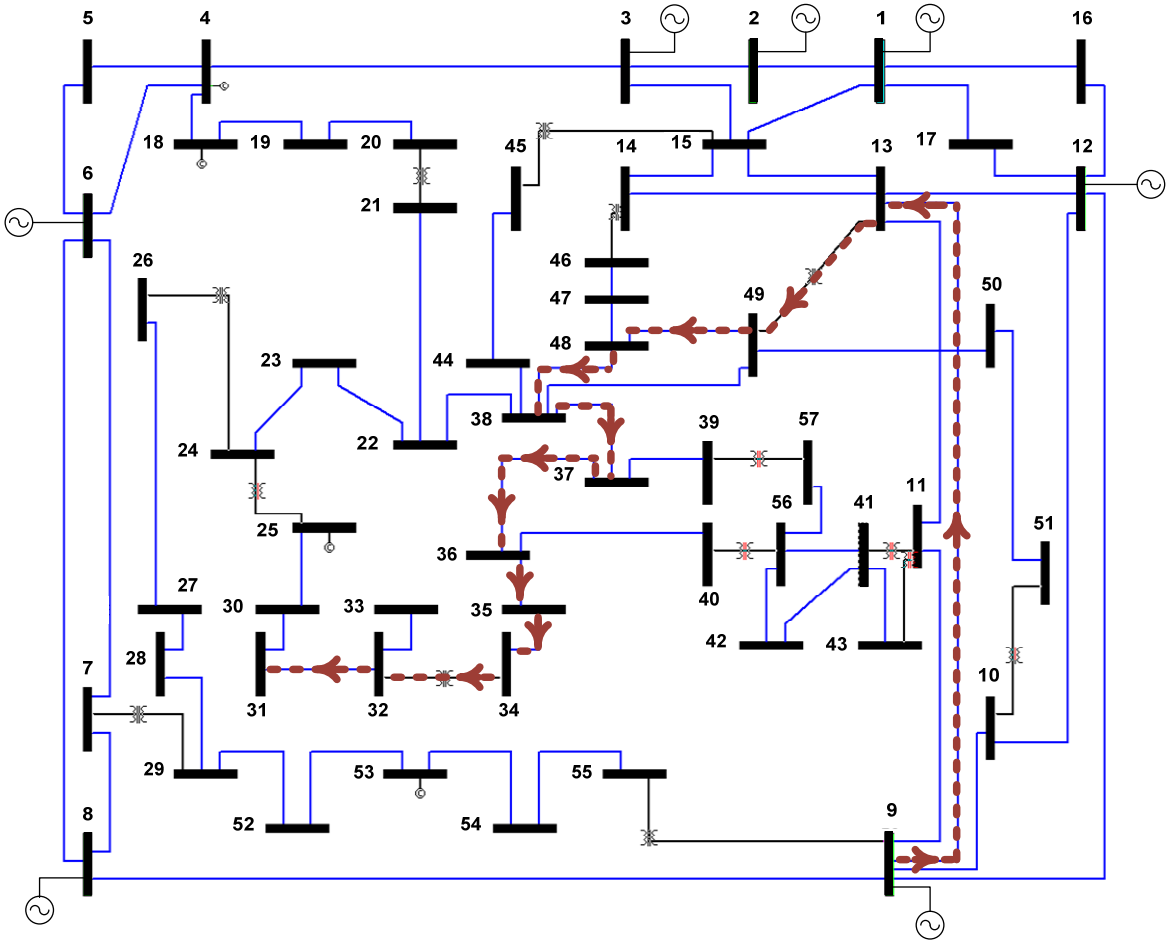

Fig. 4.25: Single line diagram of the system

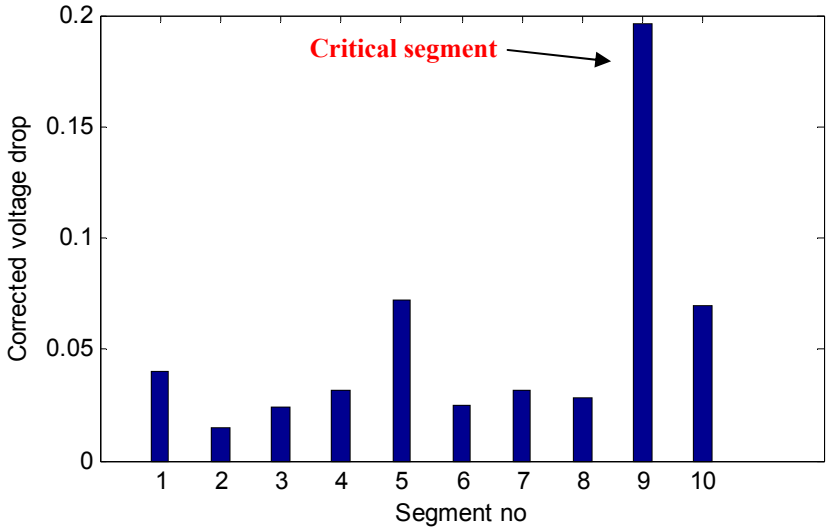

Fig. 4.26: Corrected voltage drops for the segments of the critical path

Therefore, the critical branch is 34-32. The following figure shows the results of the verification method. As seen in this figure, 34-32 is verified as the critical branch in the system.

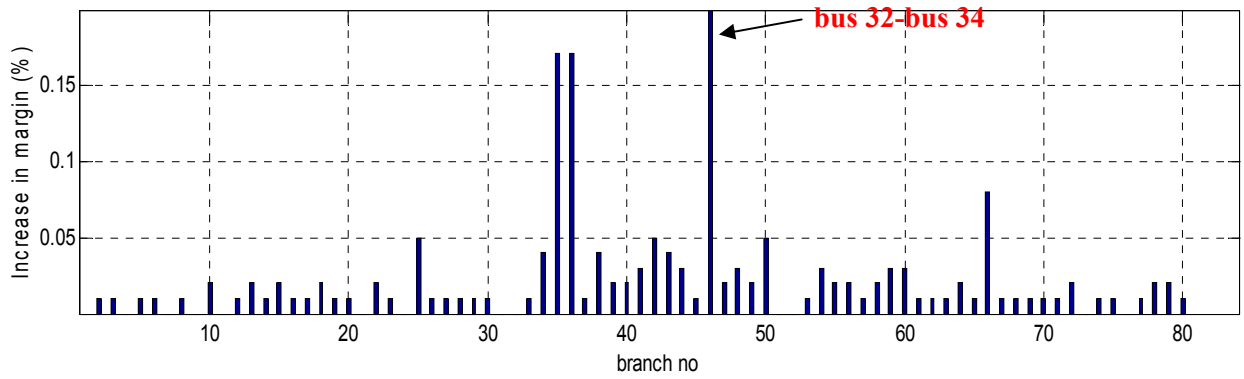

Fig. 4.27: Results of the verification method

The results of the above case studies are summarized in Table 4.3. As seen in this table, in the WECC system, the critical segment identified by the proposed method is determined as the second critical segment by the verification method. However, in all other systems including the 30-bus, IEEE 30-bus, and IEEE 57-bus systems, the result of the proposed method is exactly verified by the verification method. This indicates that the proposed method is totally acceptable and can be used as a simple and fast method for the critical segment (branch) identification.

Table 4.3: Summary of the results

System	Critical segment	
	Proposed method	Verification method
WECC 9-bus	4-9	8-9 4-9
30-bus from [70]	2-6	2-6
IEEE 30-bus	27-28	27-28
IEEE 57-bus	32-34	32-34

4.4 Conclusions

In this chapter, methods were proposed to assess the voltage stability in power systems using the channel components transform. The proposed methods include:

- Identification of the critical load buses: The contributions of load buses to the critical channel can be calculated and used as an index to rank the load buses in terms of their impact on the voltage stability. The buses with the highest contributions are the critical load buses which are more prone to voltage collapse. The critical buses are the best candidates for corrective/preventive actions such as shunt compensation or load shedding.

- Identification of the critical generators: Using CCT, a technique has been proposed to identify the critical generators which have the highest impacts on the voltage collapse. The proposed technique is based on the contributions of generators to the critical channel. The generator ranking can be utilized for optimal reactive power planning which can significantly improve the system stability margin.

- Identification of the critical branches: Based on the proposed CCT-based framework, a method was proposed to identify the critical branch. The critical branch is the one which is more under pressure and as a result, limits the stability level of the system. The identification of the critical branch is important since it can help the operator improve the stability of the system efficiently. As an example, series compensation devices such as TCSC can be installed in the critical line.

The detail algorithms of the proposed methods were presented in this chapter. The performances of the proposed methods were also verified by using several standard test systems as case studies.

Chapter 5: Large System Studies Using CCT

As shown in the previous chapters, the channel components transform (CCT) can be used to analyze different aspects of voltage stability problem. Several algorithms and methods were developed for this purpose. All the developed methods were also verified using several standard test systems. The aim of this chapter is to investigate the application of the CCT on an actual large system. For this purpose, the Alberta Integrated Electric System (AIES) shown in Fig. 5.1 [83] is used as our case study. As seen in this figure, AIES has six main regions including Northwest, Northeast, Edmonton, Central, Calgary, and South. Two representative cases of AIES are considered in this chapter.

- AIES operational base case: This base case represents the operational system. This system is used in this chapter to investigate the validity and effectiveness of the CCT-based voltage stability analysis methods. For this purpose, the CCT results are compared with the results of the verification methods.

- AIES planning base case: This base case represents the planned system which includes new transmission/generation developments and new load connections to be in service in near future. A software has been developed based on the CCT to analyze the voltage stability in power systems. The developed software works on the PSS/E platform. The AIES planning case is used to show how this software can be used for a complete and detailed voltage stability analysis.

5.1 AIES Operational Base Case

The AIES operational base case is a 2038-bus system which includes 205 PV buses and 684 PQ buses. For the ease of reference, all the system buses are renumbered from 1 to 2038. The first 205 buses are PV buses, the next 684 buses are load buses, and the remaining buses are network buses. In the following sections, the CCT is applied to this system, and similar to what

was done for standard test systems in the previous chapters, the validity of the results are discussed.

5.1.1 Critical Channel Identification

This system has 684 load buses, and as a result there are 684 channels for this system. Among all channels, there are some channels which carry very small powers such as 10^{-20} pu. It is not reasonable to rely on this kind of channels because they cannot carry important information due to their small powers. Therefore, before any analysis is started, we should filter out this kind of channels. For this purpose, the following criterion is considered.

- Filter out the i^{th} channel if $|S_{Ci}|<10^{-10}$, where S_{Ci} is the i^{th} channel power

By applying the above filtering, 15 channels are removed and the analyses are done on the remaining channels. The first step is to identify the critical channel. This can be done according to the normalized voltage drop or the channel margins. Fig. 5.2 shows the normalized voltage drops (*NVD*) of all the system channels. As this figure shows, channel 384 and channel 18 are the first and second critical channels. The same results can be obtained by using the channel margins which are illustrated in Fig. 5.3. As seen in this figure, both of these channels have very small margins when the system is close to the nose point.

Fig. 5.1: Alberta Transmission System

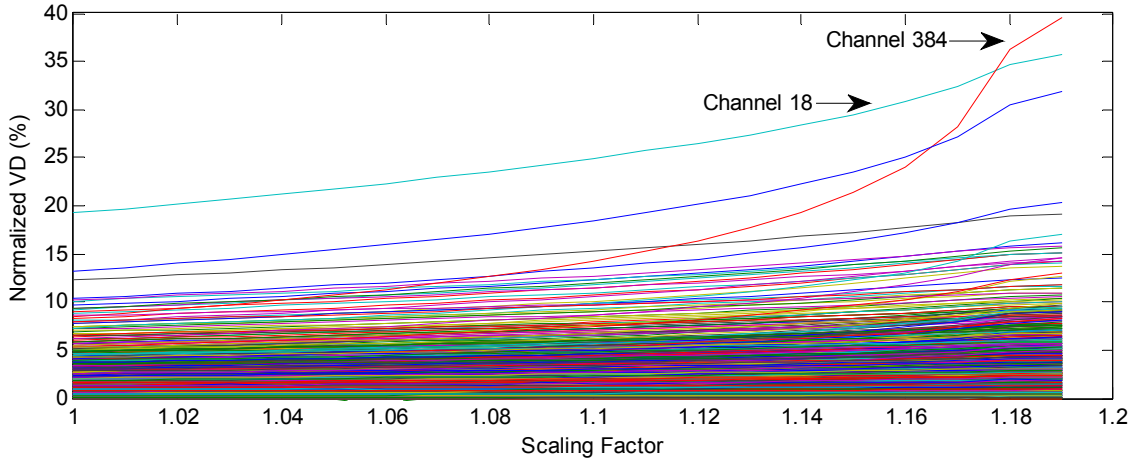

Fig. 5.2: Channel *NVD*s

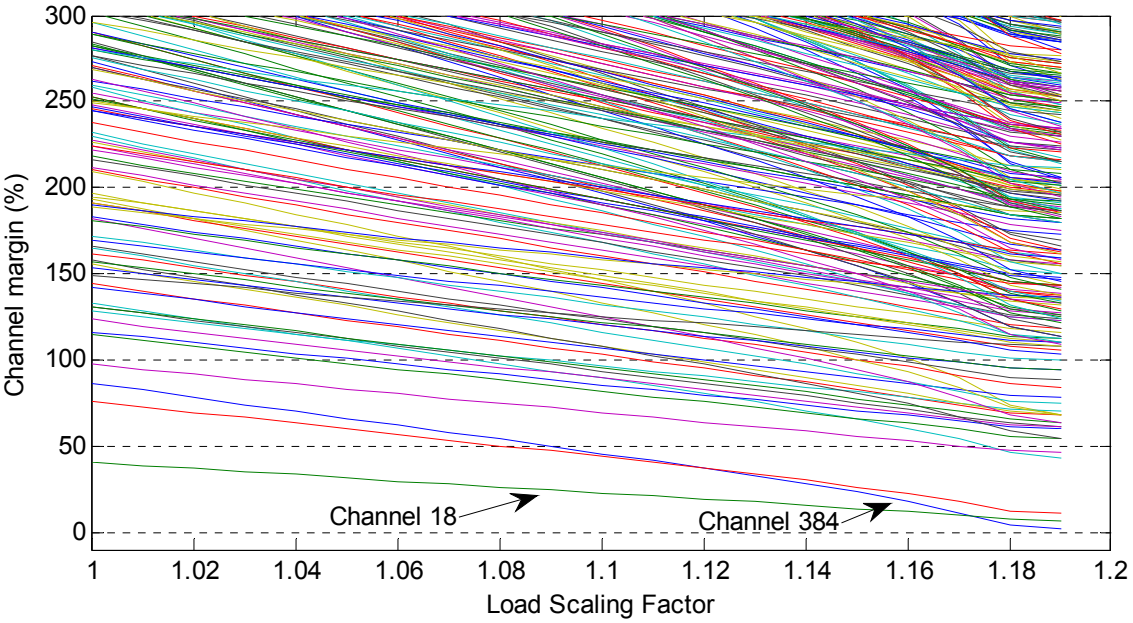

Fig. 5.3: Channel margins

Fig. 5.4 shows the *PV* curves of the top rank channels in the Alberta system. It can be seen that both channels 384 and 18 have very small margins. However, channel 18 carries much higher power. So it represents a system wide mode. This will be further investigated in the next sub-section.

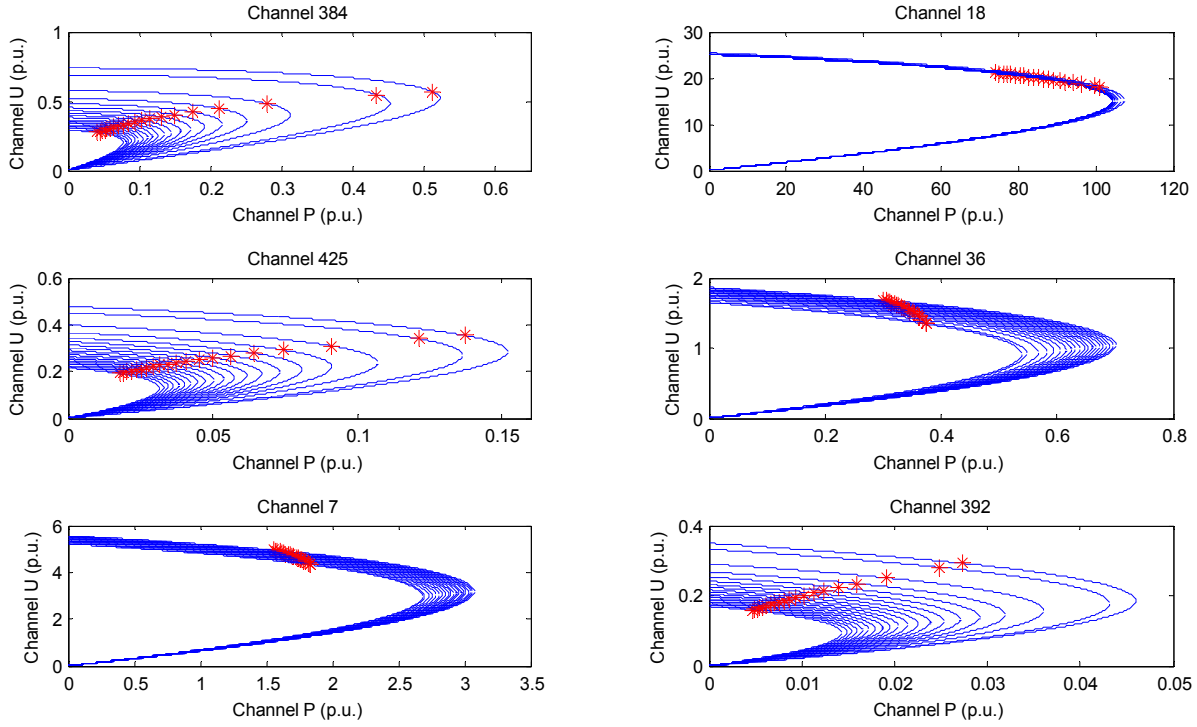

Fig. 5.4: Channel *PV* curves of 6 top-ranked channels

5.1.2 Critical Bus Identification

If the contributions of load buses to critical channels (channels 384, and 18) are computed, Fig. 5.5 and Fig. 5.6 are obtained. As these figure show, both channels identify Bus 630 as the critical bus. This bus is verified as the weakest location in the system using PSSE which gives the most critical bus in the system. Fig. 5.5 shows that channel 384 involves very small number of buses while channel 18 has a large number of buses participating. This supports the previous finding that channel 18 is a system wide channel (mode) and channel 384 is more like a local channel. Therefore, channel 18 should be considered as the critical channel.

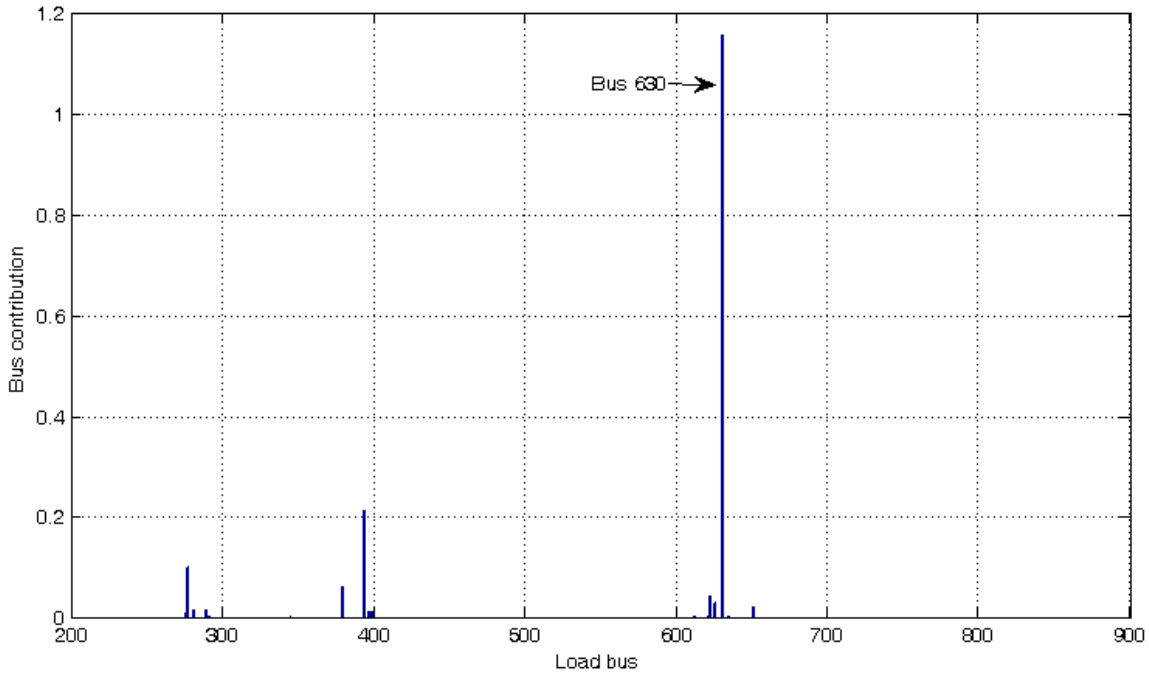

Fig. 5.5: Contribution of load buses to channel 384

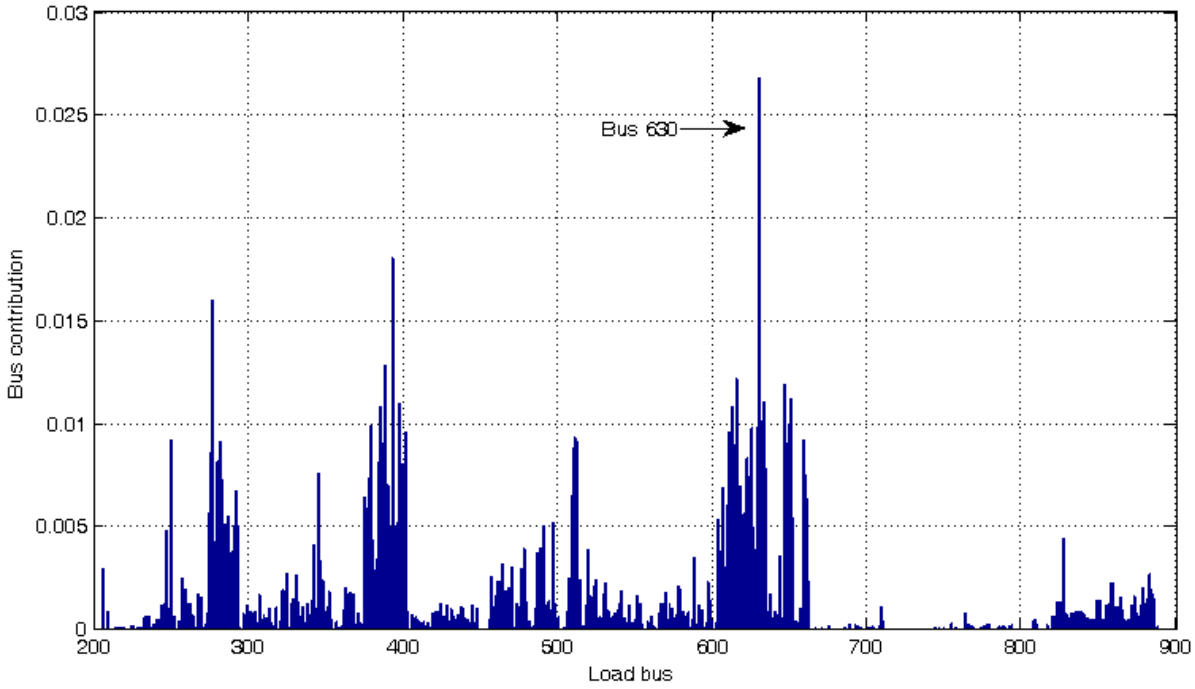

Fig. 5.6: Contribution of load buses to channel 18

5.1.3 Critical Generator Identification

In order to identify the critical generator, the contributions of all generators to the critical channel (channel 18) need to be calculated. Fig. 5.7 illustrates the results. As this figure shows, the generator connected to bus 123 is the critical generator which has the highest impact on the voltage stability.

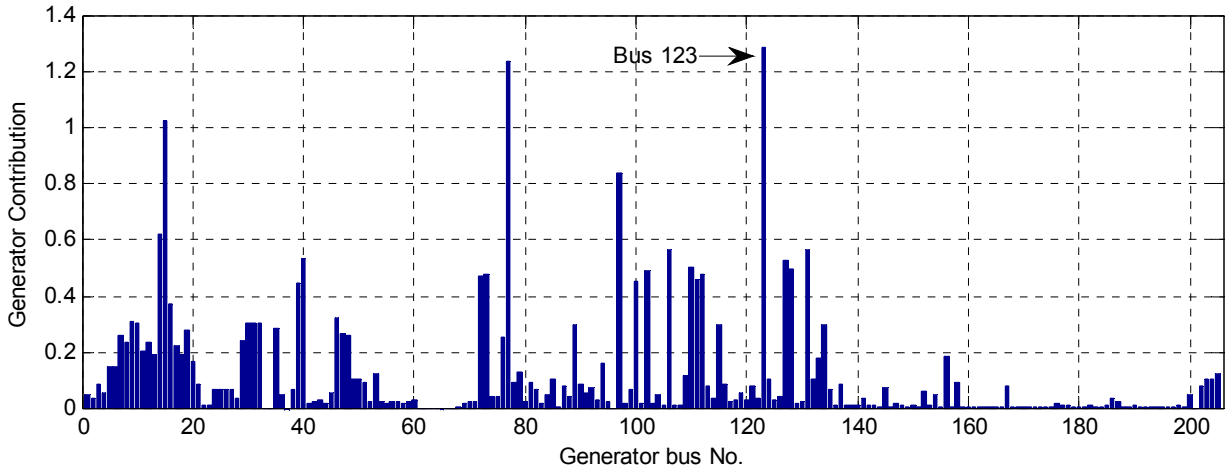

Fig. 5.7: Contributions of generators to Channel 18

In order to verify the obtained results, the sensitivities of the stability margin with respect to generator voltages are calculated. For this purpose, for each generator, a very small increase in its voltage magnitude is made and the stability margin of the system is calculated using the continuation power flow. This is performed for all the generators and they are ranked according to their associated increases in the stability margin. Fig. 5.8 illustrates the obtained sensitivities. As seen in this figure, the highest sensitivity is associated with the generator connected at bus 123. This implies that this generator is indeed the critical generator.

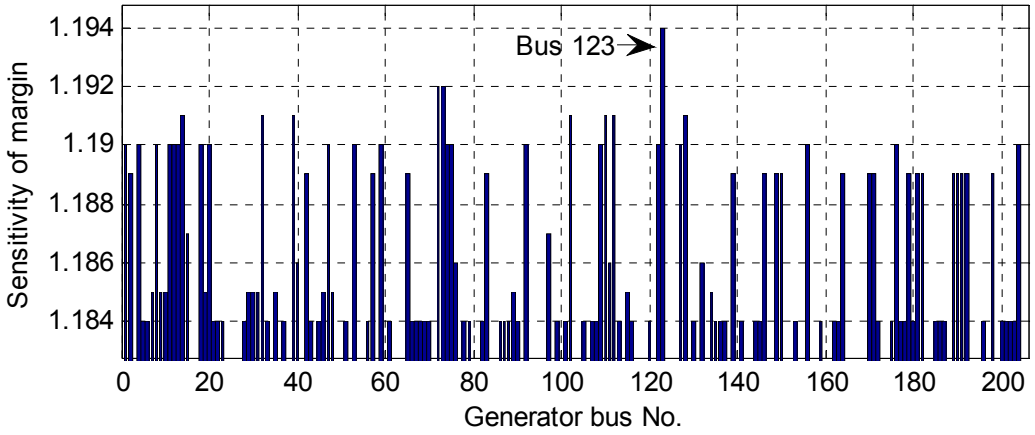

Fig. 5.8: Sensitivity of margin with respect to generator voltage

5.1.4 Critical Branch Identification

The procedure proposed before for the identification of the critical branch is applied to this case study. The obtained results are summarized in the following.

There is only one path from the critical generator (bus 123) to the critical load (bus 630). So this path which is shown below is the critical path.

Critical Path: 123 – 1049 – 1029 – 1063 – 1316 – 630

The critical path consists of five segments including:

- Segment 1: 123- 1049
- Segment 2: 1049- 1029
- Segment 3: 1029- 1063
- Segment 4: 1063- 1316
- Segment 5: 1316- 630.

Fig. 5.9 shows the corrected voltage drops of all segments of the critical path. As this figure reveals, segment 5 is the critical segment. Therefore, the critical segment (branch) in this system is the branch 1316-630.

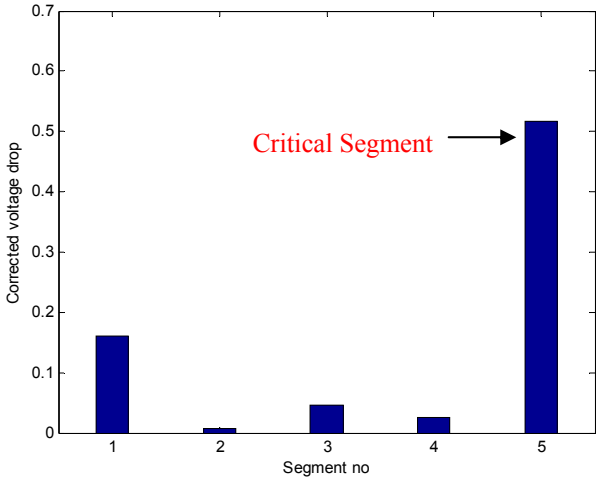

Fig. 5.9: Corrected voltage drop of the segments of the critical path

For the verification purpose, the sensitivity of the loadability margin with respect to the branch impedance is used. In this method, the reactance of the branch is reduced by a small percentage and the increased loadability margin is obtained using the continuation power flow. This is performed for all the branches and they are ranked. The critical segment would be the one which results in the highest increase in the margin. Fig. 5.10 shows the computed sensitivities. As seen in this figure, branch 1316-630 leads to the highest sensitivity. As a result, this branch is the critical branch in the system which verifies the results obtained by the proposed method.

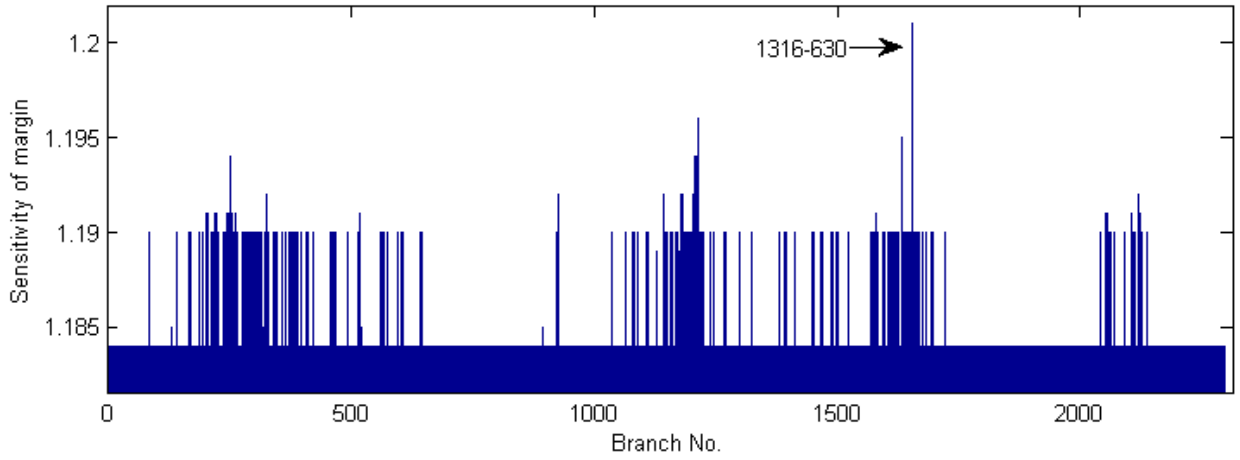

Fig. 5.10: Sensitivity of margin with respect to branch impedance

The critical load, critical generator, and the critical path are all in the Calgary region (see Fig. 5.1). The Calgary region along with the south region is shown in Fig. 5.11 in detail. In this

figure, the area in which the critical components exist are highlighted using a dash circle. To make it more clear, this area has been redrawn and shown in Fig. 5.12. In this figure, the critical generator (bus 123), the critical load (bus 630), and the critical path which is from the critical generator to the critical load are clearly shown.

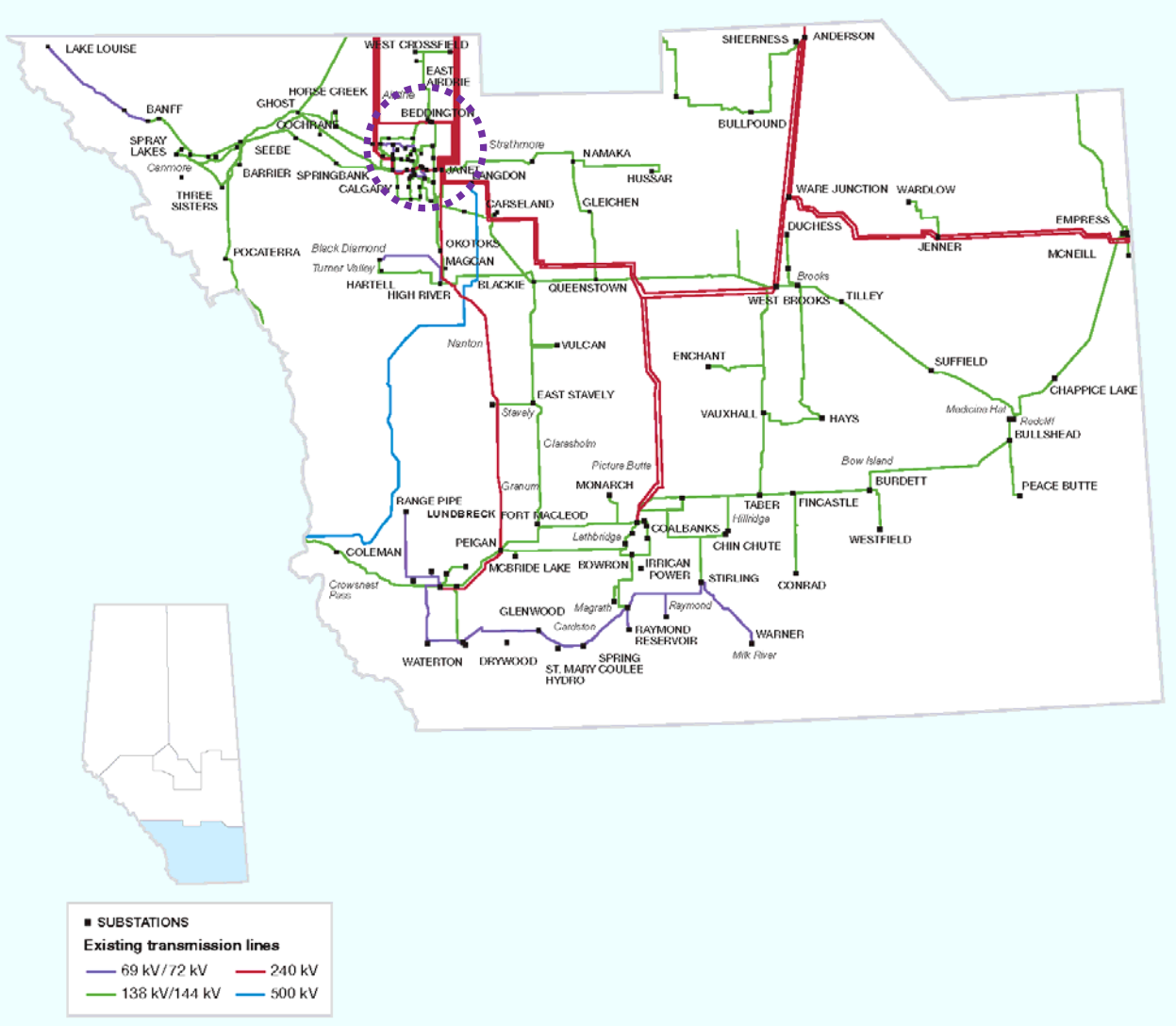

Fig. 5.11: Single-line diagram of the Calgary and South regions

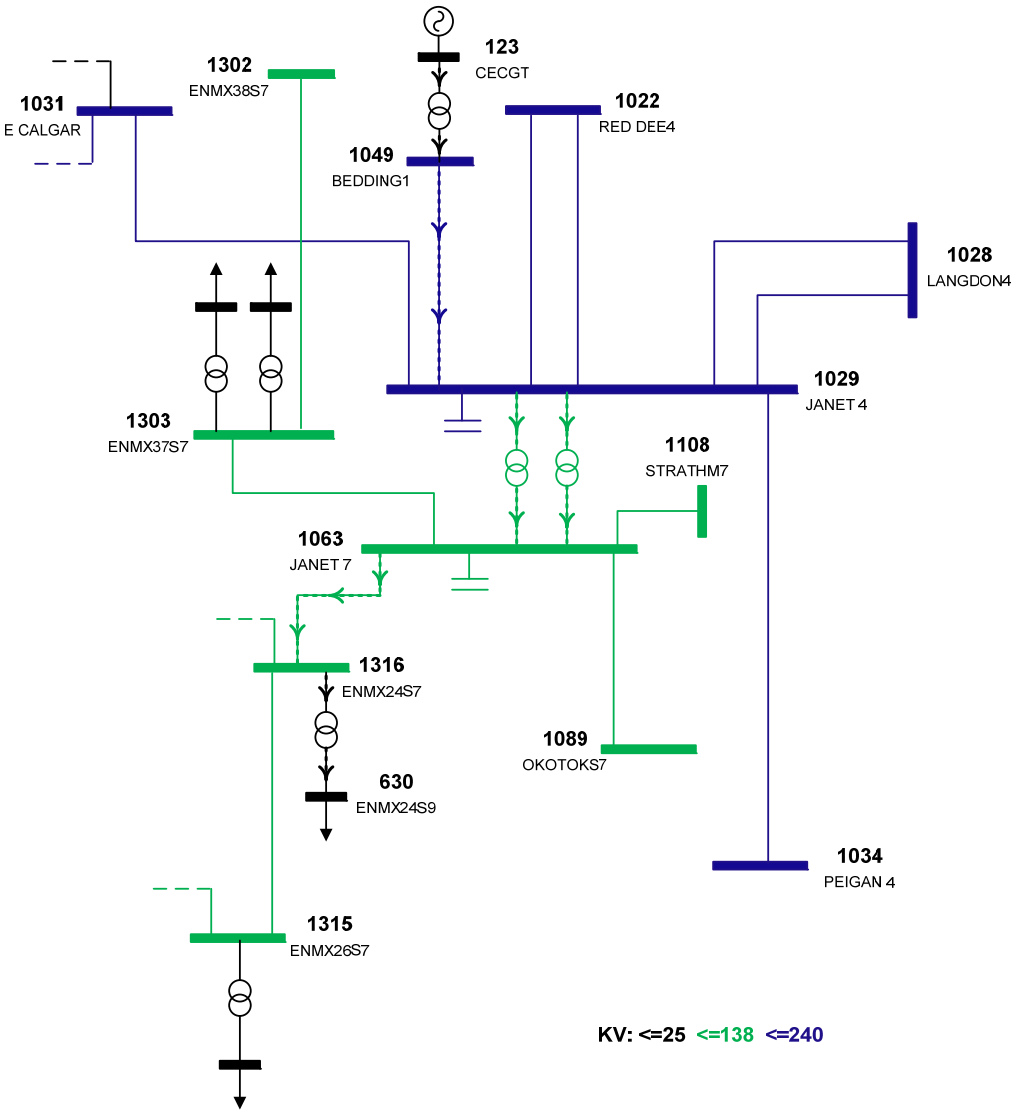

Fig. 5.12: Single-line diagram of a part of Calgary region with the critical components

5.2 AIES Planning Base Case

The CCT and associated methods have been utilized and a software has been developed. The developed software works on the PSS/E platform. By running the program for a case, the stability margin of the case, the critical channels, critical loads, critical generators, and critical transmission lines can be determined for that case. The aim of this section is to apply the software on the AIES planning base case, and show how the software can be used to analyze different aspects of voltage stability.

The system overall diagram is shown in Fig. 5.1. As will be needed for detailed studies, every region shown in Fig. 5.1 is further divided into different areas. Fig. 5.13 shows all areas of the system. Every area has been given a number and a name. The representative information about these areas is summarized in Table 5.1. The table lists the system loads and generations for different areas of the system. As this table shows, there are three areas in the system with very high demands. These areas include Calgary (area 6), Fort McMurray (area 25), and Edmonton (area 60). Also, Lake Wabamun (Area 40) has the highest generation in the system. Fort McMurray (area 25) is the next area with a high generation.

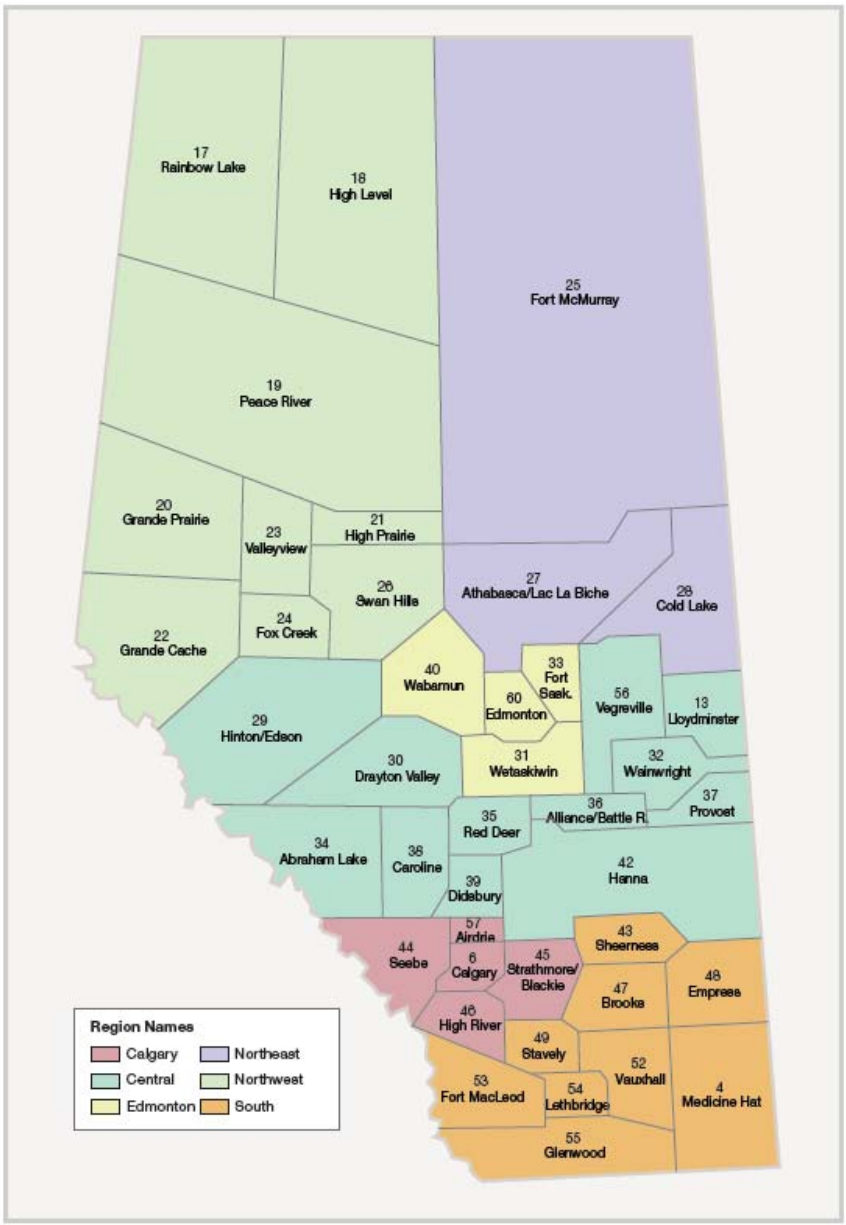

Fig. 5.13: The AIES areas

Table 5.1: AIES area loads and generations

Area Name	Area Number	Generation		Load	
		MW	MVAR	MW	MVAR
MEDICINE	4	130	72	177.2	73.9
CALGARY	6	457.2	124.7	1460.9	544.1
LLOYDMIN	13	0	0	84.6	24.5
WSCC	15	66	-67	40	13.2
RAINBOW	17	113.2	-18.3	95.8	37.6
HIGH LEV	18	0	0	18.2	6.5
PEACE RI	19	27	-7.5	184.1	60.8
GRANDE P	20	174.8	6.9	325.3	133.4
HIGH PRA	21	0	0	102.6	2.5
GRANDE C	22	150	-11	45.6	17.7
VALLEYVI	23	30	-24.1	40.5	15.7
FOX CREE	24	0	0	65.1	27.7
FORT MCM	25	1611.1	305.2	1644.9	777.3
SWAN HIL	26	5.7	-11.5	358.9	101.4
ATHABASC	27	68	35.9	153.5	62.6
COLD LAK	28	278.8	115	407.5	170.5
HINTON/E	29	0	0	132.5	60.1
DRAYTON	30	142.7	39.9	173.4	75.4
WETASKIW	31	0	0	96.7	29.9
WAINWRIG	32	0	0	111.8	43.9
FORT SAS	33	432.3	152.2	608.8	293.6
ABRAHAM	34	46.9	5.9	2.2	0.3
RED DEER	35	374	-29.5	486.2	194
ALLIANCE	36	690	-117.8	72.7	29.4
PROVOST	37	0	0	157.6	69.8
CAROLINE	38	15.6	-1	131	29.2
DIDSBURY	39	6.6	-1.9	84.4	26.5
LAKE WAB	40	4851.5	1495.6	507.3	217
HANNA	42	29.4	-15.4	157.8	43.8
SHEERNES	43	915.1	-10.4	61.2	26.3
SEEBE	44	103.5	47.8	189.8	37.4
STRATHMO	45	224	29.8	104.8	31.6
HIGH RIV	46	0	0	93.2	31
BROOKS	47	0	0	100.4	38.4
EMPRESS	48	-32.5	-75	158.5	43.7
STAVELY	49	0	0	19.1	3.8
BACKBONE	50	0	0	0	0
NORTHBAC	51	0	0	0	0
VAUXHALL	52	13	-5.5	168.1	66.2
FORT MAC	53	291	-114.6	32.9	13
LETHBRID	54	13.6	1.8	188.6	62
GLENWOOD	55	27	-46.9	43.8	18.6
VEGREVIL	56	0	0	56.9	13.6
AIRDRIE	57	24	-13.7	93.6	21.5
EDMONTON	60	-2.2	-9.4	1633	607
TOTALS		11277.4	1852.5	10871.0	4196.3

5.2.1 Developed Software

Fig. 5.14 shows the main interface of the CCT software. As this figure shows, there are three options on the top right corner. These options include:

- Scale-up power flow: The software provides two alternatives for how to apply the CCT to a case; 1) The CCT can be applied to the current operating conditions, 2) The CCT can be applied to the system nose point which is very close to the collapse point. In this case study, the second alternative is considered by selecting the associated option box in the software. As a result, the conventional PV curve approach is applied to the system first, and the system is scaled up to a point close to the collapse point. According to the PV curve approach, all the AIES loads are increased uniformly with a constant power factor. The step size of the scaling factor is selected as a small number to make sure we will get to a point close to the collapse point. Loads are represented by a voltage independent constant power model.

- Respect P limit: All the in-service generators within the AIES network are scaled up to pick up the additional load increase in proportion to their respective ratings, but they are subject to their maximum real power output limits if the "Respect P Limit" box is selected. By selecting this option, when scaling up a generator's active power, if its active power is reached, that generator is not scaled up anymore.

- Respect Q limit: This option refers to considering the maximum reactive powers of the generators. By selecting this option, a maximum reactive power output limit is implemented for each generator except the generator named 'WSCC GEN' which is connected to the bus 1520. This bus is assumed as the slack bus in the case.

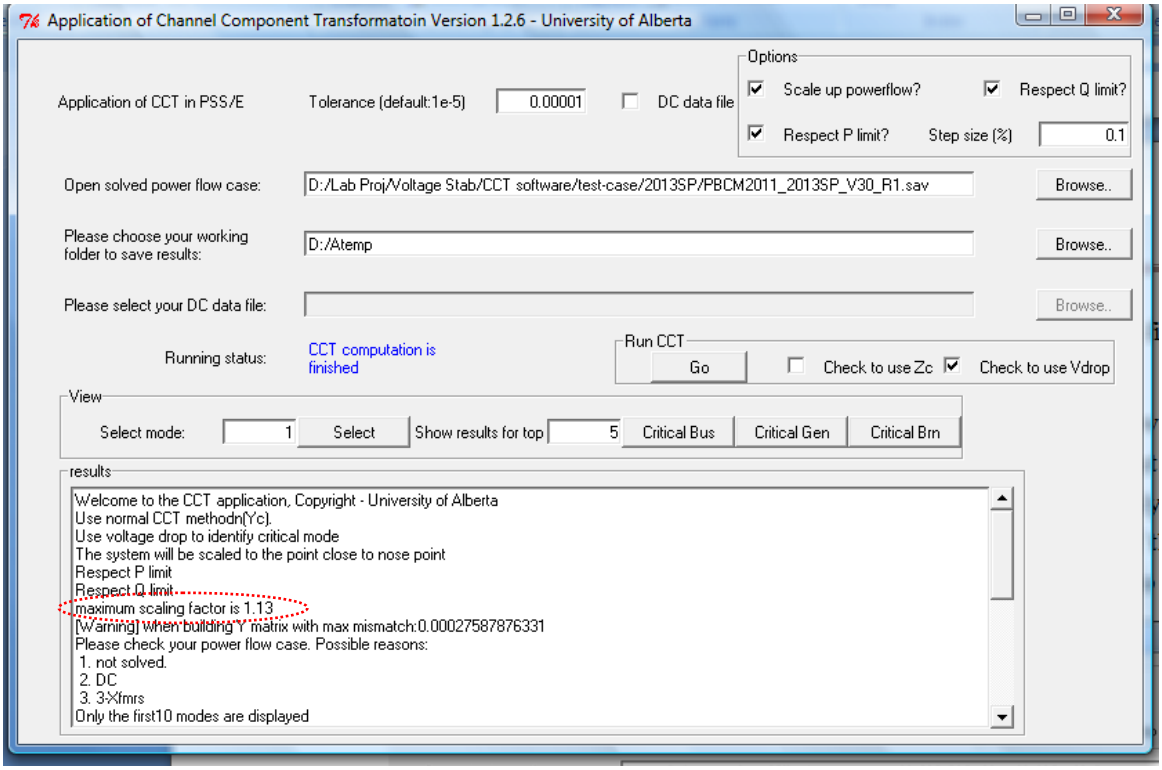

Fig. 5.14: The main interface of the CCT software

As mentioned above, the reactive power limits of generators are taken into account in the study. Before reaching the reactive limit, generators are modeled as PV buses as shown in Fig. 5.15(a) A generator's reactive limit is actually caused by the limit on the field current. A generator reaching its reactive limit will maintain a constant field current. Since the field voltage is in proportion to the field current, the generator thus behaves as a constant field voltage E (the maximum field voltage) behind its synchronous reactance X_S. Therefore, the PE model presented in [82] and [72] is used to represent such a generator. In other words, the generator is modeled as a PV bus behind the synchronous reactance as shown in Fig. 5.15(b). The specified P of the bus is still the generator's real power output, and the specified E is the maximum field voltage allowed for long-term operation. As it can be seen from the model shown in Fig. 5.15(b), the original PV bus (bus 1) now retreats to the bus 1'. Its effect is equivalent to an increase of the electrical distance from the generator to the system.

The PE modeling method has been implemented as follows. When a generator reaches its reactive limit, its field voltage (E_G in Fig. 5.15(b)) is first computed. A new bus (bus 1') is created and considered as a new PV bus with E_G as its voltage setting, and P as its power setting. Bus 1 is not a PV bus anymore. It should be treated as a network or load bus. Therefore, the

network should be modified for the purpose of the CCT application. As an example, bus 1 in Fig. 5.15(b) will be considered as a new network bus. This bus along with X_S will be moved into the network as shown in Fig. 5.15(c). The network impedance matrix and the transformation matrix are also modified. The CCT-related computations are then repeated for the modified network.

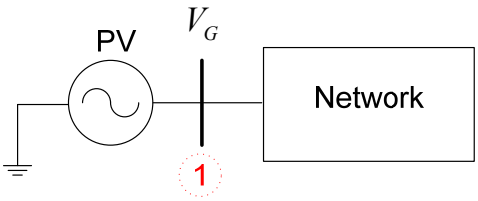

(a) PV model (before reaching the reactive limit)

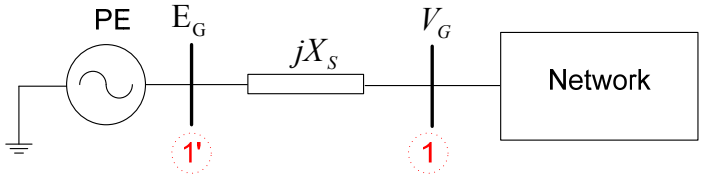

(b) PE model (after reaching the reactive limit)

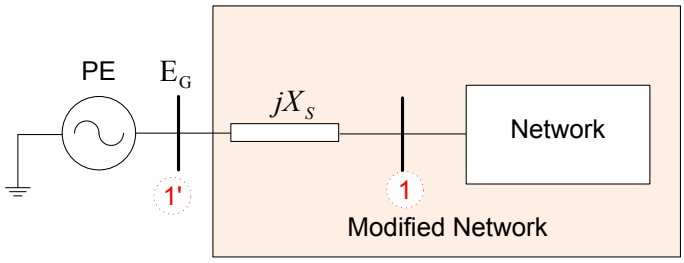

(c) Modified network

Fig. 5.15: Modeling of the generators reaching reactive power limits

By considering the above options, the CCT is applied to the base case, and the results are presented below.

5.2.2 Voltage Stability Margin

The first result is the maximum scaling factor. As highlighted in Fig. 5.14, the software results in "1.13" as the maximum scaling factor. This indicates that the voltage stability margin

of the system at the current operating conditions is %13. The total load level of the system is 10871.0 MW. Considering %13 margin, the total system load can be increased to 12284.23 MW.

According to Table 5.1, three areas in the system which have the highest load demands are Calgary, Edmonton, and Fort McMurray. One load bus is chosen in each of these areas, and its PV curve is plotted. The results are shown in Fig. 5.16. As this figure shows, the load in Edmonton is experiencing a high voltage drop as the system is scaled up. At the system nose point, its voltage is very low. Based on this figure, one may say that this bus and its associated area (Edmonton) is a relatively weak location in the system. This is to be further investigated in the next sections.

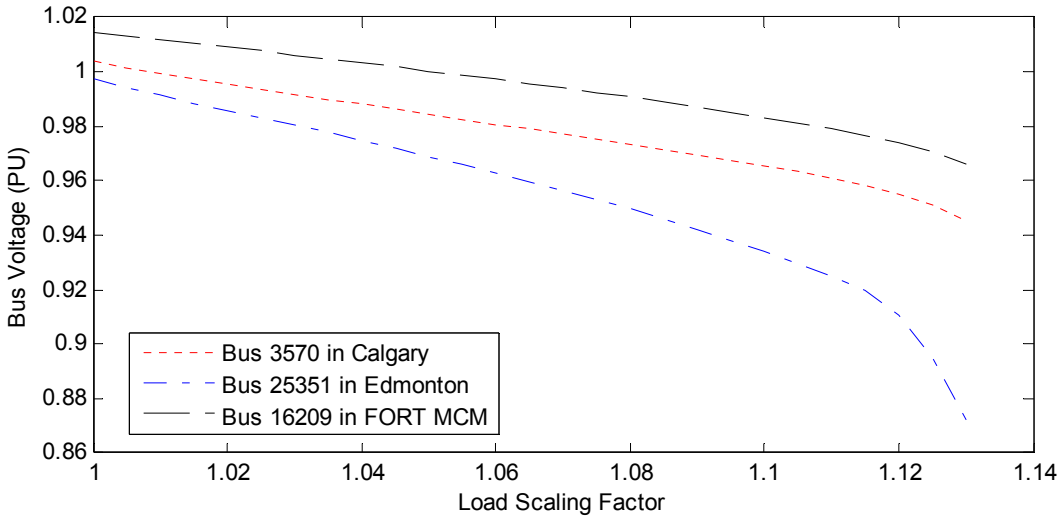

Fig. 5.16: PV curves observed at some key buses

5.2.3 Critical Channel Identification

The first 10 top channels determined by the software are shown in Table 5.2. Table 5.2 reveals that channel 90 is the critical channel in the system. After this channel, there are three channels (channels 573, 166, and 168) with very small powers (almost zero powers). If we want to analyze more than one critical channel, these three channels should not be taken into account as they may not reveal important information due to their small powers. The next critical channels would then be channels 58, 416, 43, and 25.

Table 5.2: The first 10 top channels

Rank	Channel No.	NVD (%)	Channel Power (p.u.)
1	90	20.805	0.25643
2	573	14.176	0
3	166	14.093	0.00001
4	168	13.751	0.00219
5	58	13.531	0.35869
6	416	12.520	1.08447
7	43	11.515	3.17435
8	25	11.194	29.15372
9	10	11.042	2.98697
10	17	10.819	12.79378

5.2.4 Critical Loads Identification

Considering channel 90 as the critical channel, the critical loads which have the highest contributions to this channel can be identified by the software. The first 20 critical loads are shown in Table 5.3. The load contributions are also visualized in Fig. 5.17. In this figure, all load buses are sorted based on their areas. Table 5.3 and Fig. 5.17 reveal that almost all the identified loads are from area 60 (Edmonton). The implication is that area 60 (Edmonton) is the weakest area in the system. This is consistent with what we expected before. As explained in Section 5.2.2, the load buses in Edmonton experience high voltage drops as the system goes close to the nose point. Moreover, Edmonton has high demands. So it seems reasonable that this area be the weakest area in the system.

Table 5.3: The first 20 top loads identified by the software for channel 90

Load rank	Load bus number	Area	Contribution to the critical channel (%)
1	25351	60	13.7
2	25352	60	13.2
3	25353	60	12.6
4	25331	60	11.0
5	25077	60	10.6
6	25292	60	3.6
7	25291	60	3.4
8	25343	60	2.9
9	25341	60	2.9

10	25056	60	2.8
11	25055	60	2.8
12	25051	60	2.8
13	25052	60	2.8
14	25293	60	2.8
15	25342	60	2.5
16	2357	60	1.8
17	4040	60	1.8
18	3040	60	1.8
19	4303	60	1.5
20	25198	60	1.3

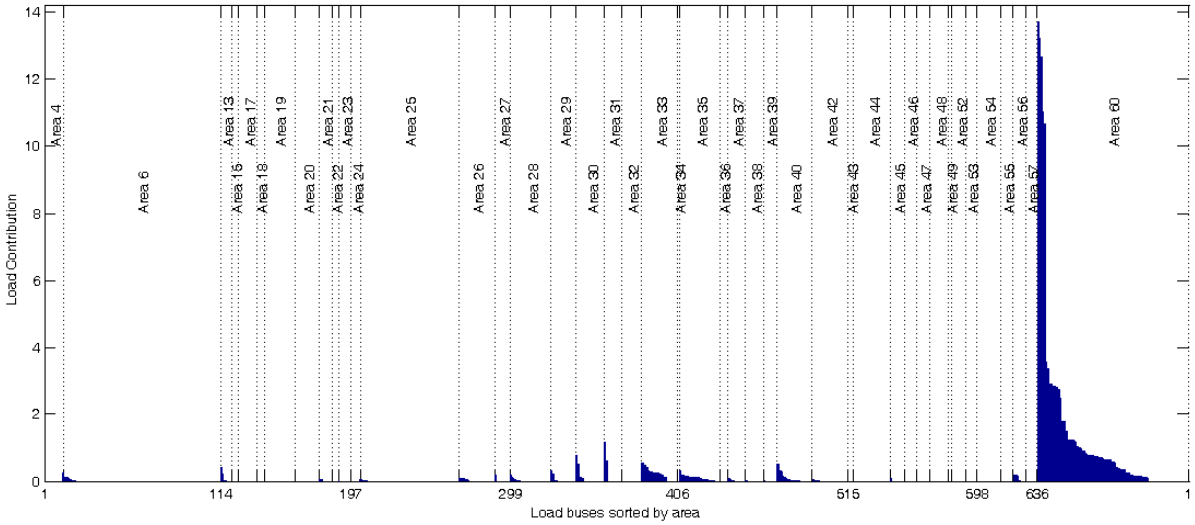

Fig. 5.17: Contributions of loads to channel 90

It is sometimes beneficial to consider other critical channels, and obtain the corresponding critical load buses. It was shown above that by using the first critical channel (channel 90), area 60 (Edmonton) is identified as the critical area. One may notice from Fig. 5.17 that channel 90 is a local channel which mostly includes loads from area 60. This was expected as this channel does not carry a large amount of power (see Table 5.2). If we are interested to find other weak areas, other critical channels need to be considered in the analyses.

According to Table 5.2, channels 573, 166, and 168 are the next top rank channels. However, their powers are almost zero. Therefore, these channels should be filtered out. The next critical channels would then be channels 58, 416, 43, and 25. The critical buses associated with these channels are shown in Table 5.4. Fig. 5.18-Fig. 5.21 visualize the load contributions

to these channels. The loads have been sorted based on their areas in these figures. Based on Table 5.4, and Fig. 5.18-Fig. 5.21, the following results are noticed:

- Area 60 (Edmonton) is identified again as the critical area when the second critical channel (channel 58) is considered.
- When the third and the fourth critical channels (channels 416 and 43) are considered, area 25 (Fort McMurray) is identified as the critical area. As mentioned before and shown in Table 5.1, area 25 is among the three areas with the highest demands. Therefore, it seems reasonable to have this area as the second critical area in the system.
- The next critical channel (channel 25) will result in area 6 (Calgary) as the critical load area. This area is also among the first three areas which have the highest demands. Another point about this channel is that as seen in Fig. 5.21, this channel contains information about many loads much more than previous channels. This implies that this channel can be considered as a system-wide channel, whereas the previous channels were local channels reflecting one or a few areas of the system. This was expected since channel 25 carries a large amount of power according to Table 5.2, whereas the other channels carry much lower powers.

Table 5.4: The first 10 top loads identified by the software for other critical channels

Load rank	Channel 58		Channel 416		Channel 43		Channel 25	
	Load bus	Area	Load bus	Area	Load bus	Area	Load bus	Area
1	25323	60	19205	25	179	25	3570	6
2	25321	60	19206	25	18293	25	4556	6
3	25322	60	17218	25	19222	25	2242	46
4	25331	60	19218	25	19227	25	4242	46
5	25077	60	5269	25	19288	25	4569	6
6	25351	60	3269	25	18224	25	4587	6
7	25352	60	15233	25	19224	25	3554	6
8	25353	60	666	25	19293	25	4972	46
9	25282	60	1221	25	19287	25	4992	6
10	25281	60	14236	25	19622	25	3567	6

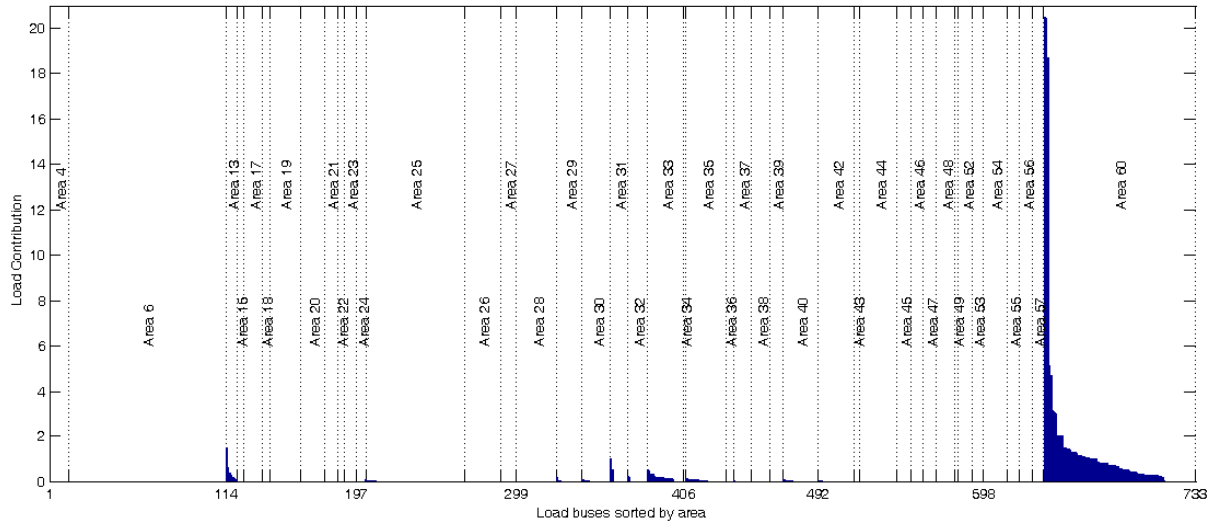

Fig. 5.18: Contributions of loads to channel 58

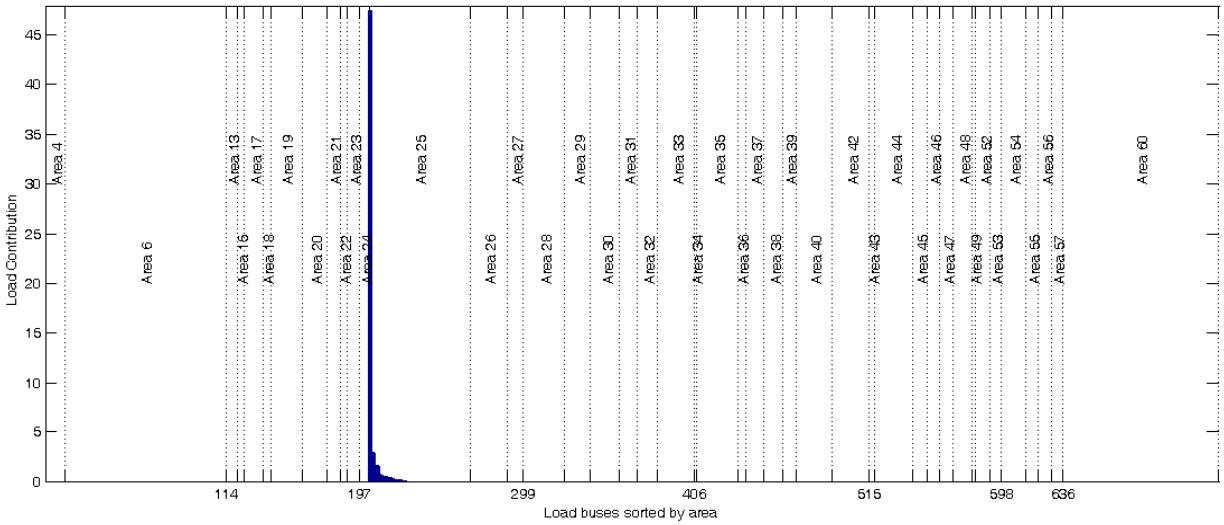

Fig. 5.19: Contributions of loads to channel 416

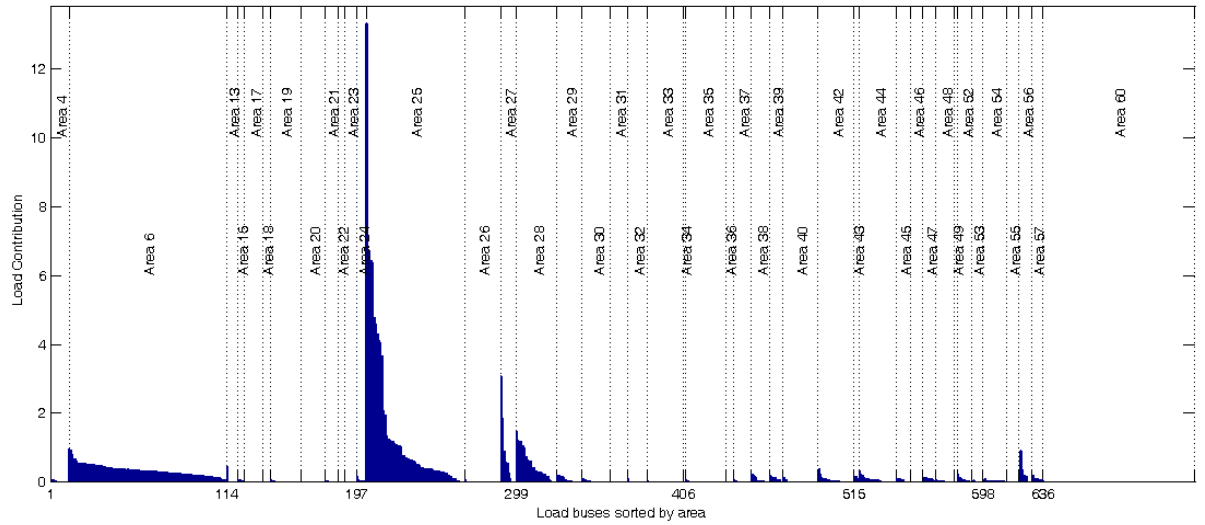

Fig. 5.20: Contributions of loads to channel 43

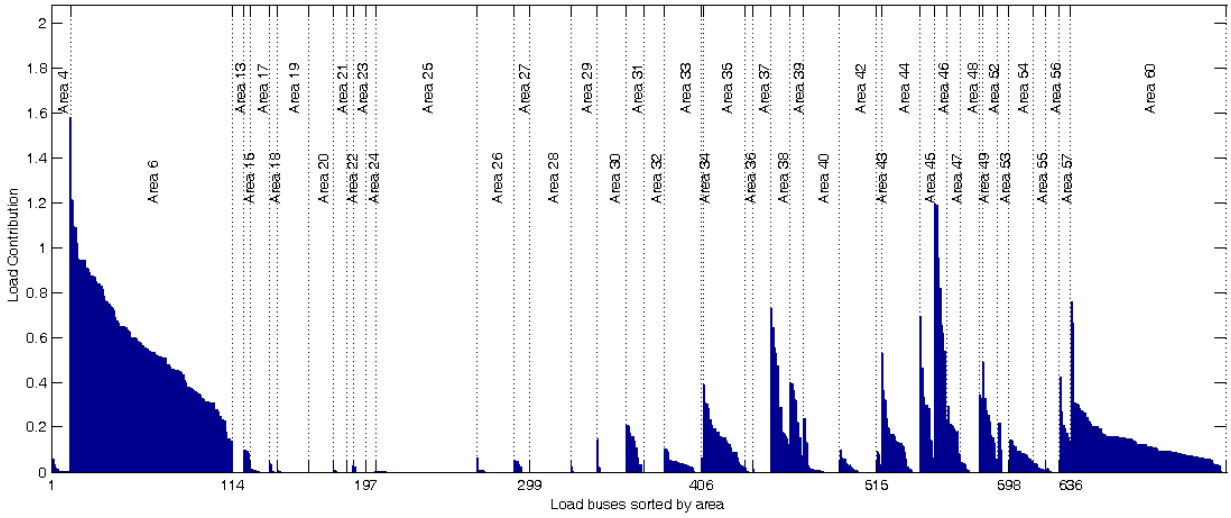

Fig. 5.21: Contributions of loads to channel 25

5.2.5 Critical Generators Identification

Table 5.5 shows the first 20 top generators identified by the software for channel 90. Fig. 5.22 illustrates the contributions of all the system generators to the critical channel. According to the table and the figure, most of the top rank generators are in area 40 (Lake Wabamun). As discussed before, and shown in Table 5.1, area 40 has the highest generation in the whole system. This area generates 4851.5 MW which is equal to %43 of all generation in the system.

This reveals that this area is a very important area in terms of generation, and it seems reasonable that this area has been identified by the software as the critical generation area.

Table 5.5: The first 20 top generators identified by the software for channel 90

Generator rank	Generator bus number	Area	Contribution
1	403	40	7.597
2	490	40	6.991
3	424	40	6.586
4	492	40	5.405
5	491	40	5.405
6	422	40	5.393
7	2031	33	4.412
8	345	40	3.826
9	342	40	3.812
10	350	40	3.803
11	129	40	3.434
12	130	40	3.362
13	3069	60	3.179
14	338	40	3.082
15	2030	33	2.750
16	625	33	2.616
17	626	33	2.567
18	627	33	2.260
19	3043	33	2.021
20	4043	33	2.007

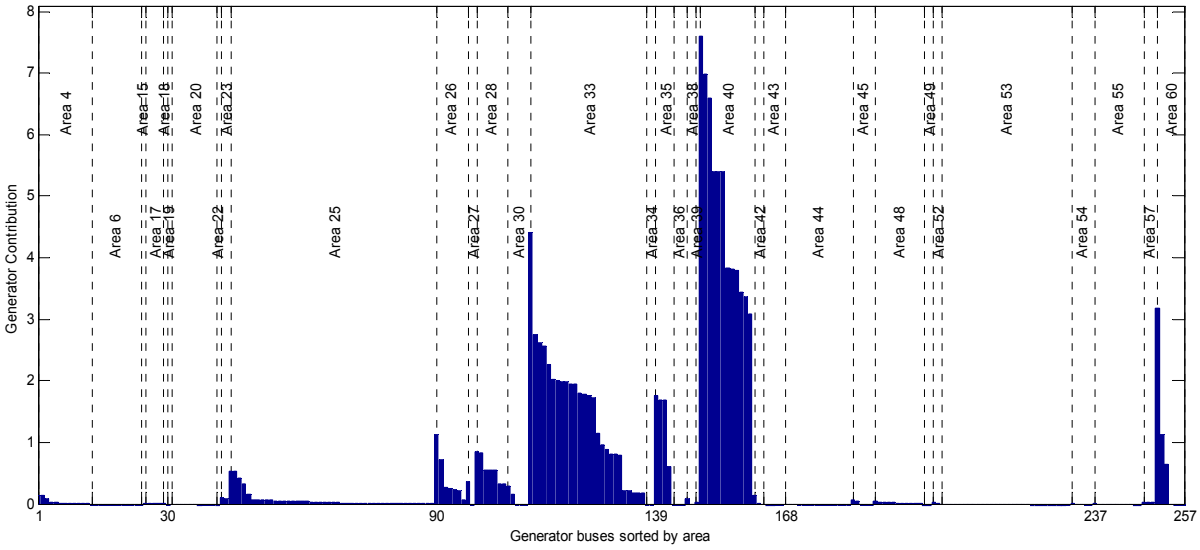

Fig. 5.22: Contributions of generators to channel 90

The first top 10 critical generators associated with other critical channels are shown in Table 5.6. Fig. 5.23-Fig. 5.26 show the contributions of generators to those critical channels. According to Table 5.6 and Fig. 5.23-Fig. 5.26, the following results are obtained:

- Channel 58 leads to area 40 (Lake Wabamun) as the critical generation area. This is the same as the first critical channel (channel 90). As shown in the previous section, these two channels (channels 90 and 58) also lead to the same area (area 60) as the critical load area. These results totally make sense since area 40 is the largest generation area which is geographically close to area 60.
- Channels 416 and 43 lead to area 25 (Fort McMurray) as the critical generation area. These two channels have previously led to the same area (area 25) as the critical load. Again the results are reasonable since area 25 is a big load area with high generation.
- Channel 25 will result in area 6 (Calgary) as the critical generation area. This channel has previously led to the same area (area 6) as the critical load. Another point about this channel is that as seen in Fig. 5.26, this channels contains information about more generators compared to the previous channels. This is consistent with what was observed for the critical loads, showing that channel 25 is a wide-area channel.

The above information has been visualized in Fig. 5.27. This figure clearly shows the critical areas associated with the critical channels.

Table 5.6: The first 10 top generators identified by the software for other critical channels

Generator rank	Channel 58		Channel 416		Channel 43		Channel 25	
	Gen bus	Area	Gen bus	Area	Gen bus	Area	Gen bus	Area
1	403,	40	18207	25	10605	25	773	6
2	26516	60	18206	25	18274	25	775	6
3	27516	60	10605	25	4760	25	774	6
4	490	40	19208	25	18206	25	4187	6
5	491	40	18208	25	2392	27	1520	15
6	492	40	19297	25	19208,	25	183	44
7	424	40	18297	25	18208	25	4502	6
8	25516	60	3273	25	2405	25	3501	6
9	422	40	18223	25	70112	25	2501	6
10	3069	60	18274	25	18302	28	4501	6

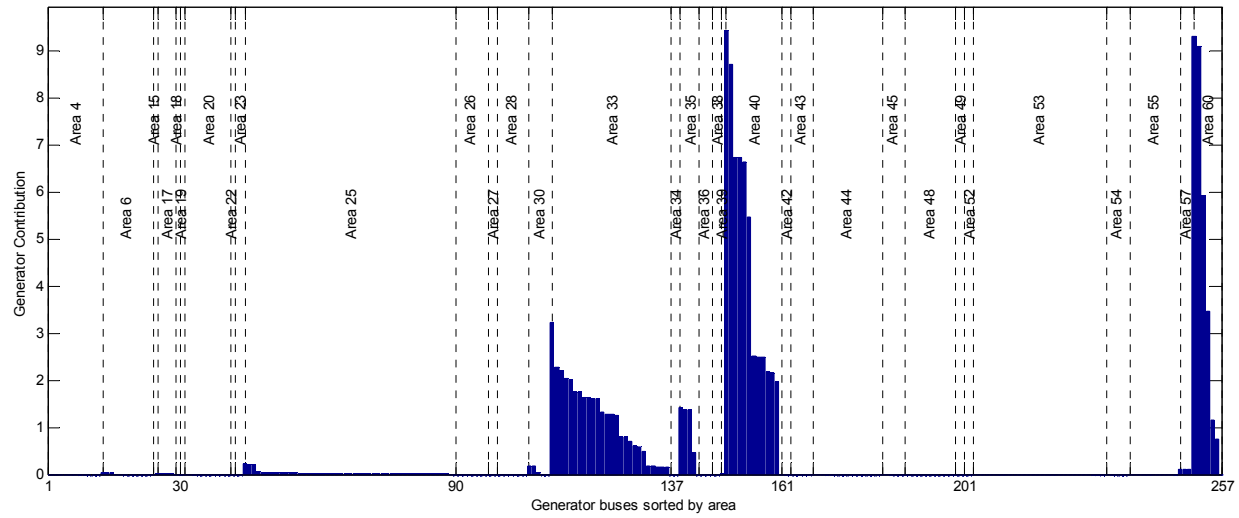

Fig. 5.23: Contributions of generators to channel 58

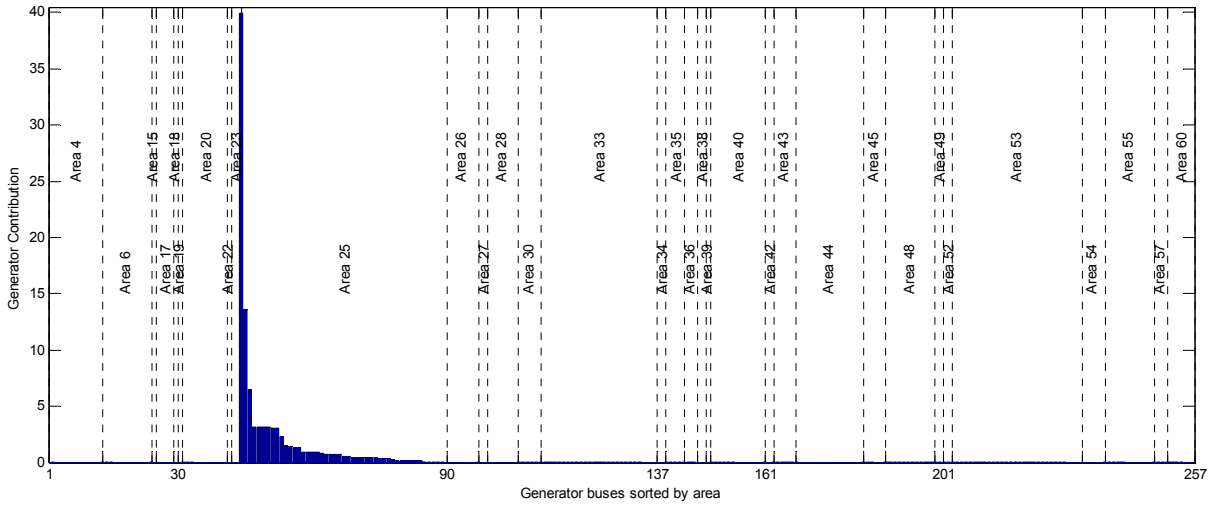

Fig. 5.24: Contributions of generators to channel 416

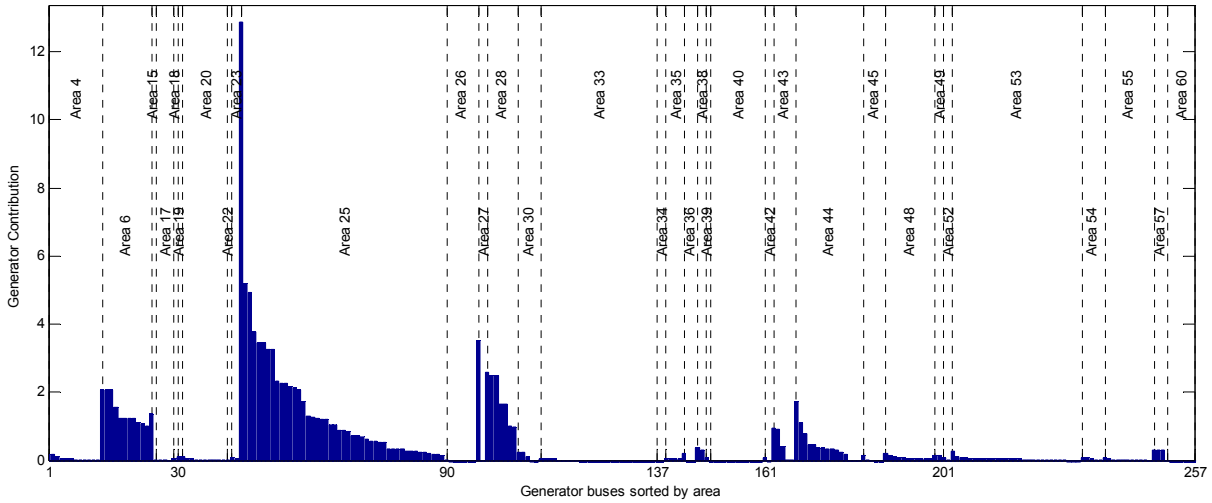

Fig. 5.25: Contributions of generators to channel 43

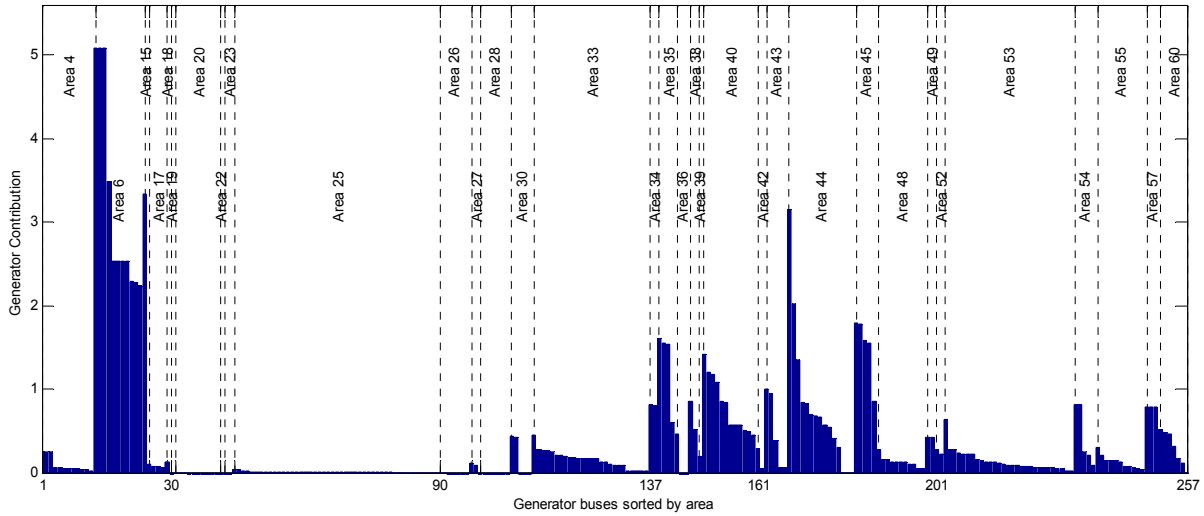

Fig. 5.26: Contributions of generators to channel 25

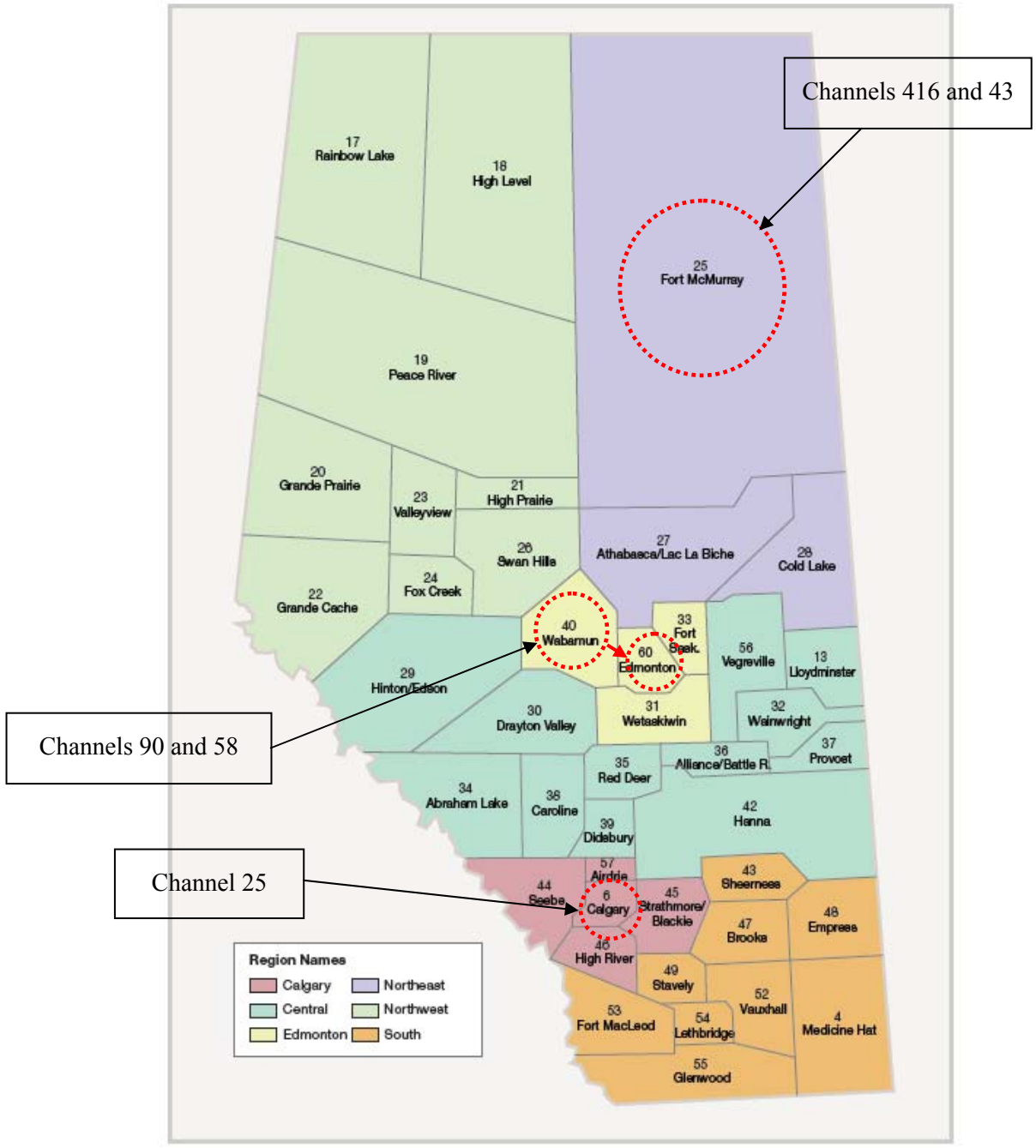

Fig. 5.27: The AIES critical areas

5.2.6 Critical Line Identification

Using the software, the following transmission path is identified as the critical transmission path (CTP).

CTP: 25351- 535 – 507 – 5506 – 506 – 518 – 128 – 258 – 510 - 403.

The consequent buses of the CTP are shown in Table 5.7. For each bus, its area and voltage level are also shown in the table. It can be seen in this table that the critical transmission path starts from the critical generator (bus 403) and ends in the critical load (bus 25351).

Table 5.7: The critical transmission path identified by the software

Consequent Bus Numbers	Bus Name	Area	Voltage level (kV)
25351	GARN 1 9	60	14.4
535	GARNEAU8	60	69
507	ROSSDALE	60	69
5506	BELLTX1	50	69
506	BELLAMY4	50	240
518	ARGYLL E	50	240
128	ELLERSLI	50	240
258	ELLERSLI	50	500
510	KEEPHIL3	40	500
403	KEEP#3GN	40	22

Among different segments of the above CTP, the software leads to the first branch i.e. 25351-535 as the critical branch. This branch is a transformer. If we want to define the critical transmission line, we need to go to the next critical segment which is 510-258. As seen in Table 5.7, this transmission line is from area 40 to area 50, and its voltage level is 500 kV. A part of system to which areas 40, 50, and 60 belong is illustrated in Fig. 5.28. The critical transmission line can be seen in this figure.

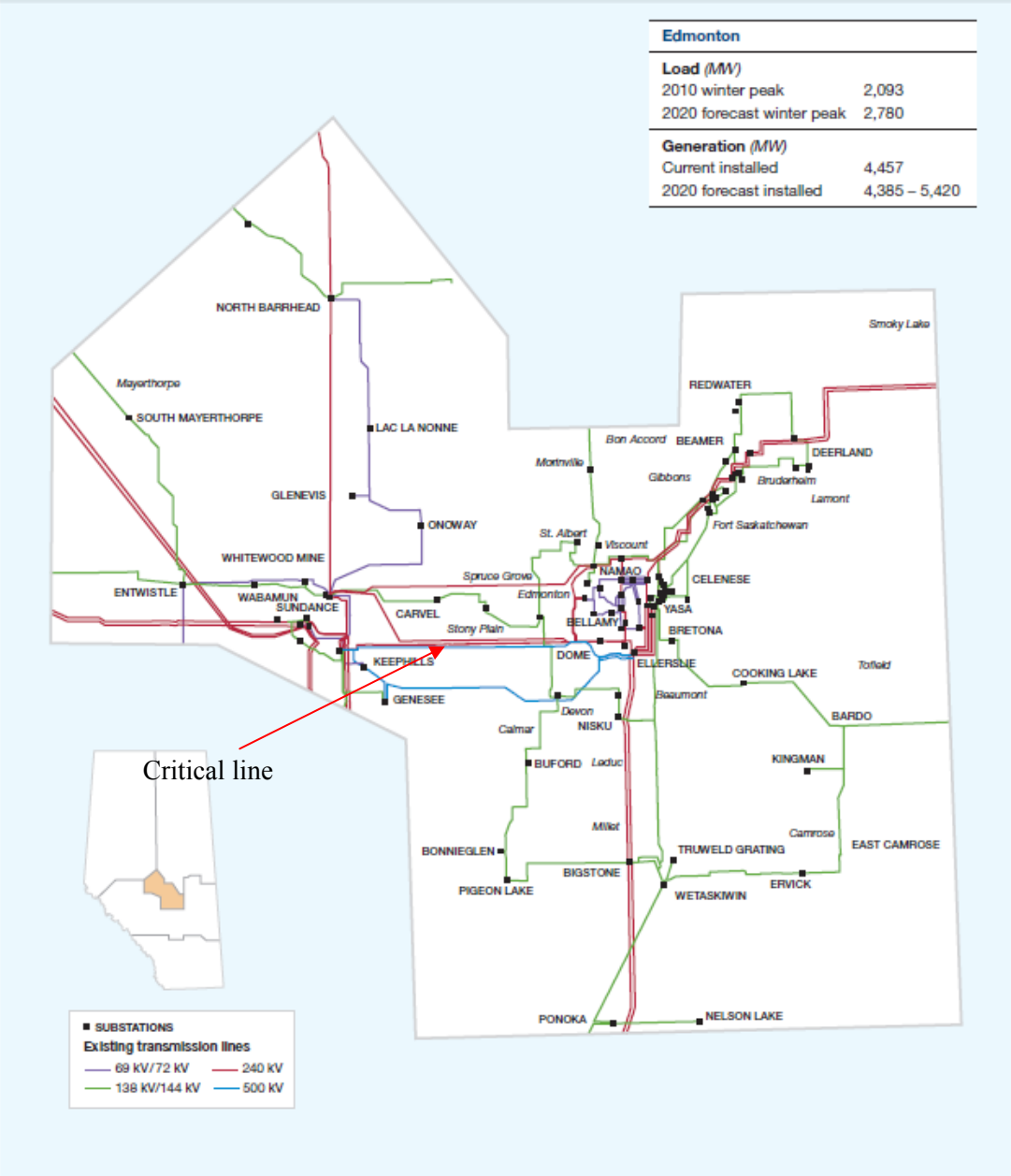

Fig. 5.28: Single-line diagram of a part of the system (around Edmonton)

5.3 Conclusions

The performance of the Channel Component Transform when it is applied to a large system was investigated in this chapter. For this purpose, the Alberta Integrated Electric System (AIES) which is a 2038-bus system was considered as the case study. The CCT was applied to this system and its voltage stability characteristics were analyzed using the proposed methods. All the obtained results were also verified using verification methods.

A software package has also been developed based on the CCT to analyze the voltage stability in power systems. The developed software works on the PSS/E platform. This chapter showed how this software could be used for the voltage stability analysis. For this purpose, a planning representative of the AIES was considered as a case study. Using the developed program, different aspects of voltage stability were then analyzed in this system. The results showed that the developed software can be easily used to perform a complete and detailed voltage stability analysis.

Chapter 6: Application of CCT to Shunt Compensation Studies

The information obtained by the voltage stability analysis can be used to manage proper countermeasures to improve the stability of the system. For this purpose, a variety of countermeasures can be taken into account [51]. Among them, reactive power planning (RPP) is one of the most effective ones since voltage collapse is typically associated with the reactive power demands of loads not being met because of limitations on the production and transmission of reactive power [11]. One of the most effective and popular types of RPP is the shunt compensation. The shunt compensation involves the installation of Var sources such as capacitor banks, static Var compensators (SVC), and static compensators (STATCOM).

When planning a shunt compensation strategy, the location and the amount of reactive supports should be determined. In the literature, this task is usually performed by solving a multi-objective optimization problem [52]. However, solving this optimization problem is a very difficult task which causes several problems especially in large power systems.

The aim of this chapter is to overcome this challenge by proposing a simple and practical approach. For this purpose, the channel components transform is used and a method for single-location shunt compensation is proposed first. The proposed method consists of three main steps:

1- Find the best location

2- Obtain an estimation for the amount of shunt compensation

3- Obtain an accurate amount by using an iterative method.

The details of the proposed algorithms are presented in this chapter. The proposed method is also applied to several test systems and the results are investigated. Moreover, the proposed method for single-location shunt compensation is extended to multi-location compensation and the obtained simulation results are presented in this report. Note that the proposed strategy is for

the shunt compensation using capacitor banks, however, it can be modified and used for any other kind of compensation such as with using SVCs.

6.1 Proposed method for single-location shunt compensation

The overall flowchart of the proposed method is illustrated in Fig. 6.1. As this figure shows, the proposed method consists of three steps. These steps are described in detail in the following sub-sections.

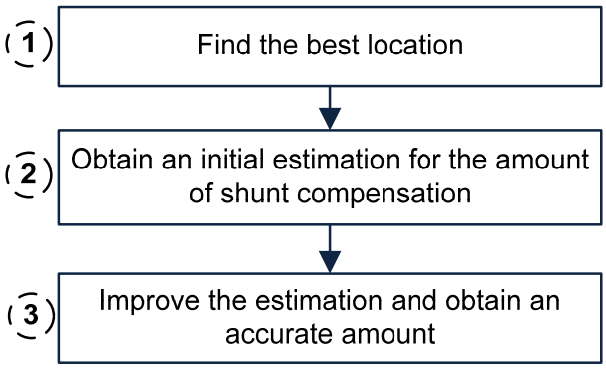

Fig. 6.1: Overall procedure of the proposed method

6.1.1 Find the best location

The best location is the location where adding a shunt compensation leads to the highest improve in the stability margin. We have already shown that CCT can identify the critical bus which is the weakest location in the system. The weakest bus seems to be the best location for shunt compensation.

To verify this claim, the sensitivity of the stability margin with respect to adding reactive support at different locations can be used. For this purpose, a small amount of reactive support is added to each load one at a time, and the resulting increase in the stability margin is computed. This is done for all the buses, and they are ranked based on their associated increases in the stability margin. As an example, Fig. 6.2 shows the result for the IEEE 57-bus system. As this figure shows, adding reactive support at bus 31 leads to the highest increase in the stability margin. In other words, bus 31 is the best location for shunt compensation. On the other hand, as shown before, this bus is the critical bus identified by the CCT.

The above study has also been performed for all the other test systems. The results are summarized in Table 6.1. According to this table, the critical bus identified by the CCT is always verified as the most effective location for adding reactive support. Therefore, the critical bus is obtained using the CCT and this bus is considered as the best location for the shunt compensation.

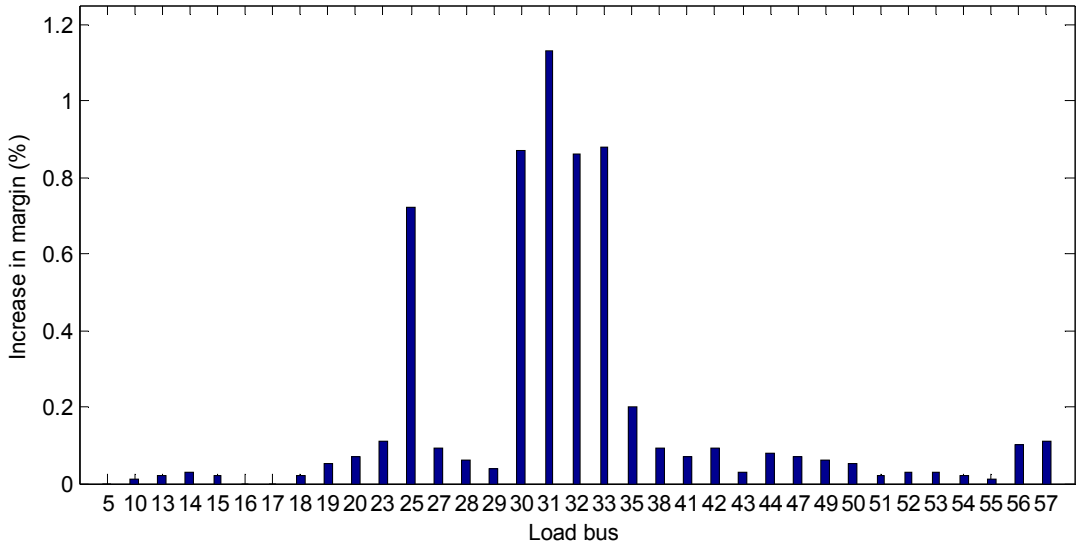

Fig. 6.2: Sensitivity of margin with respect to reactive support at different buses

Table 6.1: Comparison of the critical bus with the most effective location for the reactive support

System	Critical bus (identified by CCT)	The most effective location for reactive support (by using the sensitivity analysis)
WECC 9-bus	9	9
30-bus from [70]	8	8
IEEE 30-bus	30	30
IEEE 57-bus	31	31

6.1.2 Obtain an initial estimation for the amount of shunt compensation

Assume that the system has a low margin and the aim is to increase the margin. We know that the low stability margin of the system corresponds to the low stability margin of the critical channel. In other words, by increasing the margin of the critical channel, we can increase the system margin. Denoting the current system margin as *Initial_margin* and the required system margin as *Desired_margin*, the required increase in the margin will be

$$Margin\_increase = Desired\_margin - Initial\_margin \tag{6.1}$$

The idea is to improve the system margin by making an increase of *Margin_increase* in the critical channel's margin. This increase is to be made by adding a reactive support to the critical's channel load. The amount of this reactive support needs to be determined first.

Assume that the i^{th} channel is the critical channel. The maximum channel power, and the channel margin can be determined using the following equations.

$$S_{\max} = \frac{|F_i|^2 \left[|\lambda_i| - (X_i \sin\theta_i + R_i \cos\theta_i) \right]}{2\left[X_i \cos\theta_i - R_i \sin\theta_i \right]^2} \tag{6.2}$$

$$Channel\ margin = \frac{S_{\max} - S_i}{S_i} \times 100 \tag{6.3}$$

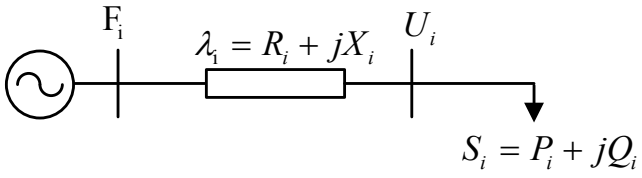

Fig. 6.3: The i^{th} channel

We want to make an increase of *Margin_increase* in the critical channel's margin by changing the channel reactive power Q_i while the channel active power P_i remains constant. Therefore, the following equality needs to be solved. In this equality, only the channel load angle θ is unknown and all other parameters which are known remain constant.

$$\frac{\frac{|F_i|^2\left[|\lambda_i|-(X_i\sin\theta_{new}+R_i\cos\theta_{new})\right]}{2\left[X_i\cos\theta_{new}-R_i\sin\theta_{new}\right]^2}-|P_i+jP_i\tan\theta_{new}|}{|P_i+jP_i\tan\theta_{new}|}\times 100 = Channel\ \ m\arg in + m\arg in\_increase \tag{6.4}$$

By solving the above equation, the required channel load angle θ_{new} is determined. Having this load angle, the new value of the channel reactive power and the required reactive support are obtained as follows.

$$Q_{new} = P_i\tan\theta_{new} \tag{6.5}$$

$$Q_{support} = Q_i - Q_{new} \tag{6.6}$$

The idea is to put a capacitor at the critical bus in order to inject the reactive power of $Q_{support}$ into the critical bus. The amount of capacitor is obtained as follows. The reactive power of the critical load Q_{Load} is changed to Q_{Load}-$Q_{support}$ first. The power flow is then performed with using the new value of the critical load's power and the voltage of the critical bus V is obtained. The amount of capacitor is then calculated using the following equation.

$$B_{estimated} = \frac{Q\,support}{|V|^2} \tag{6.7}$$

The proposed method can be summarized as the procedure shown in Fig. 6.4.

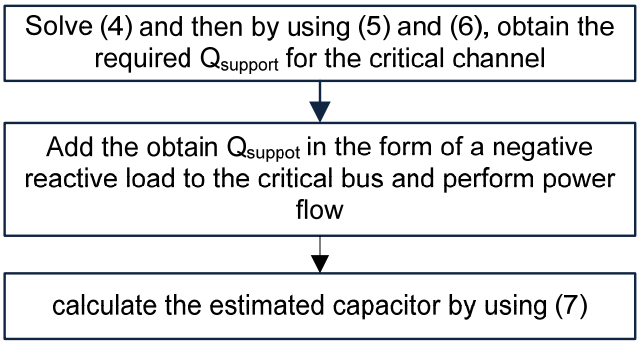

Fig. 6.4: Summary of the procedure to find an initial estimation for the capacitor

In order to check the effect of the estimated capacitor on increasing the system margin, the estimated capacitor is placed at the critical bus and using the CPF, the system margin is computed. Comparison of the obtained margin with the desired one can show how effective the estimated capacitor is.

This procedure has been applied to three test systems and the results are shown in Tables 6.2-4. Note that in all these case studies, the system is firstly stressed so that it has a low margin. Then the capacitor is estimated in order to increase the margin to %5. As these tables show, the obtained capacitor acts as an acceptable estimation which increases the system margin to a value close to the desired one.

Table 6.2: Results in WECC 9-bus system

Initial Margin (%)	Desired margin (%)	Location (critical bus)	Estimated susceptance (injected MVAr at V=1p.u)	Margin after compensation (%)
1.99	5	9	47.42	4.72

Table 6.3: Results in IEEE 30-bus system

Initial Margin (%)	Desired margin (%)	Location (critical bus)	Estimated susceptance (injected MVAr at V=1p.u)	Margin after compensation (%)
1	5	30	20.639	6.40

Table 6.4: Results in IEEE 57-bus system

Initial Margin (%)	Desired margin (%)	Location (critical bus)	Estimated susceptance (injected MVAr at V=1p.u)	Margin after compensation (%)
1.72	5	31	9.568	5.349

6.1.3 Improve the estimation and find an accurate amount

As seen in the previous step, the estimated capacitor increases the system margin to a value close to the desired margin. In this step, we want to improve the estimation so that the system margin would be exactly the same as the desired one. For this purpose, an iterative method is proposed.

Lets denote:

- M_0: the system margin without any compensation
- B_1: the susceptance of the estimated capacitor
- M_1: the system margin after placing the estimated capacitor
- B_k (k =2, 3, ..): the susceptance of the capacitor obtained at the iteration (k-1)
- M_k (k =2, 3, ..): the system margin after placing the capacitor obtained at the iteration (k-1)

The idea is to approximate the M-B curve (margin versus susceptance) as a linear curve and find a better value for B. In this approach, by using M_0, M_1, and B_1, a linear curve can be plotted. Then, according to the desired margin, we would have either Fig. 6.5(a) or Fig. 6.5(b).

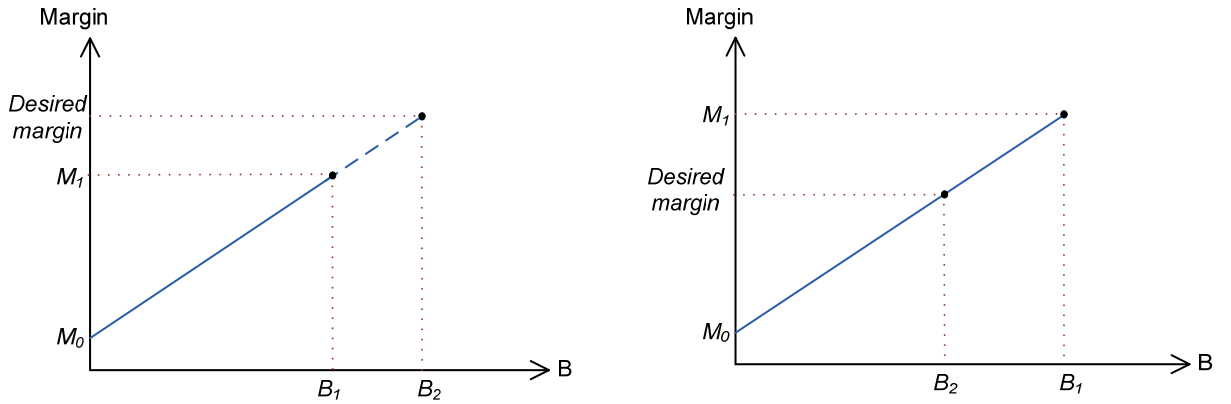

(a) when the estimated margin in lower than the desired one

(b) when the estimated margin in higher than the desired one

Fig. 6.5: Approximation of the M-B curve with a linear curve

According to Fig. 6.5, in the first iteration of the proposed method, the value of the new capacitor is calculated using the following equation.

$$B_2 = \frac{B_1}{M_1 - M_0}(M_{des} - M_1) + B_1 \tag{6.8}$$

where M_{des} is the desired margin.

After the calculation of B_2, this capacitor is placed at the critical bus and CPF is performed again. As a result, a new system margin (M_2) is obtained. If this margin is still different from the desired one, the next iteration is performed and a new value is calculated for the capacitor. This process is repeated until the obtained margin is close enough to the required margin. The general equation for obtaining the capacitor at the k^{th} iteration is as follows.

$$B_{k+1} = \frac{B_k - B_{k-1}}{M_k - M_{k-1}}(M_{des} - M_k) + B_k \tag{6.9}$$

6.2 Case study results

In this section, the proposed method is applied to three test systems and the obtained results are presented.

A) WECC 9-bus system

The first case study is the WECC 9-bus system. Table 6.5 shows the results for this system. As this table shows, the proposed iterative-based method finds an accurate value in the first iteration. Fig. 6.6 illustrates the system margin variations in different conditions. Note that every condition is specified in Table 6.5

Table 6.5: Results in WECC 9-bus system

Condition No.	Condition	B (injected MVAr at V=1p.u)	Margin (%)
0	normal conditions	0	1.99
1	initial estimation	47.42	4.720
2	1st iteration of the iterative method	52.287	5.00

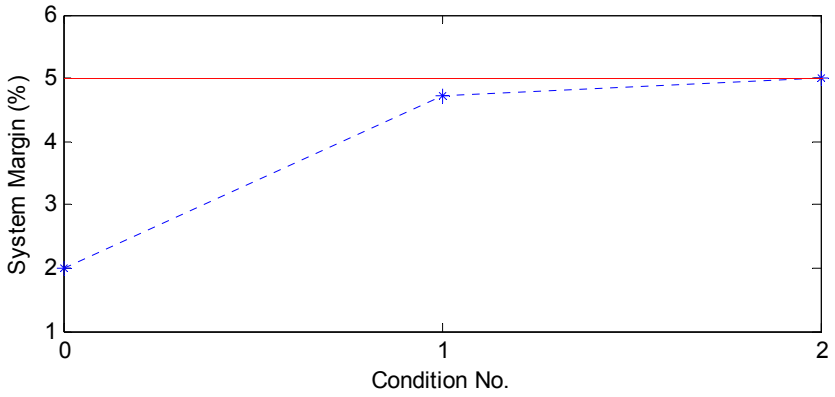

Fig. 6.6: System margin variation in different steps of the method

B) IEEE 30-bus system

The second case study is the IEEE 30-bus system. Table 6.6 shows the results for this system. Again, as seen in this table, the proposed iterative-based method finds an accurate value in the first iteration. Also, Fig. 6.7 illustrates the system margin variations in different conditions.

Table 6.6: Results in IEEE 30-bus system

Condition No.	Condition	B (injected MVAr at V=1p.u)	Margin (%)
0	normal conditions	0	1
1	initial estimation	20.639	6.4
2	1st iteration of the iterative method	15.297	5.00

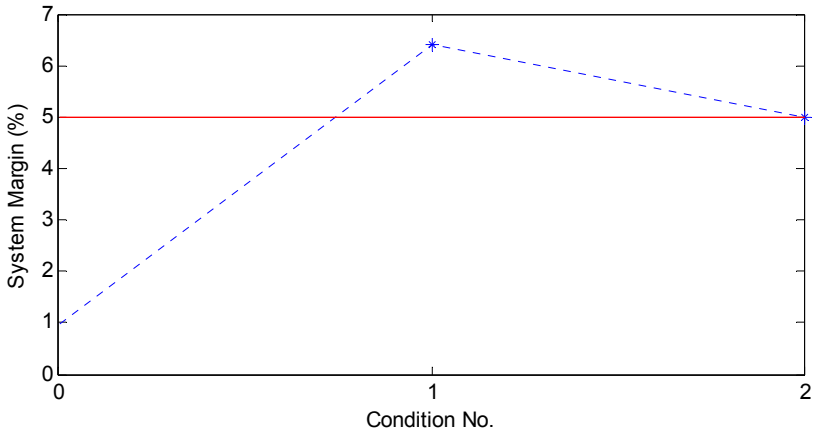

Fig. 6.7: System margin variation in different steps of the method

C) IEEE 57-bus

The last case study is the IEEE 57-bus system. Table 6.7 shows the results for this system. As seen in this table, the proposed iterative-based method finds an accurate value after two iterations. Also, Fig. 6.8 illustrates the system margin variations in different conditions.

Table 6.7: Results in IEEE 57-bus system

Condition No.	Condition	B (injected MVAr at V=1p.u)	Margin (%)
0	normal conditions	0	1.720
1	initial estimation	9.568	5.349
2	1st iteration of the iterative method	8.647	4.973
3	2nd iteration of the iterative method	8.713	5

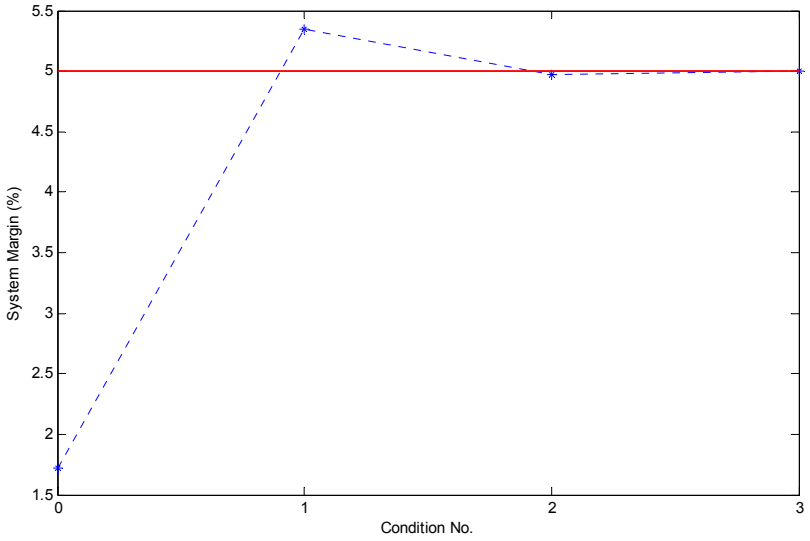

Fig. 6.8: System margin variation in different steps of the method

6.3 Extension to Multi-location Shunt Compensation

The proposed method for determining the location and amount of shunt compensation can be extended to multi-location cases. For this purpose, a maximum amount for the capacitor bank is considered and the extension is performed based on the following assumption: when a location is selected, we are interested to place a capacitor bank big enough so that either the required margin be achieved or the maximum sized be reached. This is a reasonable assumption since due to the costs associated with the installation and maintenance of each capacitor bank, the number of capacitors needs to be minimised. Considering this assumption the following strategy is proposed.

The proposed method of the single-location compensation is applied to the system first. If the obtained capacitor has a size smaller than the maximum size, this means that single-location compensation is effective enough and there is no need to place more capacitors. Otherwise, if the size of the capacitor is larger than the maximum size, the capacitor is fixed at the maximum size. The proposed method is then applied again. The critical load is found. Then, we will have one of the following cases:

1. The critical bus is different from the one obtained in the previous iteration. In this case, the method used for the first location is exactly followed again to determine the amount of the capacitor at the second location (the new critical bus).
2. The critical bus is still the same bus. In this case, the second critical bus is chosen as the best location. The method proposed for single-location is then applied but with a little modification. After $Q_{support}$ was obtained from (6.6), it should be modified to the one shown in (6.10). This modified $Q_{support}$ is then injected to the selected location and the rest of the method is performed without any change. The reason for this modification is that when injecting reactive power to a location which is not the critical bus, more reactive power needs to be injected in order to make a specific increase in the reactive power of the critical channel.

$$\text{Modified } Q_{support} = Q_{support} \times \frac{Cont_1}{Cont_2} \tag{6.10}$$

where $Cont_1$ and $Cont_2$ are the contributions of the first and second critical buses to the critical channel.

After a capacitor is determined for the second location, its size is checked. If the size is larger than the maximum size, the capacitor is fixed at the maximum size and the same procedure is used again to find the capacitor for the third location. This process is repeated until the required margin is achieved without violating the maxim size criterion. In every iteration of this process, the modified $Q_{support}$ is found using the following equation.

$$\text{Modified } Q_{support} = Q_{support} \times \frac{Cont_1}{Cont_k} \tag{6.11}$$

where k is the rank of the bus at which the capacitor is going to be installed.

The IEEE 30-bus system is considered as the case study. The maximum size of each capacitor is considered as 10 MVAr (injected at V=1 p.u.) and the proposed method is applied to this case study. As Table 6.6 showed before, by using the single-location method, a capacitor with the size of 15.297 MVAr should be placed at bus 30. Since the size is larger than the maximum size, the capacitor is fixed at the maximum size (10 MVAr) and the procedure is repeated for the second location. The results show that the critical bus is still bus 30. Therefore, the second critical bus which is bus 21 is selected as the best location. For this location, the proposed procedure results in the following table.

Table 6.8: Results in IEEE 30-bus system for the second location

Condition No.	Condition	B (injected MVAr at V=1p.u)	Margin (%)
0	normal conditions	0	3.601
1	initial estimation	14.862	4.745
2	1st iteration of the iterative method	18.179	5.00

As seen in this table, the obtained capacitor is again larger than the maximum one. So the capacitor at bus 21 is fixed to 10 MVAr and the procedure is repeated. The third critical bus which is bus 24 is selected as the best location for the third capacitor. The results for this location are presented in the following table.

Table 6.9: Results in IEEE 30-bus system for the third location

Condition No.	Condition	B (injected MVAr at V=1p.u)	Margin (%)
0	normal conditions	0	4.369
1	initial estimation	8.580	5.325
2	1st iteration of the iterative method	5.662	5.00

Since the capacitor size is smaller than the maximum size, there is no need to continue the procedure. In other words, the shunt compensation planning has been achieved. The overall results are shown in the following table.

Table 6.10: Overall results for IEEE 30-bus system when the maximum size is 10 MVAr

Location (bus no.)	B (injected MVAr at V=1p.u)
30	10
21	10
24	5.662

Comparison of the above table with Table 6.6 reveals that the required capacitor when it is placed at the critical bus is smaller than the sum of the required capacitors placed at different locations. This is consistent with what was expected since the critical bus is the best location for the shunt compensation.

6.4 Conclusions

In this chapter, a procedure based on channel components transform was proposed for shunt compensation in order to increase the stability margin of the system. In the proposed procedure, the best location is chosen based on the bus ranking results. An initial estimation for the amount of the capacitor is then obtained according to the critical channel's margin. The estimated value is then improved using an iterative method. The case study results verified the proposed method. The results also showed that the estimated value is very close to the accurate value and as a result, the iterative method needs to be performed for only a couple of iteration. The proposed method was also extended to the multi-location shunt compensation and using a case study, the proposed approach was investigated.

Chapter 7: Online Voltage Stability Monitoring Using CCT

This chapter aims to propose a wide-area scheme for the online voltage stability monitoring and analysis based on the proposed CCT-based framework. For this purpose, a practical implementation procedure will be proposed. The proposed procedure will be based on the current technologies available in power systems. These technologies mainly consist of Phasor Measurements Units (PMUs), and Supervisory Control and Data Acquisition (SCADA). A methodology for optimal placement of PMUs will also be proposed in order to minimize the number of required PMUs and as a result make the implementation procedure practical. Note that the proposed monitoring scheme may be changed and used even if PMU is not available at all. In this case, the SCADA data can be used to perform an online power flow. The power flow results may then be used instead of PMU data in the proposed scheme.

7.1 The Proposed Scheme

The main purpose of the CCT is to transform the power system into channel circuits and then extract useful information by monitoring the channel circuits. For this purpose, two tasks should be done:

1. Perform the eigen-decomposition on the impedance matrix [Z] and obtain channel impedances [Λ] and transformation matrix [T]. This can be done by using the network admittance matrix which is available from SCADA.
2. Obtain the channel quantities i.e. channel source voltages [F_{eq}], channel voltages [U], and channel currents [J] by using the generator bus voltages [E], load bus voltages and currents [V], and [I]. [E], [V], and [I] can be extracted from PMUs data, and as a result the channel quantities can be obtained and monitored online.

Therefore, the procedure shown in Fig. 7.1 can be used for the online application of the proposed framework. This procedure is run continuously, say, once for every 5 seconds. Assuming an outage event occurs, the scheme will work as follows

- Gather the network admittance matrix *Y* from SCADA. At the same time, the control devices will be considered in the equivalent network. For instance, the OLTCs (On-Load Tap Changer) will be grouped in their corresponding loads. The generators will be converted to voltage sources behind its saturated synchronous reactance when they reach the reactive power output limit and their OEL (Over Excitation Limiter) are activated.
- Construct the impedance [Z] matrix, and perform the eigen-decomposition on [Z] and obtain channel impedances [Λ] and transformation matrix [T].
- Gather synchronous generator voltage phasors [*E*], and voltage and current measurements at the load buses ([V], and [I]) from PMUs.
- Apply the transformation on [E], [V], and [I] and obtain the channel quantities.
- Compute the channel margins.
- Identify the critical channel based on channel margins.
- Use the critical channel and perform the voltage stability assessment. For example the critical loads can be identified which will be the candidates for corrective actions such as load shedding. The critical generator whose reactive power has the highest impact on the voltage stability, or the critical line which limits the power transfer can also be determined.

The main computing effort involved in the above procedure is the eigen-decomposition of the [Z]. Fortunately, this matrix does not change at each execution cycle. It changes only when major equipment is switched on/off. The 5-second execution interval also ensures that the transients associated with faults have died out and the system is in quasi-steady-state. This mode of operation is acceptable since voltage instability is mainly caused by the slow power recovery process of loads in about 15 to 30 second time frame [78]. The requirements on data communication can be also accommodated with the 5 second cycle. For cases where the PMU data are not available, state estimator results can be used assuming the state estimator can have 5 second turn around cycle.

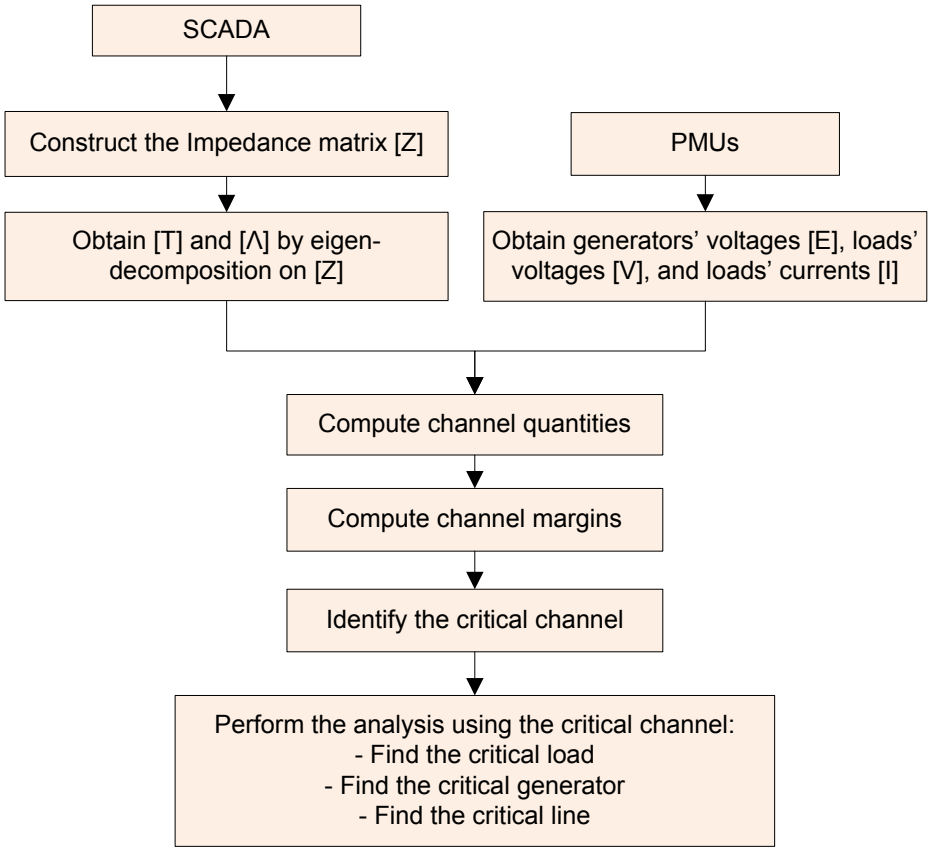

Fig. 7.1: The implementation procedure of the proposed monitoring scheme

7.2 PMU Allocation from Voltage Stability Perspective

The online application of the CCT requires installing PMUs at all generator and load buses. Since the PMU is an expensive device, this approach may not be currently practical. In other words, to make the proposed scheme more practical, we need to reduce the number of required PMUs without losing noticeable accuracy in the analysis. A strategy is proposed for this purpose in this section.

7.2.1 Proposed Allocation Strategy

The below findings can be concluded from previous chapters:

- For the voltage stability analysis and monitoring, there is no need to monitor and analyze all the system channels. It suffices to consider only a small number of the channels (critical channels).

- Only a part of system loads contribute significantly to a particular channel load. The effects of other loads on that channel are small and can be ignored.
- Only a part of system generators contribute significantly to a particular channel source voltage. The effects of other generators on that channel are small and can be ignored.

The implication is the following. A small number of channels which are the most critical can be determined. The load buses and generator buses which have significant contributions to these channels are then found. These buses will be considered as the locations for installing PMUs.

Therefore, the following strategy is proposed to reduce the number of required PMUs.

1) Stress the system to a point close to the collapse point, apply the CCT and compute the channels margins.

2) Set a value for the maximum channel margin ($Margin_{max}$), and select the channels whose margins are lower than this value as the critical channels.

3) Consider each critical channel one at a time, and perform the following process:

- Compute the contributions of load buses to the channel, and find the maximum contribution ($Cont_{max}$). Set a value for the minimum load factor (L_Factor_{min}), and compare the contribution of each load bus with the value of $Cont_{max} \times L\_Factor_{min}$. If the contribution of the load is lower than this value, that load bus is added to insignificant buses associated with the current channel.
- Compute the contributions of generator buses to the channel, and find the maximum contribution (G_Cont_{max}). Set a value for the minimum generator factor (G_Factor_{min}), and compare the contribution of each generator bus with the value of $G\_Cont_{max} \times G\_Factor_{min}$. If the contribution of the generator is lower than this value, that generator bus is added to insignificant buses associated with the current channel.

4) Compare the insignificant buses obtained for all the critical channels. Those buses which are common in all the critical channels are selected as the final insignificant buses. There is no need to install any PMU at these buses. The remaining load/generator buses are considered as the locations in which PMUs are to be installed.

With using the above PMU allocation, the application of the transform matrix to get the channel quantities is modified as follows:

- For each insignificant load bus which is not to be measured by a PMU, consider the load current as $I_i = \frac{S_i}{1}$, where, S_i is the nominal load power (load power at the base case). In fact, the voltage has been approximated by 1 p.u., and the power at the current operating condition has been approximated by the nominal power.
- For each insignificant generator bus which is not to be measured by a PMU, consider the bus voltage as 1 p.u. i.e. $E_i = 1$.
- Calculate the channel currents $[J]=[T][I]$, and the channel source voltages $[F]=[K][T][E]$.
- Calculate the channel voltages $[U]=[F]- [\Lambda]*[J]$.
- Calculate the modified channel source voltages $[F_{eq}]$.

As an illustrative example, the above strategy is applied to the AIES operational base case which is a 2038-bus system. $Margin_{max}$ is set to %40. In other words, all the channels whose margins are less than %40 when the actual system is close to the nose point are considered as the critical channels. This large value assures that if there is a change in the system topology, the critical channel would not be missed. L_Factor_{min} and G_Factor_{min} are both set to %8. Using the above predetermined values, the proposed strategy is applied to the AIES system, and the results are discussed below.

Three channels (channels 384, 18, and 425) are determined as the critical channels. This system has 684 load buses, and 205 generator buses. By applying the above strategy, however, 557 load buses and 149 generator buses are determined as the insignificant buses. In other words, only 127 load buses and 56 generator buses are selected for the PMUs locations.

To check the effect of this placement on the transform, the CCT-based offline analysis is applied to the system. But this time, the currents and voltages of the insignificant buses are not used. Instead, the above modified procedure is used to calculate the channel quantities. The obtained results show that there is no losing accuracy in the critical channels. The PV/Pδ curves of the critical channels are exactly the same as when all the load buses are used. As an example, Fig. 7.2 shows the critical channels' margins. In this figure, the solid lines are for the case that all the load/generator bus data (currents and voltages) are used, and the dash lines are for the case that only the data of the significant buses are used. As this figure shows, there is no losing accuracy in the critical channels margins. Fig. 7.3 and Fig. 7.4 illustrate the contribution of load

buses and generator buses to channel 18 for both the cases. As seen in these figures, when the PMU placement strategy is used, no change in the ranking of the top rank loads/generators is made. The implication is that by using the allocation strategy, the CCT-based analysis and monitoring can be accurately applied.

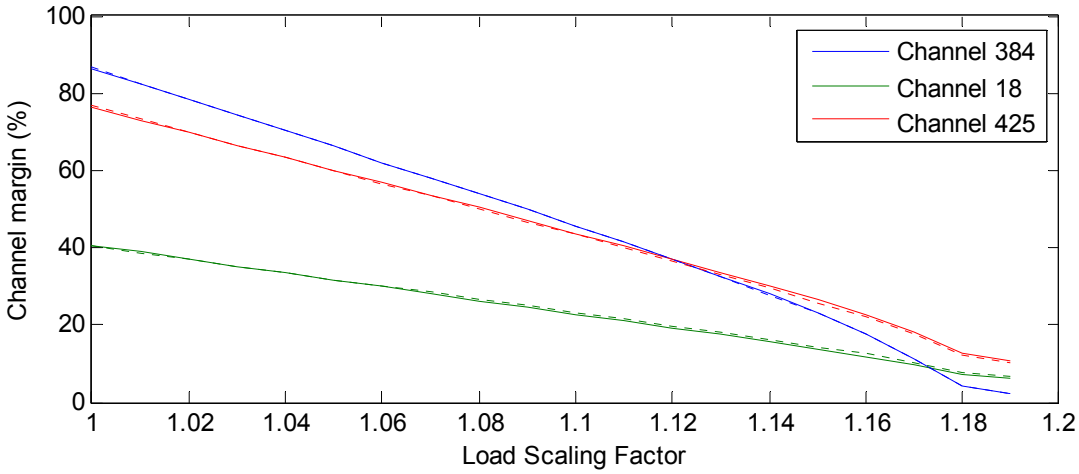

Fig. 7.2: Comparison of the critical channels margins with and without the PMU placement.

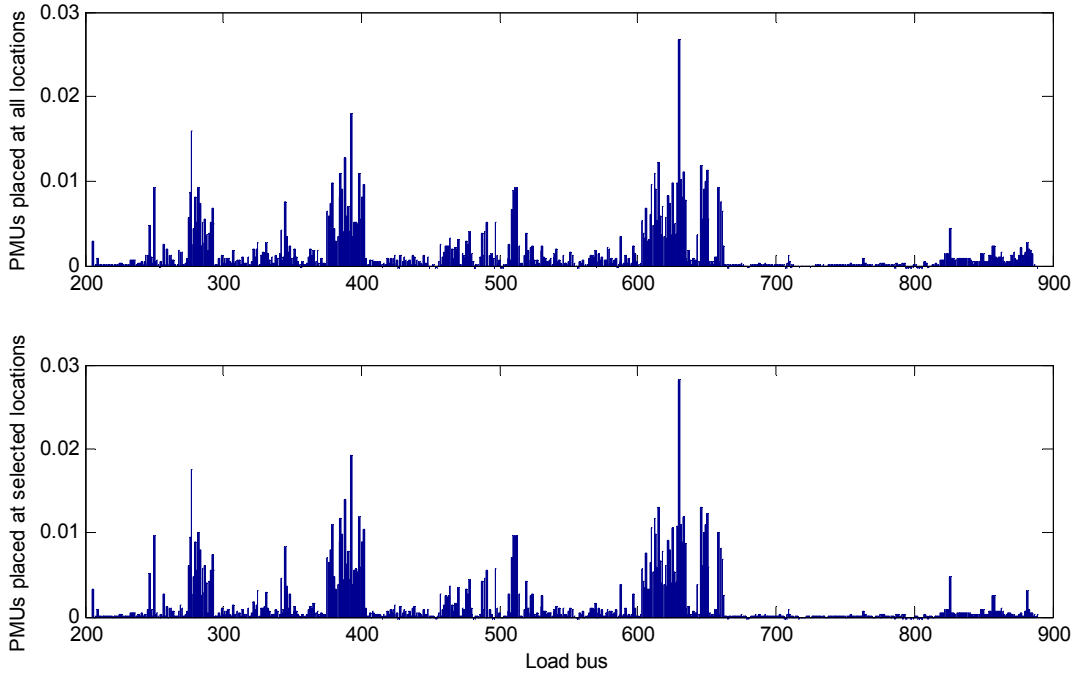

Fig. 7.3: load bus contributions to channel 18 with and without using the PMU placement strategy.

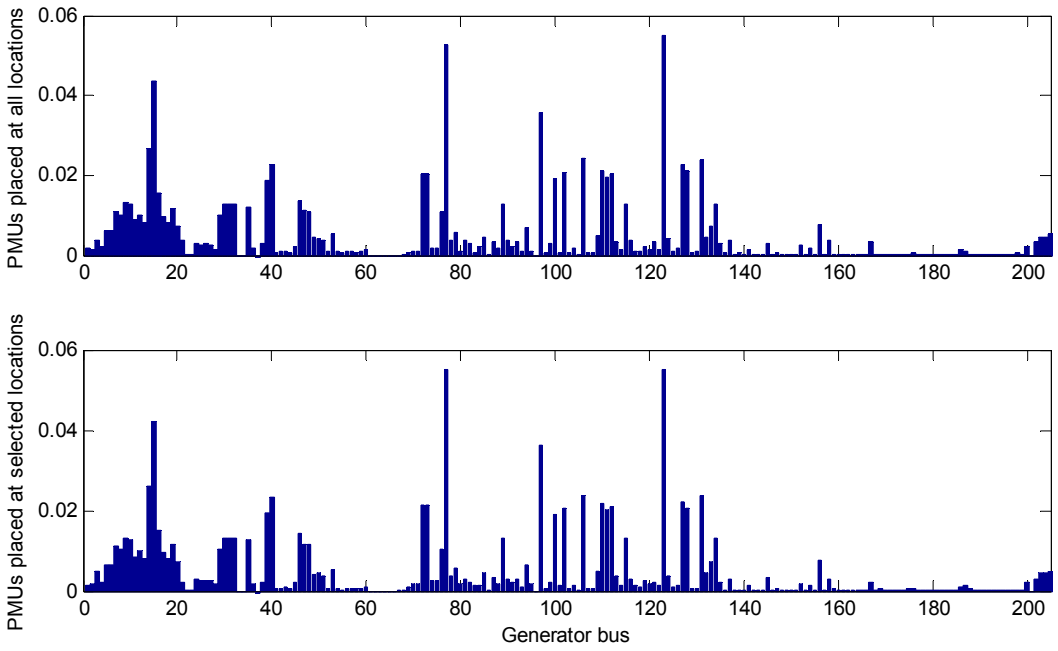

Fig. 7.4: generator bus contributions to channel 18 with and without using the PMU placement strategy.

7.2.2 Sensitivity Analysis on the Predetermined Thresholds

As explained in the previous section, two predetermined values should be set for L_Factor_{min}, and G_Factor_{min}. These two thresholds significantly affect the number of load and generator buses which are chosen for the PMUs location. The larger the thresholds values are, the smaller the number of required PMUs are. On the other hand, when the number of PMUs is decreased, the accuracy will be decreased too. Therefore, there is a trade-off between the number of PMUs and the accuracy of the monitoring and analysis. In this section, different values are considered for the thresholds and the effects on the accuracy and on the number of PMUs are analyzed. Finally, proper values are chosen for these thresholds. Obviously, if the proposed strategy is to be used in another system, similar sensitivity analysis should be performed to choose these values.

In order to analyze the effects of thresholds on the accuracy, an index should be defined first to quantify the accuracy. As explained in the previous section, the margins of the critical channels are very important to be accurately monitored. Therefore, the error between the margins before and after the PMU allocation can be used to quantify the accuracy. Let's consider the first critical channel. Let's also denote the margin of this channel before the PMU allocation as M ,

and after the PMU allocation as $\hat{M}$. Since the margins need to be compared for different load scaling factors from the base case till the nose point, the root mean squared error (*RMSE*) defined below is used.

$$RMSE = \sqrt{\frac{1}{n}\sum_{i=1}^{n}(M_i - \hat{M}_i)^2} \tag{7.1}$$

where n is the total number of data points i.e. the number of operating points from the base case to the nose point.

The above procedure is repeated for the other critical channels to obtain their RMSEs. The mean value of all critical channels RMSEs which will be called Averaged RMSE (ARMSE) is used as the final value for the error.

$$ARMSE = \frac{1}{K}\sum_{i=1}^{K} RMSE_i \tag{7.2}$$

where K is the total number of critical channels.

Now that we have defined an error, the sensitivity analysis can be performed as follows.

A. Sensitivity Analysis on L_Factor_{min}

G_Factor_{min} is set to %8 and is kept constant. Different values are then considered for L_Factor_{min} and its effects on the accuracy and the number of PMUs are analyzed. Table 7.1 summarizes the results. Note that since G_Factor_{min} is kept constant, the number of significant generator buses is the same for all the cases. So it suffices to compare the number of significant load buses only.

Table 7.1: Summary of the results for the sensitivity analysis on L_Factor_{min}

Case	L_Factor_{min} (%)	Significant load buses	*ARMSE*
1	5	178	0.0194
2	6	159	0.0253
3	7	140	0.0611
4	8	127	0.0724
5	9	116	0.0855
6	10	108	0.0971
7	11	103	0.111
8	12	97	0.126
9	13	93	0.136
10	14	85	0.176
11	15	78	0.209

The above results are visualized in Fig. 7.5. As this figure shows, by increasing L_Factor_{min}, the error is increased, but the number of significant buses and as a result the number of required PMUs is decreased. This can be seen in Fig. 7.6 which shows the sensitivity of the error with respect to the number of significant load buses. The selection of a proper value for L_Factor_{min} depends on the desired accuracy. We assume that the error should be less than 0.1, and as a result, L_Factor_{min} is set to %10 according to Fig. 7.5.

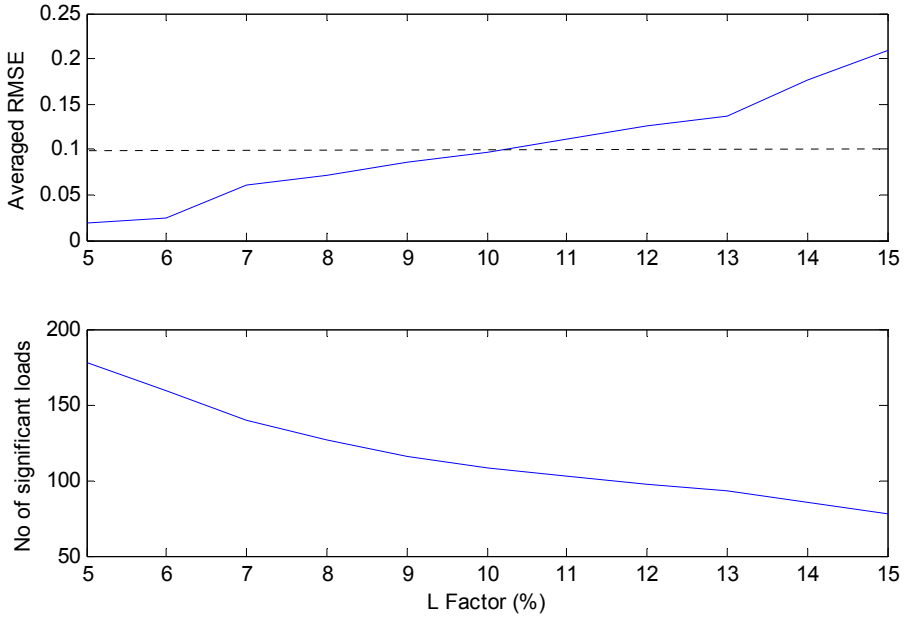

Fig. 7.5: Results of the sensitivity analysis on L_Factor_{min}.

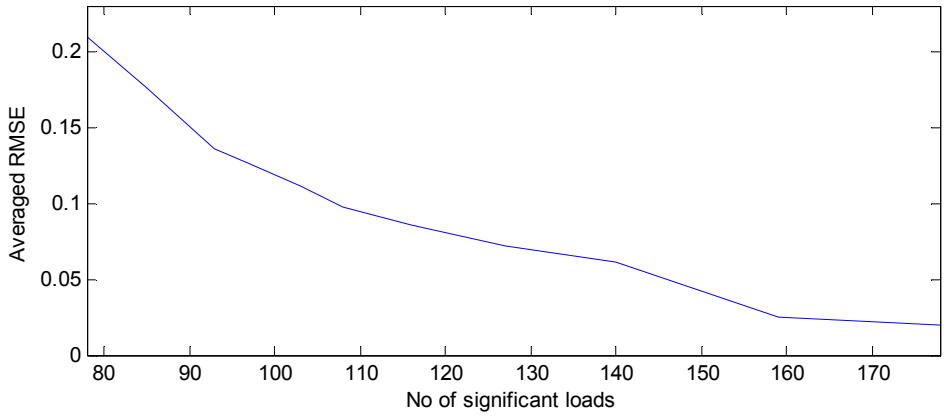

Fig. 7.6: Sensitivity of the error with respect to the number of significant loads.

B. Sensitivity Analysis on G_Factor_{min}

The previous subsection suggested that %10 is a proper vale for L_Factor_{min} in our case. Therefore, L_Factor_{min} is set to %10 and is kept constant. Different values are then considered for G_Factor_{min} and its effects on the accuracy and the number of PMUs are analyzed. Table 7.2 summarizes the results. Note that since L_Factor_{min} is kept constant, the number of significant

load buses is the same for all the cases. So it suffices to compare the number of significant generator buses only.

The above results are visualized in Fig. 7.7. As this figure shows, G_Factor_{min} does not have a significant impact on the accuracy. In other words, even if a very high value such as %80 is used, we will still have a good accuracy in terms of monitoring the margins of the critical channels. However, if the ranking of the first critical generators is important for us, we should use a smaller value so that the voltages of more generator buses can be monitored, and as a result it would be possible to accurately rank them. With respect to the above points, %40 seems to be a proper value for G_Factor_{min}.

Table 7.2: Summary of the results for the sensitivity analysis on G_Factor_{min}

Case	G_Factor_{min} (%)	Significant generator buses	*ARMSE*
1	5	82	0.097100
2	10	48	0.097102
3	20	32	0.097103
4	30	21	0.097105
5	40	13	0.097107
6	50	9	0.097110
7	60	6	0.097115
8	70	5	0.097120
9	80	5	0.097120

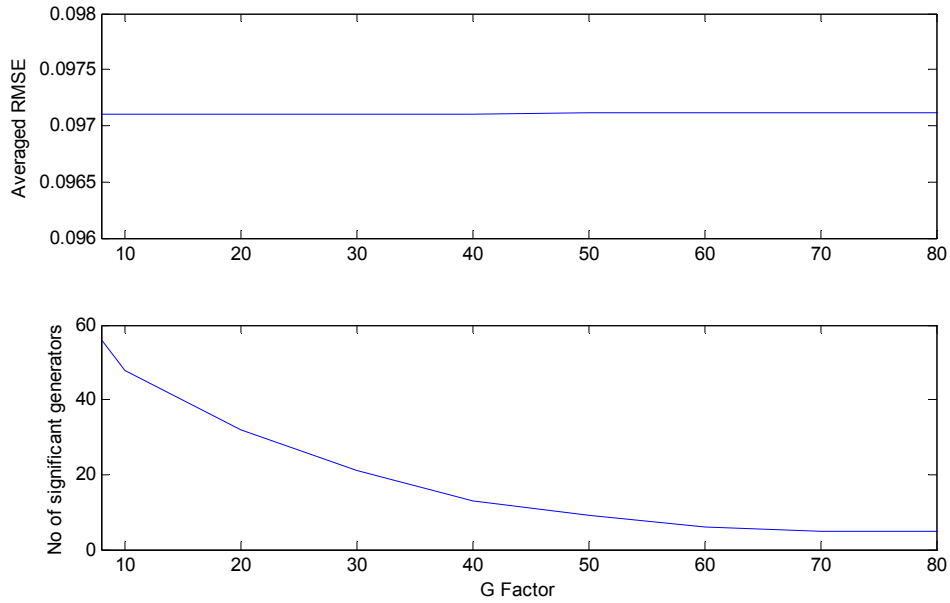

Fig. 7.7: Results of the sensitivity analysis on G_Factor_{min}.

In summary, according to the above sensitivity analysis, the following values are set for the thresholds.

$$L\_Factor_{min} = \%10, \text{ and } G\_Factor_{min} = \%40$$

With using the above values, the PMU allocation strategy will result in the following results.

- Number of significant load buses: 108
- Number of significant generator buses: 13
- Number of insignificant load buses: 576
- Number of insignificant generator buses: 192
- Total number of required PMUs: 121
- Averaged RMSE: 0.0971.

Fig. 7.8 compares the margins of the critical channels. In this figure, the solid lines are for the case that all the load/generator bus data (currents and voltages) are used, and the dash lines are for the case that only the data of the significant buses are used. As this figure reveals, the obtained PMU allocation is good and accurate.

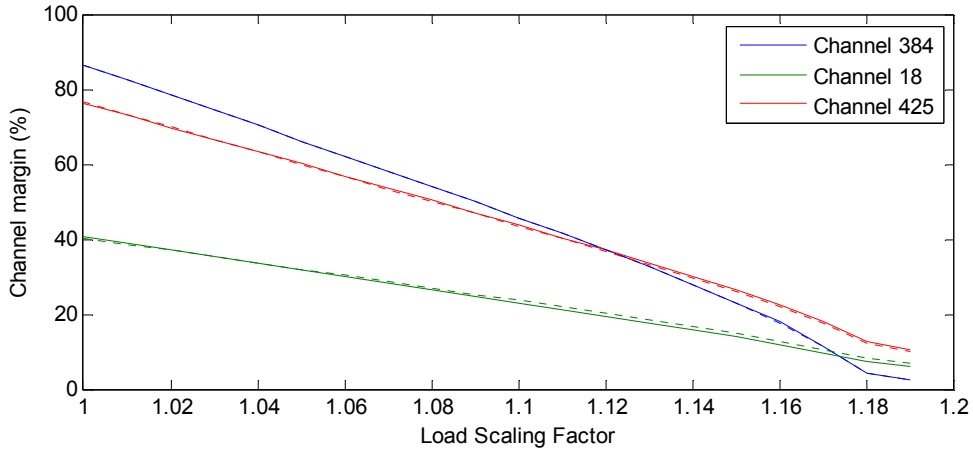

Fig. 7.8: Comparison of the critical channels margins with and without the PMU placement.

7.2.3 Effects of Contingencies on the Proposed Strategy

The proposed strategy for the allocation of PMUs is based on the current topology of the system. When the PMUs are allocated, however, it is very important that the system can be accurately monitored if a change in the topology of the system occurs. Therefore, the contingencies need to be somehow considered when the PMUs are allocated. For this purpose, a strategy is suggested in this section.

It is suggested that the proposed allocation strategy is applied to the base case first. The top rank critical contingencies are then identified. The allocation strategy is then performed again for each critical contingency one at a time. The results of all the contingencies are compared with those of the base case at the end. We might have two cases then:

1- The results are very similar. In other words, the significant load/generator buses obtained for each contingency are almost the same as those of the base case. In this case, the significant buses obtained for the base case can be used as the final PMUs locations.

2- The results are different. In other words, the significant load/generator buses obtained for each contingency are different from those of the base case. In this case, if a high accuracy is desired in case of any contingency, all the significant buses of all contingencies and the base case should be selected as the final PMUs locations.

In theory, both of the above cases are possible. In actual cases, however, case 1 is more likely to be the case. As an example, the AIES 2038-bus system is used, the above procedure is applied, and the results are discussed in the following. The following contingencies are considered.

Case 1: Outage of line 1024-1030
Case 2: Outage of line 1063-1316
Case 3: Outage of line 1004-1294
Case 4: Outage of line 1004-1301
Case 5: Outage of line 1005-1022
Case 6: Outage of line 1010-1024
Case 7: Outage of line 1022-1029
Case 8: Outage of line 1024-1233

For each contingency, the contingency is applied to the system and the offline CCT-based analysis is performed. The proposed allocation strategy is then applied to the system and the significant generator/load buses are obtained. Fig. 7.9 illustrates the significant generator buses for the base case and for all the contingencies. In this figure, each significant bus is displayed by a red square. As this figure shows, the buses obtained for the base case cover almost all the buses for all the contingencies. In other words, most of the significant buses obtained for the contingencies belong to those obtained for the base case.

Fig. 7.10 shows the significant load buses. As this figure illustrates, most of the significant buses obtained for the contingencies belong to those obtained for the base case. The implication is that using the results obtained for the base case, the system can be accurately monitored even if a contingency occurs.

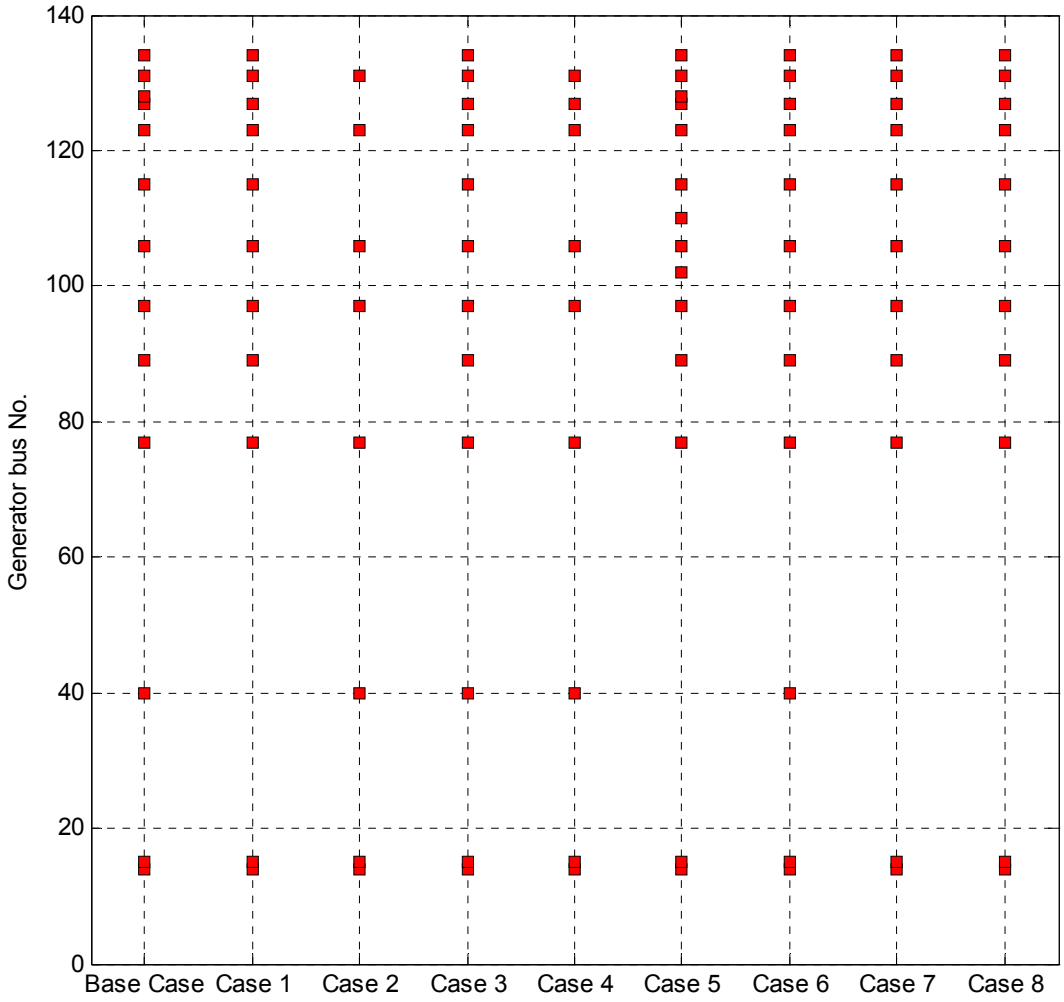

Fig. 7.9: Significant generator buses.

To verify the above claim, the following analysis is performed. The results obtained for the base case are considered, and the offline CCT-based analysis is performed for each contingency. The channel quantities are then calculated for two cases, one with using all the bus currents and voltages, and the other with using only the currents and voltages of the significant buses (the PMUs locations). The obtained channel margins are then compared for these two cases to check how accurate the results are.

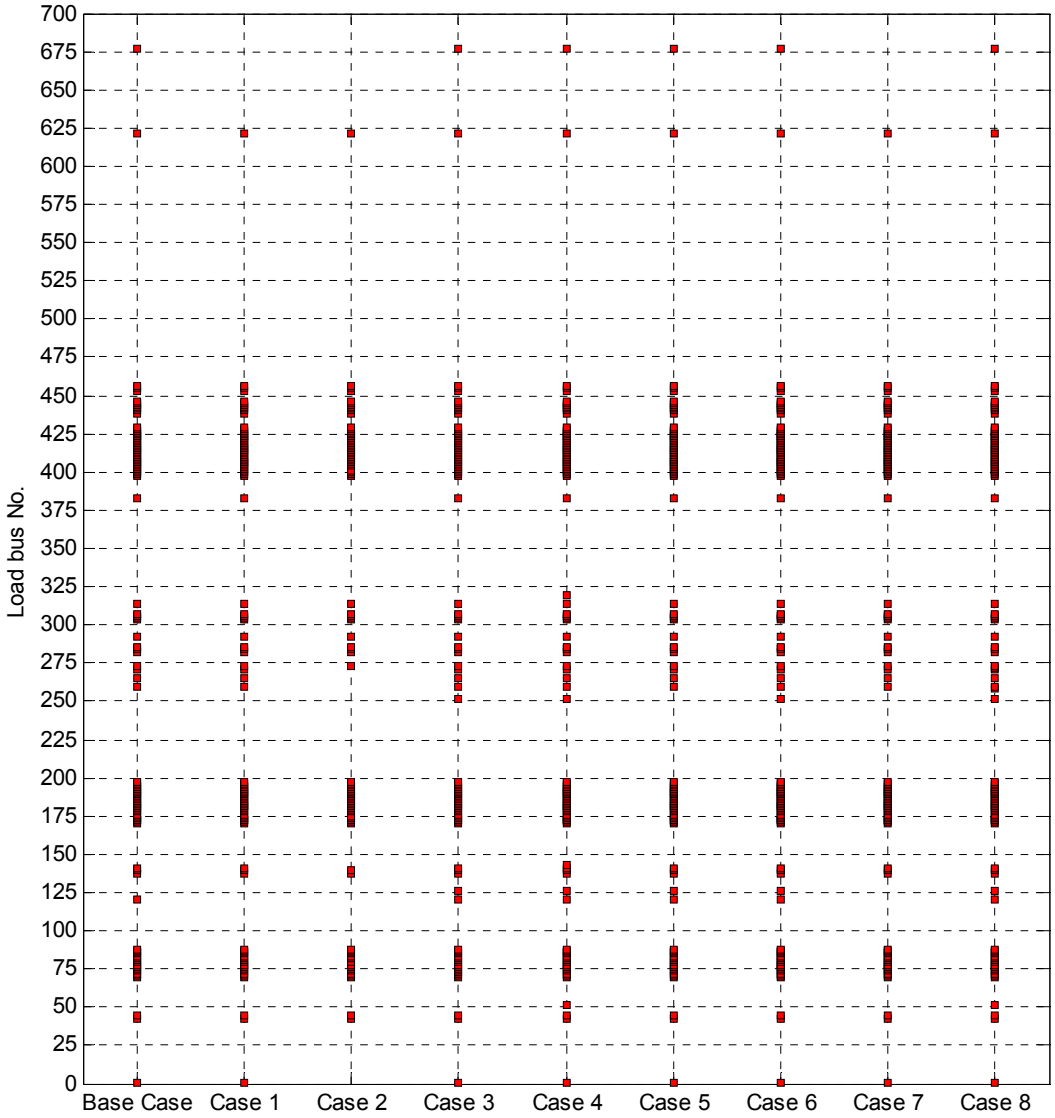

Fig. 7.10: Significant load buses.

The following figures (Fig. 7.11 - Fig. 7.18) show the critical channels' margins for different contingencies. In these figures, the solid lines are for the case that all the load/generator bus data (currents and voltages) are used, and the dash lines are for the case that only the data of the significant buses (PMUs locations) are used. According to these figures, the solid lines are very close to their associated dash lines in all the contingencies. The implication is that the critical channels can be monitored accurately with using the allocated PMUs.

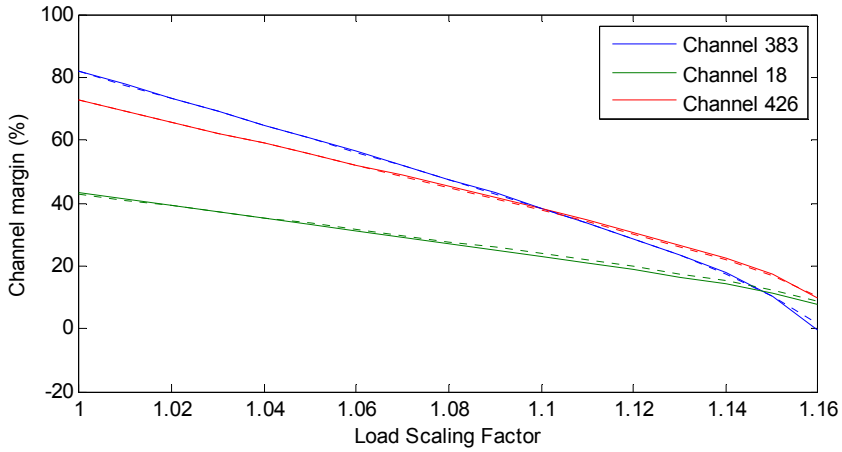

Fig. 7.11: Comparison of the channel margins with and without the PMU placement for contingency 1

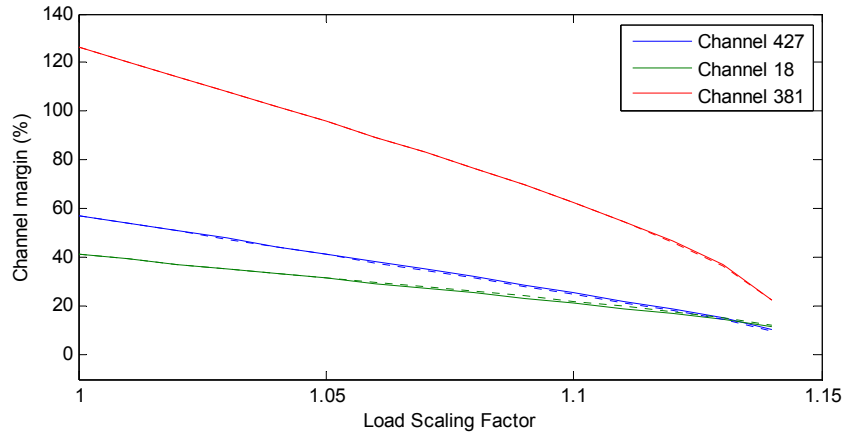

Fig. 7.12: Comparison of the channel margins with and without the PMU placement for contingency 2

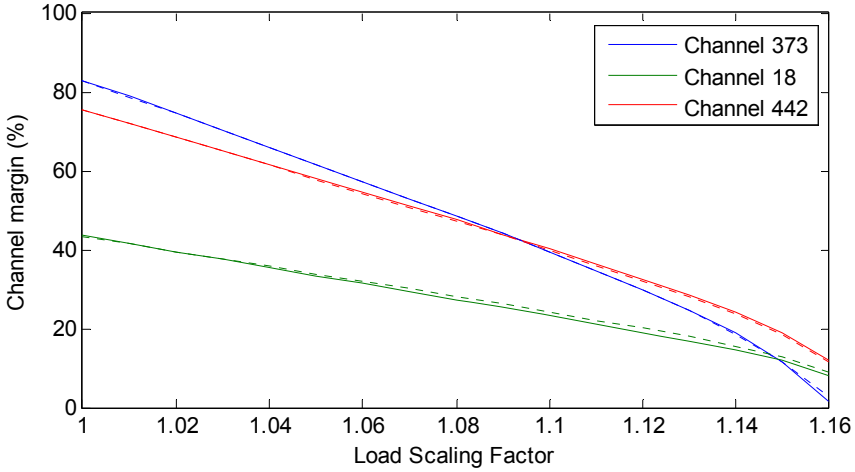

Fig. 7.13: Comparison of the channel margins with and without the PMU placement for contingency 3

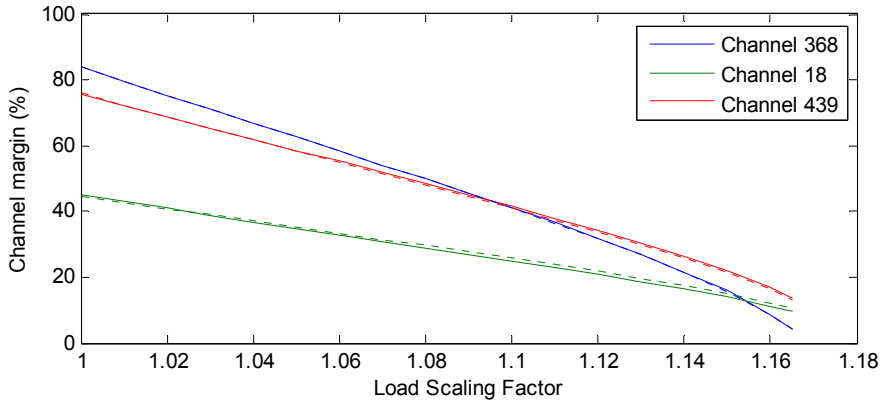

Fig. 7.14: Comparison of the channel margins with and without the PMU placement for contingency 4

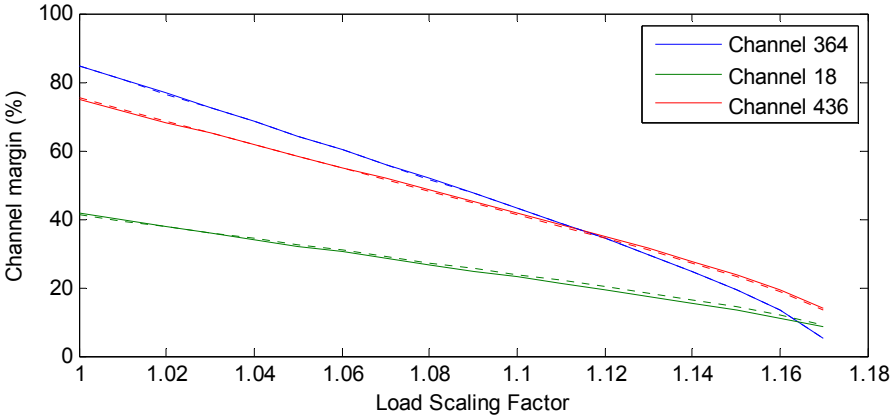

Fig. 7.15: Comparison of the channel margins with and without the PMU placement for contingency 5

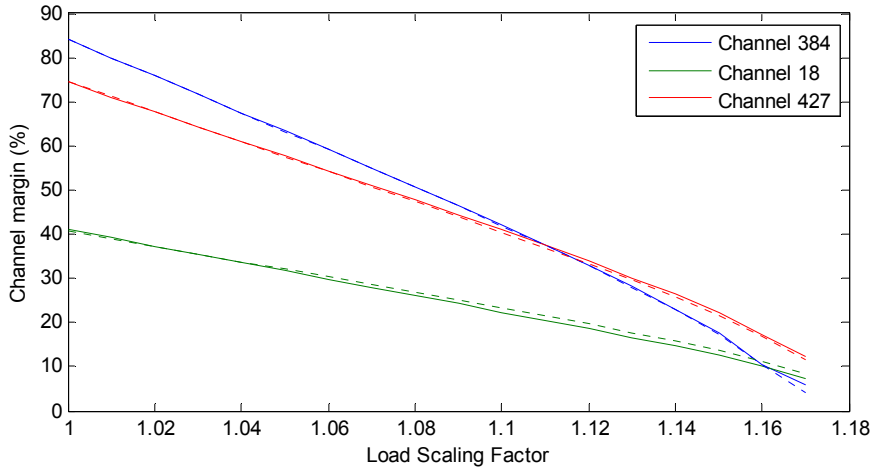

Fig. 7.16: Comparison of the channel margins with and without the PMU placement for contingency 6

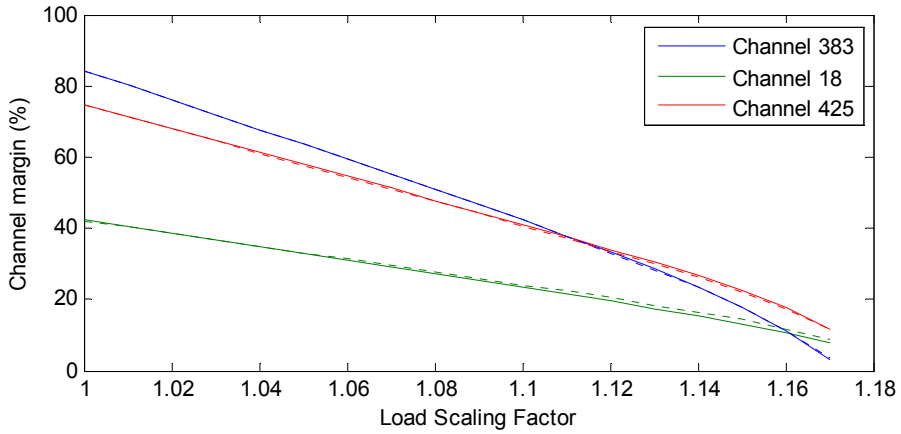

Fig. 7.17: Comparison of the channel margins with and without the PMU placement for contingency 7

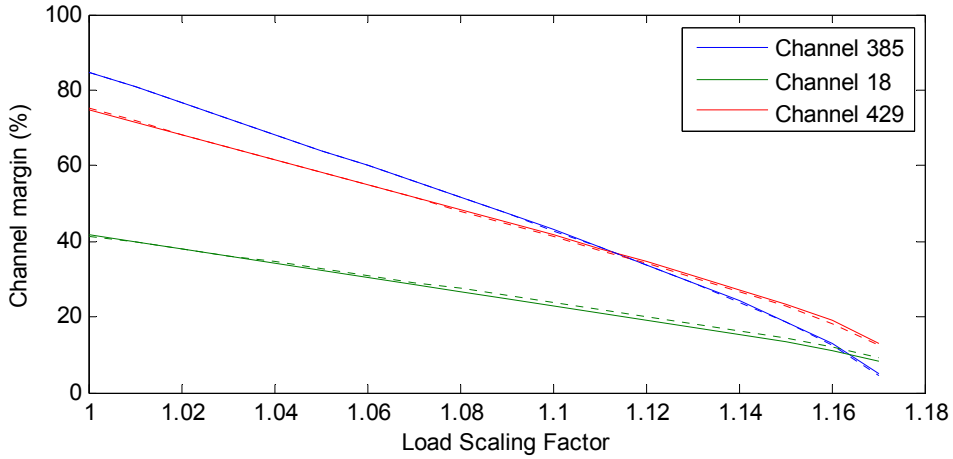

Fig. 7.18: Comparison of the channel margins with and without the PMU placement for contingency 8

7.2.4 Inclusion of Insignificant Loads in the Admittance Matrix

After the PMU allocation is performed, the data of the insignificant buses are not measured anymore. To apply the CCT, however, these data are required. There are two options to overcome this problem. One is to use the procedure explained in Section 7.2.1 which involves considering some approximations for the data of the non-monitored buses. The other option is to include the non-monitored buses in the admittance matrix. For this purpose, the loads of these buses are treated as impedances, and they are included in the admittance matrix. These buses are then treated as network buses. Therefore, the eigen-decomposition is applied again and the CCT analysis is performed.

To investigate the performance of this approach, the allocation results obtained in Section 7.2 are used and this approach is applied, and the results are investigated. Note that the load impedances are calculated based on the system data when it is at the base case, and they are assumed to remain constant for all other scaling factors. Fig. 7.19 shows the channel margins. Also, Fig. 7.20 illustrates the PV curves of the three top rank channels. As seen in these figures, channel 141 is the critical channel. This channel, however, carries small amount of power. The next critical channel is the channel 2 which has a high amount of channel power.

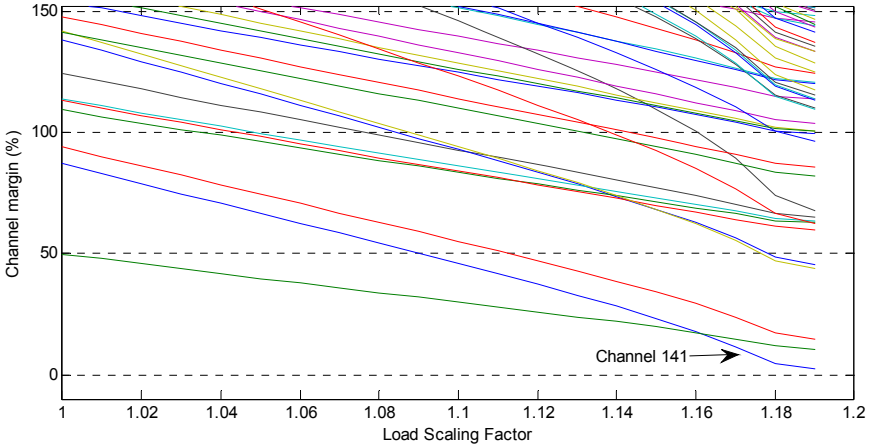

Fig. 7.19: Channels margins

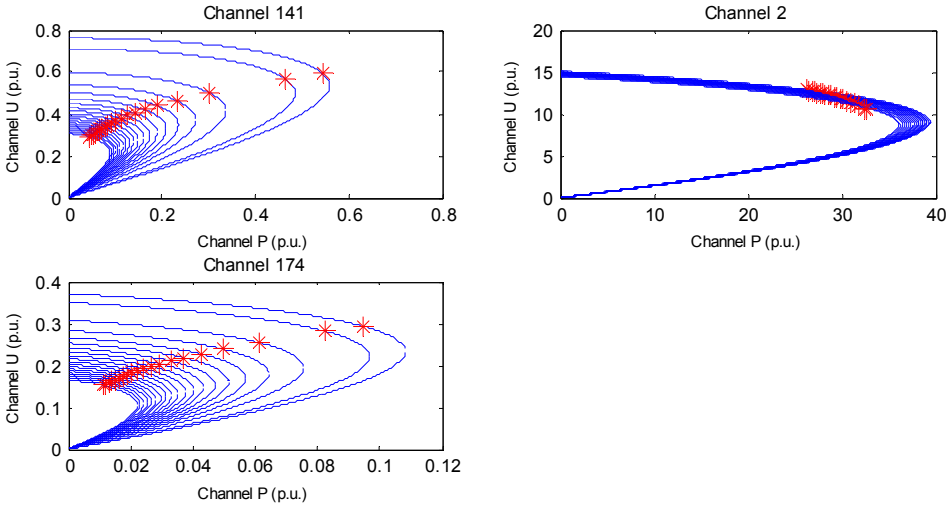

Fig. 7.20: Channel PV curves of top rank channels

Fig. 7.21 shows the contributions of load buses to channel 141. This figure leads to the following findings:

- The critical bus is bus 630 which has been verified as the actual critical load in the system.

- Only a small number of loads contribute to this channel, and the contributions of all other loads are very small. So this channel is more like a local channel.

Fig. 7.22 illustrates the contributions of load buses to channel 2. This figures shows that the critical bus is bus 630. Also, it reveals that this channel is a system channel.

Fig. 7.23 and Fig. 7.24 show the contributions of generators to channels 141 and 2, respectively. As seen in these figures, both of the channels identify bus 123 as the critical generator which can be verified by the verification method.

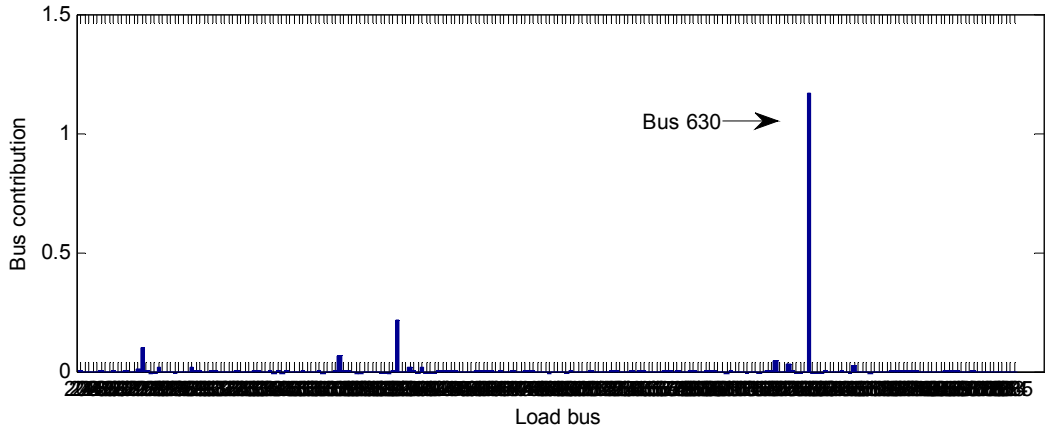

Fig. 7.21: Contributions of load buses to channel 141

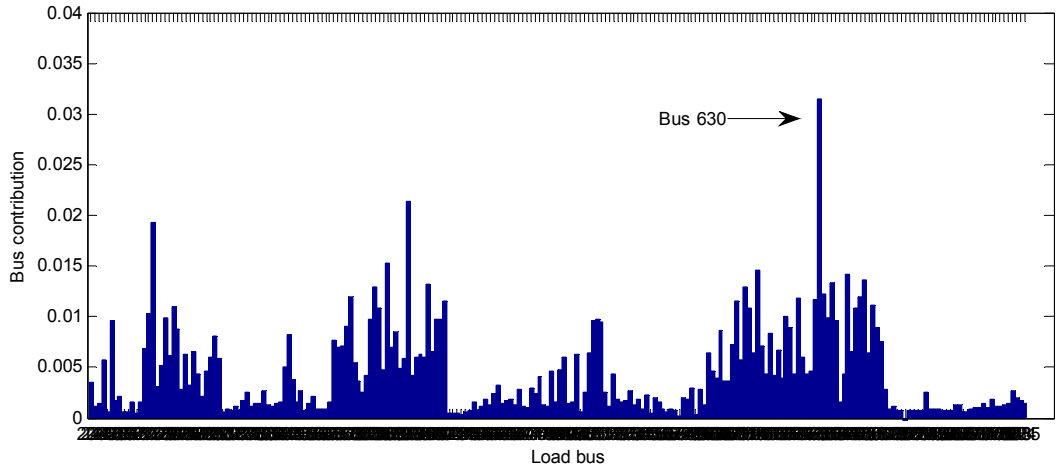

Fig. 7.22: Contributions of load buses to channel 2

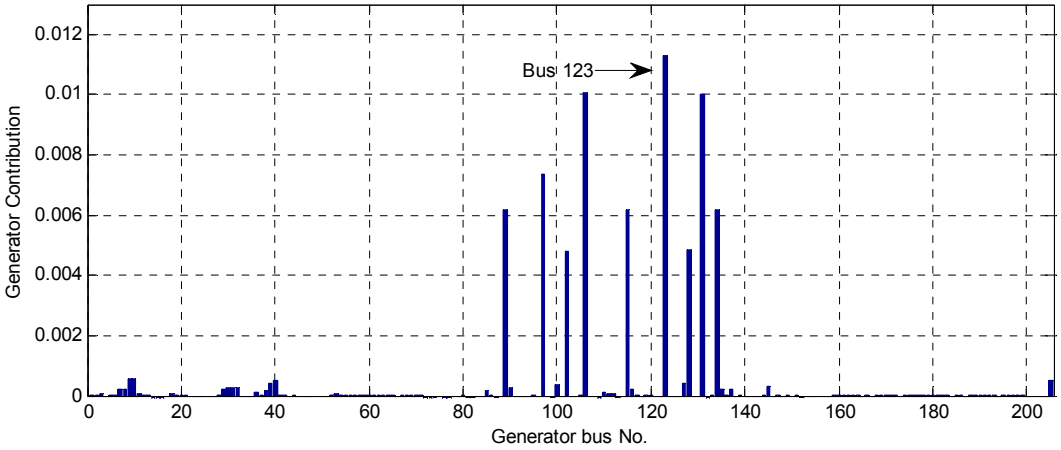

Fig. 7.23: Contributions of generator buses to channel 141

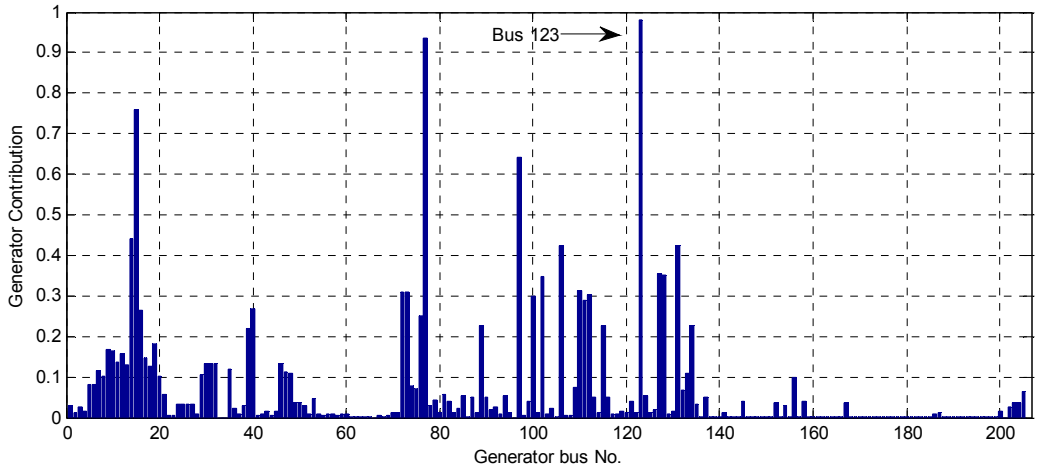

Fig. 7.24: Contributions of generator buses to channel 2

The above results show that by inclusion of insignificant load buses in the admittance matrix, the CCT analysis can still be performed accurately. The only remaining issue is the monitoring of the channels margins. Fig. 7.25 compares the margins of the three top rank channels with those of the original CCT (i.e. without inclusion of loads in the admittance matrix). As seen in this figure, the first critical channel is exactly the same as the first critical channel in the original CCT. The margins of the other two channels have the same trends as those of the original ones, but they are different in their values.

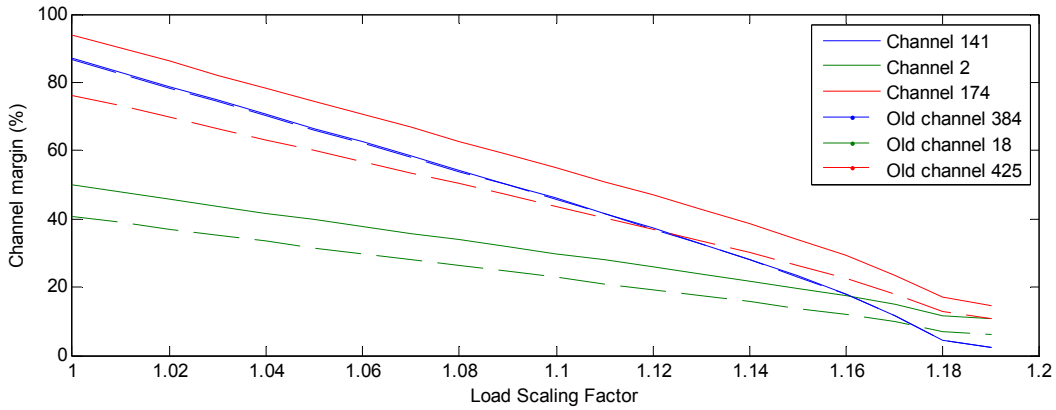

Fig. 7.25: Comparison of critical channels margins before and after the load inclusion

The overall conclusion of this subsection can be summarized as follows: With the inclusion of insignificant load buses in the admittance matrix, the first critical channel can be accurately monitored. The CCT-based analysis can also be performed accurately. However, in terms of monitoring the second and third critical channels, this approach introduces some errors. Therefore, the method proposed in Section 7.2.1 which is more accurate is recommended for this task.

7.3 Conclusions

In this chapter, a wide-area scheme for the online voltage stability monitoring and analysis along with its implementation procedure were proposed. The proposed scheme is based on the CCT-based voltage stability analysis techniques proposed in the previous chapters. A strategy has also been proposed for the allocation of PMUs. The proposed strategy finds a few critical channels first, and according to the contribution of load and generator buses to these critical

channels, finds the best locations for the PMUs. The proposed strategy has been applied to the AIES 2038-bus system and the results have been investigated in this chapter. The results have shown that using this strategy, the number of PMUs can be decreased significantly without losing any noticeable accuracy.

The performance of the allocation technique after the contingencies has also been investigated. The results have shown that using the allocated PMUs, it is possible to accurately monitor the system after any contingency.

To account for the data of the non-monitored load buses, two alternatives have been proposed. One is to approximate the load current using the nominal load power and use the approximated current in the original CCT. The other is to approximate the loads as impedances and include them in the admittance matrix. A new eigen-decomposition is then performed. The simulation results have shown that both methods are accurate in terms of the monitoring of the critical channel and analysis. However, the first approach is more accurate when monitoring other critical channels. Therefore, the first method which is more suitable is recommended.

Chapter 8: Singular Value Decomposition-based Transformation

The channel components transform is based on eigen-decomposition of the impedance matrix. Many unique features of the CCT were demonstrated in the previous chapters. However, there are two difficulties with eigenvalue decomposition [84].

- A theoretical difficulty is that the decomposition does not always exist. In other words, there might be an impedance matrix which could not be diagonalized using eigen-decomposition.

- A numerical difficulty is that, even if the decomposition exists, it might not provide a basis for robust computation. That means if some errors exist in the data (such as in the impedance matrix obtained from SCADA data), these errors could be magnified in the transformed variables. Therefore, we might not be able to get an acceptable accuracy in the results.

This chapter will show that the above difficulties can be overcome by using Singular Value Decomposition (SVD) instead of the eigenvalue decomposition. The transformation concepts and procedure will remain the same. The obtained results for several case studies will be compared to those of the original CCT.

8.1 Limitations of Eigen-decomposition

As explained above, the eigen-decomposition has two difficulties: A) non-existence difficulty, and B) Robustness difficulty. Before presenting the SVD-based transformation, these limitations are discussed in detail.

8.1.1 Non-existence difficulty

Assume that matrix [Z] is to be decomposed using eigen-decomposition. If [Z] is diagonalizable, the matrix has an eigenspace decomposition. If the matrix is not diagonalizable, then it is called defective, and, it cannot be decomposed into eigenspaces. In particular, an n × n matrix is defective if and only if it does not have n linearly independent eigenvectors.

From linear algebra we know that if an n × n complex matrix is Hermitian, then there exist n linearly independent eigenvectors for this matrix. In other words, any Hermitian matrix can be diagonalized using eigen-decomposition. If a complex matrix is not Hermitian, there would be no guarantee that it can be diagonalized. Matrix [Z] is Hermitian if and only if it satisfies the following conditions

$$Z = Z^H \tag{8.1}$$

Where H stands for complex conjugate transpose.

A power system impedance matrix [Z] is symmetric i.e. $Z = Z^T$ (where T stands for transpose) but it is not Hermitian i.e. $Z \neq Z^H$. Since the impedance matrix is not Hermitian, there is no guarantee that we are able to decompose it into a diagonal matrix using eigen-decomposition.

8.1.2 Robustness difficulty

The eigenvalues of some matrices could be sensitive to perturbations. In other words, small changes in the matrix elements could lead to large changes in the eigenvalues. This is discussed in the following. Assume that [Z] has a full set of linearly independent eigenvectors and can be decomposed using eigenvalue decomposition as follows:

$$Z = T^{-1}\Lambda T \tag{8.2}$$

This can be rewritten as

$$\Lambda = TZT^{-1} \tag{8.3}$$

Now let δZ denote some change in Z. Then,

$$\Lambda + \delta\Lambda = T(Z + \delta Z)T^{-1} \tag{8.4}$$

Hence

$$\delta \Lambda = T(\delta Z)T^{-1} \tag{8.5}$$

Taking matrix norms,

$$\| \delta \Lambda \| \leq \| T \| \| T^{-1} \| \| \delta Z \| = k(T) \| \delta Z \| \tag{8.6}$$

where k(T) is the matrix condition number. Note that the key factor is the condition of T, the matrix of eigenvectors, not the condition of Z itself. The above analysis implies that a perturbation in Z can be magnified by a factor as large as k(T).

As mentioned before, the Z matrix is obtained from SCADA data. Since these data are measured using some measurement equipments, one would expect some errors. Those errors will introduce some errors in Z matrix. This kind of errors is an example for perturbation in Z. Similarly, roundoff errors introduced during the computation of eigenvalues have the same effect as perturbations in the original matrix [84]. Consequently, these errors may be magnified in the computed eigenvalues. If the condition number of the transformation matrix is small (close to 1), this magnification may not be significant, and therefore, the results obtained by the eigen-decomposition would be accurate. However, if the transformation matrix has a large condition number, the errors would be significantly magnified, leading to unreliable results.

8.2 SVD-based Transformation

The defining equations for singular values and vectors are

$$\begin{aligned} Z T_1 &= T_2 \Sigma \\ Z^H T_2 &= T_1 \Sigma^H \end{aligned} \tag{8.7}$$

where Σ is a diagonal matrix the same size as Z. The diagonal elements of Σ are the singular values of the impedance matrix Z. The singular vectors can always be chosen to be perpendicular

to each other, so the matrices T_1 and T_2, whose columns are the normalized singular vectors, satisfy the following condition, indicating that T_1 and T_2 are unitary matrices.

$$\begin{aligned} T_1^H T_1 &= 1 \\ T_2^H T_2 &= 1 \end{aligned} \tag{8.8}$$

Consequently,

$$Z = T_2 \Sigma T_1^H \tag{8.9}$$

with diagonal Σ and unitary T_1 and T_2. This is known as the singular value decomposition, or SVD, of the matrix Z.

Equation (2.3) can be rewritten as

$$\begin{aligned} V &= KE - ZI = KE - T_2 \Sigma T_1^H I \\ T_2^H V &= T_2^H KE - \Sigma T_1^H I \end{aligned} \tag{8.10}$$

Denote $U = T_2^H V$ as the channel voltage, $J = T_1^H I$ as the channel current, and $F = T_2^H KE$ as the channel voltage source. This leads to the following decoupled channel networks whose circuit representations are shown in Fig. 8.1.

$$\begin{bmatrix} U_1 \\ U_2 \\ \dots \\ U_n \end{bmatrix} = \begin{bmatrix} F_1 \\ F_2 \\ \dots \\ F_n \end{bmatrix} - \begin{bmatrix} \sigma_1 & 0 & 0 & 0 \\ 0 & \sigma_2 & 0 & 0 \\ 0 & 0 & . & 0 \\ 0 & 0 & 0 & \sigma_n \end{bmatrix} \begin{bmatrix} J_1 \\ J_2 \\ \dots \\ J_n \end{bmatrix} \tag{8.11}$$

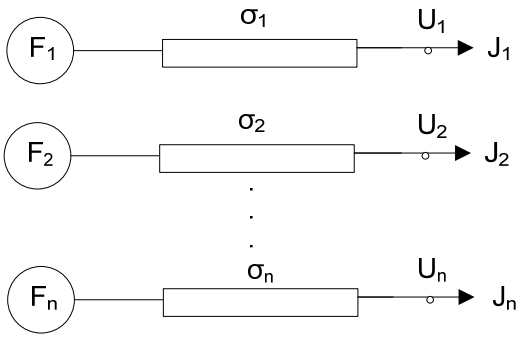

Fig. 8.1: Channel domain representation of a complex network

As seen above, similar to the eigen-decomposition, the SVD-based transformation converts a complex network into a set of decoupled simple one-source, one-load networks. The only difference is that since the singular values are always real, the channel impedances (σ_i) shown in Fig. 8.1 are purely resistive. The rest of the transformation procedure remains the same as that of the eigen-decomposition.

8.3 Advantages of the SVD-based Transformation

The singular value decomposition has the following advantages over the eigen-decomposition.

A) Existence

It is well proven that SVD exists for any matrix. In other words, the matrix does not have to be diagonalizable in order to have a SVD. Therefore, when using SVD instead of eigen-decomposition, the existence problem is not a concern anymore.

In fact, squared singular values of Z are the eigenvalues of $Z^H Z$ i.e.

$$Z^H Z = (T_1 \Sigma^H T_2^H)(T_2 \Sigma T_1^H) = T_1 \Sigma^2 T_1^H = T_1 \Sigma^2 T_1^{-1} \tag{8.12}$$

$Z^H Z$ is always a Hermitian matrix, and as it was explained before, eigenvalues always exist for a Hermitian matrix.

B) Robustness

The singular value decomposition always uses orthonormal basis. That means matrices T_1 and T_2 are unitary matrices, so they preserve length and angles and do not magnify errors. Similar to that of the eigen-decomposition, a perturbation analysis can be performed for SVD as follows.

$$\Sigma + \delta\Sigma = T_2(Z + \delta Z)T_1^{-1} \tag{8.13}$$

Hence

$$\delta\Sigma = T_2(\delta Z)T_1^{-1} \tag{8.14}$$

Since T_1 and T_2 are unitary matrices, they preserve norms. Consequently,

$$\| \delta\Sigma \| = \| \delta Z \| \tag{8.15}$$

Therefore, perturbations of any size in the impedance matrix cause perturbations of the same size in its singular values. There is no need to define condition numbers for singular values because they would always be equal to one.

The above analysis shows that if there is any error in the impedance matrix (such as errors that exist in the measured data), or if there is any roundoff error in the computations, they will not be magnified when using SVD-based transformation.

8.4 Case Study Results

The SVD-based transformation is applied to several case studies to examine its performance when analyzing voltage stability. The results will be compared with those of the CCT (the eigen-decomposition-based transformation).

- **Simple Case Studies**

The first case study is the simple one-source three-load system used in Section 3.1. The network itself is shown in Fig. 2.6. Let's consider the system parameters as Z=j0.3;

Z_a=Z_b=Z_c=j0.2; E =1.0. Also, the loads are considered purely active as S_a=0.3, S_b=0.25, and S_c=0.4. The above conditions are the same as those considered in Section 3.1. If the SVD-based transformation is applied on the system, the following channel quantities are obtained.

$$[\Sigma] = \begin{bmatrix} 1.1 & 0 & 0 \\ 0 & 0.2 & 0 \\ 0 & 0 & 0.2 \end{bmatrix}, \quad and \quad [F] = \begin{bmatrix} j1.73 \\ 0 \\ 0 \end{bmatrix}$$

It can be seen that similar to the results of the CCT, only channel 1 has a voltage source. The impedances are, however, purely resistive. The above parameters lead to zero active power transfer in channel 1. Therefore, there would be no PV curve. However, if the QV curves are plotted for channel 1, Fig. 8.2 is obtained. This figure is similar to the PV curve shown in Fig. 3.3 as both figures reach their nose points when the system reaches its maximum loadability point.

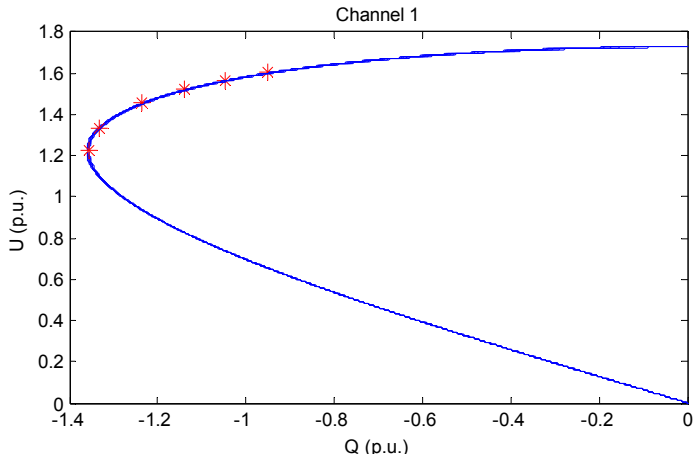

Fig. 8.2: Channel QV curve for the first case study

The second case study involves the same network configuration but Z_a, Z_b, and Z_c are not equal (Z_a=0.35, Z_b=0.2, and Z_c=0.1, similar to Section 3.1). . The SVD-based transformation will lead to the following channel quantities.

$$[\Sigma] = \begin{bmatrix} 1.129 & 0 & 0 \\ 0 & 0.28 & 0 \\ 0 & 0 & 0.14 \end{bmatrix}, \quad and \quad [F] = \begin{bmatrix} j1.720 \\ -j0.168 \\ j0.1099 \end{bmatrix}$$

All channels have non-zero voltage sources in this case. Therefore, all channels need to be analyzed. The channel QV curves for this case study are shown in Fig. 8.3. This figure confirms the results of Section 3.1 that voltage collapse occurs when one of the channels (channel 1) reaches its maximum power transfer limit.

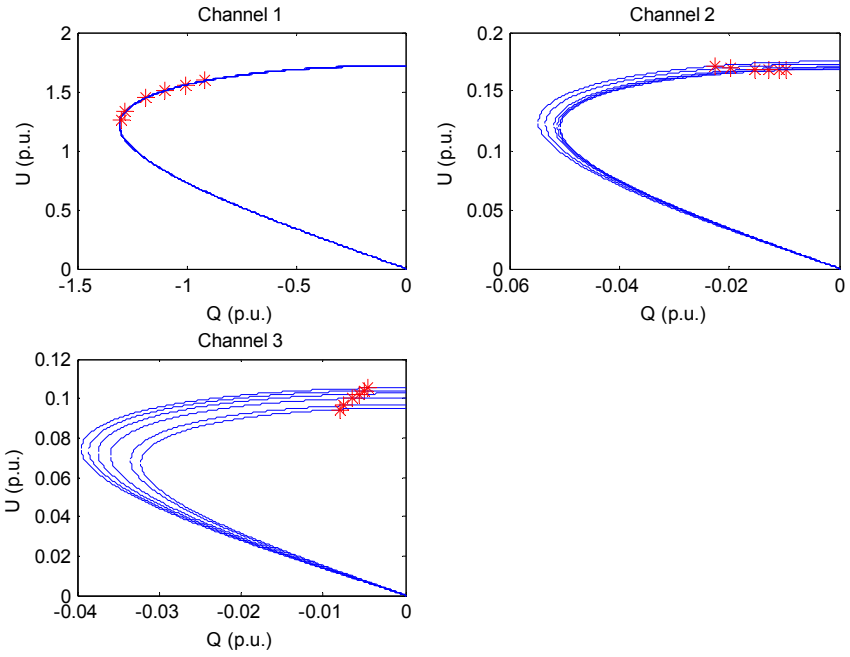

Fig. 8.3: Channel QV curves for the second case study

- **WECC 9-bus system**

WECC 9-bus system is considered as the next case study. By applying the SVD-based transformation on this system, the following PV/QV curves are obtained. As seen in the figures, both PV and QV curves show that channel 1 is the critical channel whose operating point goes very close to the nose point when the system is close to the collapse point. This is confirmed by the channel margins shown in Fig. 8.6.

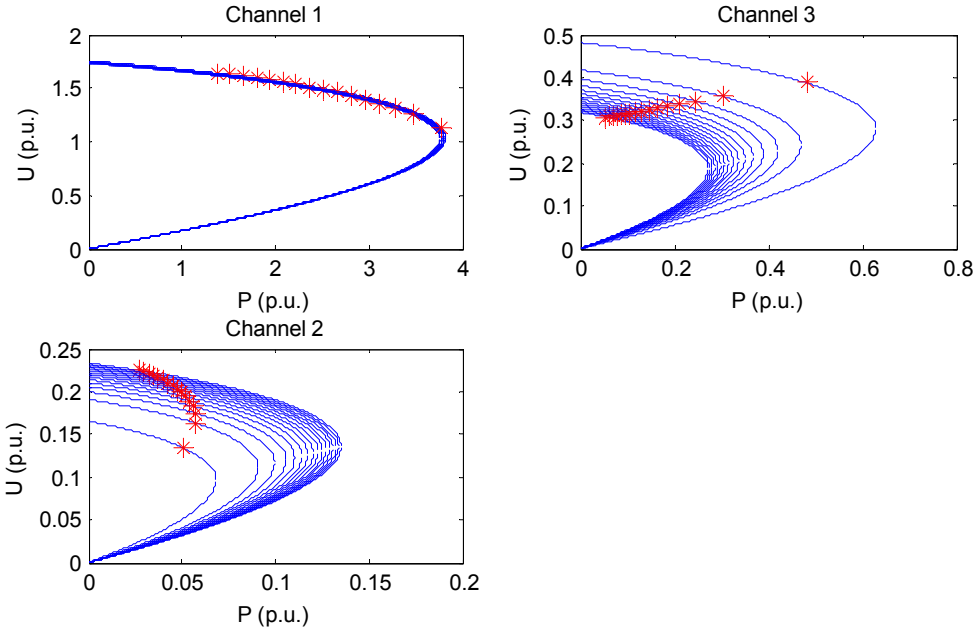

Fig. 8.4: Channel PV curves for WECC 9-bus system

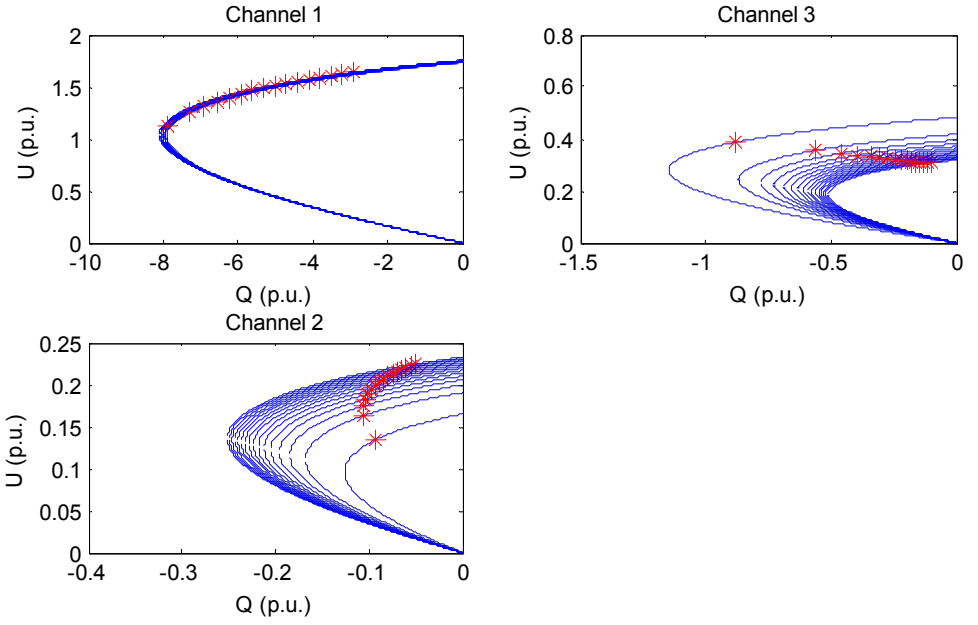

Fig. 8.5: Channel QV curves for WECC 9-bus system

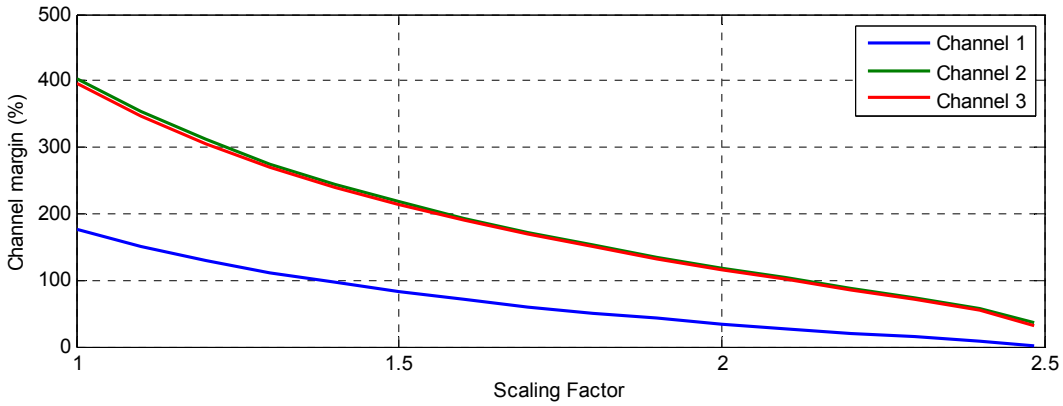

Fig. 8.6: Channel margins for WECC 9-bus system

Fig. 8.7 compares the channel margins obtained from the SVD-based transformation with those of the CCT. As seen in this figure, the margins (especially the critical channel's margin) obtained by both methods are the same.

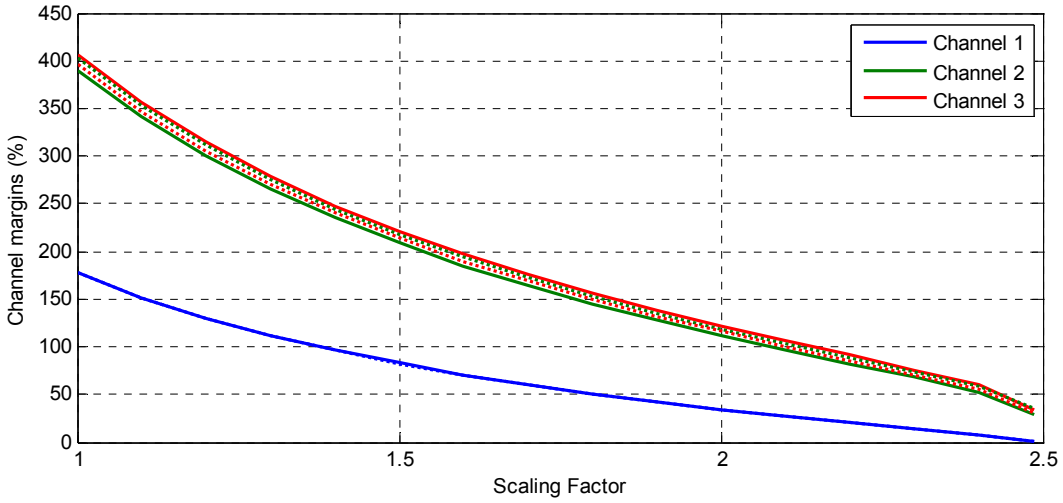

Fig. 8.7: Comparison of channel margins obtained by the CCT and the SVD-based transformations (solid lines: CCT, dash lines: SVD-based transformation)

The load and generator rankings obtained by the SVD-based transformation are also shown in Fig. 8.8 and Fig. 8.9. If we compare these results with those of the CCT illustrated in Fig. 4.1 and Fig. 4.5, we will see that the rankings are exactly identical.

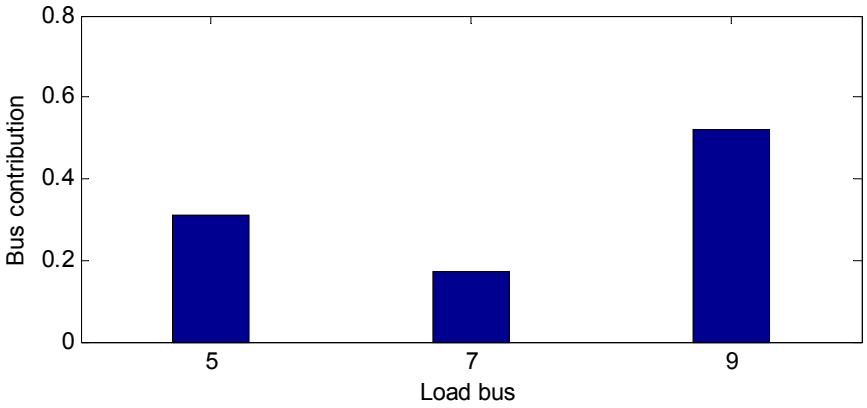

Fig. 8.8: Contribtions of load buses to the critical channel

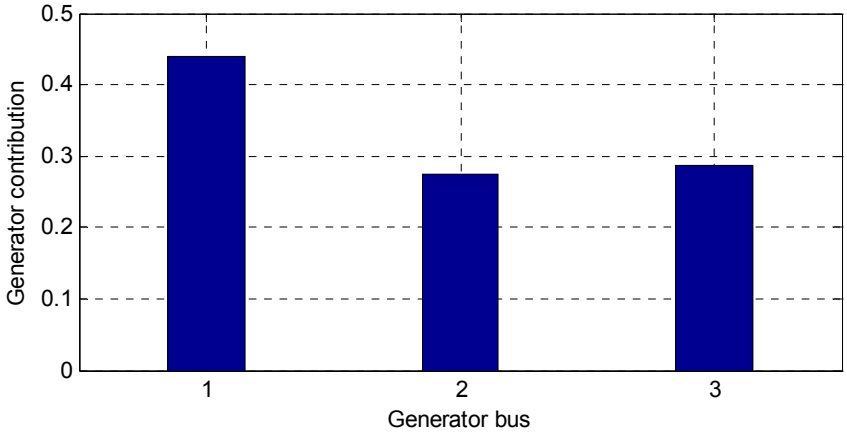

Fig. 8.9: Contribtions of generator buses to the critical channel

- **IEEE 30-bus**

Fig. 8.10 and Fig. 8.11 show the top PV/QV curves for the IEEE 30-bus systems. As both of these figures show, channel 1 is the critical channel whose operating point goes very close to the nose point. Also, Fig. 8.12 compares the channel margins obtained by the SVD-based transformation and the CCT. According to this figure, the margins of critical channels are exactly the same.

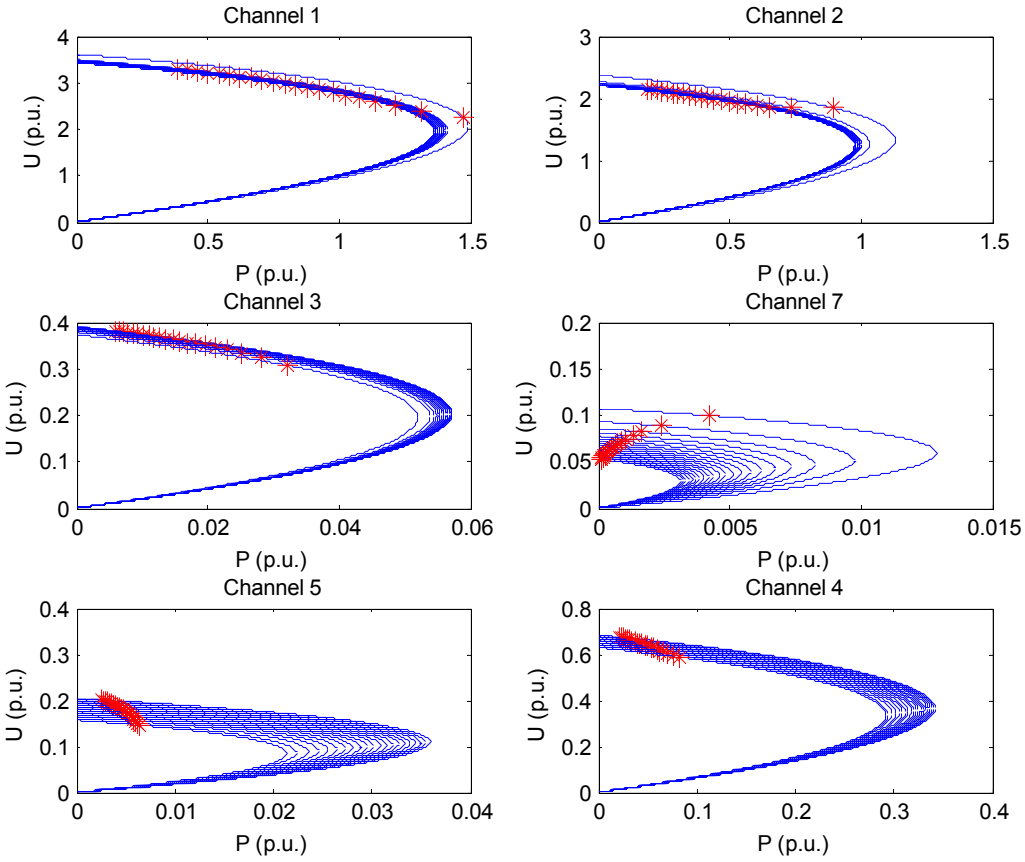

Fig. 8.10: Channel PV curves for IEEE-30 bus system

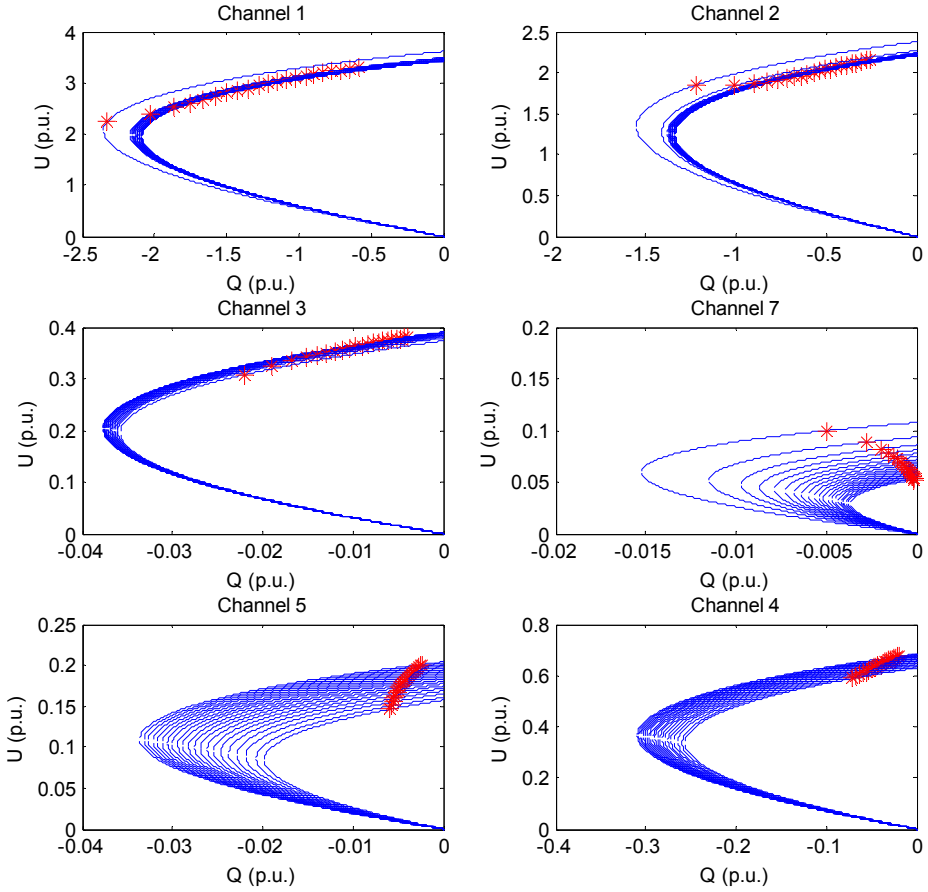

Fig. 8.11: Channel QV curves for IEEE-30 bus system

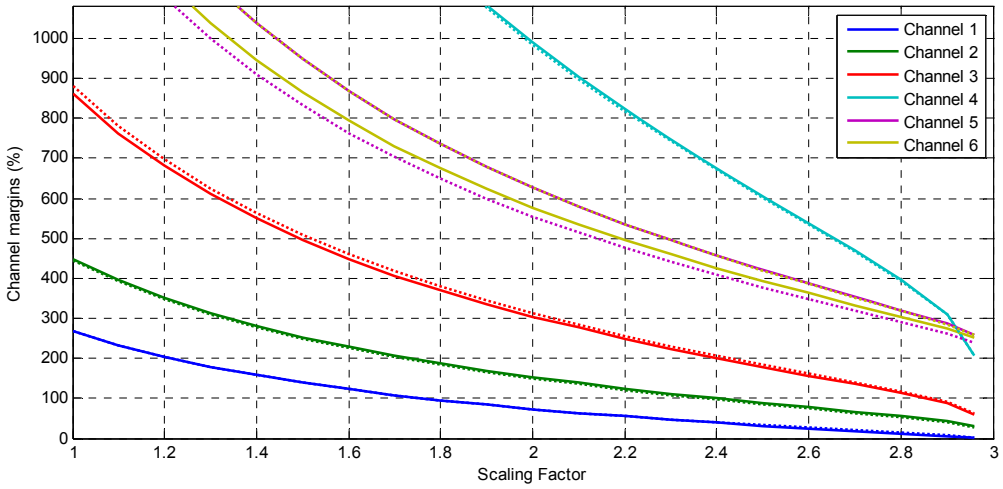

Fig. 8.12: Comparison of channel margins obtained by the CCT and the SVD-based transformations (solid lines: CCT, dash lines: SVD-based transformation)

The load and generator rankings obtained by the SVD-based transformation are also shown in Fig. 8.13 and Fig. 8.14. If we compare these results with those of the CCT illustrated in chapter 4, we will see that the rankings are exactly identical.

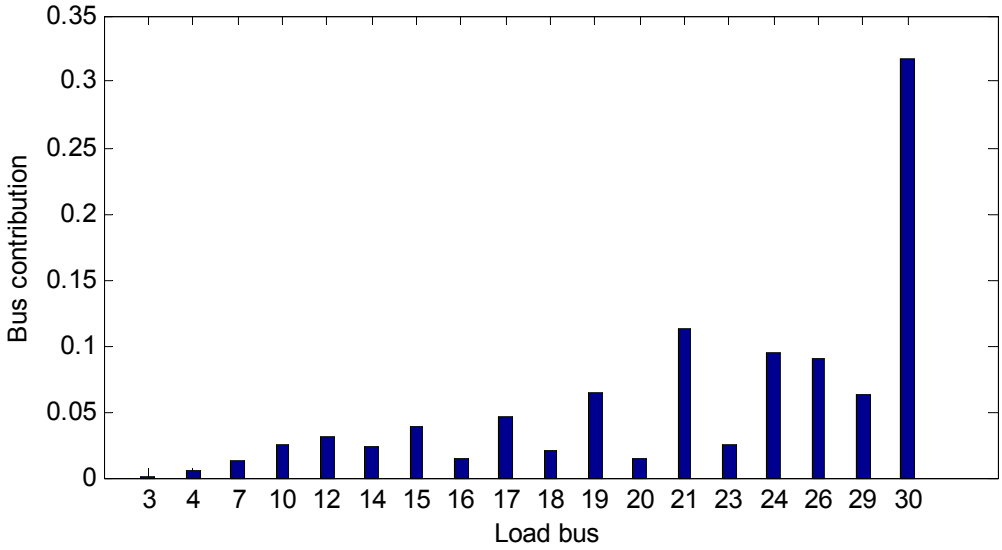

Fig. 8.13: Contribtions of load buses to the critical channel

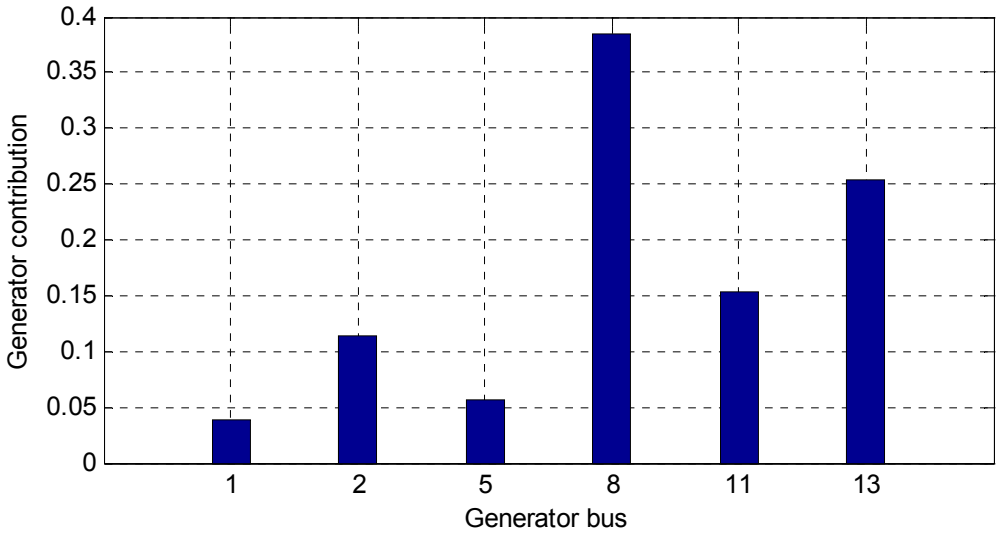

Fig. 8.14: Contribtions of generator buses to the critical channel

- **IEEE 57-bus**

Fig. 8.15 and Fig. 8.16 show the PV/QV curve results for the IEEE 57-bus systems. As both of these figures show, channel 1 is the critical channel whose operating point goes very close to the nose point. Also, Fig. 8.17 compares the channel margins obtained by the SVD-based transformation and the CCT. According to this figure, the margins of critical channels are exactly the same.

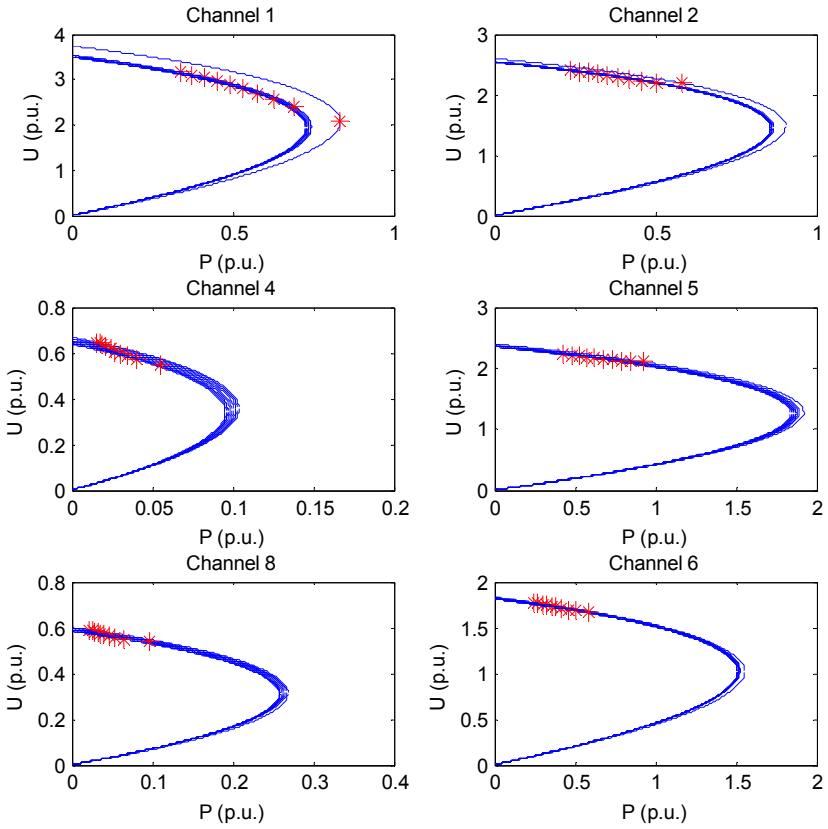

Fig. 8.15: Channel PV curves

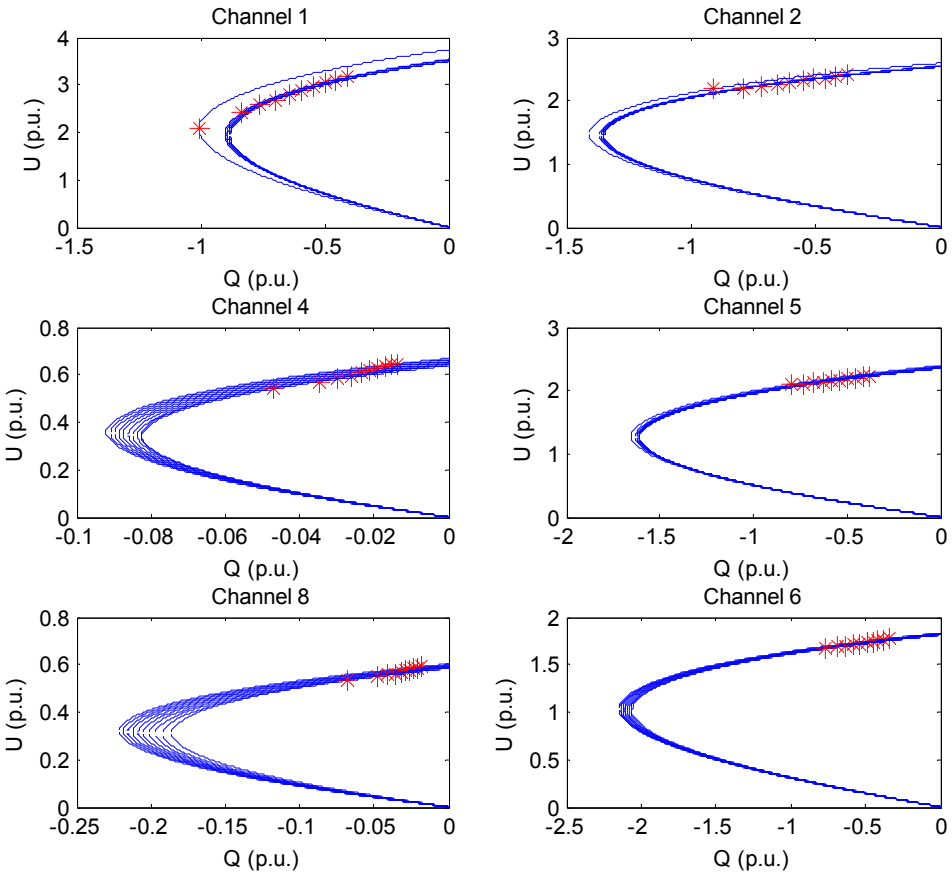

Fig. 8.16: Channel QV curves

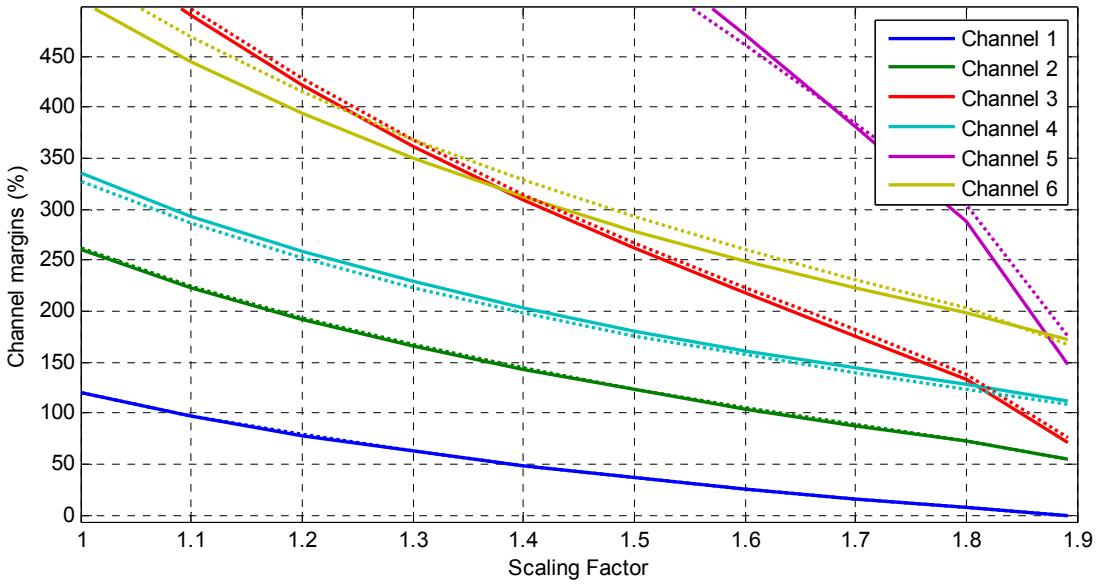

Fig. 8.17: Comparison of channel margins obtained by the CCT and the SVD-based transformations (solid lines: CCT, dash lines: SVD-based transformation)

The load and generator rankings obtained by the SVD-based transformation are also shown in Fig. 8.18 and Fig. 8.19. If we compare these results with those of the CCT illustrated in chapter 4, we will see that the rankings are exactly identical.

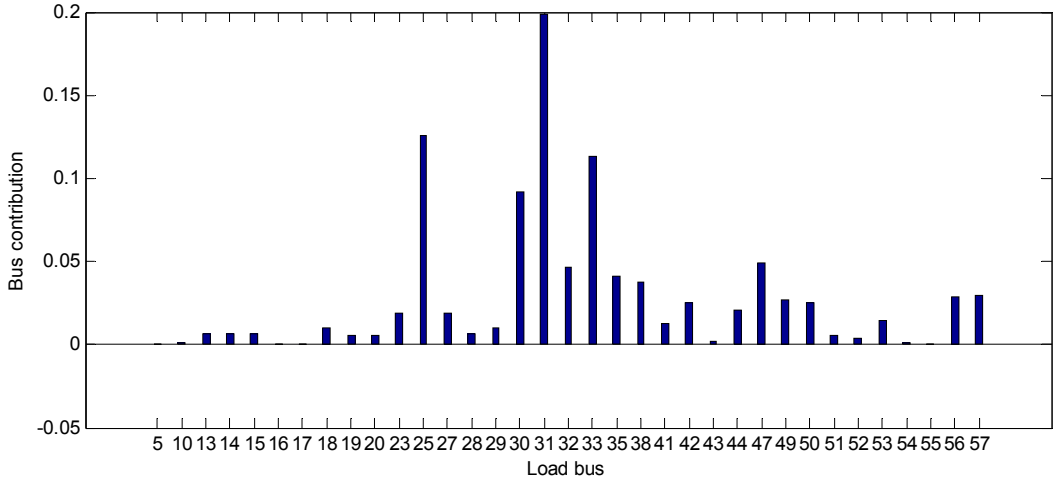

Fig. 8.18: Contribtions of load buses to the critical channel

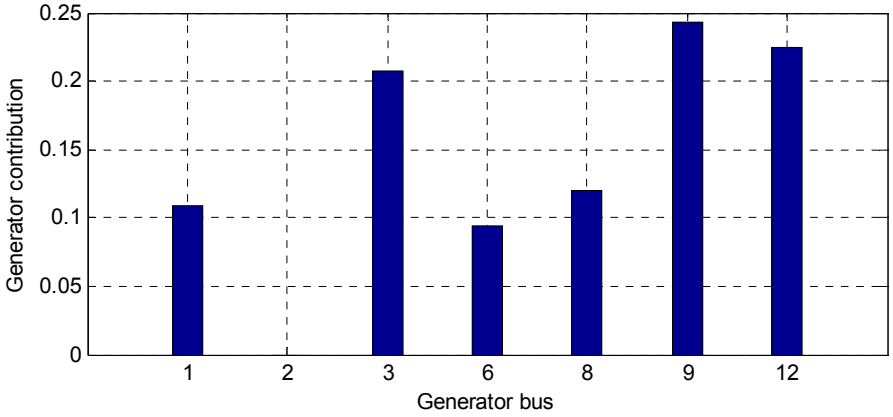

Fig. 8.19: Contribtions of generator buses to the critical channel

The results reported above verify that the proposed SVD-based transformation can be successfully applied to voltage stability analysis. Comparison of the obtained results with those of the CCT show that the SVD-based transformation leads to the same margins for the critical channels, the same ranking for the loads, and the same ranking for the generators.

8.5 Conclusions

The channel components transform which is an eigen-decomposition-based transformation showed many unique features in analyzing voltage stability in previous chapters. In this chapter, the difficulties which might be faced by CCT were discussed. The main difficulties include the non-existence difficulty and the robustness difficulty. These difficulties were discussed in detail. It was shown that using the singular value decomposition instead of the eigen-decomposition could help overcoming the difficulties. Therefore, a new transformation based on singular value decomposition was proposed. The proposed transformation was then applied to several test systems to analyze the voltage stability characteristics. The obtained results were compared to those of the CCT. The comparison showed that the SVD-based transformation leads to the same margins for the critical channels, the same ranking for the loads, and the same ranking for the generators. The implication is that the proposed SVD-based transformation can be successfully applied to voltage stability analysis. Since it does not face the non-existence and the robustness difficulties, the SVD-based transformation might be preferred instead of the original CCT.

Chapter 9: Conclusions and Future Work

This chapter summarizes the main findings of the thesis and provides suggestions for extending and improving this research.

9.1 Thesis Conclusions and Contributions

In this thesis, a new framework called Channel Component Transform (CCT) has been proposed to analyze the behavior of complex power systems. The framework has been used to analyze one of the important problems in power systems i.e. power system voltage stability. Case studies show that the proposed method can indeed reveal new information about a power system and is a quite promising technique. The overall results of the work can be summarized as follows.

- The main feature of the CCT is that it can decouple a complex network into a set of decoupled single-source, single-branch and single-load networks called channel networks. The decoupled circuits are much easier to analyze and they can reveal insightful characteristics of a power system, such as the modes of voltage instability and paths of critical power flow. Similarly, if the variations of the transformed variables can be evaluated, one may be able to predict the complex behaviors of the actual network.

- Using the proposed transformation, actual PV curves of a complex power network could be decomposed into channel PV curves. This is a promising feature since the channel PV curves can be easily derived from the channel circuits even in online applications. Channel PV curves can be used instead of actual PV curves for voltage stability analysis and monitoring. This is achieved by evaluating the criticality of each channel in that domain and finding the critical channel which is most responsible for the voltage collapse. Once the critical channel is found, the voltage stability analysis and monitoring can be performed by only analyzing and monitoring this channel.

- With the proposed transform, the *PV* curves can also be examined from the perspective of power-angle relationship in the channel domain. The results help one to gain improved understanding on the role of bus voltage angles in voltage collapse. Without the proposed transform, it is impossible to obtain any meaningful $P\delta$ curves since there are many physical bus angles in an actual power system, and which bus angle differences need to be examined are difficult to determine.

- The contributions of load buses to the critical channel can be calculated and used as an index to rank the load buses in terms of their impact on the voltage stability. Extensive case study results and comparisons with the already established methods have verified the performance of the proposed method. Identification of the critical buses can help us to establish some practical applications for the transform. For example, an online wide-area load shedding scheme based on the critical buses may be developed to prevent the voltage collapse

- Using CCT, a technique has been proposed to identify the critical generators which have the highest impacts on the voltage collapse. The proposed technique is based on the contributions of generators to the critical channel. This could be a significant contribution since no such method has been proposed before. The generator ranking can be utilized for optimal reactive power planning which can lead to a valuable improvement in the system stability margin.

- Based on the proposed CCT-based framework, a method has been proposed to identify the critical branch. The critical branch is the one which is more under pressure and as a result, limits the stability level of the system. The identification of the critical branch is very important because it can help the operator improve the stability of the system efficiently. As an example, series compensation devices such as TCSC can be installed in the critical line.

- The CCT and all the associated methods proposed in this report have been applied to several standard test systems and an actual large system, the Alberta Integrated Electric System (AIES). The obtained results are very promising, indicating that the CCT-based voltage stability analysis can be very effective and practical. A CCT-based software package has also been developed which works on PSSE platform. By

applying the software on the AIES, this thesis showed the effectiveness of the software in performing complete and detailed voltage stability analysis.

- A procedure based on CCT was proposed for shunt compensation in order to increase the stability margin of the system. In the proposed procedure, the best location is chosen based on the bus ranking results. An initial estimation for the amount of the capacitor is then obtained according to the critical channel's margin. The estimated value is then improved using an iterative method. The case study results verified the proposed method. The results also showed that the estimated value is very close to the accurate value and as a result, the iterative method needs to be performed for only a couple of iterations. The proposed method was also extended to multi-location shunt compensation.

- The proposed framework can be implemented for the online monitoring of voltage stability. For this purpose, a wide-area monitoring scheme has been presented in this thesis. The proposed scheme is based on the current technologies available in power systems. These technologies mainly consist of Phasor Measurements Units (PMUs), and Supervisory Control and Data Acquisition (SCADA). A methodology for optimal placement of PMUs has also been proposed in order to minimize the number of required PMUs and as a result make the implementation procedure more practical.

- Despite all the unique features of the CCT, there might be some difficulties. The main difficulties which include the non-existence difficulty and the robustness difficulty were discussed in this thesis. Although these difficulties are not likely to happen, an alternative has been proposed to overcome these difficulties. For this purpose, a new transformation based on singular value decomposition was proposed. The proposed transformation was then applied to several test systems to analyze the voltage stability characteristics. The obtained results showed that the proposed SVD-based transformation can be successfully applied to voltage stability analysis.

9.2 Suggestion for Future Work

Voltage stability analysis and monitoring is just one of the applications of the CCT. Indeed, the proposed transform and associated framework can lead to several other applications. As an

example of these applications, a reactive power planning strategy on the network side has been proposed in this thesis. The proposed strategy uses the critical channel information and bus ranking results to determine the location and amount of shunt compensations. Some of the other potential applications seen at this stage could be as follows:

- Optimal scheduling of generators (RPP on the generation side): Similar to the proposed procedure for RPP on the network side, an iterative procedure can be proposed. The suggested procedure is as follows: The conventional optimal power flow (OPF) is firstly performed. The generators' contributions to the critical channel are also determined. These contributions are then used to define penalty factors for generators' reactive powers. The active power dispatch obtained by OPF is kept fixed, and by using the penalty factors, OPF is performed again. New generators' contributions and associated penalty factors are then calculated and OPF is performed again. This procedure is repeated until the required margin is achieved.

- Optimal allocation of series compensation devices: The critical transmission lines identified by the proposed framework are the ones which more limit the stability of the system. They will be the best candidate for series compensation techniques. Therefore, the critical lines identified by CCT can be utilized to propose a practical method for optimal allocation of series compensation devices (such as TCSC) in order to improve voltage stability.

- Effective load shedding schemes: Similar to the proposed procedure for the shunt compensation, an iterative algorithm can be proposed for optimal load shedding. The suggested algorithm could be as follows: The best location for load shedding is chosen based on the bus ranking results. An initial estimation for the amount of the load to be shed is then obtained according to the critical channel's margin. The estimated value can then be improved using an iterative method. This can be repeated for next critical loads until the required margin criteria are met.

- Establish a framework for angular stability analysis: Similar to the PV curve decomposition, the CCT can be applied to decompose Pδ curves. The Pδ curve decomposition for the purpose of voltage stability analysis has been conducted and presented in this thesis. The decomposition for the purpose of transient stability analysis could be done as well. For this purpose, the "multiphase" network model

shall be developed from the generator's perspective. The corresponding network equation will be

$$V_G = KV_S + ZI_G \tag{9.1}$$

where V_G is the voltage of the generators excluding the swing one, and V_S is the voltage of the swing generator. A transformation similar to the CCT with using the eigen-decomposition of the new Z matrix can then be applied and a transformed channel domain model, shown in Fig. 9.1, can be obtained. In this model, every circuit has a voltage source F acting as the infinite bus. Therefore, each channel circuit can be considered as an one-machine infinity bus (OMIB) system and its transient stability may be analyzed using the channel Pδ curves. There is no doubt that similar to the voltage stability analysis, a lot more research is needed to find the transient stability characteristics of a system in channel domain.

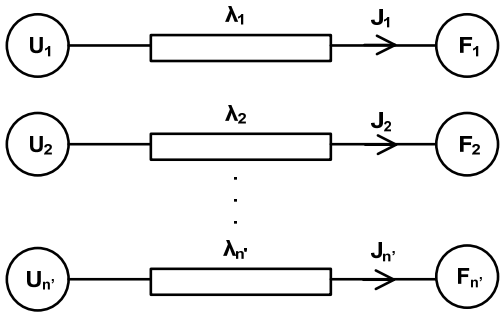

Fig. 9.1: Channel domain representation for transient stability analysis

Chapter 10: References

[1] IEEE/CIGRE Joint Task Force on Stability Terms and Definitions, “Definition and classification of power system stability”, IEEE Trans. on Power Systems, vol. 19, no. 2, pp. 1387-1401, May 2004.

[2] A. G. Phadke, “Synchronized phasor measurements in power systems,” IEEE Comput. Appl. Power, vol. 6, no. 2, pp. 10–15, Apr. 1993.

[3] P. Pourbeik and C. Rehtanz, conveners, Wide Area Monitoring and Control for Transmission Capability Enhancement, Fin. Rep. CIGRE Working Group C4.601, Jan. 2007.

[4] A. G. Phadke, H. Voslkis, R. M. de Morales, T. Bi, R. N. Nayak, Y. K. Sehgal, S. Sen, W. Sattinger, E. Martinez, O. Samuelsson, D. Novosel, V. Madani, and Y. A. Kulikov, “The wide world of wide-area measurements,” IEEE Power Energy Mag., vol. 6, no. 5, pp. 52–65, Nov. 2008.

[5] D. Novosel, V. Madani, B. Bhargava, K. Vu, and J. Cole, “Dawn of the grid synchronization,” IEEE Power Energy Mag., vol. 6, no. 1, pp. 49–60, Jan. 2008.

[6] M. Zima, M. Larsson, P. Korba, C. Rehtanz, and G. Andersson, "Design Aspects for Wide-Area Monitoring and Control Systems," Proceedings of the IEEE, vol.93, no.5, pp. 980-996, May 2005.

[7] Chih-Wen Liu, Mu-chun Su, Shuenn-Shing Tsay, and Yi-Jen Wang, "Application of a novel fuzzy neural network to real-time transient stability swings prediction based on synchronized phasor measurements," IEEE Trans. Power Syst., vol.14, no.2, pp.685-692, May 1999.

[8] M. Glavic, T. Van Cutsem, “Wide-area Detection of Voltage Instability from Synchronized Phasor Measurements. Part I: Principle”, IEEE Trans. On Power Systems, vol. 24, no. 3, pp. 1408-1425, Aug. 2009.

[9] A. M. Abed, “WSCC Voltage stability criteria, undervoltage load shedding strategy, and reactive power reserve monitoring methodology”, IEEE PES Summer Meeting 1999, vol. 1, pp. 191-197, Jul. 1999.

[10] V Ajjarapu and C. Christy, "The continuation power flow: A tool for steady state voltage stability analysis," IEEE Trans. Power Syst., vol. 7, no. 1, pp. 416-423, Feb. 1992.

[11] C. Cañizares, Ed., Voltage Stability Assessment: Concepts, Practices, and Tools, 2002, ISBN 0 780 378 695. Special publication of the IEEE Power System Stability Subcommittee.

[12] B. Gao, G. K. Morison, and P. Kundur, “Voltage Stability Evaluation Using Modal Analysis”, IEEE Trans. Power Syst., vol.7, no. 4, pp. 1529-1542, Nov. 1992.

[13] Y. Mansour, W. Xu, F. Alvarado, and C. Rizzin, "SVC placement using critical modes of voltage instability," IEEE Trans. Power Syst., vol. 9, no. 2, pp. 757- 763, May 1994.

[14] D. L Hau Aik, and G. Andersson, “Use of Participation Factors in Model Voltage Stability Analysis of Multi-infeed HVDC Systems”, IEEE Trans. Power Deliv., vol. 13, no. 1, pp. 203-211, Jan. 1998.

[15] T. Van Cutsem and C. Vournas, Voltage Stability of Electric Power Systems. Norwell, MA: Kluwer, 1998.

[16] Y. Mansour, Ed., Suggested techniques for voltage stability analysis: IEEE Working Group on Voltage Stability, 1993.

[17] L. C. P. Da Silva, V. F. da Costa, and W. Xu, "Assessment of generator impact on system power transfer capability using modal participation factors," Proc. Inst. Elect. Eng.—Gen., Transm., Dist., vol. 149, no. 5, p. 564, 2002.

[18] R. J. Thomas and A. Tiranuchit, "Voltage instabilities in electric power networks," Proceedings of the 18th Southeastern Symposium on System Theory, Apr. 1986, pp. 359-363.

[19] A. Tiranuchit and R. J. Thomas, "A posturing strategy against voltage instabilities in electric power system," IEEE Trans. Power Syst., vol. 3, no. 1, pp.87-93, Feb. 1988.

[20] P. A. Löf, T. Smed, G. Andersson, and D. J. Hill, "Fast calculation of a voltage stability index," IEEE Trans. Power Syst., vol. 7, no. 1, pp. 54-64, Feb. 1992.

[21] C. A. Canizares, A. Z. de Souza, and V.H. Quintana, "Comparison of performance indices for detection of proximity to voltage collapse," IEEE Trans. Power App. Syst., vol. 11, no. 3, pp. 1441-1450, Aug. 1996.

[22] J. Peshon, D. S. Piercy, W. F. Tinney, and O. J. Tveit, "Sensitivity in power systems," IEEE Trans. Power App. Syst., vol. PAS-87, 1968.

[23] CIGREWorking Group, "Indices Predicting Voltage Collapse Including Dynamic Phenomena," Report of CIGRE Working Group 38.02.11, 1994.

[24] M. Suzuki and K. Masegi, "Direct calculation of voltage-stability limit of electric power systems," Electrical Engineering in Japan, Vol. 111, No. 7, pp. 40-48. 1991.

[25] C. Concordia, "Voltage stability simplified," International Journal of Electrical & Energy Systems, vol. 14, no. 5, pp. 364-366, Oct. 1992.

[26] M. Begovic and A. Phadke, "Control of voltage stability using sensitivity analysis," IEEE Trans. Power Syst., vol. 7, no. 1, pp. 114–123, Feb. 1992.

[27] T. Van Cutsem, Y. Jacquemart, J.-N. Marquet, and P. Pruvot, "A comprehensive analysis of mid-term voltage stability," IEEE Trans. Power Syst., vol. 10, no. 2, pp. 1173–1182, May 1995.

[28] I. Dobson, "Observations on the geometry of saddle-node bifurcation and voltage collapse in electric power systems," IEEE Trans. Circuits Syst. I, vol. 39, no. 3, pp. 240–243, Mar. 1992.

[29] S. Greene, I. Dobson, and F. Alvarado, "Sensitivity of the loading margin to voltage collapse with respect to arbitrary parameters," IEEE Trans. Power Syst., vol. 12, no. 1, pp. 262–272, Feb. 1997.

[30] C. Moors and T. Van Cutsem, "Determination of optimal load shedding against voltage instability," in Proc. 13th Power System Computation Conf., Trondheim, Norway, Jul. 1999, pp. 993–1000.

[31] F. Capitanescu and T. Van Cutsem, "Preventive control of voltage security: A multi-contingency sensitivity-based approach," IEEE Trans. Power Syst., vol. 17, no. 2, pp. 358–364, May 2002.

[32] F. Capitanescu, T. Van Cutsem, "Unified sensitivity analysis of unstable or low voltages caused by load increases or contingencies", IEEE Trans. Power Syst., Vol. 20, No. 1, pp. 321-329, Feb. 2005

[33] Yanfeng Gong, "Development Of An Improved On-Line Voltage Stability Index Using Synchronized Phasor Measurement ", Phd Dissertation, Department Of Electrical & Computer Engineering, Mississippi State University, 2006.

[34] Y. Tamura, H. Mori, and S. Iwamoto, "Relationship between voltage instability and multiple load flow solutions in electric power systems," IEEE Trans. Power App. Syst., vol. 102, no. 5, pp. 1115-1125, May 1983.

[35] Y. Tamura, K. Sakamoto, and Y. Tayama, "Current issues in the analysis of voltage instability phenomena," Proc. Bulk Power System Phenomena – Voltage Stability and Security, EPRI, pp.5-39, January 1989.

[36] P. Kessel and H. Glavitsch, "Estimating the voltage stability of a power system," IEEE Trans. Power Syst., vol. 1, no. 3, pp. 346-354, Jul. 1986.

[37] T. Q. Tuan, J, Fandino, N. Hadjsaid, J. C. Sabonnadiere, H. Vu, "Emergency load shedding to avoid risks of voltage instability using indicators," IEEE Trans. Power Syst., vol. 9, no. 1, pp. 341-351, Feb. 1994.

[38] K. Vu, M. M. Begovic, D. Novosel, M. M. Saha, "Use of Local Measurements to Estimate Voltage Stability Margin", IEEE Trans. Power Syst., vol. 14, no. 3, pp. 1029-1035, Aug. 1999.

[39] D. E. Julian, R. P. Schulz, K. T. Vu, W. H. Quaintance, N. B. Bhatt, D. Novosel, "Quantifying proximity to voltage collapse using the voltage instability predictor (VIP)", Proc. IEEE PES Summer Meeting, Seattle, Jul. 2000, pp. 16-20.

[40] M. Moghavvemi and O. Faruque, "Real-time contingency evaluation and ranking technique", IEE Proc.-Gener. Transm. Distrib. Vol. 145, no.5, pp. 517-524, Sept. 1998.

[41] I. Smon, G. Verbic, and F. Gubina, "Local voltage-stability index using Tellegen's theorem", IEEE Trans. Power Syst., vol. 21, no. 3, pp. 1267-1275, Aug. 2006.

[42] M. Larsson, C. Rehtanz, and J. Bertsch, "Real-time voltage stability assessment of transmission corridors", presented at the IFAC Symp. Power Plants and Power Systems Control, Seoul, Korea, 2002.

[43] F. Gubina and B. Strmcnik, "Voltage stability proximity index determination using voltage phasors approach", IEEE Trans. Power Syst., vol. 10, no. 2, pp. 788-794, May 1995.

[44] F. Gubina and B. Strmcnik, "A simple approach to voltage stability assessment in radial networks", IEEE Trans. Power Syst., vol. 12, no. 3, pp. 1121-1128, Aug. 1997.

[45] A. Wiszniewski, "New criteria of voltage stability margin for the purpose of load shedding", IEEE Trans. Power delivery, vol. 22, no.3, pp. 1367-1371, July 2007.

[46] M. Glavic and T. Van Cutsem, "Detecting with PMUs the onset of voltage instability caused by a large disturbance," in Proc. 2008 IEEE Power Eng. Soc. General Meeting, Pittsburgh, PA, Jul. 2008.

[47] C. D. Vournas, N. G. Sakellaridis, "Tracking Maximum Loadability Conditions in Power Systems", Proc. Bulk Power System Dynamics and Control-VII, Paper 104, Charleston, Aug. 2007.

[48] B. Milosevic, M. Begovic, "Voltage Stability Protection and Control using a Wide-Area Network of Phasor Measurements", IEEE Trans. Power Syst., vol. 18, no. 1, pp. 121-127, Feb. 2003.

[49] B. Genet, J-C. Maun, "Voltage Stability Monitoring using Wide- Area Measurement System", Proc. of IEEE PowerTech Conf., Lausanne (Switzerland), paper 392, Jun. 2007.

[50] M. Glavic and T. Van Cutsem, "Wide-area detection of voltage instability from synchronized phasor measurements. Part II: Simulation results," IEEE Trans. Power Syst., vol. 24, no. 3, pp. 1417–1425, Aug. 2009.

[51] T. Van Cutsem, "Voltage instability: Phenomena, countermeasures, and analysis methods," Proc. IEEE, vol. 88, pp. 208–227, 2000.

[52] W. Zhang, F. Li, L. M. Tolbert, "Review of Reactive Power Planning: Objectives, Constraints, and Algorithms," IEEE Trans. Power Syst., vol. 22, no. 4, pp. 2177-2186, 2007.

[53] Y. L. Chen, "Weak bus oriented reactive power planning for system security," IEE Proc. Generation, Transmission and Distribution, vol. 143, no. 6, pp. 541–545, Nov. 1996.

[54] B. Kermanshahi, K. Takahashi, and Y. Zhou, "Optimal operation and allocation of reactive power resource considering static voltage stability," in Proc. 1998 Int. Conf. Power System Technology (POWERCON '98), Aug. 18–21, 1998, vol. 2, pp. 1473–1477.

[55] Y. L. Chen and C. C. Liu, "Multiobjective Var planning using the goal attainment method," IEE Proc. Generation, Transmission and Distribution, vol. 141, no. 3, pp. 227–232, May 1994.

[56] Y. L. Chen, "Weighted-norm approach for multiobjective Var planning," IEE Proc. Generation, Transmission and Distribution, vol. 145, no. 4, pp. 369–374, Jul. 1998.

[57] Y. L. Chen and C. C. Liu, "Optimal multi-objective Var planning using an interactive satisfying method," IEEE Trans. Power Syst., vol. 10, no. 2, pp. 664–670, May 1995.

[58] R. Ramos, J. Vallejos, and B. Barán, "Multi-objective reactive power compensation with voltage security," in Proc. 2004 IEEE/PES Transmission and Distribution Conf. and Expo.: Latin America, Brazil, Nov. 2004, pp. 302–307.

[59] C. Cañizares, W. Rosehart, A. Berizzi, and C. Bovo, "Comparison of voltage security constrained optimal power flow techniques," in Proc. PES Summer Meeting, vol. 3, 2001, pp. 1680–1685.

[60] F. Dong, B.H. Chowdhury, and M.L. Crow, "Improving voltage stability by reactive power reserve management," IEEE Trans. Power Syst., vol. 20, no. 1, pp. 338–345, Feb. 2005.

[61] C. M. Affonso, L. C. P. da Silva, F. G. M. Lima, et al. "MW and MVar management on supply and demand side for meeting voltage stability margin criteria" IEEE trans. power syst., vol.19, pp.1538~1545, Aug. 2004.

[62] Claudio A. Canizares and Zeno T. Faur, "Analysis of SVC and TCSC controllers in voltage collapse", IEEE Trans. Power Syst., vol. 14, no. 1, pp. 158-165, Feb. 1999.

[63] C. P. Gupta, S. C. Srivastava and R. K. Varma, "Enhancement of static voltage stability margin with reactive power dispatch using FACTS devices", Proc. of the 13th Power System Computations Conference, Trondheim (Norway), pp. 1009-1015, 1999.

[64] Y. Wang, I. Rahimi Pordanjani, W. Li, W. Xu, and E. Vaahedi, "A strategy to minimize the load shedding amount for voltage stability prevention", IET Generation, Transmission & Distribution, vol.5, no.3, pp.307-313, March 2011.

[65] T. Menezes, L. C. da Silva, and V. F. da Costa, "Dynamic VAR sources scheduling for improving voltage stability margin," IEEE Trans. Power Syst., vol. 18, no. 2, pp. 969–971, May 2003.

[66] T.V. Menezes , L.C.P. da Silva , C.M. Affonso and V.F. da Costa , "MVAR management on the pre-dispatch problem for improving voltage stability margin" , IEE Proc. Gen. Transm. Distrib. , vol. 151 , no. 6 , pp 665-672 , Nov. 2004.

[67] S. Skogestad and I. Postethwaite, Multivariable Feedback Control, Analysis and Design. New York: Wiley, 1996.

[68] Joong-Rin Shin, Byung-Seop Kim, Jong-Bae Park, and K.Y. Lee, "A New Optimal Routing Algorithm for Loss Minimization and Voltage Stability Improvement in Radial Power Systems," IEEE Trans. Power Syst., vol.22, no.2, pp.648-657, May 2007.

[69] Allen. J. Wood, and Bruce F. Wollenberg, "Power Generation, Operation, and Control," 2nd Edition, John Wiley & Sons, NY, Jan 1996.

[70] O. Alsac, and B. Stott, "Optimal Load Flow with Steady State Security," IEEE Trans. Power App. Syst., vol. PAS 93, no. 3, pp. 745-751, 1974.

[71] V. C. Nikolaidis and C. D. Vournas, "Design strategies for load-shedding schemes against voltage collapse in the Hellenic system", IEEE Trans. Power Syst., vol. 23, no. 2, pp. 582-591, May 2008.

[72] Z. Huang , L. Bao and W. Xu , "Generator ranking using modal analysis" , IEE Proc. Gen. Transm. Distrib. , Vol. 150 , No. 6 , pp 709-716 , Nov. 2003.

[73] A. Chakrabortty, J.H. Chow, and A. Salazar, "A Measurement-Based Framework for Dynamic Equivalencing of Large Power Systems Using Wide-Area Phasor Measurements," IEEE Transactions on Smart Grid, vol.2, no.1, pp.68-81, March 2011.

[74] T. Overbye, P. Sauer, C. DeMarco, B. Lesieutre, M. Venkatasubramanian, Using PMU Data to Increase Situational Awareness. PSERC Publication 10-16, Sep. 2010.

[75] H. W. Dommel, ElectroMagnetic Transients Program. Reference Manual (EMTP Theory Book). Portland, OR: Bonneville Power Administration, 1986.

[76] A. G. Phadke, "Synchronized phasor measurements—a historical overview," in Proc. IEEE Power Eng. Soc. Asia Pacific Transmission Distribution Conf. Exhib., Oct. 6–10, 2002, vol. 1, pp. 476–479.

[77] I.Musirin, T.K.A.Rahman "Novel Fast Voltage Stability Index (FVSI) for Voltage Stability Analysis in Power Transmission System" 2002 Student Conference on Research and Development Proceedings, Shah Alam, Malasia, July 2002.

[78] Y. Wang; I. R. Pordanjani, W. Li, W. Xu, T. Chen, E. Vaahedi, and J. Gurney, "Voltage Stability Monitoring Based on the Concept of Coupled Single-Port Circuit," IEEE Trans. Power Syst., vol.26, no.4, pp.2154-2163, Nov. 2011.

[79] M. Lin, "Static and transient voltage stability assessment of hybrid AC/DC power systems," Mississippi State University; 2010.

[80] A. Salloum, "Optimal location and sizing of dynamic VArs for fast voltage collapse," Arizona State University; 2011.

[81] C. Taylor, "Power system voltage stability," MC Graw Hill, New York, 1994.

[82] L. Da Silva, Y. Wang, W. Xu, and V. Da Costa, "Comparative Studies on Methods of Modeling Generator Var Limit for Power-Flow Calculations", Electric Power Components and Systems, vol. 29, no. 6, pp. 561-576, 2001.

[83] 2011 Long-term Transmission Plan, AESO "http://www.aeso.ca/".

[84] Moler CB. Numerical computing with MatLaboratory, 1st ed. USA: Society for Industrial and Applied Mathematic; 2004.

[85] R. D. Zimmermann, and D. Gan, "Matpower a Matlab power system simulation package, " User's Manual,", Version 2.0, Dec. 1997.

[86] Siemens PTI, PSS/E 30.2 Program Operational Manual, Volume II, 2005.

[87] P. Kundur, Power System Stability and Control. New York: McGraw- Hill, 1994.

[88] E. A. Leonidaki, G. A. Manos, and N. D. Hatziargyriou, "An effective method to locate series compensation for voltage stability enhancement," Elec. Power Syst. Res, vol. 74, no. 1, pp. 73–81, Apr. 2005.

Appendix A. Load Models in Channel Domain

If the channel loads are treated as constant power loads, the channel operating point might go beyond the nose of the associated channel PV curve while the system is still stable. Our extensive research has revealed that the phenomenon is caused by the coupling of loads in channel domain. This coupling was discussed in section 3.3.1 from the mathematic point of view and a channel load model consisting of a constant power and a constant current source was proposed in order to overcome this difficulty. A discussion is provided in this appendix to justify the proposed channel load representation from the system point of view.

A.1 A discussion on the PV curve of a two-bus system

In this section, the effect of load model on the voltage stability conditions is discussed first in a simple two-bus system shown in Fig. A.1.

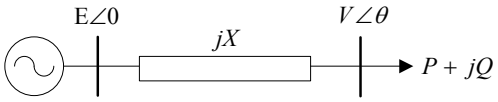

Fig. A.1: A simple two-bus system

For this system, the relationship between the voltage magnitude at the load bus and the load power is given as

$$V^4 + V^2[2(P_L R + Q_L X) - E^2] + Z^2(P_L{}^2 + Q_L{}^2) = 0 \tag{A.1}$$

The above equation defines a curve in (P,V) plane which is known as the PV curve. On the other hand, one more equation can be written according to the load characteristics. For example, if the load is considered as a constant power load, we have

$$\begin{aligned} P_L &= k(P_{con}) \\ Q_L &= k(Q_{con}) \end{aligned} \tag{A.2}$$

where P_{con} and Q_{con} are constants and k is an independent demand variable called scaling factor.

If the load characteristic i.e. (A.2) is plotted in the (P,V) plane, it will intersect the PV curve at two points as shown in Fig. A.2. These points are two feasible solutions of a forth-order equation obtained by including (A.2) in (A.1). For a stable system, the upper side points (C_1, and C_2 in Fig. A.2) are the operating points of the system. Also, the system will be at the voltage collapse point if the load characteristic becomes tangent to system PV curve and two solutions coalesce in one point ($C_{critical}$ in Fig. A.2). According to Fig. A.2, if the load is a constant power load, $C_{critical}$ will be at the nose point of the PV curve. Therefore, for a constant power load, the operating point will never go beyond the nose point of the PV curve in a stable system.

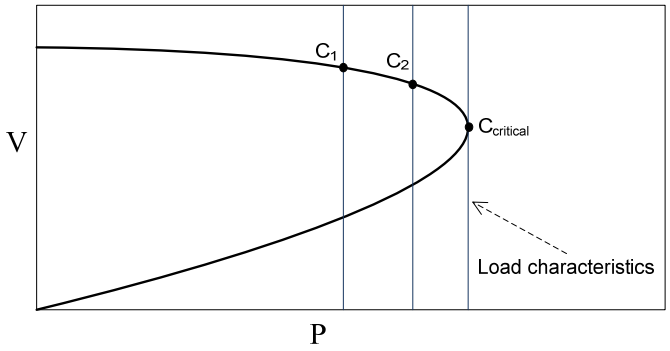

Fig. A.2: PV curve and load characteristic of a constant power load

Now let's consider that the load is not a constant power. For example, if we consider the load as a mixture of a constant power and a constant current load, the load characteristic will be

$$\begin{aligned} P_L &= k(P_{con} + aV) \\ Q_L &= k(Q_{con} + bV) \end{aligned} \tag{A.3}$$

where a and b are constants and define the constant current part of the load.

The previous system is considered again, but this time, the load is considered to be a mixture of a constant power and a constant current. If the load characteristic is plotted in the (P,V) plane, Fig. A.3 is obtained. According to this figure, the critical operating point lies beyond the nose

point of the PV curve. This indicates that the operating point of a stable system can be on the lower half-side of the PV curve. For example, C_3 in Fig. A.3 which is beyond the nose point of the PV curve is a stable operating point of the system.

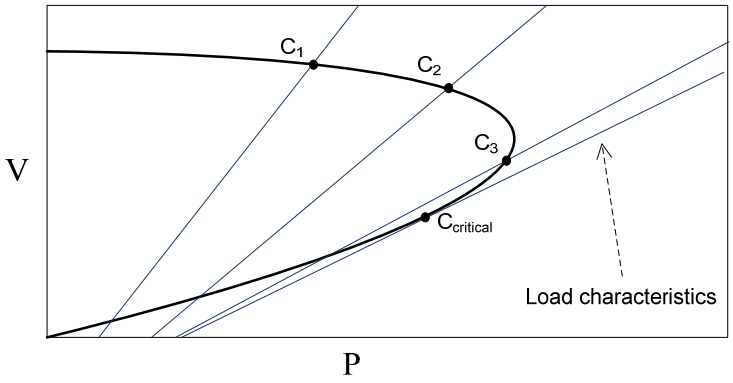

Fig. A.3: PV curve and load characteristic of a load consisting 25% PQ and 75% constant current

According to what was explained above, the following conclusion can be obtained from this discussion; If the load is considered as a constant power, the operating point of a stable system cannot lie beyond the nose point of the associated PV curve. However, if the load is not a constant power, the system operating point can lie beyond the nose point of the PV curve while the system is still stable. This conclusion gives us the idea that a similar phenomenon might happen in channel domain. In other words, channel loads might not be purely constant power loads and as a result the channel operating point can go beyond the nose point of the channel PV curve.

A.2 Selection of a Proper Model for Channel Loads

At the first step of the channel load modeling, a proper model should be chosen. For this purpose, a discussion on a simple system is conducted and according to the results, a model is chosen for the channel loads.

A 3-generator, 3-load power system shown in Fig. A.4 (a) is considered as the case study. Note that we especially let $Z_{12} = Z_{23} = Z_{13}$, and $Z_{11} = Z_{22} = Z_{33}$. The resulting Thevenin [*Z*] matrix will have the following form:

$$[Z] = \begin{bmatrix} Z_s & Z_m & Z_m \\ Z_m & Z_s & Z_m \\ Z_m & Z_m & Z_s \end{bmatrix}$$

where Z_s and Z_m can be obtained from the admittance matrix. One can see that this matrix is identical to that of a three-phase line (Fig. A.4 (b)). As a result, the symmetrical components transform can be used as a special case of the channel components transform. The channel domain is the sequence domain. The channel circuits are the 012 sequence circuits.

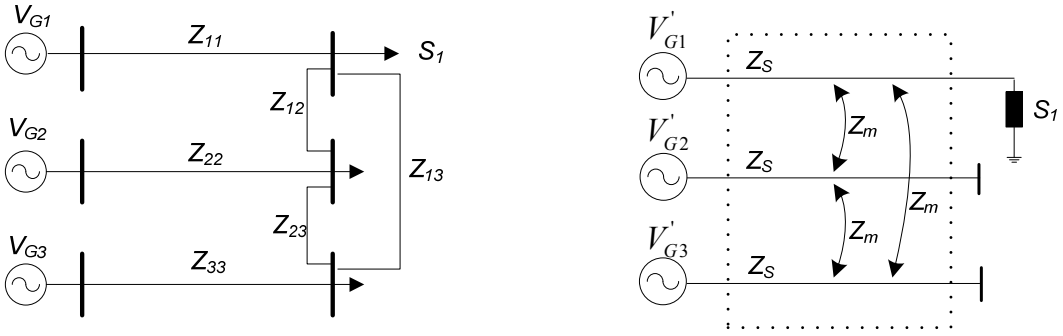

(a) Three bus study system (b) equivalent three-phase representation

Fig. A.4: 3-generator, 3-load system and its equivalent three-phase model.

Furthermore, we assume that only bus 1 is loaded and there are no loads at the other load buses. This loading pattern essentially represents a single-phase short circuit situation, except that the short-circuit impedance is the bus 1 load. Based on the SCT theory, the sequence (channel) circuits can be connected in series as shown in Fig. A.5 to compose the equivalent circuit diagram.

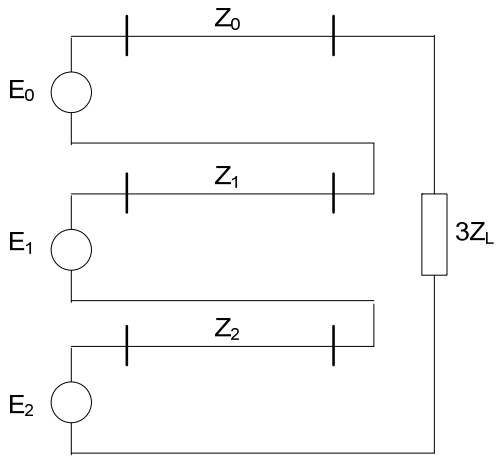

Fig. A.5: Equivalent channel circuit diagram

The above circuit diagram shows the relationship between the actual system and the decoupled modal circuits. The maximum power transfer happens in physical domain when the load (Z_L) gets the maximum power. According to Fig. A.5, this happens when the following condition is satisfied.

$$\frac{|3 * Z_L|}{|Z_0 + Z_1 + Z_2|} = 1 \tag{A.4}$$

Let's consider an example. The impedances are considered as $Z_{11} = Z_{22} = Z_{33} = 0.3j$, and $Z_{12} = Z_{23} = Z_{13} = 0.45j$. The generator voltages are considered as $0.945\angle 6.07^o$, $0.612\angle 22.38^o$, and $0.565\angle 36.11^o$. These voltages are kept constant and Z_L in Fig. A.5 is decreased until it reaches the maximum power transfer. As a result, the PV curve of the load in Fig. A.5 will be as shown in Fig. A.6. Also, the associated channel PV curves are shown in Fig. A.7.

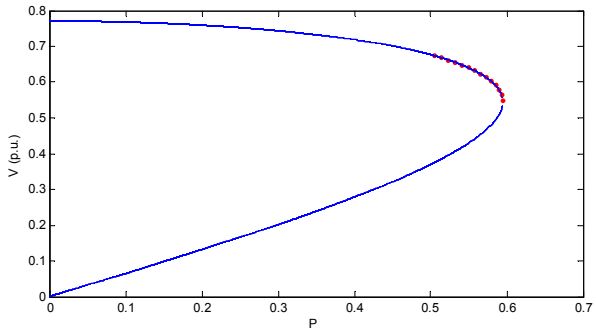

Fig. A.6: PV curve of the equivalent circuit shown in Fig. A.5

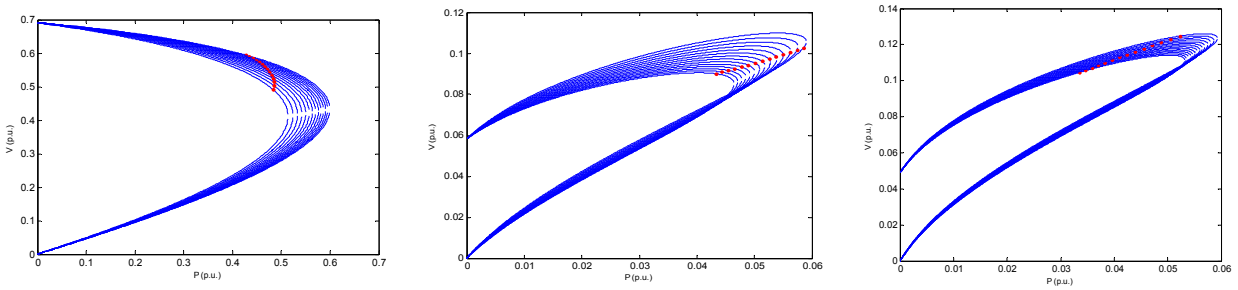

(a) zero sequence (channel 1) (b) positive sequence (channel 2) (c) negative sequence (channel 3)

Fig. A.7: Channel PV curves

According to Fig. A.6 and Fig. A.7, when the actual system is at its nose point, the operating point in channel 2 lies beyond its nose point. To investigate this phenomenon, let's consider the channel equivalent circuits. Based on Fig. A.5, the channel circuit for channel 2 is as shown in Fig. A.8.

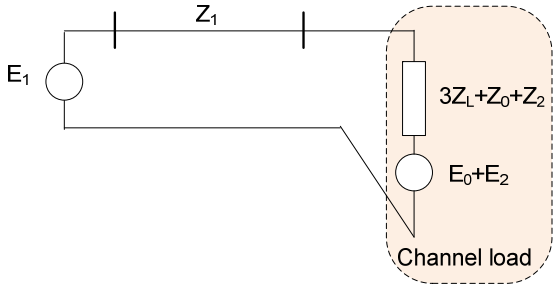

Fig. A.8: Channel circuit for channel 2 (positive sequence)

If the whole channel load shown in Fig. A.8 is treated as a PQ load, the maximum power transfer happens in the channel when,

$$\frac{\left|3Z_L + Z_0 + Z_2 - \left(E_0 + E_2\right)/I_1\right|}{\left|Z_1\right|} = 1 \tag{A.5}$$

The real and imaginary parts of the impedances Z_L, Z_0, Z_1, and Z_2 are usually positive. Therefore, when the actual system is at the nose point i.e. Z ratio in Fig. A.5 is equal to one, Z ratio in (A.5) might be less than one only because of the term $-\left(E_0 + E_2\right)/I_1$. In other words, inclusion of the voltage sources in the channel load might make the operating point pass the nose of the channel PV curve. However, if the voltage sources are considered as what they really are,

and the rest of the load is treated as a PQ load, the channel PV curve will still be the same as Fig. A.7. But this time, according to what was explained before, being beyond the nose point does not mean that the channel is unstable. For example, if the load characteristic of channel 2 is plotted, Fig. A.9 is resulted. According to this figure, although the operating point is beyond the nose point, the channel is still in the stable region.

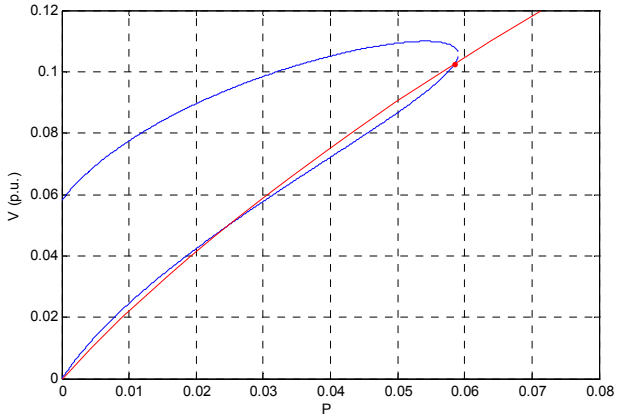

Fig. A.9: PV curve of channel 2 with the load characteristic

The above discussion revealed that in each channel load, there might be a constant voltage source which comes from the voltage sources of the other channels i.e. coupling effect. This constant voltage source might have a significant influence on the placement of the channel operating point on the PV curve. Therefore, a method is required in order to obtain this constant voltage source so that its effect could be excluded from the channel load.

On the other hand, when the physical load is considered as a constant impedance at each system operating point, the Thevenin equivalent of the channel load shown in Fig. A.8 can be replaced by the Norton equivalent which was used in Section 3.3.2.

A.3 Verification of the Proposed Method for Channel Load Modeling

The previous sections of this appendix have shown that the channel load can be modeled as a Thevenin (or Norton) equivalent circuit. In Section 3.3.2, a method were proposed to obtain the parameters of this equivalent circuit. Basically, there are two ways to verify the performance of the proposed method:

- ***Indirect verification***

In this approach, the proposed method is used and the CCT with the modeled channel loads is applied to different voltage stability studies. The comparison of the results with those of the standard methods can determine the effectiveness of the CCT-based strategy which also includes the proposed channel load modeling. This kind of verification has been done in the main body of this thesis. As discussed in detail, all the results including the critical load/generator/branch identification were verified by the standard methods. Although it was not presented in the thesis, not such good results could be obtained without using the channel load modeling. The implication is that the proposed channel load modeling has a reliable and acceptable performance and therefore, is good enough for the CCT-based studies.

- ***Direct verification***

In this approach, the parameters of the channel loads should be estimated using another method and the results should be compared with those of the proposed method. For this purpose, a method similar to Thevenin circuit identification method [38] is used to identify the channel load parameters.

In this method, the system loads are considered as constant impedances at each operating point and a Thevenin circuit for the channel load (as shown in Fig. A.10) is obtained which is associated with that operating point.

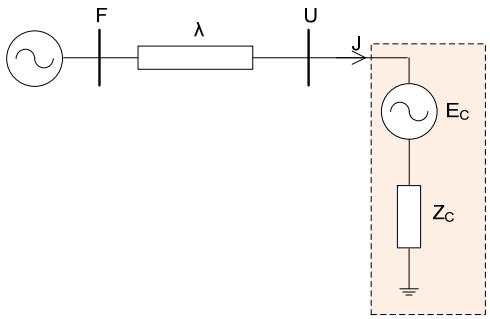

Fig. A.10: Channel-domain circuit with the modeled load

The aim is to calculate the model parameters (E_C and Z_C) for each channel and for each operating point. For each channel, at least two sets of data (U and J) are required. One set can be obtained from the system data when it is at the current operation condition. The second set of

data is obtained by applying a small change in the voltage source (F) of the associated channel while keeping the load side (E_C and Z_C) constant. As explained in the previous sub-section, E_C is composed of the voltage sources of the other channels, and Z_C is composed of the loads and channel impedances. Therefore, in order to keep E_C and Z_C constant, the voltage source of all other channels and the impedances of all system loads should be kept constant. In other words, a change should be applied in only and only the voltage source of the associated channel to obtain the second data set. For this purpose, a procedure is proposed in the following.

Assume that modeling of the load for channel 1 is the aim. Therefore, the voltage source of channel 1 should be changed while those of the other channels are constant i.e.

$$F_{1\_new} = F_1 + \Delta F_1$$
$$F_{i\_new} = F_i\ ,\ i \neq 1$$

This requires changing the generator voltages. New generator voltages [E_{new}] are obtained by solving the following equation.

$$\begin{bmatrix} F_{1\_new} \\ F_2 \\ \cdots \\ F_n \end{bmatrix} = [C] \begin{bmatrix} E_{1\_new} \\ E_{2\_new} \\ \cdots \\ E_{m\_new} \end{bmatrix} \tag{A.6}$$

Then, we consider the system loads as constant impedances and the new loads' voltages [V_{new}] and currents [I_{new}] are obtained by solving the following two equations simultaneously.

$$[V_{new}] = [K][E_{new}] - [Z][I_{new}] \tag{A.7}$$
$$[V_{new}] = [Z_L][I_{new}] \tag{A.8}$$

The transform is then applied on the obtained [V_{new}], and [I_{new}] along with [E_{new}], and a new set of channel data U_{new} and J_{new} is obtained. Using this new data set along with the one obtained based on the normal operating point of the system i.e. U and J, the channel load parameters Z_C and E_C are obtained by solving the following equation set.

$$\begin{cases} U = Z_C J + E_C \\ U_{new} = Z_C J_{new} + E_C \end{cases} \tag{A.9}$$

The E_C obtained by the above procedure (verification method) can then be compared with the one obtained by the proposed method. As an example, the following figure shows this comparison for the WECC 9-bus system. Solid lines show the results obtained by the proposed method and dashed lines show the results obtained by the verification method. Note that we have three channels in this system. As seen in this figure, the results are very close to each other verifying the proposed method.

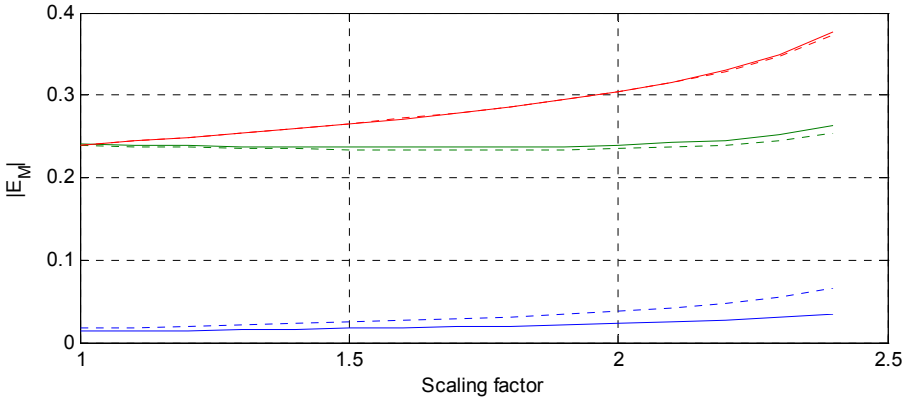

Fig. A.11: Comparison of E_C obtained by the proposed method and by the verification method

Appendix B. A Discussion on the Critical Branch Identification

A method was proposed and verified for the critical branch identification in this thesis. The proposed method uses the information obtained by the CCT i.e. the identified critical load and generator, finds the critical transmission path, and then finds the critical branch using the voltage phasors of the actual system. Although the proposed method was verified as an accurate and reliable method, one may wonder why a more direct CCT-based method is not used. For example, with respect to the success of generator/load contributions to the critical channel in identifying the critical generator/loads, one may expect that a similar contribution index can be defined to determine the impact of the branches in the critical channel. In this respect, we expected that we could find the weak branches by examining the current or power flow pattern associated with the critical channel. We have conducted research on this subject and found out that this approach does not work. The aim of this appendix is to briefly present the concept, the methodology, and case study results regarding this approach.

The equations to determine the power flow pattern associated with the critical channel are straight forward. We know that the nodal voltages can be obtained from channel voltages using the following equation.

$$[V]=[T]^{-1}[U] \tag{B.1}$$

Assume that channel 1 is the critical channel, we can determine the nodal voltage component that belongs to channel 1 as follows:

$$\begin{bmatrix} V_1 \\ V_2 \\ \dots \\ V_n \end{bmatrix}_{Channel\,1} = \begin{bmatrix} T_{11} & T_{12} & . & T_{1n} \\ T_{21} & . & . & . \\ . & . & . & . \\ T_{n1} & T_{n2} & . & T_{nn} \end{bmatrix}^{-1} \begin{bmatrix} U_1 \\ 0 \\ \dots \\ 0 \end{bmatrix} \tag{B.2}$$

The same procedure can be applied to obtain voltage sources. Therefore, the voltage of all load buses V_L and generator buses V_G can be easily determined using the above procedure. On

the other hand, we obtained an equation for the voltage of network buses V_N in terms of V_L and V_G in section 2.3 as follows.

$$V_N = -Y_{NN}^{-1}(Y_{NG}V_G + Y_{NL}V_L) \tag{B.3}$$

Using the above equation and the obtained V_L and V_G, the voltage of network buses V_N can be calculated. Therefore, the voltage of all buses would be available. It would be easy then to obtain the powerflow pattern of the system which corresponds to the critical channel.

Once the power flow pattern associated with the critical channel is obtained, we can determine the critical branch. For this purpose, one of the following two methods can be used.

- Normalized Voltage Drop (*NVD*): This method is somewhat similar to the critical channel identification presented in section 3.4. According to the discussions of section 3.4, the voltage drop in a single branch can indicate the stability level of the branch. The higher the voltage drop, the lower the stability level. The idea is to extend this concept to a multi branch system. In this approach, the critical branch is likely to have the highest normalized voltage drop among all the branches. Therefore, the *NVD* of each branch is calculated according to (B.4) and by using the obtained bus voltages which correspond to the critical channel. The branch which has the highest *NVD* should be the critical branch.

$$NVD_{ij} = \frac{|V_i| - |V_j|\cos\delta_{ij}}{|V_i|} \times 100 \tag{B.4}$$

where V_i is the sending end voltage, V_j is the receiving end voltage, and δ_{ij} is the phase angle difference between the sending-end and the receiving end.

- Line Stability Index (*FVSI*): The line stability index or novel fast voltage stability index (FVSI) proposed in [77] is based on the concept of power flow in a single line. For a typical transmission line, the stability index is calculated by (B.5). This index should be calculated for all the branches by using the power flow pattern associated with the critical channel. The branches are then ranked based on the calculated indices.

$$FVSI_{ij} = \frac{4Z^2 Q_j}{V_i^2 X} \tag{B.5}$$

where Z is the line impedance, X is the line reactance, Q_j is the reactive power flow at the receiving end and V_i is the sending end voltage.

A 6-bus system shown in Fig. B.1 is considered as the first case study. The parameters of this system are provided in Tables B.1 and B.2. This system has 3 load buses, 3 generator buses, and no network bus. Therefore, it is very easily to obtain the power flow pattern of the system associated with the critical channel without any difficulty.

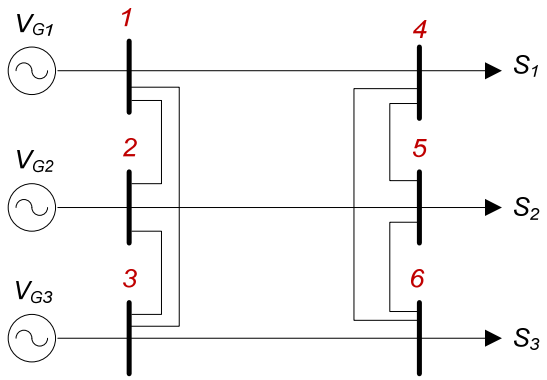

Fig. B.1: a simple 6-bus system

Table B.1: Branch data

Branch No.	From bus	*To bus*	*R* (p.u.)	*X* (p.u.)
1	1	2	0.1	0.2
2	1	3	0.05	0.4
3	1	4	0.05	0.3
4	2	3	0.05	0.25
5	2	5	0.1	0.3
6	3	6	0.02	0.1
7	4	5	0.01	0.2
8	4	6	0.02	0.1
9	5	6	0.05	0.3

Table B.2: Generator and load data

Bus	P_G (p.u.)	$\|V_G\|$ (p.u.)	P_L (p.u.)	Q_L (p.u.)
1	Slack bus	1.05	---	---
2	0.9	1.05	---	---
3	0.5	1.07	---	---
4	---	---	0.8	0.7
5	---	---	0.7	0.2
6	---	---	1	0.5

The CCT-based voltage stability analysis is applied first to this system. The results show that channel 1 is the critical channel in this system (see Fig. B.2). Therefore, the load/generator voltage components that belong to channel 1 should be calculated first. When the system is close to the nose point, the obtained voltages are as follows:

$$V_G = \begin{bmatrix} 1.58\angle -8.4 \\ 1.89\angle -18.5 \\ 0.399\angle -10.3 \end{bmatrix} \qquad V_L = \begin{bmatrix} 0.59\angle -34.7 \\ 0.69\angle -35.8 \\ 0.45\angle -34.8 \end{bmatrix}$$

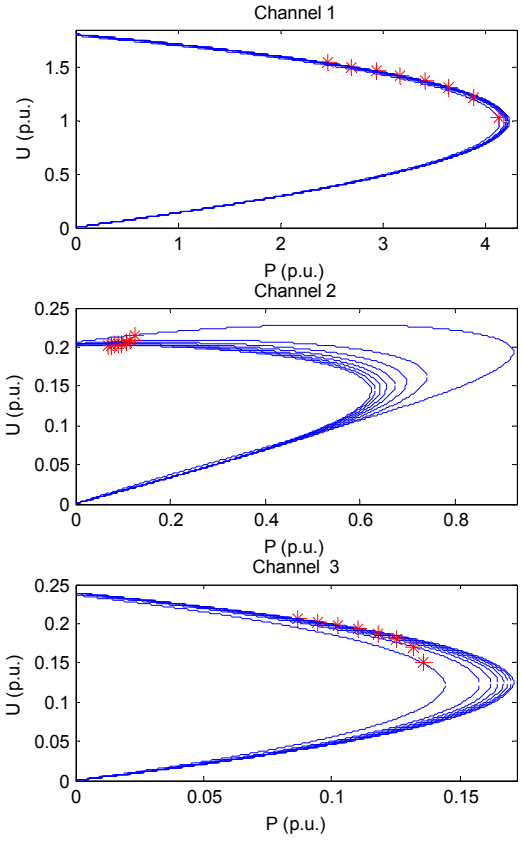

Fig. B.2: The channel PV curves for the simple case study

According to the above results, the voltage difference between generator 2 and generator 3 are very high. This leads to a great amount of current and voltage drop on the line which connects these two buses i.e. line 4. So it seems that this line should be the critical one. This can be confirmed if the *NVD* and *FVSI* are calculated for the branches. Fig. B.3, and Fig. B.4 show the calculated *NVD* and *FVSI*, respectively. As these figures reveal, both methods lead to line 4 as the critical line.

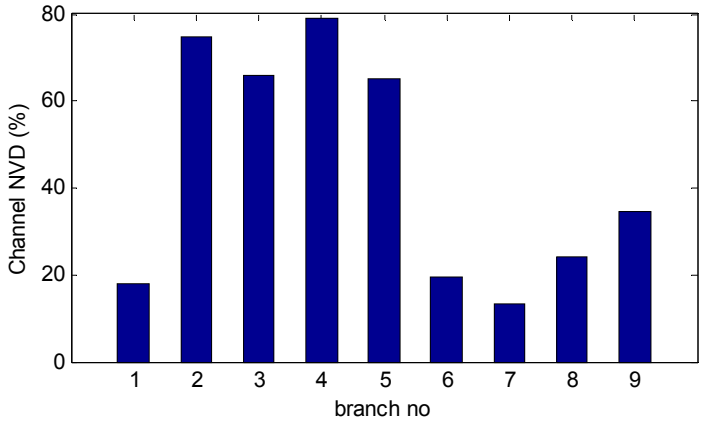

Fig. B.3: The *NVD* for the power flow pattern associated with the critical channel

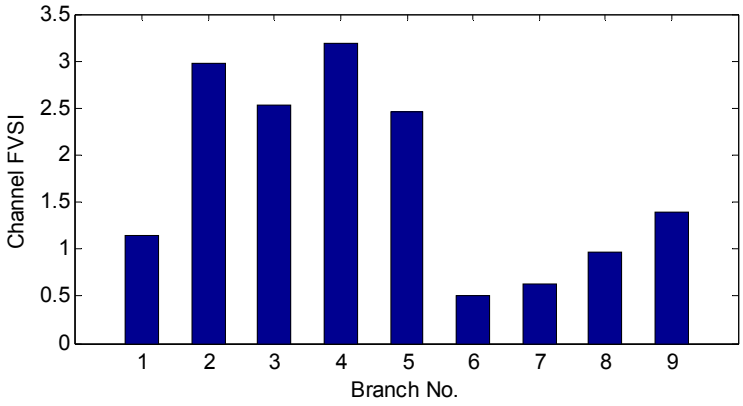

Fig. B.4: The *FVSI* for the power flow pattern associated with the critical channel

On the other hand, if the verification method (the sensitivity-based method) is applied to this system, Fig. B.5 is obtained. As clearly seen in this figure, line 4 is not the critical line. It does not even belong to the first three critical lines. This is totally reasonable because line 4 connects

a generator to another generator and it is not likely that such a line would be the critical one in a system.

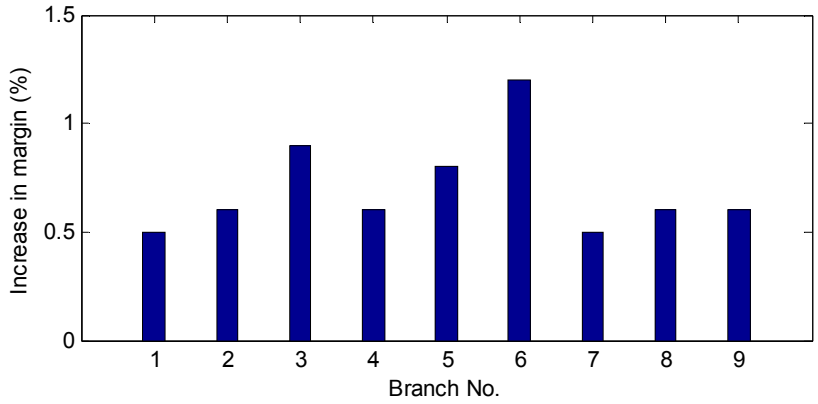

Fig. B.5: Branch ranking obtained by the verification method

The IEEE 30-bus system is considered as the next case study. Fig. B.6 and Fig. B.7 show the calculated *NVD* and *FVSI*, respectively. As these figures reveal, both methods lead to line 1 as the critical line. Again, line 1 is a line which connects a generator to another generator. Therefore, this result seems to be wrong at the first place. This can be confirmed by looking at the results of the verification method shown in Fig. B.8. As seen in this figure, line 1 does not belong to the first few critical lines in this system.

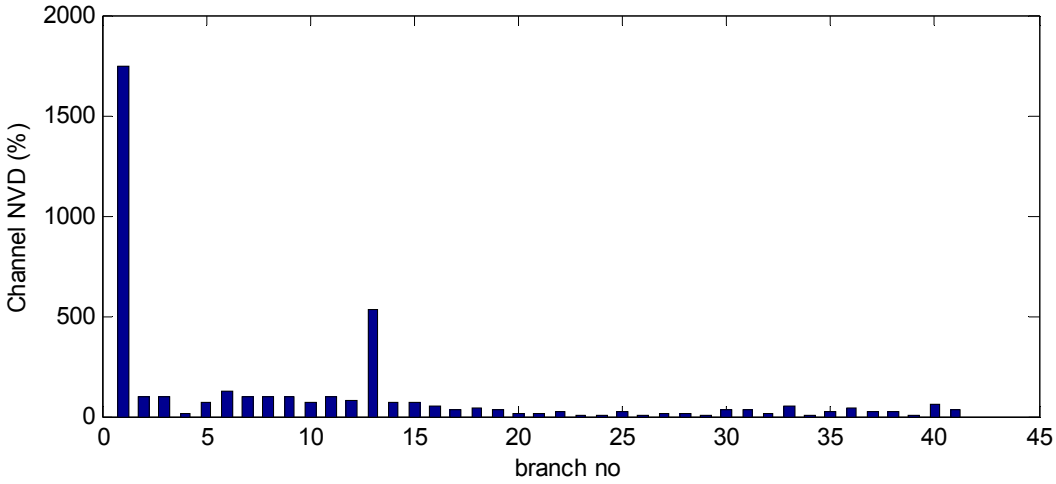

Fig. B.6: The *NVD* for the power flow pattern associated with the critical channel

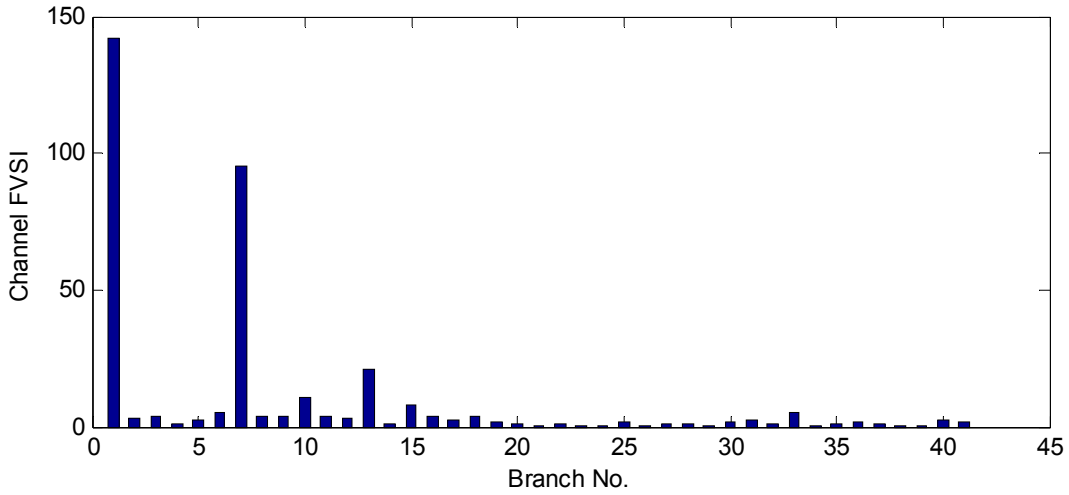

Fig. B.7: The *FVSI* for the power flow pattern associated with the critical channel

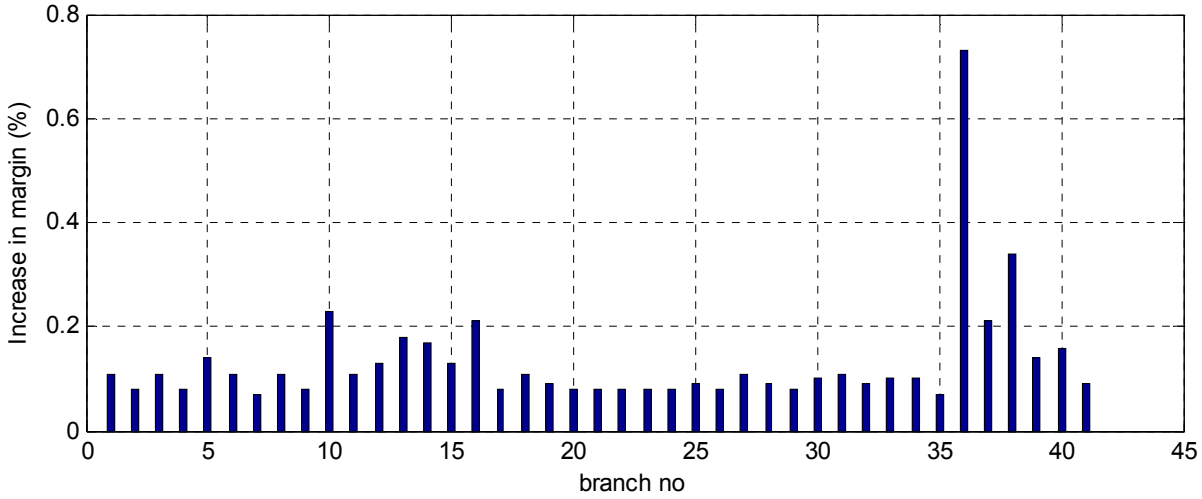

Fig. B.8: Branch ranking obtained by the verification method

Several other test systems have also been considered as case studies. To save space, their results are not reported here. However, the conclusions of the results are all the same. The methods which directly use the power flow pattern associated with the critical channel cannot be used for the critical line identification.